
Fundamental Physics Opportunities with the Next-Generation Event Horizon Telescope

Dimitry Ayzenberg, Lindy Blackburn,
Richard Brito, Silke Britzen,
Avery E. Broderick, Raúl Carballo-Rubio,
Vitor Cardoso, Andrew Chael, Koushik
Chatterjee, Yifan Chen, Pedro V. P. Cunha,
Hooman Davoudiasl, Peter B. Denton,
Sheperd S. Doeleman, Astrid Eichhorn,
Marshall Eubanks, Yun Fang,
Arianna Foschi, Christian M. Fromm,
Peter Galison, Sushant G. Ghosh,
Roman Gold, Leonid I. Gurvits,
Shahar Hadar, Aaron Held, Janice Houston,
Yichao Hu, Michael D. Johnson, Prashant
Kocherlakota, Priyamvada Natarajan,
Héctor Olivares, Daniel Palumbo,
Dominic W. Pesce, Surjeet Rajendran,
Rittick Roy, Saurabh, Lijing Shao,
Shammi Tahura, Aditya Tamar, Paul Tiede,
Frédéric H. Vincent, Luca Visinelli,
Zhiren Wang, Maciek Wielgus, Xiao Xue,
Kadri Yakut, Huan Yang, Ziri Younsi

Abstract The Event Horizon Telescope (EHT) Collaboration recently published the first images of the supermassive black holes in the cores of the Messier 87 and Milky Way galaxies. These observations have provided a new means to study supermassive black holes and probe physical processes occurring in the strong-field regime. We review the prospects of future observations and theoretical studies of supermassive black hole systems with the next-generation Event Horizon Telescope (ngEHT), which will greatly enhance the capabilities of the existing EHT array. These enhancements will open up several previously inaccessible avenues of investigation, thereby providing important new insights into the properties of supermassive black holes and their environments. This review describes the current state of knowledge for five key science cases, summarising the unique challenges and opportunities for fundamental physics investigations that the ngEHT will enable.

Contents

1	Introduction	3
1.1	ngEHT: array architecture and vision	4
1.2	Outline and notation	6
1.2.1	List of acronyms used in this review	7
1.3	Author contributions	8
2	Studies of the photon ring	10
2.1	The photon shell and ring	10
2.2	Science Cases	13
2.2.1	Demonstrating existence of the $n = 1$ ring	13
2.2.2	Static modeling of the $n = 1$ ring	15
2.2.3	Harnessing time dependence for photon ring detection	16
2.3	Open Questions	19
3	Measuring black hole mass and spin	21
3.1	Introduction	21
3.2	Overview of ngEHT observables for measuring mass and spin	21
3.2.1	Light ring imaging	22
3.2.2	Hotspot tracking	24
3.2.3	Photon ring autocorrelations	25
3.2.4	Polarization spirals in direct and indirect images	26
3.2.5	Probes of extremal BH/signatures of NHEK	27
3.3	Overview of complementary measurements of mass and spin	28
3.3.1	Probing Sgr A* with S-stars	28
3.3.2	Observation of Sgr A* EMRIs with LISA	29
3.3.3	Pulsars around the Sgr A* black hole	30
3.3.4	Quasi-periodic oscillations	32
3.3.5	Near-IR flares and orbiting hot spots	33
4	Searching for ultralight fields with the ngEHT	34
4.1	The theory	35
4.2	Constraints from black-hole spin measurements	36
4.3	Direct gravitational effects	39
4.3.1	Observing the superradiant instability evolution	39
4.3.2	Black holes with synchronised bosonic hair	41
4.3.3	Photon ring astrometry for real bosons	43
4.3.4	Boson and Proca stars	44
4.3.5	Motion of S-stars	45
4.4	Polarimetric measurements for axion-induced birefringence	46
4.5	Open issues	49
4.5.1	Other types of interactions	49
4.5.2	Parametric instability of axion clouds	50
4.5.3	Plasma heat-up from axion clouds in a magnetic field	51
5	Tests of GR and the Kerr hypothesis with the ngEHT	53
5.1	Scenarios for physics beyond GR	55
5.1.1	Modified gravity	55
5.1.2	Specific spacetimes and compact objects beyond GR	59
5.1.3	New-physics effects in light propagation and matter dynamics	62
5.2	Science cases	64
5.2.1	Horizonless spacetimes and their central brightness depression	64
5.2.2	Parametric tests of the Kerr paradigm	69
5.2.3	Image signatures of event horizons: the inner shadow	72
5.2.4	Resolvable multi-ring structures	76
5.3	ngEHT challenges for numerical simulations	77
5.4	Outlook	80
6	Exploring binary black holes with ngEHT	82
6.1	Multiple supermassive black hole systems	85
6.2	Taxonomy of SMBHBs	86
6.2.1	Telescopic binaries	88
6.2.2	Astrometric binaries	88
6.2.3	Spectroscopic binaries	89

6.2.4	Relativistic transiting binaries	90
6.2.5	Reverberation binaries	90
6.3	Multi-messenger detection of supermassive black hole binaries	91
6.3.1	Multi-messengers with pulsar timing arrays	92
6.3.2	Multi-messengers with LISA	93
6.3.3	The role of VLBI in multi-messenger studies	93
6.4	Emission models of supermassive binary black holes	94
6.4.1	Hybrid modeling	94
6.4.2	Model selection: binary vs Lense-Thirring	94
6.4.3	Simple emission models	95
6.5	Simplified physical models: approximate, semi-analytic emission models	95
6.5.1	Physical models: GRMHD simulations of accreting SMBH binaries	95
6.6	Summary of prospects of probing SMBH binaries with the ngEHT	98
6.7	Challenges & future prospects	99
	Conclusions	100
	Acknowledgments	100
	References	101
	Author affiliations	154

1 Introduction

Recent very-long-baseline interferometry (VLBI) observations of supermassive black holes (SMBHs) have opened a new path to observe and study strong field gravity. Black holes (BHs) lie at the edge of our understanding of the fundamental laws of physics. The mechanisms governing their genesis and evolution are poorly understood, but there is substantial evidence for the pivotal role they play in star formation, galactic evolution, cosmic energy exchange and transport, accretion and outflows, and the generation of ultra-high-energy (UHE) emissions. From a fundamental physics perspective, BHs hold a tremendous potential for advancing scientific knowledge. They are considered central to possible energy extraction mechanisms *from vacuum* of their surrounding deep gravitational potentials, wherein gravitational lensing can be so strong that the trajectories of light rays are “closed”. The Einstein field equations (EFEs) break down in BH interiors, raising the prospect that the geometry close to the event horizon may carry observable imprints which will prove crucial in the development of a more comprehensive description of the gravitational interaction. Such developments will require conclusive experimental evidence for the existence of astrophysical BH event horizons and for a detailed mapping of their geometry. The last decade has been vital for the field. In 2015 the first direct detection of gravitational waves (GWs) opened up the remarkable new tool of GW astronomy to study compact objects. GWs have been successfully used to probe BHs and neutron stars in the highly dynamical regime.

The achievement of hitherto unprecedented resolving power in traditional observational astronomy using optical, infrared, and radio VLBI over the past few decades has led to significant progress in the study of BH systems. Of particular importance in the context of this review are the multidecadal observations of the orbital motions of S-stars in the Galactic Centre (GC) by the Keck telescope (Do et al., 2019a) and the VLTI (Abuter et al., 2022). These observations constrained the central mass of the GC to be $\sim 4 \times 10^6 M_{\odot}$ (see Table 2), providing compelling evidence for the existence of a supermassive compact object, presumably a SMBH. Parallel advances in mm wavelength VLBI during these years provided a means to spatially resolve the immediate environment of the compact object in the GC at frequencies where the surrounding hot plasma becomes optically thin. This led to the discovery of horizon-scale features

of the GC SMBH Sagittarius A*, hereafter Sgr A*, (Doeleman et al., 2008), and similar scale structures around the M87 SMBH, hereafter M87* (Doeleman et al., 2012). Subsequent growth of mm-VLBI arrays led to the Event Horizon Telescope (EHT) Collaboration (EHTC) producing the first ever images of these two SMBHs (EHT Collaboration, 2019a, 2022a). These results present a bright ring feature in both SMBH images, demonstrating the persistence of this feature across a scale of more than three orders of magnitude in mass (see Figure 1), as anticipated from the scale-invariance of general relativity (GR). Both images also demonstrate manifestly similar image morphologies, with pronounced central brightness depressions and ring diameters consistent with the predictions of GR. These recent breakthroughs are complementary to GW observations, probing spacetime geometries which can be understood as “static” (i.e., effectively stationary) by detecting radiation produced by matter in the vicinity of the BH’s purported event horizon.

In this review we assess the potential of a next-generation Event Horizon Telescope (ngEHT) to extract information on foundational issues related to BHs and near-horizon physics, presenting an overview of the most promising future prospects for studies of BHs and strong field gravity in the next decade. The ngEHT program is expected to transform our understanding of SMBH sources via substantial improvements in angular resolution, image dynamic range, multi-wavelength capabilities, and long-term monitoring, as well as rendering several new SMBH systems accessible to event horizon-scale study. The structure of the persistent ring feature in EHT images of Sgr A* and M87* is currently not sufficiently resolved to unambiguously confirm the presence of a “photon ring”¹. The ngEHT will use measurements of the emission near SMBHs to probe their spacetime geometry, measuring the BH mass and spin, as well as enabling tests of the no-hair theorem of astrophysical BHs.

1.1 ngEHT: array architecture and vision

The current EHT results were all achieved using an observing campaign in 2017 that included 8 telescopes at 6 geographic sites. In an interferometric array such as the EHT, each baseline joining a pair of telescopes samples a single Fourier component of the sky image. EHT observations of Sgr A* had 15 intersite baselines, while EHT observations of M87* had 10 intersite baselines (the South Pole Telescope cannot observe M87*). The EHT observations recorded a single 4 GHz band, centered on 228 GHz. Since the initial EHT observing campaign, the array has been expanded to include 3 additional sites, has doubled the recorded bandwidth, and has recently added the ability to observe at 345 GHz (Crew et al., 2023).

The ngEHT is a project that is designing an array that would substantially enhance the observational capabilities of the EHT (Doeleman et al., 2019). Over two phases of deployment, the ngEHT will add up to ~ 10 additional sites worldwide by ~ 2030 (see Figure 2). The ngEHT will also include three simultaneous observing bands at 86, 230, and 345 GHz. Apart from providing spectral information, this configuration will allow substantially improved phase coherence at high frequencies because the dominant sources of ngEHT phase errors are non-dispersive (see, e.g., Issaoun et al., 2023; Rioja et al., 2023). Together, these improvements will augment the angular resolution of

¹ In the absence of attenuating material media, gravitational field theory predicts a formally infinite hierarchy of successively thinner and fainter photon rings: see Sec. 2.

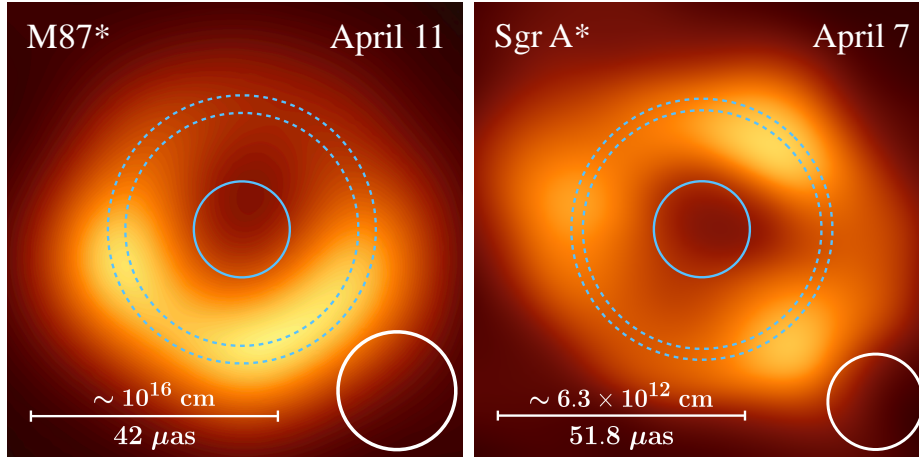


Fig. 1 EHTC images of M87* (left) and Sgr A* (right). The central solid blue circles show the largest possible diameter (in GR) of each BH’s event horizon, i.e., the Schwarzschild value of $4 r_g$, where r_g is the BH gravitational radius (see Sec. 2). The size of the event horizon in the observed image would appear slightly larger than the solid blue circles, due to gravitational lensing. Note that the event horizons fit within the central dark regions of both images (the central brightness depression). Pairs of dashed blue circles delineate the estimated diameter range of the bright ring from image domain analysis of M87* ($42 \pm 3 \mu\text{as}$) and Sgr A* ($51.8 \pm 2.3 \mu\text{as}$). These ranges are consistent with the prediction of the Schwarzschild BH shadow diameter ($2\sqrt{27} r_g$). The white circles in the lower right of both panels show the $20 \mu\text{as}$ FWHM circular Gaussian beam (EHT 2017). See [EHT Collaboration \(2019a\)](#) and [EHT Collaboration \(2022a\)](#) for further information. Figure reproduced from [Younsi \(2024\)](#).

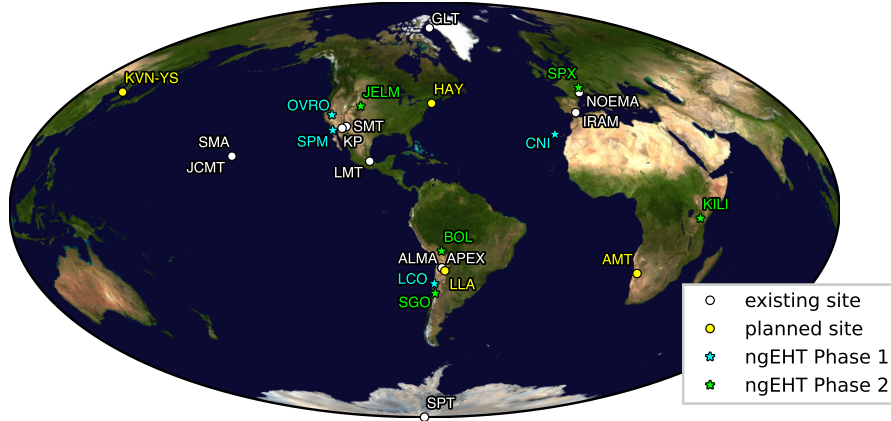


Fig. 2 Vision for the ngEHT array. Current EHT sites are shown in white, candidate ngEHT Phase 1 sites are blue, and candidate ngEHT Phase 2 sites are green. In addition, yellow markers show four additional sites that are planned to come online over the next five years: the 37 m Haystack Telescope (HAY; [Kauffmann et al., 2023](#)), the 15 m Africa Millimetre Telescope (AMT; [Backes et al., 2016](#)), the Large Latin American Millimeter Array (LLA; [Romero, 2020](#)), and the Yonsei Radio Observatory of the Korea VLBI Network (KVN-YS; [Asada et al., 2017](#)). For additional details on the ngEHT array, see [ngEHT Array](#). Figure reproduced from [ngEHT Science](#).

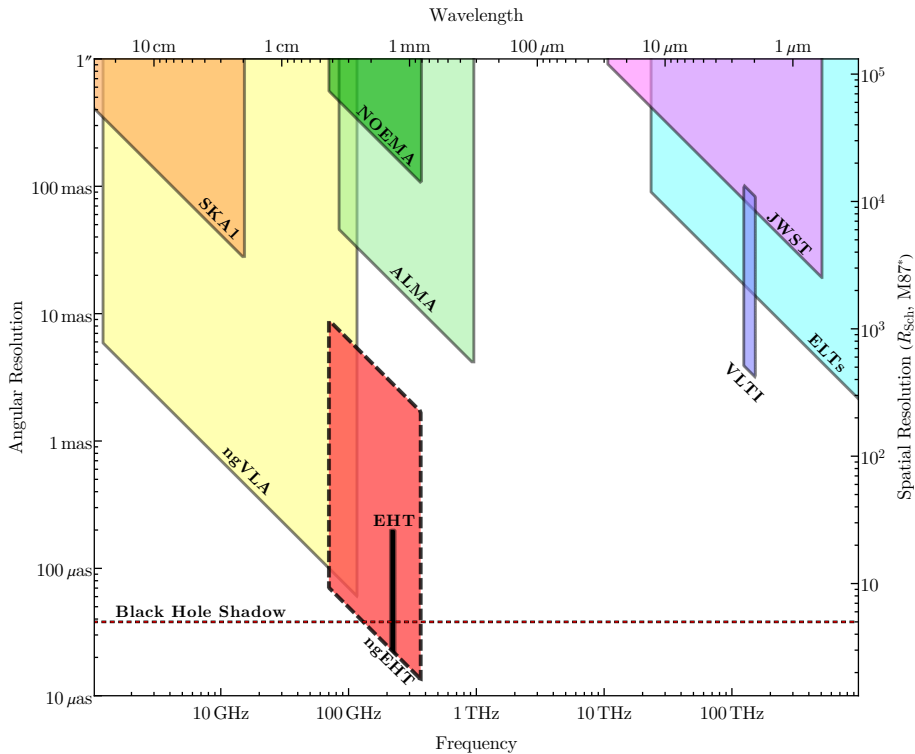


Fig. 3 Observing frequencies and imaging angular resolutions for current and next generation facilities. The EHT and ngEHT have significantly finer imaging resolution than any other telescope. The ngEHT will significantly expand the frequency coverage of the EHT and will provide access to larger angular scales. Figure reproduced from [ngEHT Science](#).

current EHT images by approximately 50% and will increase the angular scales that the array can image by an order of magnitude (see [Figure 3](#)). They will also increase the dynamic range of BH images by 1–2 orders of magnitude and will ultimately support dense observations year-round, significantly improving the current temporal coverage of EHT observations (~ 1 week per year). For a summary of the ngEHT array, see [Doeleman et al. \(2023, hereafter ngEHT Array\)](#). For a summary of the complete set of ngEHT science goals, see [Johnson et al. \(2023, hereafter ngEHT Science\)](#).

1.2 Outline and notation

This review article is organised as follows. In [Sec. 2](#) we review the status and prospects of ngEHT studies of the photon ring to provide evidence of strong field gravitational lensing by SMBHs and yield novel tests of GR. Next, in [Sec. 3](#) we present an overview of ngEHT observables for measuring SMBH mass and spin, followed by an overview of other studies which can complement those the ngEHT will perform. In [Sec. 4](#) we discuss the capability of the ngEHT to search for ultralight bosonic fields below the eV scale, together with the implications of these studies for the structure of the central compact object and its surrounding plasma. [Section 5](#) presents an overview of tests of

GR and the Kerr hypothesis with the ngEHT. Different physical scenarios in beyond-GR theories are classified, with their implications for testable violations of the Kerr hypothesis discussed, together with a summary of key science cases for testing features of compact objects in and beyond GR. Finally, in Sec. 6 we discuss the prospects of studies of SMBH binaries with the ngEHT. Candidate sources are identified and the challenges and prospects of probing SMBH binaries with the ngEHT are explored.

In this review we venture to provide a framework for the exploration and development of these exciting new prospects. Studies such as those discussed in this review will consolidate our understanding of the different ways ngEHT-driven VLBI observations can probe the properties of SMBHs and enable new tests of fundamental physics.

The acronyms used in this review are summarised in Table 1. We adopt the geometrical unit convention in which $G = c = 1$, and unless otherwise stated assume the metric signature to be $[-, +, +, +]$. When specifying vectors and tensors, Greek indices (e.g., μ, ν) span $(0, 1, 2, 3)$ and Latin indices (e.g., i, j) span $(1, 2, 3)$, where 0 denotes the temporal component and $(1, 2, 3)$ denote spatial components.

1.2.1 List of acronyms used in this review

AGN	Active Galactic Nucleus
Athena	Advanced Telescope for High ENergy Astrophysics
BAL	Broad absorption line
BH	Black hole
BBH	Binary black hole
CFT	Conformal field theory
CMB	Cosmic microwave background
CCTP	Conjugate closure trace product
CTA	Cherenkov Telescope Array
DM	Dark matter
DAGN	Dual AGN
ECO	Exotic compact object
EdGB	Einstein dilaton Gauss Bonnet
EdM	Einstein dilaton Maxwell
EFEs	Einstein field equations
EFT	Effective field theory
EHT	Event Horizon Telescope
EHTC	Event Horizon Telescope Collaboration
EMRI	Extreme mass-ratio inspiral
EVPA	Electric vector position angle
FFE	Force-Free Electrodynamics
FWHM	Full width half maximum
GC	Galactic Center
GR	General relativity
GRMHD	General-relativistic magnetohydrodynamics
GRRT	General-relativistic radiative transfer
GW	Gravitational wave
GWB	Gravitational wave background
HD	Hellings & Downs
IMBH	Intermediate-mass black hole

IR	Infrared
ISCO	Innermost stable circular orbit
JWST	James Webb Space Telescope
LIGO	Laser Interferometer Gravitational-Wave Observatory
LISA	Laser Interferometer Space Antenna
LLAGN	Low luminosity AGN
LT	Lense-Thirring
M87	Messier 87
MAD	Magnetically arrested disk
MCMC	Markov Chain Monte Carlo
MRI	Magnetorotational instability
ngEHT	Next-Generation Event Horizon Telescope
NGC	New General Catalogue
ngVLA	Next-Generation Very Large Array
NHEK	Near horizon extremal Kerr
NIR	Near Infrared
PN	Post-Newtonian
PTA	Pulsar Timing Array
QPO	Quasi-periodic oscillation
RIAF	Radiatively inefficient accretion flow
SANE	Standard and normal evolution
SCO	Stellar compact object
SDSS	Sloan Digital Sky Survey
SEP	Strong equivalence principle
SFPR	Source Frequency Phase Referencing
Sgr A*	Sagittarius A*
SKA	Square kilometer array
SMBH	Supermassive black hole
SMBHB	Supermassive black hole binary
SNR	Signal-to-noise ratio
UHE	Very high energy
VHE	Very high energy
VLA	Very Large Array
VLBI	Very-Long-Baseline Interferometry
VLBA	Very Long Baseline Array
VLTI	Very Large Telescope Interferometer
SWG	Science working group

1.3 Author contributions

The ngEHT Fundamental Physics Science Working Group (SWG) was coordinated by **Vitor Cardoso and Ziri Younsi**. The topic “Studies of the photon Ring” was led by **Shahar Hadar and Daniel Palumbo**. The topic “Measuring black hole mass and spin” was led by **Dimitry Ayzenberg, Lijing Shao and Huan Yang**. The topic “Searching for ultralight fields with the ngEHT” was led by **Richard Brito and Yifan Chen**. The topic “Tests of GR and the Kerr hypothesis with the ngEHT” was led by **Astrid Eichhorn and Aaron Held**. The topic “Exploring binary black

holes with the ngEHT” was led by **Silke Britzen and Roman Gold**. All authors contributed to the writing of the document.

2 Studies of the photon ring

There are three classical tests of GR: the precession of the planet Mercury, the deflection of light by the Sun and the gravitational redshift of light. The first observation of light deflection by the Sun was measured by Arthur Eddington and his team during the 1919 eclipse (Crispino and Kennefick, 2019; Will, 2014). They recorded a deflection angle of $\delta \sim 1.7$ arcseconds. This is consistent with the weak field prediction of GR where, for a small dimensionless compactness r_g/r_0 , the angle is given by $\delta \approx 4r_g/r_0$. Here r_0 is the perihelion of the light ray’s trajectory and $r_g := GM/c^2$ is the gravitational radius of the deflector, wherein M is the mass of the Sun, G is Newton’s gravitational constant and c is the speed of light.

In the strong field regime, near extremely compact objects such as BHs, the very same principles of GR predict that the deflection angle should become unbounded at the so-called *photon shell*: the spacetime region, close to the BH event horizon, where light rays may orbit indefinitely at fixed (Boyer-Lindquist) radius (see Perlick, 2004, for a review and historical account). The Schwarzschild radius of a BH is defined as $r_S := 2GM/c^2 \equiv 2r_g$ and corresponds to the radius of the event horizon of a Schwarzschild BH. For the Schwarzschild metric, the photon shell is located at $3r_g$, i.e., at a coordinate radius of only $0.5r_S$ away from the event horizon.

The light rays of the photon shell are unstable; when they are slightly perturbed, time evolution drives them away from the shell, and eventually they either reach asymptotic infinity or fall into the BH. Nevertheless, in this process they experience extreme lensing, with order-unity deflection angles (in radians), and carry an imprint of the spacetime geometry at the photon shell region. The extreme gravitational lensing close to the photon shell is accompanied by an extreme “Shapiro-like” delay, directly responsible for the late-time appearance of collapsing spacetimes or of transient electromagnetic phenomena in the BH vicinity (Podurets, 1965; Ames and Thorne, 1968; Cardoso et al., 2021a; Ferrari and Mashhoon, 1984; Cardoso et al., 2009).

The detection of extreme gravitational lensing may therefore provide new ways to observe gravitational phenomena in the strong-field regime. The goal of this Chapter is to discuss how EHT and ngEHT observations can be used to provide evidence and quantification of the strong deflection of light by BHs.

2.1 The photon shell and ring

Geodesic motion in the Kerr spacetime has been studied since the pioneering work of Carter (1968) and numerous papers thereafter (see, e.g., Walker and Penrose, 1970; Chandrasekhar, 1983; Hackmann et al., 2010). In this section we discuss the unstably bound null geodesics of Kerr, which are of central importance for the interpretation of BH images. These are null-geodesic orbits with fixed Boyer-Lindquist radial coordinate (Boyer and Lindquist, 1967). They are pivotal for astrophysical observations of BHs since they define the universal features in the observational appearance of the BH, as will be described below.

In what follows we adopt Boyer-Lindquist coordinates $x^\mu = (t, r, \theta, \phi)$ and denote the photon 4-momentum by p_μ . We denote the BH mass by M and its angular momentum by J . The BH spin parameter is defined as $a := J/M$, and the dimensionless spin parameter is defined as $a_* := J/M^2 \equiv a/M$. Null geodesics (photons) in the Kerr spacetime are specified by two constants of motion: the energy-scaled

angular momentum component parallel to the axis of symmetry $\lambda = L/E$, where $L \equiv p_\phi$ and $E \equiv -p_t$, and the energy-scaled Carter constant $\eta = Q/E^2$, where $Q = p_\theta^2 + (p_\phi^2 \csc^2 \theta - a^2 p_t^2) \cos^2 \theta$.

The energy itself only determines the frequency of the photon moving along the geodesic and not its trajectory. The existence of a quadratic Killing tensor and the resulting separability of the Hamilton-Jacobi equation for the Kerr spacetime give rise to the Carter separation constant, Q , which characterizes the polar motion. Together with the null condition $p_\mu p^\mu = 0$, the geodesic motion may be reduced to a problem of quadratures, i.e., expressed as a system of four coupled first-order ordinary differential equations for the geodesic path.

We now focus on a specific, special subset of the Kerr BH's null geodesics which orbit at a fixed Boyer-Linquist radius $r = \tilde{r}$. These orbits play a central role in this section and they are interchangeably referred to as spherical/bound/critical photon orbits. As mentioned above, the radial equation is cast in the form of one-dimensional radial motion in an effective potential, $V_r(r)$. Solving $V_r(\tilde{r}) = V_r'(\tilde{r}) = 0$ determines a one-parameter family of critical parameters $\lambda(\tilde{r})$ and $\eta(\tilde{r})$ for which spherical photon orbits exist. These bound photon orbits comprise the *photon shell*, and are labeled by their radius \tilde{r} (Darwin, 1959; Bardeen et al., 1972; Luminet, 1979; Teo, 2003; Gralla et al., 2019; Johnson et al., 2020). The fact that $V_r''(\tilde{r}) < 0$ for all these orbits shows that they are *unstable*. The impact parameters λ and η may be thought of as coordinates on an observer's screen, and the above-described set $\{\lambda(\tilde{r}), \eta(\tilde{r})\}$ defines the critical curve, with \tilde{r} a parameter along it.

The spherical photon orbits, which constitute the photon shell, exist in the range $\tilde{r}_- < \tilde{r} < \tilde{r}_+$, where the outermost (retrograde, +) and innermost (prograde, -) equatorial circular photon orbits are located at the radii:

$$\tilde{r}_\pm = 2M \left\{ 1 + \cos \left[\frac{2}{3} \arccos(\pm |a_*|) \right] \right\}. \quad (1)$$

For $a_* = 0$, these two radii coincide and there is a unique spherical photon orbit radius which defines the so-called Schwarzschild photon sphere. Note that in the Schwarzschild geometry geodesics are planar, as a result of spherical symmetry.

Near-critical null geodesics are governed by the properties of the photon shell. Essentially, they are controlled by a triplet of critical parameters: the Lyapunov exponent $\gamma(\tilde{r})$ (Johnson et al., 2020), describing the instability rate of the orbits, and the temporal and azimuthal periods, $\tau(\tilde{r})$, $\delta(\tilde{r})$, respectively (Teo, 2003; Gralla and Lupsasca, 2020a,b).

In an optically thin setting, each light source in the vicinity of the BH will have multiple (mathematically, an infinite number of) images on an observer's screen. The different images may be indexed by the number of half-orbits executed by the photons that create them, where the half-orbit number n is the number of polar turning points (i.e., in the motion in θ) the photon undergoes between its emission and observation. The weakly-lensed direct image, $n = 0$, is therefore accompanied by extremely lensed subrings $n = 1, 2, \dots$, composed of photons that orbited the BH before detection. The subring images are increasingly thin, and appear exponentially close to the critical curve, both as $\sim e^{-\gamma n}$. More precisely, if (ρ, φ) are polar coordinates on the observer screen and $\langle I^n \rangle$ is the n^{th} subring's contribution to the time-averaged specific intensity, the subrings obey the asymptotic relation (Johnson et al., 2020):

$$\langle I^{n+1}(\tilde{\rho} + \delta\rho, \varphi) \rangle = \langle I^n(\tilde{\rho} + e^\gamma \delta\rho, \varphi) \rangle, \quad (2)$$

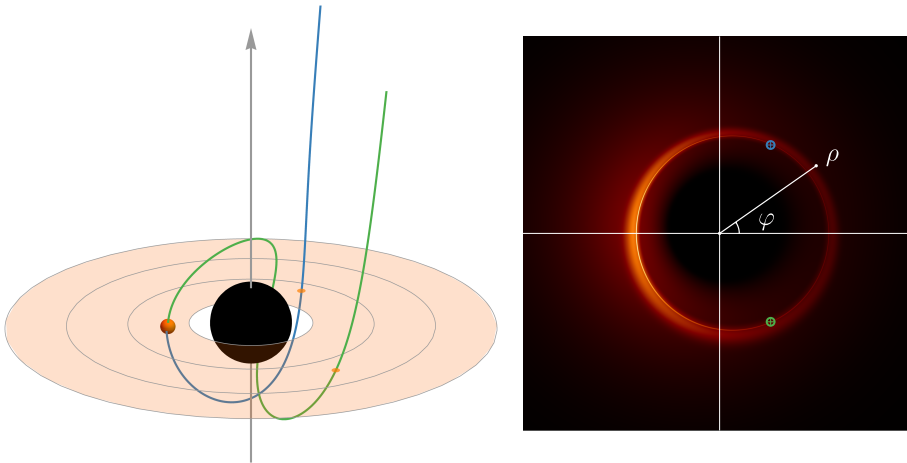


Fig. 4 Left: near-critical null geodesics emanating from a flare (orange sphere) in an optically thin equatorial emission disk around a Kerr BH with $a_* = 0.94$. The blue light ray has half-orbit number $n = 1$, while the green ray has $n = 2$. Right: image of the disk as would be seen by an infinite-resolution distant observer at an inclination of 17° . Strongly lensed light rays, which undergo multiple half-orbits, appear on the observer screen close to the “critical curve”, displaying enhanced brightness, and compose the photon ring. Correlated images of the same spacetime event (e.g., the flare) appear at different angles and times along the ring (blue and green dots on the right image). Figure from [Hadar et al. \(2021\)](#).

where $\tilde{\rho}(\varphi)$ parameterizes the critical curve on the screen, $\delta\rho$ is a small deviation from it, and we assume that, on average, the source is axisymmetric and reflection-symmetric with respect to the equatorial plane. Practically, for most configurations the first indirect image, $n = 1$, coarsely straddles the critical curve, while the $n \geq 2$ very closely follows it.

The *photon ring* ([Bardeen, 1973](#); [Luminet, 1979](#); [Johannsen and Psaltis, 2010](#); [Gralla et al., 2019](#); [Johnson et al., 2020](#)) is the sum of the $n \geq 1$ subrings. Due to the exponential demagnification of subsequent rings, the majority of the photon ring flux in a general viewing geometry will lie in the $n = 1$ subring. For time-averaged images (or equivalently, axisymmetric flows), only the Lyapunov exponent, which describes the demagnification between subsequent winding numbers, is necessary to describe the relative structure of each photon ring. In other words, for a flow viewed over many realizations of the turbulence, the spatial structures that emerge on average are all simply related to the Lyapunov exponent. For the temporal and transient observables discussed in [Sec. 2.2.3](#), τ and δ also come into play.

The photon ring, in particular its thickness, has not yet been resolved by the EHT. The ngEHT is expected to sample the $n = 1$ with its longest baselines, especially at 345 GHz. This could provide a unique probe of spacetime, given low enough optical and Faraday depths (see, e.g. [Himwich et al., 2020](#); [Mościbrodzka et al., 2021](#); [Ricarte et al., 2021](#); [Palumbo and Wong, 2022](#)). The relation between the $n = 0$ and $n = 1$ sub-images is a general probe of the spacetime, and its measurement could provide some constraining power on BH parameters, as well as enable novel tests of GR ([Wielgus, 2021](#); [Broderick et al., 2022](#); [Staelens et al., 2023](#)).

Below, we consider the science cases enabled by detection of the photon ring, namely: demonstrating the existence of the photon ring, static model fitting of the

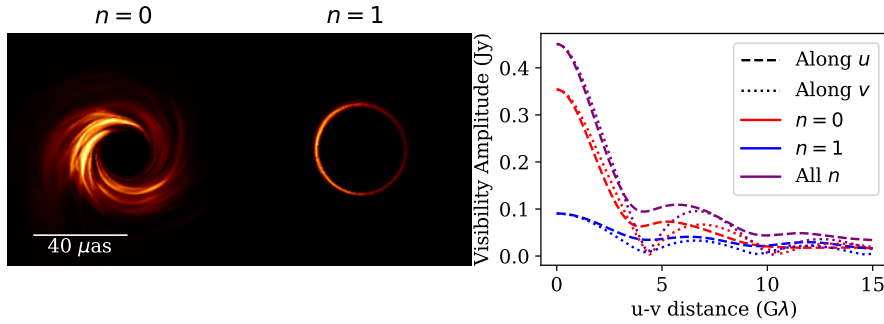


Fig. 5 Left: $n = 0$ and $n = 1$ images from a MAD GRMHD simulation viewed with parameters appropriate for M87* at 230 GHz. Right: visibility response along the u and v axes of the decomposed and full image. At the baseline lengths accessible to the ngEHT, the $n = 0$ and $n = 1$ image have comparable correlated flux density.

$n = 1$ ring, and dynamical tracking of features of the space time. Both spatial and temporal sensitivity to photons in the $n = 1$ ring offer opportunities for sensitive measurements of mass and spin, as will be further described in Sec. 3.

2.2 Science Cases

2.2.1 Demonstrating existence of the $n = 1$ ring

The presence of a photon ring arises as a qualitative consequence of extreme compactness of the central compact object and the existence of a photon shell. Hence, its qualitative detection alone constitutes an important confirmation of our understanding of strong gravity in a broader sense than precision-testing GR or constraining alternative spacetime metrics. Equipped with 345 GHz detectors, the ngEHT could approach a $13 G\lambda$ baseline length. At this baseline length a hint of $n = 1$ photon ring presence could be detected simply as a systematic excess of long baseline flux density with respect to the values measured on shorter baselines, informing us about additional power at high spatial frequencies. However, robust, physically-informed probes are necessary to make strong statements about photon ring existence. We outline a few potential approaches here.

As shown in Johnson et al. (2020) and reproduced here in Figure 5, the $n = 1$ ring in realistic simulations of M87* will be detectable above the 10 mJy thermal noise level of typical EHT baselines (EHT Collaboration, 2019b). However, we observe that teasing out the $n = 1$ structure in the general case of turbulent general-relativistic magnetohydrodynamics (GRMHD) will involve distinguishing two emission sources entering at comparable correlated flux density in VLBI measurements. Though the $n = 1$ ring will not be strictly resolved, data analysis methods that permit super-resolved structure (geometric and emissivity modeling, as well as some imaging methods) may enable measurements of photon ring properties. The main challenge for the ngEHT will be demonstrating that the data prefer the presence of a thin ring.

Fortunately, the BH spacetime is stationary relative to the evolving accretion flow, meaning that large volumes of data taken over many realizations of the turbulent

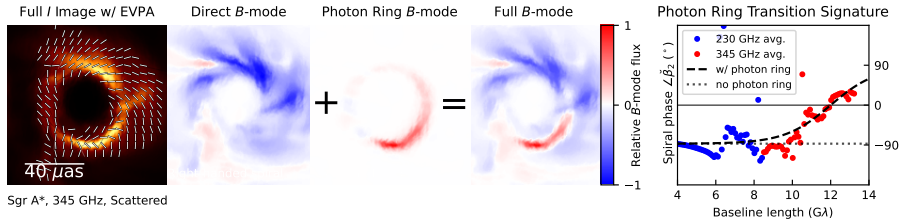


Fig. 6 Polarized interferometric indication of the Sgr A* photon ring. Left: a MAD GRMHD simulation of Sgr A* with $R_{\text{low}} = 1$, $R_{\text{high}} = 80$, and viewed at 30° , after corruption by interstellar scattering. Middle panels: divergence-free B -mode polarization defined relative to the image center, showing the sign flip between the direct and indirect image. Right panel: the phase of the polarimetric spiral quotient defined in Palumbo et al. (2023) after averaging over 24 hours of the simulation movie at left, which reveals the presence of the photon ring B -mode reversal even without phase information constraining the image center. This detection mechanism is only possible with long-baseline 345 GHz detections which just barely reach the indirect image-dominated regime.

plasma should indicate a single value of BH parameters like mass and spin. Nonetheless, demonstrating that any detailed structure consistent with the photon ring is present is challenging: of all the improvements to the ngEHT, by far the most important in realizing this goal is the expansion to 345 GHz with associated frequency phase transfer from simultaneous observations at 86 GHz (for M87*) or 230 GHz (for Sgr A*). Higher frequency means longer baselines and thus sharper angular resolution. Moreover, at higher frequencies the characteristic optical and Faraday depths in the accretion flow decrease, tending to favor larger fractions of the observed flux in the photon ring where the optical path length is longer (see, e.g., EHT Collaboration, 2021b).

One promising application of the ngEHT’s novel 345 GHz coverage is a polarimetric test for the existence of the photon ring. As discussed in greater detail in Sec. 3.2.4, in the low-inclination, low-spin limit, the photon ring exhibits a simple negation of the divergence-free “ B -mode” of polarization. Recent studies of favored models for M87* and Sgr A* suggest that a gain-insensitive polarized interferometric observable, $\tilde{\beta}_2$, can detect this reversal, with the first hints of the Sgr A* photon ring available on the longest 345 GHz baselines of the ngEHT (Palumbo et al., 2023). This observable, which extends the analysis of rotationally symmetric polarization described in Palumbo et al. (2020) and used in EHT Collaboration (2021b), effectively contains the same information as the interferometric fractional polarization \tilde{m} expressed in a rotating basis. Figure 6 demonstrates that, for magnetically arrested disk (MAD) flows of modest inclination in Sgr A*, the longest baselines in the 345 GHz ngEHT detect the phase transition to the $n = 1$ ring under varying model assumptions.

Given the reality of the comparable signal-to-noise ratio (SNR) of $n = 0$ and $n = 1$ interferometric visibilities at ngEHT baselines in realistic accretion flows, the ngEHT will necessarily report measurements of the $n = 1$ ring that are strongly dependent on model specification. Whether the ngEHT measurement is treated as proof of existence by the astronomical community is dependent on the defensibility of the assumptions made in model fitting and in testing our methods against simulations. As an example, Broderick et al. (2020b) demonstrated a hybrid approach in which a geometrically agnostic image grid is model fit in parallel with an optional ring component; demonstration of the existence of the ring is then reliant on Bayesian information criteria,

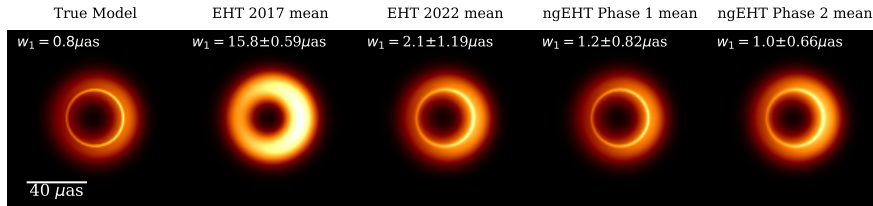


Fig. 7 Geometric model fits containing two geometric “m-rings” with identical prior volume adapted from [Tiede et al. \(2022\)](#). The fits assume that the two rings, 0 and 1, have hierarchical widths. Increasing data quality and coverage eventually requires the presence of a sharp ring. Here w_1 specifies the mean and 1σ uncertainty on the thinner ring’s thickness. Starting with the EHT 2022 array, all arrays have joint 230 GHz and 345 GHz coverage, the most crucial difference in capability of recovering sharp features.

evaluating whether the data prefers the presence of the ring based on Bayesian evidence. In [Sec. 2.2.2](#) we outline several approaches for static modeling of the $n = 1$ ring that are usable not only as probes of parameter values, but also as tests of detection.

2.2.2 Static modeling of the $n = 1$ ring

As discussed in [Johnson et al. \(2020\)](#), the exponential demagnification of subsequent photon rings leads to cascading baseline regimes where individual subrings dominate. However, at the longest baselines accessible to the Earth, i.e., $\sim 10 G\lambda$ at 230 GHz and $\sim 15 G\lambda$ at 345 GHz, the direct $n = 0$ and indirect $n = 1$ image structure are of comparable flux density, as discussed earlier in [Sec. 2.2.1](#). Here, we mention a few approaches under development and highlight the philosophical path forward for static modeling of the $n = 1$ ring.

Due to a tendency for imaging algorithms to favor smoothness and structure at a single (pixel) spatial scale, imaging VLBI data is ill-suited to experiments seeking to measure photon ring structures. In order to measure a sharp feature like the $n = 1$ ring, methods which permit (or enforce) the sharp sub-image are necessary. Geometric model fitting is ideal for general probes of what size of features may be permitted by data. For example, one can imagine fitting a pair of smooth rings with priors on diameter and thickness which permit one to be thick (presumably capturing the direct image) and another to be razor-thin (presumably capturing the indirect image). A sufficiently lenient prior would yield a posterior on these parameters which indicates whether the data rejects, permits, or demands a sharp feature to be present. An example of such a fit for a variety of array architectures and frequencies is shown in [Figure 7](#). The underlying true model contains a thin ring and a thick ring, but only the combined data of the ngEHT 230 and 345 GHz arrays are sufficient to require recovery of the thin ring. This type of test, in which priors are deliberately uninformative, is a useful pessimistic test of whether the ngEHT will find a photon ring. Alternatively, one may enforce the presence of a thin ring through the prior volume and allow its diameter to vary widely. This approach was shown to be very successful in finding the photon rings present in GRMHD simulations ([Broderick et al., 2020b](#)).

Emissivity modeling, however, provides the most direct approach. By taking GR as given, one may fit ngEHT data with lensed models of the underlying accretion flow. Such approaches innately capture features of the BH accretion system that are not

directly probed by imaging or modeling of the sky intensity distribution. In particular, given a specification of the emitting material, the assumption of GR predicts direct and indirect lensed images of the flow without the typical cost of adding additional model components. Thus, any emissivity model-fitting approach will elegantly enable parallel constraints on the properties of the accretion flow and the spacetime itself. The effects of non-GR spacetimes on photon ring properties are discussed in Sec. 5.

Fluid models of turbulent plasma are generally too expensive to evaluate in a forward modeling framework, so simplifications of the flow are required. The most established model for use with VLBI data is the radiatively inefficient accretion flow (RIAF), a static axisymmetric three-dimensional model of the emission that has been shown to successfully capture quiescent structures of GRMHD (Broderick et al., 2009, 2011, 2014). Meanwhile, Tiede et al. (2020) demonstrated promising temporal sensitivity to mass and spin with a model consisting of infalling hotspots. Most recently, Palumbo et al. (2022) used the equatorial toy models in Gelles et al. (2021b) and Narayan et al. (2021) to produce a simple, axisymmetric forward model for the polarized image of the accretion flow while avoiding radiative transfer.

At first glance, emissivity modeling obviates the typical calibration to GRMHD simulations performed in previous EHT analysis by directly measuring spacetime parameters while marginalizing over potential emitting structures (EHT Collaboration, 2019e,f). Though the possibility for (potentially artificially) wider varieties of emission structures is useful for creating reliable measurements of BH parameters and would address common criticisms of EHT measurements such as those in Gralla et al. (2019), model misspecification provides a more fundamental limitation on the success of these approaches. The task remains to find emissivity model specifications that perform well on realistic GRMHD simulations, and to build trust in the results from these approaches, which typically produce (occasionally erroneously) tighter posteriors on system parameters than other methods.

2.2.3 Harnessing time dependence for photon ring detection

A complementary method to measure the photon ring relies on image variability. Light rays emitted by any source near the BH travel to the telescope along multiple curved paths, arriving at different times and image positions. Therefore, the variability of an optically-thin source must induce intensity correlations between different image positions and times in the (time-dependent) image. The indirect, $n \geq 1$ “light echoes” are part of the photon ring and the temporal and angular separations between them are largely universal, i.e. depend on the spacetime geometry in the photon shell. Consequently, a successful measurement of light echoes will constitute a detection of the photon ring. Moreover, determining their quantitative details will allow measurements of mass and spin (see Secs. 2.1 and 3) and, eventually, strong-field tests of GR, as we detail below.

The turbulent environment in the vicinity of a SMBH is expected to produce significant emissivity fluctuations in large regions of the parameter space. This has been observationally demonstrated using archival M87* data by Wielgus et al. (2020). Horizon-scale variability was also recently confirmed with sub-mm VLBI with the EHT as reported in Wielgus and et al (2022) and EHT Collaboration (2022b). As explained above, the BH spacetime convolves these source fluctuations in an intricate yet universal manner determined by its lensing properties. This leads to spatio-temporal correlations

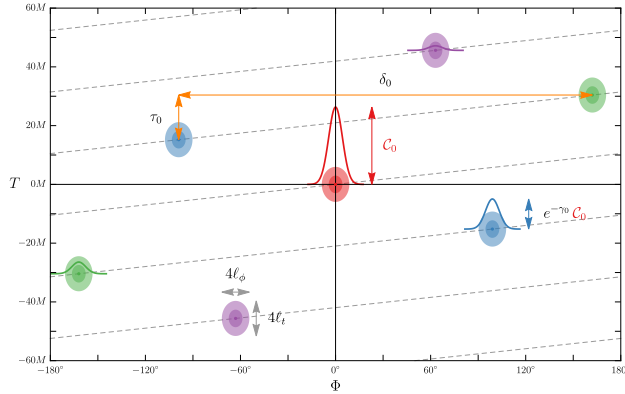


Fig. 8 Universal, self-similar structure in the autocorrelation function $\mathcal{C}(T, \Phi = \varphi - \varphi')$, Equation (3), for polar observations of an equatorial disk surrounding a Kerr BH with $a_* = 0.94$. The colored peaks arise from pairs of correlated photons with the same half-orbit numbers $n = n'$ (red), and different half-orbit numbers $|n - n'| = 1$ (blue), $|n - n'| = 2$ (green), and $|n - n'| = 3$ (purple). The (identical) shapes of the correlation peaks are determined by source properties, while their locations and relative magnitudes are determined by the spacetime geometry. Here γ_0 , δ_0 , and τ_0 are photon ring critical exponents (Johnson et al., 2020; Gralla and Lupsasca, 2020a). Figure from Hadar et al. (2021).

of intensity fluctuations across the image, and especially across the photon ring, where the light echoes appear.

An observable which efficiently distills these correlations from the data is the two-point correlation function of intensity fluctuations on the photon ring (Hadar et al., 2021):

$$\mathcal{C}(T, \varphi, \varphi') = \langle \Delta I(t, \varphi) \Delta I(t + T, \varphi') \rangle, \quad (3)$$

where $\Delta I(t, \varphi)$ is the intensity fluctuation (integrated over the width of the ring) at time t and angle φ in the image of the ring.

Importantly, the structure of this correlation function displays universal features. For optically thin emission, it will display a series of peaks in the space spanned by the angles and time separation $\{T, \varphi, \varphi'\}$. The peaks indicate a high degree of correlation, arising from the fact that different image fluctuations arise from the same source fluctuation in the BH's vicinity. The locations and relative magnitudes of the correlation peaks depend only on the BH's spacetime geometry and not on the emission details and we therefore refer to them as universal. The shape of the peaks does depend strongly on the geometric and statistical properties of the accretion flow. An example of the expectation for \mathcal{C} in the case of polar observation is shown in Figure 8.

Preliminary order-of-magnitude estimates in Hadar et al. (2021) indicate an apparent possibility of measuring the correlation function \mathcal{C} using an Earth-based array by upgrading certain aspects of the EHT, in particular the overall observation time. The main advantage of this observable is that it is in principle sensitive to the photon ring even when the latter's width is unresolved. Resolving the diameter (which was already achieved by the EHT) and essentially attaining adequate temporal resolution should be sufficient for its measurement. The ngEHT is expected to provide an orders-of-magnitude improvement over the EHT in the relevant SNR thanks to the addition of

dedicated stations, which will greatly enhance the overall observation time. The time cadence of image reconstruction, therefore, must be comparable or smaller than the BH’s natural geometric timescale. For M87* observations ($r_g/c \approx 9$ hours) this is not an issue, but for Sgr A* ($r_g/c \approx 21$ seconds) this requirement poses a challenge.

An observability estimate follows from the general principle: $\text{SNR} \sim \sqrt{N_{\text{eff}}}$, where N_{eff} is the effective number of samples. Here N_{eff} depends on the source temporal and angular correlation lengths, and on the magnitude of fluctuations. These are uncontrolled parameters which can be estimated for M87* and Sgr A*. Furthermore, N_{eff} also depends on improvable parameters like temporal and angular resolution, and, importantly, on the observation time (linearly) and the number of stations (roughly quadratically). For M87*, [Hadar et al. \(2021\)](#) estimated that \sim months of monitoring with ngEHT may give first estimates of \mathcal{C} . For Sgr A*, estimates crucially depend on the expected temporal resolution, as discussed above. Note that the estimate described here is but a preliminary step and assessing in full the observability of \mathcal{C} demands significant further work. See [Sec. 2.3](#) for a discussion of possible future improvements of the method.

A related approach to the utilization of time-dependent emission and its light echoes was described in [Wong \(2021\)](#), wherein the characteristic signatures of localized emission events, such as orbiting hotspots, were considered. Such events were shown to lead to “BH glimmer”, created by light echoes of the direct image. The higher-order images appear around the photon ring at multiple angles and times, the values of which are determined by the lensing properties of the Kerr geometry. The glimmer pattern across positions and times on the ring carries geometric information on the mass, spin and Kerr nature of the lensing object.

Another interesting proposal concerning autocorrelations was put forward in [Chesler et al. \(2021\)](#). This work proposed the coherent (i.e., phase-dependent) two-point autocorrelation function as a potential observable. In principle, electric fields contain information that intensities (which are phase-independent) do not convey. However, for \sim mm observations [Chesler et al. \(2021\)](#) argued that this observable was out of practical reach since it is suppressed by the ratio of the observing wavelength to the BH length-scale. It remains to be seen whether coherent correlators could be relevant for other types of observations, or other observables.

The optical signatures of orbiting hotspots around BHs were first considered in [Broderick and Loeb \(2005\)](#). Their observability with the EHT was the focus of [Tiede et al. \(2020\)](#), where the effects of shearing of the spot were incorporated within a semi-analytical model. In addition, it was argued that the observation of multiple such hotspots would allow to “tomographically” map the spacetime in the vicinity of the BH. Theoretical predictions for the the astrometric signatures and flux variability of horizon-scale flares were studied in [Saida \(2017\)](#) and [GRAVITY Collaboration et al. \(2020\)](#). These were then applied to Sgr A*’s three flares observed by GRAVITY in 2018, showing their consistency with a hotspot closely orbiting the BH. The time-dependent signatures of infalling gas clouds in VLBI, and their dependence on BH parameters, were studied in [Moriyama and Mineshige \(2015\)](#) and [Moriyama et al. \(2019\)](#).

In [Narayan et al. \(2021\)](#), [Gelles et al. \(2021a\)](#), and [Vos et al. \(2022\)](#), the polarimetric signatures of orbiting hotspots were investigated, studying their dependence on the BH’s parameters, the magnetic field structure, and the hotspot parameters. Subsequently, these models were applied in [Wielgus et al. \(2022\)](#) to data recorded by ALMA immediately after the Sgr A* X-ray flare, on 11 April 2017. The observed variability

was interpreted as arising from an equatorial hotspot, orbiting clockwise in a vertical magnetic field.

In fact, an important signature of strong lensing already lies at the level of the total luminosity. The latter’s late-time fall-off after a transient accretion process is predicted to provide an imprint of the photon ring (Podurets, 1965; Ames and Thorne, 1968; Cardoso et al., 2021a). As emitting matter falls towards the BH, e.g., a star or inhomogeneity in the accreting material, the late-time dependence of the luminosity is *not* that due to redshift close to the horizon, but is actually governed by the Lyapunov exponent, γ , due to the extreme lensing of photons. In particular, the luminosity of bodies being accreted onto non-spinning BHs decreases as $\mathcal{L} \sim e^{-t/(3\sqrt{3}M)}$ as the object approaches the horizon. Detection of this time dependence would be a strong, complementary indication of extreme gravitational lensing.

2.3 Open Questions

The work outlined and referenced in this section has demonstrated that ngEHT measurements of the photon ring have the capacity to constrain the mass-to-distance ratio and spin of M87*. However, much work remains to formalize what will constitute a reliable detection of the photon ring, as well as the specific pathways to connect measurements of the $n = 1$ ring to constraints on non-GR spacetimes.

For instance, estimates of the $n = 1$ subring size using the EHT 2017 data of M87* were published by Broderick et al. (2022). The measurement used the hybrid modeling approach discussed above, which combines a low-resolution image raster with a sharp ring (Broderick et al., 2020b). The authors demonstrated that this method successfully measures the $n = 1$ photon ring properties in a set of five GRMHD images. However, because any photon ring detection with the EHT or ngEHT will require some degree of superresolution, these measurements are strongly dependent upon the underlying methodology and assumptions.

The Broderick et al. (2022) results do not constitute a detection of the photon ring for a number of reasons. First, tests of hybrid imaging in Tiede et al. (2022) find that the hybrid imaging methodology readily produces false positives: hybrid imaging strongly prefers a photon ring even when applied to synthetic data from images with no photon ring, even if the fitted ring is constrained to be thin. In addition, the fitted ring parameters are substantially biased by the direct ($n = 0$) emission. Moreover, distinct tests in Tiede et al. (2022), Palumbo et al. (2022) and Lockhart and Gralla (2022) each show that the EHT 2017 data of M87* do not constrain the presence or absence of the photon ring. In short, the use of hybrid imaging for photon ring detection and measurement requires additional study and development to be reliable, and its applicability to both the EHT and ngEHT is an active area of research.

Regarding the constraints on non-Kerr metrics that may be possible with ngEHT photon ring measurements, Wielgus et al. (2020) and Kocherlakota et al. (2023) have worked out observable differences in ring size in face-on viewing geometries for a number of GR and non-GR BH alternatives. For example, in parameterised tests of GR, the spacetime is modified by the presence of extra deformation parameters other than the spin and mass defined as the “hairs”. Constraining the values of these parameters can act as a test of GR in the strong field limit. These deformation parameters can distort the characteristic shape and size of the photon ring, allowing for some stringent constraints given a strong detection of the ring. The same can be extrapolated to other

compact objects and solutions of modified gravity theories where these photon rings tend to have distinct features which can further help in ruling out some of these models. In addition, it remains to be seen whether and how ngEHT observations could provide robust, universal ways to infer spacetime symmetries.

There remains much work to be done before static or dynamical modeling of the accretion flow emissivity distribution will be able to closely approximate all structures observed in GRMHD simulations. In particular, the RIAF, hotspot, and equatorial models mentioned in this text do not typically include outflows (self-consistent or otherwise), while simulation efforts in [EHT Collaboration \(2021b\)](#) show significant emission along the jet funnel as opposed to the disk in models consistent with the EHT data on M87*. Capturing the full space of possible emission geometries is the most natural way to produce well-motivated uncertainties on BH parameters from sub-mm VLBI. [Levis et al. \(2022\)](#) has provided a useful first step towards inference of arbitrary emission regions in a fixed Schwarzschild spacetime without detailed radiative transfer. Future, more general approaches will be crucial for understanding the level of confidence of ngEHT measurements and their sensitivity to GRMHD calibration.

Finally, it will be important to look into several open issues regarding time-domain signatures of the photon ring. As already alluded to, translation of the autocorrelation observable directly into (semi-)raw visibility amplitudes, bypassing the need for image reconstruction with each step of a “movie”, could be very useful for analyzing rapidly varying sources such as Sgr A*. It will be important to obtain a good heuristic grip on the observables described in [Sec. 2.2.3](#) away from small inclinations, for varying source models, and at all possible spins, as well as to discern the effects of deviations from the universal regime, i.e., the contribution of the correlation between the $n = 0$ and $n = 1$ subrings. Ultimately, an end-to-end study of realistic synthetic data generated from “slow light” GRMHD movies of both Sgr A* and M87* sampled with realistic cadence is required, imaging each snapshot with the best imaging algorithms available. This effort is already underway. An outstanding challenge will be to flesh out additional interesting observables which may benefit from source variability and to define their associated requirements for the ngEHT.

3 Measuring black hole mass and spin

3.1 Introduction

According to the uniqueness results, a stationary BH in vacuum is fully characterized by its mass, spin, and electric charge (Robinson, 1975; Chrusciel et al., 2012; Cardoso and Gualtieri, 2016). Astrophysical BHs are expected to be electrically neutral due to quantum discharge effects, electron-positron pair production, and charge neutralization by astrophysical plasmas (Gibbons, 1975; Goldreich and Julian, 1969; Ruderman and Sutherland, 1975; Blandford and Znajek, 1977). Therefore, mass and spin are the only fundamental quantities that determine the BH geometry within GR (Zajaček et al., 2018). Measuring the masses and spins of BHs will help constrain their formation channels and growth mechanisms (Volonteri, 2010; Volonteri et al., 2021), map out the population demographics (Shankar et al., 2004), and examine BH feedback models (Terrazas et al., 2020). The spin of BHs is also relevant for probing ultra-light fields, as discussed in Sec. 4.

Observables obtained by the ngEHT have been proposed to probe the strong-gravity regime of the BH spacetime, which in turn constrain the BH mass and spin, assuming the Kerr metric. Some of them (i.e., BH/light ring imaging) have already been employed for the measurement of mass and spin for M87* and Sgr A*. Others may require specific signatures of accretion flows (e.g., hotspots), additional information (e.g., polarization) and/or temporal measurements (e.g., autocorrelation), which should become accessible through the ngEHT. In particular, they can provide an unprecedented opportunity to probe properties of near-extremal BHs, which are deeply connected to the holography principle.

The mass and spin measurement of Sgr A* will likely be conducted earlier and more accurately by other means, e.g., through a combination of S-star orbits, possible clouds, pulsars, or lurking stellar-mass BHs. The ngEHT measurements can thus most likely be verified by comparing to these alternative methods (Will, 2008; Psaltis et al., 2016). Here, we discuss how the combined information can be used to break possible degeneracy of parameters in any individual approach, in order to achieve better measurement precision.

3.2 Overview of ngEHT observables for measuring mass and spin

The EHT collaboration has announced the observation results for two supermassive BHs so far: M87* (EHT Collaboration, 2019a) and Sgr A* (EHT Collaboration, 2022a). By measuring the emission region diameter and combining with calibrations from GRMHD simulations, the mass of M87* is determined to be $(6.5 \pm 0.7) \times 10^9 M_\odot$, corresponding to an angular diameter of the shadow $42 \pm 3 \mu\text{as}$. The angular diameter of Sgr A* is measured to be $51.8 \pm 2.3 \mu\text{as}$ and the corresponding mass is constrained within $4.0_{-0.6}^{+1.1} \times 10^6 M_\odot$, consistent with constraints from the S-stars. The most precise measurements of the mass are reported by the VLTI as $(4.297 \pm 0.013) \times 10^6 M_\odot$ (Abuter et al., 2022), and by Keck as $(3.951 \pm 0.047) \times 10^6 M_\odot$ (Do et al., 2019b). These differ because of the difference in R_0 between the two results: scaling the Keck measured mass to the VLTI distance yields $4.299 \pm 0.063 \times 10^6 M_\odot$ (Abuter et al., 2022). The current EHT-based mass value, due to its 20–80 times larger error, is not sufficiently precise to distinguish between these two aforementioned values.

The spin magnitude of M87* is poorly constrained but the image morphology is consistent with the shadow of a spinning (instead of non-spinning) Kerr BH. If the spin axis and M87's large-scale jet are aligned, then the BH spin vector is pointed away from the Earth, with recent studies showing this can still be the case even for misaligned accretion flows (Chatterjee et al., 2020). On the other hand, the Sgr A* images disfavor scenarios where the BH is viewed at high inclination, as well as non-spinning BHs and those with retrograde accretion disks.

Table 2 Mass measurements for the SMBH at the center of the Milky Way.

	GRAVITY/VLTI ^a	Keck ^b	EHT ^c
Sgr A*	$(4.297 \pm 0.012) \times 10^6 M_{\odot}$	$(3.975 \pm 0.058) \times 10^6 M_{\odot}$	$(4.0_{-0.6}^{+0.1}) \times 10^6 M_{\odot}$

^a Abuter et al. (2022), ^b Do et al. (2019b), ^c EHT Collaboration (2022a).

3.2.1 Light ring imaging

As discussed in Sec. 2, within the EHT image there exists a theoretically infinite sequence of lensed images of the emission region. The locations of these photon rings asymptote to the boundary of the shadow, the size and shape of which encodes the mass and spin of the BH (Medeiros et al., 2020; Johannsen and Psaltis, 2010; Takahashi, 2004; Falcke et al., 2000; Luminet, 1979; Hilbert, 1917). Actual observables are likely, by virtue of being luminous, the low-order images, i.e., primary, secondary, and tertiary images, corresponding to the $n = 0, 1,$ and 2 photon rings in Broderick et al. (2022) and Johnson et al. (2020). The relative locations of the lensed images at different orders depend on mass and spin, enabling a measurement of both. Because this remains true even for polar observers, observing the secondary presents a unique pathway to measuring spins in M87* and Sgr A*.

The expected width of the $n = 1$ photon ring is $\lesssim 1 \mu\text{as}$, and thus well below the diffraction limit of Earth-bound mm-VLBI. Nevertheless, combined modeling and imaging techniques might provide an ability to both extract the highly uncertain primary image and constrain properties of an additional narrow ring-like image feature (Broderick et al., 2020b). This procedure leverages high SNR to separate the $n = 1$ photon ring and diffuse primary emission on Earth-sized baselines, and assumes that one does not encounter a noise floor of systematic uncertainties.

While it is possible to extract the ring diameter with EHT coverage (Broderick et al., 2020b), measuring the width and total flux in the $n = 1$ photon ring will only be possible with the additional stations and sensitivity of the ngEHT. The first EHT analyses of M87* already super-resolve the source, achieving a typical resolution of $\sim 10 \mu\text{as}$. Given the strong priors that accompany a specified ring model, the degree of super-resolution in the determination of the ring width, w , is approximately:

$$\begin{aligned} \frac{\sigma_w}{b} &\sim \frac{1}{2\pi u w N \sqrt{n_s} \text{SNR}} \\ &\sim 1\% \times \left(\frac{\text{SNR}}{7}\right)^{-1} \left(\frac{u}{10 \text{ G}\lambda}\right)^{-1} \left(\frac{w}{1 \mu\text{as}}\right)^{-1} \left(\frac{N}{20}\right)^{-1} \left(\frac{n_s}{10}\right)^{-1/2}, \end{aligned} \quad (4)$$

where N is the number of stations, n_s is the number of independent scans, $b = 1/u \sim 20 \mu\text{as}$ is the nominal beam, u is the maximum baseline length in λ , and SNR is the

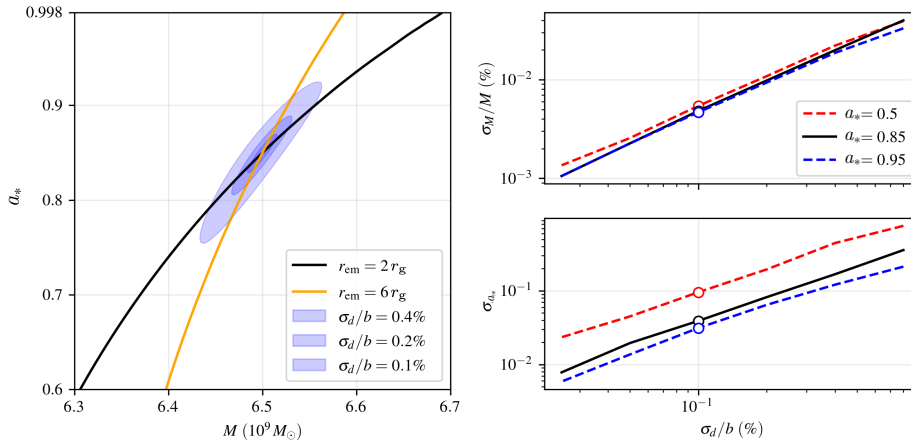


Fig. 9 Left: predicted joint constraints on mass and spin from measurements of the primary and secondary images (i.e., the $n = 0$ and $n = 1$ photon rings) of the emission about a BH with mass $M = 6.5 \times 10^9 M_\odot$ and spin $a_* = 0.85$, appropriate for M87*. The two lines show the degenerate constraint when the emission is dominated by that at $2 r_g$ (black) and $6 r_g$ (orange). The combined 1σ regions are indicated in blue for diameter measurements of various precision, ranging from $\sigma_d/b = 0.1\%$ to 0.4% . Right: estimates of the precision of mass (top) and spin (bottom) for different intrinsic BH spins, as a function of diameter measurement precision. The open points show the fiducial value in Equation 5.

thermal signal-to-noise ratio. Thus, $N \times \text{SNR} \gtrsim 140$ is needed to eventually achieve the sub- $1 \mu\text{as}$ precision needed to resolve the $n = 1$ photon ring width in a single observation.

A single measurement of the diameter of the $n = 1$ photon ring alone would provide a mass measurement that has a bounded systematic uncertainty. For equatorial emission seen by a polar observer, the diameter of the $n = 1$ photon ring ranges from $4.30 M/D$ to $6.17 M/D$ as the radius of the peak emission moves from the horizon to infinity (Broderick et al., 2022), where D is the source distance. Thus, the conclusive detection of a photon ring necessarily eliminates the current dominant systematic uncertainty for mass estimates of M87*.

The differing behavior of the primary and secondary image dependence on the emission location provides a means to probe spin. A single simultaneous measurement of the primary emission location and $n = 1$ photon ring results in a degenerate constraint on the mass and spin of M87*. Similar to the ring width, it should be possible to constrain the diameter of the photon ring considerably better than the nominal beam:

$$\frac{\sigma_d}{b} \sim \frac{1}{\pi N \sqrt{n_s} \text{SNR}} \sim 0.1\% \times \left(\frac{\text{SNR}}{7}\right)^{-1} \left(\frac{N}{20}\right)^{-1} \left(\frac{n_s}{10}\right)^{-1/2}, \quad (5)$$

where the significant improvement arises because the ring diameter, unlike the ring width, is well resolved by Earth-sized baselines. Because the emission region in M87* is highly variable (EHT Collaboration, 2019a,b,c,d,e,f, 2021a,b), two such measurements of the primary emission and the $n = 1$ photon ring diameter made at widely separated times, and thus for different characteristic emission radii, produce estimates for both. An illustrative example for M87* is shown in Figure 9, in which the radius of the peak emission moves from $2 r_g$ to $6 r_g$ between observations. Measuring the radii of the direct emission and the $n = 1$ photon ring in either epoch results in degenerate measurements

of mass and spin shown by the two lines. Combining the two epochs produces a joint measurement of mass and spin, where the precision depends on the difference in the emission region location, the true BH spin, and the degree of super-resolution in the measurement of the $n = 1$ photon ring diameter.

3.2.2 Hotspot tracking

M87* and Sgr A* both exhibit localized variability in the emission region. In M87* this variability appears as ejections within the jet, which are instrumental to measuring the jet velocity on milliarcsecond scales (Jeter et al., 2020; Ly et al., 2007; Walker et al., 2016; Hada et al., 2016). In Sgr A* it appears as broad-spectrum flaring, extending from the millimeter to the X-ray (Genzel et al., 2003; Gillessen et al., 2006; Dodds-Eden et al., 2009; Witzel et al., 2012; Neilsen et al., 2013; Ponti et al., 2017; Fazio et al., 2018), and at least a subset of these have been associated with orbiting features (Abuter et al., 2018). Simultaneous X-ray and infrared (IR) observations of Sgr A* variability hint at the multiwavelength emission properties of orbiting hotspots (Boyce et al., 2019) and their close links to particle acceleration mechanisms (e.g., Ball et al., 2019). The dynamical nature of the “hotspots” enable high-precision measurements of BH mass and spin (Broderick and Loeb, 2005, 2006; Doeleman et al., 2009b; Abuter et al., 2018; Tiede et al., 2020).

Flare reconstructions are fundamentally strong lensing experiments, relating the direct emission and higher-order lensed images from a dominant, compact emission region. The chief systematic uncertainty is the astrophysics of the flare emission itself, including its unknown orbit, temporal evolution, density, temperature, and rate of shear. For these reasons, relating flare orbital periods to those expected for circular geodesics (i.e., Keplerian motion), is not a direct measure of spacetime properties. However, the relationship between the primary and secondary images is independent of the orbital dynamics, requiring only motion to selectively relate different regions of the image plane (Broderick and Loeb, 2005, 2006). Reconstructing a single flare observed over a handful of orbits would yield a sub-1% accuracy spin measurement, while simultaneously recovering the astrophysical hotspot parameters over a wide range of flare models, BH parameters, and in the presence of an obscuring accretion flow and intervening scattering in the Galactic disk (Tiede et al., 2020). Yet, flares could cool on shorter time scales than the orbital time scale, and shearing may render it impossible to observe significantly more than one full orbit.

Each flare observed by ngEHT would produce an independent measurement of the gas rotation, which can provide constraints of BH spin (Conroy et al., 2023). The observation of flares occurring at multiple orbital radii probes the spacetime at different locations, therefore providing an immediate test of the Kerr metric, which demands all such spin measurements be consistent with each other (Tiede et al., 2020). The observation of flares at different frequencies provide a means to test the achromatic nature of lensing in GR. Thus, observations of multiple flaring epochs enables a tomographic mapping of the BH spacetime.

The most significant practical limitation is the need to observe multiple, high-brightness flares, dominated by orbiting features. For both M87* and Sgr A*, this is most readily accomplished with a monitoring campaign that triggers target of opportunity observations. While the full (u, v) -coverage of the ngEHT is preferable, modeling with even a 10 station subset, e.g., only the proposed new ngEHT sites, would suffice for dynamical flare modeling to produce high-precision spin estimates.

3.2.3 Photon ring autocorrelations

As discussed in Sec. 2, the two-point correlation of intensity fluctuations on the photon ring encodes information about the background spacetime, which can be used to measure the BH mass and spin. Here we provide more details about the underlying principle and the estimation of the SNR.

The correlation function \mathcal{C} is expected to be described by localized peaks with separations in time and azimuthal angle around the ring. For example, if two light rays are emitted from the same point source and perform half-orbits of the BH k and k' times, respectively, before reaching the observer, they will contribute to a peak in the correlation function. These peaks can be labeled by $m = k - k'$ and should share an identical profile based on the source statistics. The peak width is set by the correlation length of fluctuations in the source, while the locations and relative heights of the peaks are dependent on the BH parameters. Specifically, each successive peak is suppressed by $e^{-\gamma}$ and is translated by (τ, δ) , where γ , τ , and δ are the critical exponents that describe geodesics near the critical curve. The critical exponents have been computed analytically for the Kerr spacetime (Johnson et al., 2020; Gralla and Lupsasca, 2020a). For a geodesic approaching the critical radius, the ratio of distances from the critical radius of successive half-orbits k is:

$$\frac{\delta r_{k+1}}{\delta r_k} \approx e^{-\gamma}. \quad (6)$$

While these near-critical geodesics stay near the critical radius, they continue to move in the other directions. The elapsed time Δt and the swept azimuthal angle $\Delta\phi$ for each half-orbit, which approach a constant value for large half-orbit number k , are given by:

$$\Delta t \approx \tau + \delta t_k, \quad \Delta\phi \approx \delta + \delta\phi_k, \quad (7)$$

and $\delta t_k, \delta\phi_k \sim e^{-k\gamma} \rightarrow 0$ as $k \rightarrow \infty$. Observing the correlation structure would provide measurements of the critical parameters (γ, τ, δ) and, as these are dependent on the BH spacetime, would in turn allow for estimates of the BH mass and spin. The SNR for the correlation of N independently sampled pairs of intensity functions for individual images can be estimated as (Hadar et al., 2021):

$$\text{SNR} \sim \frac{l_\phi \theta_{\text{ph}}}{\theta_{\text{obs}}} \text{SNR}_\infty, \quad (8)$$

where SNR_∞ is the SNR for an idealized case of infinite resolution and the m^{th} correlation peak

$$\text{SNR}_\infty \sim e^{-|m|\gamma} \sqrt{\frac{2\pi t_{\text{obs}}}{l_\phi l_t}}. \quad (9)$$

Here t_{obs} is the observing time, l_t and l_ϕ are the correlation lengths in the t and ϕ directions, respectively, θ_{ph} is the angular radius of the photon ring, and θ_{obs} is the finite angular resolution of the observation.

Based on this SNR estimate and as mentioned in Sec. 2, detecting the $m = 1$ peak of M87* with the EHT would require observations every few days over a span of many months or even several years. Due to Sgr A*'s significantly shorter gravitational timescale, the limiting factor becomes the ability to form an image with very short (\sim minutes) observations. An ngEHT-like array with the capability to create movies of

Sgr A* would be sufficient and the SNR for the $m = 1$ peak of Sgr A* would be about two orders of magnitude larger than the SNR for M87* for the same observing duration, primarily because of the shorter coherence time for Sgr A* (Hadar et al., 2021). Reaching a high enough SNR to detect the $m = 2$ and higher-order correlation peaks, however, would require a significantly improved array and many years of observations.

Whilst observations that can detect the $m = 1$ correlation peak may be possible with the proposed ngEHT array, more work needs to be done to pin down the various technical requirements. In addition, it is not yet clear how the SNR of the peaks translates into uncertainties in the mass and spin measurements. More work is also required to determine if correlations in the astrophysical structure of the disk could contaminate the correlation function.

3.2.4 Polarization spirals in direct and indirect images

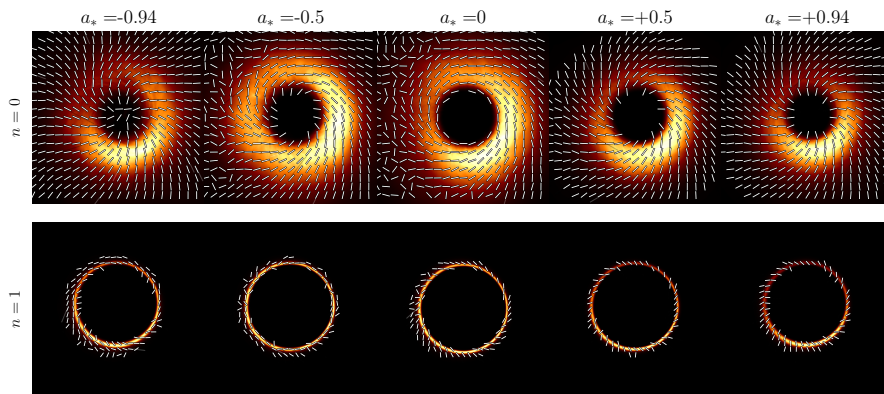


Fig. 10 Time-averaged images of the direct ($n = 0$) image and first lensed ($n = 1$) image from MAD GRMHD simulations at various spins, rotated so that the approaching jet is oriented 288° East of North (adapted from Palumbo and Wong, 2022). Ticks show the EVPA. Polarization spirals about the ring become more radial at higher spin magnitudes, reverse direction over radius in retrograde flows ($a_* < 0$), and approximately reflect through the origin across sub-image index n . These images use the R_{high}^2 electron heating prescription, each having $R_{\text{high}} = 80$, a reasonable value for both M87* and Sgr A* (Mościbrodzka et al., 2016; EHT Collaboration, 2019e, 2022c). The simulations themselves were generated with *iharm3d* (Gammie et al., 2003) and ray traced with *ipole* (Mościbrodzka and Gammie, 2018). See Wong et al. (2022) for additional details on the ray tracing.

Although the astrophysical details of the accreting plasma often confound measurements of spacetime properties, occasionally the emission illuminates BH properties. Figure 10 shows time-averaged images of MAD simulations decomposed into direct and indirect images for a variety of spins. In these images a number of features with a direct connection to spin are seen. Most apparent is the electric vector position angle (EVPA) spiral, which becomes more radial at higher spin magnitudes, as first identified in Palumbo et al. (2020). Emami et al. (2023) studied the spiral trend in detail, finding that this effect arises from frame dragging causing the plasma velocity and magnetic field to become more toroidal in structure at higher spins, causing the polarization (perpendicular to the magnetic field) to appear more radial in structure. We see

also that the sub-image polarization spiral has opposite handedness compared to the direct image spiral. This feature arises from the complex conjugation of the Walker-Penrose constant (Walker and Penrose, 1970) across sub-images, derived in Himwich et al. (2020). This conjugation has a simple behavior in the face-on, zero-spin limit, and leads to an approximate reflection of the polarization through the origin, as observed in GRMHD in Palumbo and Wong (2022) and is related to a depolarization near the photon ring observed in Jiménez-Rosales et al. (2021). The detailed relationship between the direct and indirect image polarization is a direct probe of spin. Lastly, we see that in retrograde models, the spiral changes direction from the large scale accretion rotation direction at large radii to the interior, strongly frame-dragged region, as investigated in Ricarte et al. (2022).

Taken together, there are several pathways through which images with high resolution and dynamic range can be used to elucidate spin, given prior assumptions and understanding of the underlying accretion flow properties. These features are more difficult to observe in models undergoing standard and normal evolution (SANE), but both EHT results and results from the GRAVITY collaboration support the conclusion that M87* and Sgr A* are in the MAD state (Gravity Collaboration et al., 2020). These features are also more difficult to observe in individual snapshots, but the ngEHT is proposed to observe M87* with a roughly weekly cadence, enabling analysis of average, quiescent structure, while the same can be done with Sgr A* in the course of a few days. Polarized emission from the accretion flow will be a crucial tool in probing the BH spacetimes of M87* and Sgr A*, and should complement more general approaches which attempt to circumvent astrophysical details. Cases with a single-baseline for polarimetry were studied by Palumbo et al. (2023).

3.2.5 Probes of extremal BH/signatures of NHEK

As rotating BHs approach the extremal limit, a non-degenerate near-horizon region emerges with an enhanced conformal symmetry, often referred as near horizon extremal Kerr (NHEK). Thanks to the presence of NHEK, there are a set of zero-damping quasinormal modes with slow decay rates (zero in the extremal limit) (Yang et al., 2013), and the field perturbations display self-similar behavior (Gralla and Zimmerman, 2018). The NHEK perturbations are important as their prescription determines how an infalling particle never overspins a near-extremal BH to produce a naked singularity, as required by Weak Cosmic Censorship (Sorce and Wald, 2017). The additional conformal symmetry also allows the construction of the Kerr/CFT conjecture (Guica et al., 2009) which relates a 2+1 conformal field to the NHEK region. It is therefore of fundamental theoretical interest to probe and test the signatures of the NHEK, with ngEHT and/or other observations.

Astrophysical BHs may reach dimensionless spins of up to $a_* \sim 0.998$, assuming Shakura-Sunyaev thin-disk accretion (Shakura and Sunyaev, 1973). For these rapidly spinning BHs, the Green's function exhibits a transient power-law growth in the near-horizon region and a transient power-law decay at far distances (Yang et al., 2013), as compared with the exponential signature of the Green's function for generic spins. This power-law behavior of the Green's function, as a manifestation of collectively excited zero-damping modes, is a direct signature of NHEK and its enhanced symmetry. One possible way to test this signature is through the measurement of photon ring auto-correlations. For near extremal Kerr BHs, the correlation function follows a power law (instead of exponential) relation between different peaks separated by

angle and time, which may be resolved through performing measurements with sufficient accuracy. Roughly speaking, in order to distinguish between a power-law decay from an exponential decay in the correlation function, at least the correlations of the $m = 0, m = 1$ pair and the $m = 0, m = 2$ pair are needed, although it is challenging to detect the $m = 2$ peaks since this requires observation over many years (see discussion in previous subsection). With only the $m = 0, m = 1$ pair, it is possible to perform a consistency test between the measured correlation and the inferred correlation if the Green's function follows a $1/t$ power-law decay. Such correlation may also be interpreted as $e^{-\gamma(M, a_*)}$ for appropriate (M, a_*) , but the degeneracy may be broken by including constraints of (M, a_*) from other observables. In this setting, the SNR of the correlation in Equation 8 should be modified as:

$$\text{SNR} \sim \frac{l_\phi \theta_{\text{ph}}}{\theta_{\text{obs}}} \left(\frac{C}{|m|\tau} \right) \sqrt{\frac{2\pi t_{\text{obs}}}{l_\phi l_t}}, \quad (10)$$

where C is a numerical factor to be determined by the Green's function. The higher the SNR, the better the statistical confidence that can be claimed for the consistency test. It is also noteworthy that this power-law signature is comprised of a subclass of photon orbits close to the equatorial plane of the BH. A further observer-inclination-angle-dependent modification should be incorporated in order to further refine Equation (10).

Another possible avenue is to search for related signatures in the BH image and/or the transient images of hot spots (Gralla et al., 2018), since part of the co-rotating light rings reside on the horizon (with deviation much smaller than the gravitational radius). Recent studies have investigated MHD accretion flows onto BHs with $a_* = 0.998$, in both the Kerr spacetime and in other theories of gravity (Younsi et al., 2023; Chatterjee et al., 2023b,c). Defining $\epsilon \equiv (1 - a_*)^{1/3}$, the flux of the hotspot generally scales as $\epsilon/\log \epsilon$ (Gralla et al., 2018), i.e., diminishing flux in the extremal limit. The redshift factor of the emission varies with orbital phase, with peak blueshift factor being $\sqrt{3}$ and redshift factor being $1/\sqrt{3}$. The redshift/blueshift factor of Iron $K\alpha$ lines may be used for such a test. It is, however, unclear what the most relevant observables for ngEHT measurements in this context will be. In addition, the number of high-spin candidates for ngEHT measurement is currently highly uncertain.

3.3 Overview of complementary measurements of mass and spin

Accurate measurements of mass and spin are vital to understand the nature of BHs and explore their discovery potential. In order to draw firm conclusions, it is important to cross-check such measurements with other independent observations. In many cases, the mass and spin estimates may exhibit degeneracy to certain degrees. To break such degeneracy it is useful to have complementary measurements which can be combined appropriately. We briefly discuss below alternative measurements of BH mass and spin from S-stars, pulsars, GWs, and quasi-periodic oscillations (QPOs).

3.3.1 Probing Sgr A* with S-stars

The Sgr A* SMBH in the Galactic Center is surrounded by a dense cluster of young stars, commonly referred to as S-stars. Some of them have been discovered with small periastron distances and high eccentricities (Schodel et al., 2002; Meyer et al., 2012;

(Abuter et al., 2022) and are powerful probes of the properties of Sgr A*. By monitoring the orbit of the star S2, the GRAVITY instrument (Abuter et al., 2017, a near-infrared interferometer mounted at the ESO VLTI) has detected the leading order relativistic effects, i.e., the relativistic redshift (Abuter et al., 2018; Do and et al, 2019) and Schwarzschild precession (Abuter et al., 2020, 2022), constraining the mass of the central object to a very good precision (see Table 2) (Abuter et al., 2022). The typical precision of mass measurement with S-stars is in the range 0.01% – 0.1%, since the tightness of the mass measurement depends on the relative ratio of the astrometric accuracy to the semimajor axis and the ratio of the redshift accuracy to the orbital velocity (Weinberg et al., 2005; Zhang et al., 2015), and does not depend directly on the semimajor axis or eccentricity.

The spin and quadrupole moment of Sgr A* can be constrained by detecting spin-induced effects and quadrupole-induced precession in the motion of S-stars (Will, 2008; Psaltis et al., 2016; Zhang et al., 2015; Waisberg et al., 2018). The spin of Sgr A* induces Lense-Thirring precession on the S-star orbits and rotates the orbital plane around the spin axis. This precession should be observable both in astrometry and radial velocity space (Will, 2008; Zhang et al., 2015; Waisberg et al., 2018). To constrain the spin parameter, S-stars need to be found within milliparsec-scale distance of Sgr A*, where the key parameter is the pericenter distance d_{peri} . Detecting quadrupole-induced effects will be even more challenging. Explicit simulations for the GRAVITY+ project (Abuter et al., 2022) show that the simple time-averaged estimates by Merritt et al. (2010) were too pessimistic, as tracking the orbits will reveal the moment of the deviation, which for spin or quadrupole effects will coincide with a pericenter passage. The combination of astrometry from GRAVITY+ and spectroscopy from ELT-MICADO should be able to deliver a spin measurement within a few years of operation, assuming a star with suitable d_{peri} can be tracked.

The S-stars found to-date do not pass close enough to Sgr A*, thus the measurements of spin and quadrupole parameters have not yet been achieved (Iorio, 2020; Gravity Collaboration et al., 2022). The upgraded GRAVITY+ instrument, with higher sensitivity, may possibly find closer S-stars with sufficient brightness, and will continue to monitor S2 over a longer period of time, thereby yielding estimates of the spin and quadrupole moment of the central object (Psaltis et al., 2016; Zhang et al., 2015; Yu et al., 2016; Waisberg et al., 2018; Gravity Collaboration et al., 2022). Two or more S-stars in closer orbits are often required, so that the combination of position and redshift data provide complementary information to measure the spin of Sgr A* (Will, 2008; Zhang et al., 2015). Figure 11 shows the constraints of mass and spin parameters of Sgr A* with two stars assumed to have orbital periapsis distances of $800 r_g$ and $1000 r_g$ and eccentricities of 0.9 and 0.8, respectively, whilst assuming an astrometric precision of $10 \mu\text{as}$ (Psaltis et al., 2016). These studies did not account for the improvement possible with ELT spectroscopy, which will bring into reach stars of spectral types that show rich spectra in the near-IR, potentially achieving radial velocity uncertainties as low as $\sim 0.1 \text{ km/s}$ (Evans et al., 2015; Simon et al., 2019), two orders of magnitude better than what is currently possible with S2.

3.3.2 Observation of Sgr A* EMRIs with LISA

Extreme mass ratio inspirals (EMRIs) where stellar-mass compact objects orbit SMBHs are an important class of GW source for milliHertz GW detectors (Amaro-Seoane et al., 2017; Pan and Yang, 2021a). Stellar-mass BHs and compact stars orbiting around

Sgr A* are potential compact binary sources (referred to here as Sgr A* EMRIs) that can be explored with the future Laser Interferometer Space Antenna (LISA) GW observatory (Naoz et al., 2020; Gourgoulhon et al., 2019). Such observations will provide a promising direction for measuring the spin of Sgr A*. The prospect of such measurements has been studied recently in Gourgoulhon et al. (2019) and Tahura et al. (2022) in the case of circularized binaries with orbital separations $\leq 10^2 r_g$ (here r_g denotes the gravitational radius of Sgr A*; see also Yang et al. (2022) for an analysis with brown dwarfs), which are well motivated by several formation scenarios (Emami and Loeb, 2021, 2020; Pan et al., 2022; Pan and Yang, 2021b). As the location and distance of Sgr A* from the Solar System are known, the waveform template bank for such systems requires fewer parameters, leading to a threshold SNR of detection (~ 10) which is much smaller than a typical threshold (~ 20) for EMRIs detectable by LISA (Babak et al., 2010). Fisher analyses with Monte-Carlo samplings of the direction and magnitude of the spin of Sgr A* suggest that the spin can be measured within $\sim 2\%$ uncertainty. Such precision may thus be better than that achievable via future S-star and pulsar observations, and a comparison among them is presented in Figure 11. Furthermore, one can estimate the direction of the spin of Sgr A* with similar accuracy from GW observations with LISA (Tahura et al., 2022).

There are various issues worth noting in this scenario of spin measurement. First of all, it relies crucially on the abundance of stellar-mass BHs near Sgr A* and whether they are massive enough to produce signals above the threshold SNR. In addition, distributed dark matter may create an orbital precession degenerate to that of the spin-induced one (see also Sec. 4). However, according to analysis in Heifel et al. (2022), these effects will be easily distinguishable via observations of the star S2. Finally, eccentric Sgr A* EMRIs can be generated in the mass segregation scenario (Linial and Sari, 2022; Emami and Loeb, 2020, 2021; Alexander and Hopman, 2009; Binney and Tremaine, 2011), for which the higher harmonics of orbital frequency also contribute to the gravitational waveform. Since the higher harmonics of the frequency should be closer to the most sensitive band of LISA, the event SNRs for such EMRIs are expected to be higher than the circular ones considered in Tahura et al. (2022), resulting in more precise parameter estimation. However, detailed studies in this regard are yet to be performed.

3.3.3 Pulsars around the Sgr A* black hole

Timing of pulsars near Sgr A* provides an alternative way to probe the spacetime geometry. In particular, such observations are in principle capable of measuring the three lowest-order moments of the BH, namely its mass (M), spin vector (\vec{S}), and quadrupole moment (Q) with high precision (Kramer et al., 2004; Bower et al., 2018, 2019; Della Monica et al., 2023). Similar to measurements of BH shadows, observations of pulsars can be used to test the Cosmic Censorship Conjecture, the uniqueness properties of BHs, and modified gravity (Liu et al., 2012; Psaltis et al., 2016; Dong et al., 2022b).

Pulsar timing is essentially a ranging experiment, which measures the projected pulsar orbit along the line of sight. Although until now no such pulsars have been discovered in the vicinity of Sgr A*, targeted searches are ongoing. Population studies and the expected sensitivity and range of new telescopes, e.g., the Square Kilometre Array (SKA; Wharton et al., 2012; Shao et al., 2015; Goddi et al., 2016; Weltman et al., 2020) demonstrate that one might discover such a pulsar, although others have been cautious (Dexter and O’Leary, 2014). If a pulsar is discovered in a close orbit around

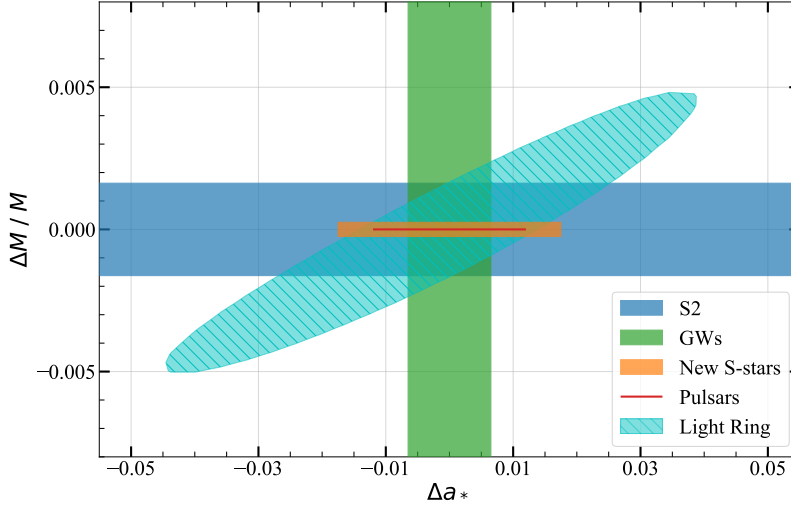


Fig. 11 Fractional error in the mass of Sgr A* ($\Delta M/M$ with ΔM denoting $1\text{-}\sigma$ error in M) vs. $1\text{-}\sigma$ error in the dimensionless spin of Sgr A* (Δa_*) achieved from various observations. The dimensionless spin parameter is defined as $a_* = |\vec{S}|/M^2$ (Kramer et al., 2004). Observation of the star S2 with GRAVITY places a constraint on M with $\Delta M = 1.3 \times 10^4 M_\odot$ (Abuter et al., 2022), shown by the horizontal range in blue. Implementing such bounds on mass, GW observations with LISA can achieve $\Delta a_* = 0.013$ (Tahura et al., 2022) (vertical range in green). The orange bar shows the precision of mass and spin measurements the future GRAVITY instrument can achieve ($\Delta M/M \simeq 0.05\%$ and $\Delta a_* = 0.035$), given that S-stars are found closer to Sgr A* (Psaltis et al., 2016; Zhang et al., 2015). Projected pulsar timing observations can obtain $\Delta a_* = 0.024$ (horizontal range of the red line), while $\Delta M/M$ is of the order 10^{-6} (Psaltis et al., 2016), which is much smaller than the scale of the above figure. The $\delta_d/b = 0.2\%$ case in Figure 9 is reproduced here for comparison, as labeled by “Light Ring”. Future pulsar timing and GRAVITY experiments have the potential to provide the most precise spin measurements.

Sgr A*, the orbital dynamics are determined by the BH spacetime, and/or in the sequence of the post-Newtonian expansion, the mass, spin, and quadrupole moments that show up in the equation of motion at different post-Newtonian orders. Different values of these parameters predict different evolution behaviours of the orbit, which in turn leave traces in the pulsar timing data. Therefore, with a dedicated experiment, the multipole moments of Sgr A*’s spacetime geometry can be extracted with precision.

Figure 11 shows an example from simulations reported by Psaltis et al. (2016). An eccentric orbit with $e = 0.8$ and an orbital period $P_b = 0.5$ yr is assumed. In order to account for the external perturbations from matter around Sgr A*, only data around three passages of periastris are used. Within such a scenario the mass and spin can already be constrained with sub-percent-level accuracy. The degenerate directions of these constraints are very different from other measurements with the S-stars and BH shadows. Therefore, a combination of these with pulsar data would reduce the uncertainty in BH parameter measurements, although the precision of the pulsar measurement trumps all other experiments. However, one must emphasize that the different

independent methods will serve as important cross-validation of each other, and finding any discrepancy between methods would have important consequences.

3.3.4 Quasi-periodic oscillations

QPOs may probe the strong field regime of BHs as their timescales correspond roughly to those of matter orbiting in the innermost regions of the accretion disc, assuming that the cause of emission variations is due to motions in the gravitational field and not due to quasi-periodic heating mechanisms (e.g., Kato et al., 2010; Dolence et al., 2012; Shcherbakov and McKinney, 2013; Dokuchaev, 2014; Miyoshi et al., 2011; Brink et al., 2015).

For sources suitable for dynamical imaging by the ngEHT, namely Sgr A*, QPOs have been reported in the radio band on timescales of the order of tens of minutes, usually falling in the range of time periods $T \sim 17 - 57$ mins (Miyoshi et al., 2011; Shcherbakov and McKinney, 2013; Dokuchaev, 2014) and occur roughly in integer ratios (Miyoshi et al., 2011; Brink et al., 2015). However, even for well studied sources such as Sgr A*, the inference of BH spin from QPO measurements has not produced consistent results. Shcherbakov and McKinney (2013) assumed a model spin to be $a_* = 0.9375$ which predicts the QPO with $T \sim 35$ mins and is different from the results of Dolence et al. (2012), who assumed the same BH spin. Dokuchaev (2014) attempted to explain the QPOs as light curves of orbiting hot spots on nearly circular orbits. By analysing the observed QPOs of periods 11.5 mins and 19 mins, the spin was inferred to be $a_* \approx 0.65$, which is consistent with the (broad) range inferred from mm-VLBI (Broderick et al., 2009). Dokuchaev’s model associated the $T \sim 11.5$ mins QPO with the period of rotation of the BH horizon and the $T \sim 19$ mins to the latitudinal oscillation period of hot spots (Dokuchaev, 2014) moving on nearly circular orbits. However, there are certain limitations on sensitivity of orbiting hotspots to spin measurements (Matsumoto et al., 2020; Gelles et al., 2021a). Nevertheless, due to multi-wavelength observations of QPOs (Dolence et al., 2012), inferring spin from QPOs modelled in terms of hotspot motion seems a viable avenue to explore. The recent EHT results of Sgr A* (EHT Collaboration, 2022a) showed that observations were consistent with models that had spins of $a_* = 0.5$ and $a_* = 0.94$ and these are rather close to the QPO-based spin inference discussed above.

The importance of hot spots for probing the spacetime and its role in determining spin has already been discussed in Sec. 3.2.2. Herein, we note that the QPO frequencies based on modelling of hot spots discussed in Dokuchaev (2014) are independent of the astrophysical model, hence it is possible that BH spin measurements can be obtained which are agnostic to at least some astrophysical uncertainties.

In a similar vein, if we further align with the hot spot model for studying QPOs, as has been done across the multi-wavelength spectrum (Schnittman and Bertschinger, 2004; Schnittman, 2005; Zamaninasab et al., 2008; Johannsen and Psaltis, 2011b; Dolence et al., 2012), the quantity *in radio astronomy* which is sensitive to modelling variability in these hotspots is the closure phases (Doeleman et al., 2009b), which can show periodicity over several cycles. In particular, the periodicity of orbital hotspots manifests in closure phases at both, 230 GHz and 345 GHz (Doeleman et al., 2009b). As was also noted in Doeleman et al. (2009b), detection of periodicity is enhanced by the addition of more telescopes in the western hemisphere and, comparatively, increase in bandwidth is of lesser importance. On the other hand, increased bandwidth is desirable for studying polarisation of the source (Doeleman et al., 2009a,b). Thus, the possibility

of measuring spins from QPOs can directly inform instrumentation requirements for the ngEHT and combining the observations at 230 GHz and 345 GHz can potentially provide stronger constraints on BH spins of astrophysical sources such as Sgr A*.

3.3.5 Near-IR flares and orbiting hot spots

Near-IR observations with adaptive optics resolution at the 8m–10m-class telescopes revealed quasi-periodic light curves of Sgr A* (Genzel et al., 2003; Hamaus et al., 2009), although the number of cycles observed was too low to firmly conclude whether a periodic process was truly causing the variations (Witzel et al., 2012). If true, the oscillation period obviously sets a lower bound on the spin.

The situation has now become much more compelling with the discovery of astrometric loops during NIR flares observed with GRAVITY (Abuter et al., 2020). The data directly show that hot spots revolve clockwise around Sgr A* in a near-Keplerian motion at radii of around $8 r_g$, with a close-to face-on geometry. Strong support for this picture comes from simultaneous polarimetry of the near-IR flares. These flares show loops in the Q-U plane, with the same revolution time. This can be explained by a poloidal magnetic field geometry and the low inclination angle of the Sgr A* system.

Whether the flares (and other quasi-periodic features) can actually be used to probe the spacetime around Sgr A* is not yet clear. Simulations by Ressler et al. (2018) show that the geometry of the inner accretion disc, along which the hot spot motions, are governed by the influx of angular momentum from the incoming material, i.e., stellar winds of massive stars in the case of Sgr A*. The orientation of the mean flares' angular momentum vector is consistent with that of the disk of massive young stars moving clockwise at radii between 1–10 arcseconds (Paumard et al., 2006; Lu et al., 2009; von Fellenberg et al., 2022).

4 Searching for ultralight fields with the ngEHT

Shortly after Peccei and Quinn proposed a resolution of the strong CP problem (Peccei and Quinn, 1977b,a), *i.e.*, the puzzling smallness of the CP violating parameter in QCD, it was realized that it would lead to the appearance of a light pseudo-scalar, the “axion” (Weinberg, 1978; Wilczek, 1978). Laboratory and astrophysical data constrain the axion to be an “ultralight boson” with a mass below the eV scale (Workman et al., 2022). Cosmological constraints imply a lower bound on the typical QCD axion mass (Preskill et al., 1983; Abbott and Sikivie, 1983; Dine and Fischler, 1983), close to which it could be a viable dark matter candidate. Similar ultralight bosons have since been proposed in a plethora of beyond Standard Model theories (Svrcek and Witten, 2006; Abel et al., 2008; Arvanitaki et al., 2010; Goodsell et al., 2009; Marsh, 2016; Freitas et al., 2021). Such particles, like the QCD axion, can be compelling dark matter candidates, but are extremely hard to detect or exclude with usual particle detectors. Their low mass makes them a special type of dark matter candidate with de Broglie wavelengths that can be as large as a galaxy (Hu et al., 2000; Robles and Matos, 2012; Schive et al., 2014; Hui et al., 2017; Ferreira, 2021). This feature can lead to interesting unique properties when compared to other dark matter candidates. For example, ultralight bosons can form solitonic structures where the balance between gravitation and “quantum” pressure leads to a flat core profile in the inner region of galaxies. This mechanism, proposed to address small-scale puzzles in the observations of galaxies (Hu et al., 2000; Robles and Matos, 2012; Schive et al., 2014; Hui et al., 2017; Broadhurst et al., 2020; De Martino et al., 2020; Pozo et al., 2021), also provides a lower limit on the mass of dark matter (Bar et al., 2018), comparable to limits from cosmology (see, e.g., Kobayashi et al., 2017). Depending on the masses and couplings of the bosons, such self-gravitating structures or “boson stars” could even mimic BHs (Liebling and Palenzuela, 2023).

Quite remarkably, very light bosonic particles can also dramatically influence the dynamics of rotating BHs, specially when the BH horizon scale is of the order of the Compton wavelength of the boson. Then, rotating BHs can become unstable against the production of light bosonic particles due to a energy-extraction process known as BH superradiance, akin to the Penrose process and the Blandford-Znajek process (Penrose and Floyd, 1971; Zel’dovich, 1971; Blandford and Znajek, 1977; Brito et al., 2015b). This process drives an exponential growth of the field in the BH exterior, while spinning the BH down, forming a dense bound state or “cloud” around the rotating BH. This mechanism leads to several observable consequences, affecting the mass and spin of SMBHs, as well as their images made possible by the EHT and the ngEHT instruments.

The goal of this section is to discuss how the EHT and the ngEHT can be used to study the existence of ultralight bosons. We will consider three main observables: in Sec. 4.2 we first discuss how precise measurements of the mass and spin of astrophysical BHs allow the exclusion of minimally coupled bosons. Section 4.3 is devoted to the discussion of several direct gravitational signatures that can be used to constrain or detect the existence of ultralight bosons. Namely, in Sec. 4.3.1 we discuss how the ngEHT could detect ultralight bosons through the direct observation of the long-term evolution of the superradiant instability and then present examples where the existence of ultralight bosons could lead to geometries which can differ from Kerr. In particular, we discuss the so-called Kerr BHs with bosonic hair in Sec. 4.3.2, whereas in Sec. 4.3.3 we discuss how the oscillating metric perturbations induced by superradiant clouds made of real bosons could be detected using the photon ring autocorrelation. We then

also mention compact bosonic self-gravitating configurations in Sec. 4.3.4 which are discussed in more detail in Sec. 5.2.1. Section 4.3.5 discusses how the motion of S-stars around Sgr A* can constrain the total mass of the cloud in a certain mass window. In Sec. 4.4 we then discuss how for axion-like particles which interact with photons the formation of an axion cloud can lead to periodic oscillations of the orientation of the linear polarization of photons. Finally, in Sec. 4.5 we close with some open issues.

4.1 The theory

Our starting point is the generic Lagrangian density for massive, minimally coupled bosons:

$$\mathcal{L} = \frac{R}{16\pi} - \frac{1}{2}\nabla^\mu a \nabla_\mu a - V(a) - \frac{1}{4}B^{\mu\nu}B_{\mu\nu} - \frac{1}{2}m_V^2 X_\nu X^\nu + \mathcal{L}_{\text{EH}}(H) - \frac{m_T^2}{4}(H^{\mu\nu}H_{\mu\nu} - H^2), \quad (11)$$

where ∇_μ is the covariant derivative. For axion-like particles a , the potential is $V(a) = m_a^2 f_a^2 [1 - \cos(a/f_a)]$, where m_a is the axion mass, f_a is the decay constant characterizing some high energy scale. For a small self-interaction, i.e. $a/f_a \ll 1$, the potential $V(a) \approx m_a^2 a^2/2$ simply becomes a mass term.

The theory above also includes a possible new vector field X^μ of mass m_V and corresponding tensor $B^{\mu\nu} \equiv \nabla^\mu X^\nu - \nabla^\nu X^\mu$, and a tensor field $H^{\mu\nu}$ of mass m_T . The theory above only considers the Fierz-Pauli term for massive tensors, and describes a broad class of nonlinear theories expanded around vacuum Kerr background (Brito et al., 2013, 2015b, 2020). From now on, we will collectively refer to the mass parameter of these new fields as $m_b = (m_a, m_V, m_T)$. Note that the physical mass of the boson is $\hbar m_b$.

The corresponding equation of motion for such massive fields can be studied in a fixed Kerr background, as long as backreaction effects are small, which is the case for bosonic dark matter or for bosons produced from superradiance alone (see, e.g., Brito et al., 2015a; Herdeiro and Radu, 2017). A convenient procedure is to separate angular variables², expanding the wavefunction Ψ describing a boson of spin s in a given set of angular functions carrying two indices. One of them, l , specifies the total angular momentum. The other, namely the azimuthal number, m , is associated with the projection of the angular momentum along the z -axis (Brito et al., 2015b). A Fourier analysis of the resulting ‘‘radial’’ equation, i.e., assuming a general time dependence $\sim e^{-i\omega t}$ results in a single ordinary differential equation, which is in fact an eigenvalue problem for ω .

For any bosonic field Ψ , there is an unstable mode which grows exponentially in time as $\Psi \sim e^{\omega_I t}$, where the instability rates, ω_I , can be found in Brito et al. (2015b) and have the general dependence (Detweiler, 1980; Cardoso and Yoshida, 2005; Dolan, 2007; Pani et al., 2012; Baryakhtar et al., 2017; Cardoso et al., 2018a; Dolan, 2018; Baumann et al., 2019; Brito et al., 2020):

$$\omega_I \sim \Upsilon_{slm} \alpha^{4l+5+S} (m \Omega_{\text{BH}} - m_b), \quad (12)$$

² For generic BH spins, separation of variables has only been achieved for massive scalar and vector fields (Brill et al., 1972; Dolan, 2007; Frolov et al., 2018; Dolan, 2018). For massive tensors no such separation is known, but the full problem, involving a system of elliptic partial differential equations, has recently been solved in Dias et al. (2023).

where $S = -s, -s + 1, \dots, s - 1$, s is the spin projection along the z -axis and the Υ_{slm} coefficients can be found in Brito et al. (2015b). In the above, Ω_{BH} is the angular velocity of the BH and $\alpha \equiv Mm_b$ is the gravitational coupling. The only exception to the scaling (12) is a special dipole mode that exists for massive spin-2 fields (Brito et al., 2013; Dias et al., 2023). This special mode scales as $\omega_I^{\text{dipole}} \propto \alpha^3 (\Omega_{\text{BH}} - \omega_R)$, where $\omega_R \sim 0.73 m_b$, and has an instability timescale much shorter than any other superradiant mode. Precise values of ω_I^{dipole} for generic BH spins and values of α can be found in Dias et al. (2023).

The instability occurs only for large enough rotations, a clear sign of its superradiant nature. Owing to the results above, the modes of a boson field around a spinning BH are amplified if the BH angular velocity at the horizon is larger than the angular phase velocity of the incident wave, i.e., $m \Omega_{\text{BH}} > m_b$. These modes populate the BH over a volume with radius comparable to the Compton wavelength $1/m_b$.

Superradiance is most effective for highly spinning BHs and when the boson Compton wavelength is comparable to the BH gravitational radius $r_g \equiv M$ (Brito et al., 2015b). For a minimally coupled scalar, the growth is dominated by a dipolar mode which can grow on a timescale:

$$\tau = \frac{1}{\omega_I} \sim \frac{M}{10^6 M_\odot} \text{ yr}, \quad (13)$$

where M the BH mass. This is the shortest possible instability timescale and requires large BH spins and a gravitational coupling $\alpha \sim 0.42$, or:

$$m_b \sim 5.6 \times 10^{-17} \left(\frac{10^6 M_\odot}{M} \right) \text{ eV}. \quad (14)$$

The instability deposits the BH rotational energy into the boson field, which forms a bosonic structure outside the horizon, co-rotating with the BH, and with a length scale $\sim 1/(Mm_b^2)$.

We should note that additional interaction terms can be added to action (11), such as couplings of the axion to photons. In the presence of self-interactions or additional couplings, the exponential growth due to the superradiant instability could be terminated once the field value becomes sufficiently large (Yoshino and Kodama, 2012; Fukuda and Nakayama, 2020; Baryakhtar et al., 2021; Ikeda et al., 2019; East, 2022; Omiya et al., 2023; Spieksma et al., 2023; Chen et al., 2023b). On the other hand, the presence of additional interactions can also lead to unique signatures, as we discuss in more detail in Sec. 4.4.

4.2 Constraints from black-hole spin measurements

From the discussion of the previous section we can infer for example that a BH of mass $\sim 10^{10} M_\odot$ like M87* can be superradiantly unstable for ultralight bosons of masses $\sim 10^{-21}$ eV from Equation (14). This ultralight boson mass is close to the range of “fuzzy” dark matter (Davoudiasl and Denton, 2019), which is relevant for dynamics on galactic scales (Ferreira, 2021).

The instability time scale can be extremely short compared to typical astrophysical time scales and, therefore, relevant for astrophysical BHs (cf. Equation 13). The instability removes rotational energy from astrophysical BHs, and hence a robust observable for this effect concerns the BH “Regge” plane: if a bosonic field of a certain mass exists,

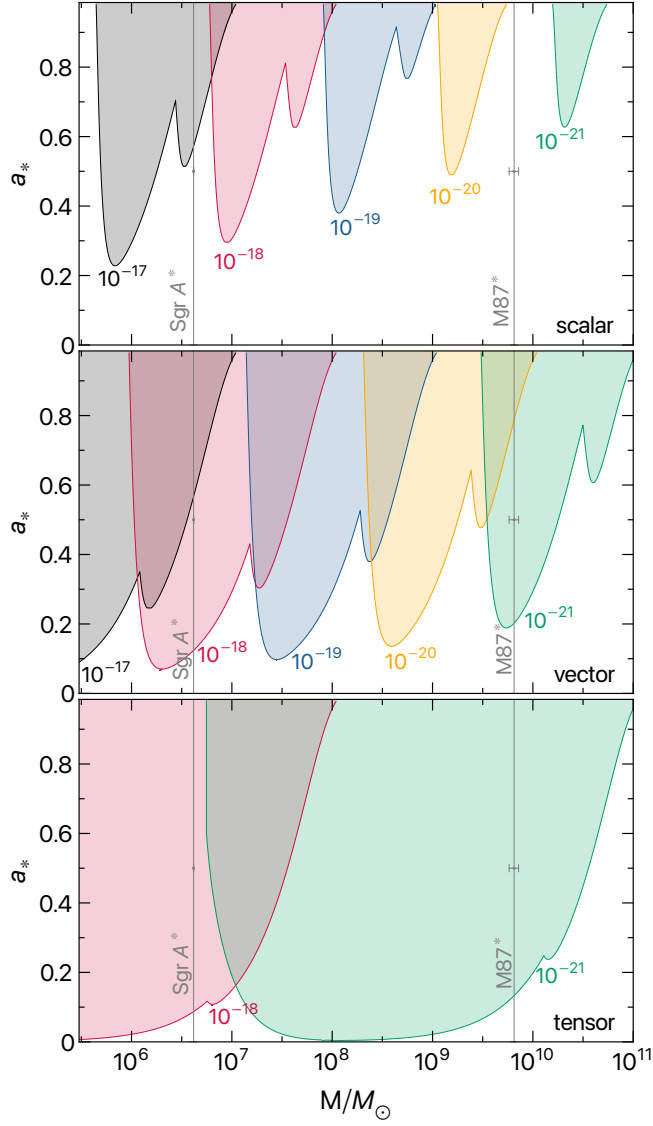


Fig. 12 Exclusion regions in the BH spin-mass diagram obtained from the superradiant instability of Kerr BHs against massive bosonic fields for the two most unstable modes. The top, middle, and bottom panels refer to scalar, vector and tensor fields, respectively. For each mass of the field (reported in units of eV), the separatrix corresponds to an instability time scale equal to the Salpeter time $\tau_{\text{Salpeter}} \approx 4.5 \times 10^7$ yr, i.e., inside each colored region the instability timescale would be shorter than τ_{Salpeter} . For illustration we consider bosons with masses ranging from 10^{-21} eV to 10^{-17} eV. For the massive tensor case we only show two masses to minimize clutter in the figure. The gray lines and error bars denote the measured mass of Sgr A* (Abuter et al., 2022) and M87* (EHT Collaboration, 2019a).

BHs with certain masses/spins will slow down on short timescales and should not be seen, up to observational uncertainties. For very weakly self-interacting bosons, the process depends primarily on the mass and spin of both the BH and the fundamental boson. By requiring the predicted instability timescale to be smaller than the typical accretion timescale (which tends to instead spin-up the BH), one can then draw regions in the parameter space where highly spinning BHs should not reside, if bosons within the appropriate mass range exist in nature (Arvanitaki et al., 2010; Brito et al., 2013, 2015a; Davoudiasl and Denton, 2019). This is illustrated in Figure 12 for scalar, vector and tensor fields, where we show exclusion regions in the BH spin-mass diagram for bosons with masses ranging from 10^{-21} eV to 10^{-17} eV.

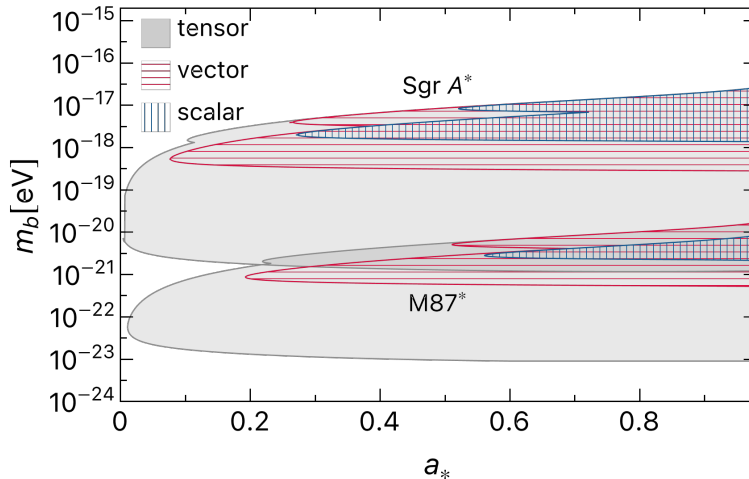


Fig. 13 Exclusion regions for the two most unstable modes as a function of the spin of Sgr A* and M87* when fixing Sgr A*'s mass to $M \simeq 4 \times 10^6 M_\odot$ (Abuter et al., 2022) and M87*'s mass to $M \simeq 6.5 \times 10^9 M_\odot$ (EHT Collaboration, 2019a). As in Figure 12, the separatrices correspond to an instability time scale equal to the Salpeter time $\tau_{\text{Salpeter}} \simeq 4.5 \times 10^7$ yr.

Such a spin-down effect allows use of BH spin measurements to constrain the existence of ultralight bosons (see Brito et al. (2015b) for a review of current constraints). Measurements of BH mass and spin with ngEHT are discussed in detail in Sec. 3. Given that the BH mass is generally much better constrained than the BH spin, the uncertainty in the measurement of the BH mass has a minimal impact on these constraints. To illustrate the possible constraints that could be obtained from Sgr A* and M87* given their measured mass, in Figure 13 we show the exclusion regions as a function of the BH spin. In particular, Figure 13 shows that obtaining a lower limit on its spin is enough to place some constraints on a range of boson masses (with the specific boson mass range constraint dependent on the magnitude of the measured BH spin; Davoudiasl and Denton, 2019). For example, from Figure 13 one can see that for a conservative spin measurement of M87* with $a_* \gtrsim 0.5$ (Cruz-Osorio et al., 2022), one could exclude scalar fields with masses around $\sim 3 \times 10^{-21}$ eV. On the other hand, a non-zero spin for Sgr A* would constrain bosons with masses around $\sim 3 \times 10^{-18}$ eV. Given the shorter instability timescale for vector and tensor fields compared to scalar fields, constraints

for vector and tensor fields are stronger. This is especially true for tensor fields due to the very short instability timescale of the special dipole mode (Dias et al., 2023). For example, measuring the spin of M87* to be $a_* \gtrsim 0.2$ would be enough to impose constraints for vector fields with masses $\sim 10^{-21}$ eV, whereas for tensor fields the measurement of a non-zero spin in Sgr A* and M87* would be enough to exclude massive tensor fields with masses in the whole range from $\sim 10^{-23}$ eV up to $\sim 10^{-17}$ eV (Dias et al., 2023). Boson masses of this order-of-magnitude are particularly interesting since this mass range is so far mostly unconstrained (Brito et al., 2015b; Ferreira, 2021).

A key ingredient in the spin-down calculation is the timescale on which astrophysical processes spin up a BH. If a BH is accreting at the Eddington limit, the characteristic timescale for significant spin-up is largely independent of the BH mass and is given by the Salpeter time $\tau_{\text{Salpeter}} \approx 4.5 \times 10^7$ yr (Shankar et al., 2009). Super-Eddington accretion could reduce this timescale further. On the other hand, EHT observations have indicated that both M87* and Sgr A* are currently significantly sub-Eddington $\dot{M}/\dot{M}_{\text{Edd}} \sim 2 \times 10^{-5}$ and $\dot{M}/\dot{M}_{\text{Edd}} \sim 10^{-9}$, respectively (Kuo et al., 2014; EHT Collaboration, 2019e, 2022a), which would increase the spin-up times accordingly. The impact of the time scale shifts the location of the constraints to the lower mass side³. As the spin up time increases, lighter masses can be ruled out. The power law dependence on the timescale, however, is weak and has an exponent that can be obtained from Equation (12).

Finally, we point out that while ruling out ultralight bosons with spin measurements of BHs is relatively straightforward, making a discovery of ultralight bosons via this effect is much more challenging, although technically possible. If one had a reasonable estimate of the initial spin distribution of BHs or believed that the spins of BHs were generally large, and if one measured the masses and spins of a large population of BHs, then one would see a characteristic dependence between the maximum spin of a BH and its mass if an ultralight boson existed in the relevant mass range (see, e.g., Arvanitaki et al., 2017; Brito et al., 2017; Ng et al., 2021, where this possibility was studied in the context of BH spin measurements obtained via GW observations of stellar-origin and massive BH binaries). In practice, however, the discovery of ultralight bosons using this method would likely be prone to very large modelling uncertainties.

4.3 Direct gravitational effects

4.3.1 Observing the superradiant instability evolution

We now turn to considering the possibility that superradiant evolution within a given timescale may be observable (Roy and Yajnik, 2020; Creci et al., 2020; Roy et al., 2022; Chen et al., 2022c). VLBI techniques have recently allowed the observation of the image of the dark shadow surrounding M87* (EHT Collaboration, 2019a) and Sgr A* (EHT Collaboration, 2022a) by a global network of radio telescopes. This has opened up the possibility to test physics in the strong gravity regime via BH imaging. As mentioned above, one such interesting phenomenon in strong gravity is the exponential growth of ultralight bosons near a BH via superradiance. This leads to rapid extraction of spin

³ For sufficiently short astrophysical spin-up timescales no constraints on ultralight bosons can be derived for any measured spin. Given the expected limits from the Salpeter time, it is expected that constraints can be derived assuming sufficiently large spins are measured.

and energy from the BH, which could be detectable as a change in the shadow of the BH image.

To further discuss this phenomenon, we consider the evolution of minimally coupled, massive bosonic fields, as in Equation (11). We assume that the backreaction due to the presence of the boson fields is negligible on the Kerr background and that the propagation of the boson fields acts as a perturbation over the background Kerr metric. As was mentioned, such a hypothesis is justified by the fact that the total mass of the boson cloud adds up to a fraction of the BH mass that is distributed over a large volume $\sim M^3/m_b^6$, with m_b the mass of the generic boson field, therefore exerting negligible distortion on the background spacetime (Brito et al., 2015b; Roy et al., 2022).

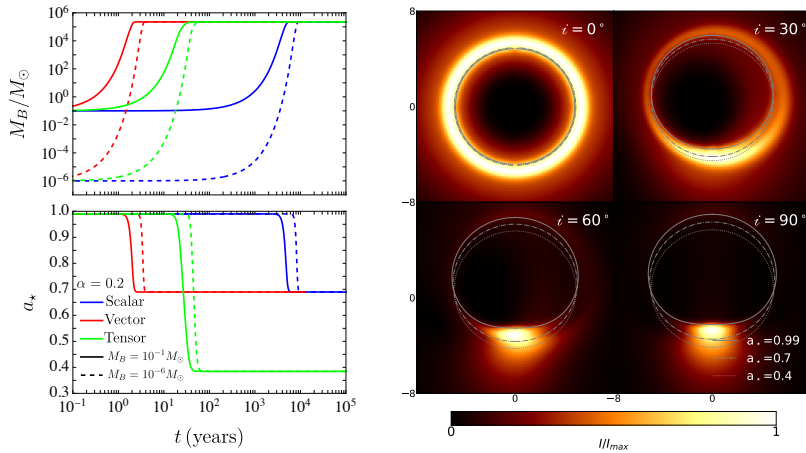


Fig. 14 Left panel: the evolution of the mass of the boson cloud M_B (top) and of the dimensionless BH spin parameter a_* (bottom), as a function of time in years for (initial) $\alpha = 0.2$ and for different choices of the bosonic nature: scalar field (red), vector field (blue), tensor field (green), with the set of quantum numbers as given in the text. The initial mass of the boson cloud is $M_B = 10^{-1} M_\odot$ (solid line) and $M_B = 10^{-6} M_\odot$ (dashed line). We assume an initial BH mass $M = 4.3 \times 10^6 M_\odot$ and initial spin $a_* = 0.99$. Right panel: evolution of shadow contours (gray lines) during different stages of superradiance for a vector with initial $\alpha = 0.2$ and a BH viewed at different inclination angles. The background depicts the intensity map with an initial value of $a_* = 0.99$. The coordinate origin is taken to be the BH location and the axes are specified in units of the initial gravitational radius.

To better assess this, we have solved the equations describing the evolution of the occupancy number of the boson cloud, $N(t) = M_B/m_b$, where M_B is the mass of the cloud, the dimensionless BH spin parameter a_* due to superradiance, and the mass change of the BH. We have neglected the change in the mass of the BH due to accretion, since we work on timescales that are shorter than the Salpeter timescale. The exponent of α in Equation (12) predicts that some of the modes experiencing the fastest superradiant evolution have $l = 1, S = 0$ (scalar field), $l = 1, S = -1$ (vector field), or $l = 2, S = -2$ (quadrupole mode of a tensor field). For illustration purposes we do not include the evolution of the massive tensor field dipolar mode, which has a much shorter instability timescale (Dias et al., 2023). Other than this special dipolar mode, the spectrum of the unstable modes for a massive vector field generally lead to the shortest timescales (Pani et al., 2012; Baryakhtar et al., 2017; Cardoso

et al., 2018a; Dolan, 2018). For example, the timescale for the superradiance evolution associated with a scalar field with $\alpha = 0.2$ around a BH of mass $M \sim 10^6 M_\odot$ is $t \sim \mathcal{O}(10^4)$ years, while repeating the estimate for a vector field with the same parameters reduces the timescale to $t \sim \mathcal{O}(10)$ years).

Figure 14 shows the evolution of the mass of the boson cloud M_B (top left) and a_* (bottom left) due to superradiance caused by a scalar field (red), a vector field (blue) and a quadrupole mode of the tensor field (green), assuming the mass of Sgr A* as $M = 4.3 \times 10^6 M_\odot$ with initial spin parameter $a_* = 0.99$, for an initial coupling $\alpha = 0.2$, corresponding to the mass $m_b \approx 6 \times 10^{-18}$ eV, for two different choices of the initial mass of the boson cloud: $M_B = 10^{-1} M_\odot$ (solid line) and $M_B = 10^{-6} M_\odot$ (dashed line). For this example, the change in the BH mass is $\sim 3\%$ for the scalar and vector fields, and $\sim 5\%$ for the tensor field. The initial value of the boson cloud mass only affects the timescale (and not the relative change in the BH mass) since the evolution of both the spin parameter and the BH mass are proportional to the total number of bosons.

At this point, we note that SMBHs are very old, hence the probability of observing superradiance in one of the observations is vanishingly small, since the instability should have saturated by now. There are, nevertheless, circumstances where this might happen, if, for example, a bosonova suddenly leads to cloud destruction (Yoshino and Kodama, 2012), and the exponential extraction of the BH spin restarts. A varying boson mass predicted in quintessence models (TsujiKawa, 2013) that recently entered the superradiant region is also possible.

Examples of evolution of the shadow contours are shown on the right panel of Figure 14. The center of the shadow is clearly separated from the BH located at the origin, with the distance increasing with a_* and the inclination angle i . Thus the drift of the shadow center, which evolves in the axis perpendicular to the spin projection, can be a smoking gun of superradiant evolution at large i (Chen et al., 2022c). For example, at $i = 60^\circ$, a $10 \mu\text{as}$ drift is possible for both vector and tensor fields. On the other hand, using photon ring autocorrelation (Hadar et al., 2021), one can record yearly variations in the azimuthal lapse, δ_0 , which is sensitive to the BH spin (Gralla and Lupsasca, 2020a) at low i . These two ways are thus complementary and both benefit from long-duration observation times.

4.3.2 Black holes with synchronised bosonic hair

The growth of a bosonic field around a Kerr BH due to superradiance may or may not lead to an equilibrium state. If the bosonic field is complex, the BH-bosonic field system can form true stationary configurations: *BHs with synchronised bosonic “hair”* (Herdeiro and Radu, 2014, 2015a; Herdeiro et al., 2016). Such BH equilibrium configurations exist with both scalar and vector (Proca) fields, under a general synchronisation mechanism (see Herdeiro et al., 2015; Delgado et al., 2019, 2021, for more details and generalizations).

Focusing on the scalar case, i.e., Equation (11) with $X_\mu = 0$, $H_{\mu\nu} = 0$ and $V(a) = m_a^2 |a|^2 / 2$, but now with the field a complex and $(\nabla a)^2$ also becoming $|\nabla a|^2$, one can construct fully non-linear BH solutions in GR minimally coupled to a complex massive bosonic field a . Although the metric is assumed to be stationary and axially-symmetric, the full solution is not, due to the explicit time dependence assumed in the harmonic ansatz for the scalar $a \sim e^{i(k\varphi - wt)}$, where k and w are respectively the azimuthal harmonic integer and the field frequency (Herdeiro and Radu, 2015a). This

allows one to evade some well-known *no-hair theorems* (Herdeiro and Radu, 2015b). Although some of the solutions can display quite unusual BH shadow shapes and very distinct gravitational lensing signatures (Cunha et al., 2015, 2019; Cunha and Herdeiro, 2018; Vincent et al., 2016a), one of the regions in the domain of existence with most potential to describe astrophysical and viable solutions lies in the proximity to the Kerr limit. In that region one may find configurations that might be formed within astrophysical timescales.

The growth timescale of a scalar field due to superradiance is extremely sensitive to the resonance of the BH mass scale M with the Compton wavelength of the ultralight particles. In addition, BHs with bosonic hair are also not absolutely stable and can suffer from their own superradiant instabilities (Ganchev and Santos, 2018; Degollado et al., 2018). One possibility is that M87* started as a Kerr BH and grew scalar hair within an astrophysical timescale (e.g., $\lesssim 0.1\%$ of the Hubble time (Degollado et al., 2018)), transforming into a BH with bosonic hair state that is effectively stable to its own superradiant instabilities over cosmological timescales (Ganchev and Santos, 2018; Degollado et al., 2018), provided that one restricts to the interval:

$$m_a M_{\text{M87}} \in [0.1, 0.3] \quad \implies \quad m_a \in 1-3 \times 10^{-20} \text{ eV}. \quad (15)$$

Within this range, each hairy BH solution can be identified by a two-parameter set of values $\{p, M m_a\}$, where $p = 1 - M_H/M$ measures the fraction of the spacetime mass stored in the bosonic hair. Here M_H denotes the Komar mass of the horizon and M denotes the total (ADM) mass. The parameter, p , satisfies $0 \leq p \leq 1$, interpolating between vacuum Kerr BHs in the test limit of a for ($p = 0$), and horizonless boson stars for ($p = 1$). Fully dynamical numerical evolution of complex *vector* fields growing from vacuum Kerr by superradiance (East and Pretorius, 2017) suggest a maximal possible value of $p \sim 9\%$ (Herdeiro and Radu, 2017). If the process is approximately conservative, then an upper limit of $p \sim 10\%$ should exist regardless of the spin of the bosonic field (Herdeiro et al., 2022).

The shadow areal radius \mathcal{R} of BHs with bosonic scalar hair can be compared with the Kerr case, for the same total mass M . Such a comparison is appropriate if most of the scalar hair is spread over a length scale of $\sim 10 M$, which is typically the case for the hairy BH solutions under consideration here. Under these circumstances, signature effects of the scalar field can be expected to be subdominant on far-away measurements of the total mass M , using, e.g., stellar orbital motions over length scales $\gg M$. Assuming $i = 17^\circ$ for M87*, the relative shadow deviation $\delta\mathcal{R}$ depends very weakly on $M m_a$ and is accurately parameterized by a function of p alone (Cunha et al., 2019):

$$\delta\mathcal{R}(p) \equiv 1 - \frac{\mathcal{R}_{\text{hairy}}}{\mathcal{R}_{\text{Kerr}}} \simeq p + p(p-1)A, \quad \text{with } A \simeq 0.111159. \quad (16)$$

Since $\mathcal{R}_{\text{Kerr}} \simeq 19 \mu\text{as}$, the detection of bosonic scalar hair close to the upper limit of $p \sim 10\%$ requires an ngEHT angular resolution close to $1.7 \mu\text{as}$, whereas a finer measurement of p below 1% would require resolutions smaller than $\sim 0.1 \mu\text{as}$. Constraining the value of p for M87* via ngEHT observations would directly measure how much mass can exist in a bosonic field in equilibrium with the SMBH.

Naively, one might expect similar results to also hold for BHs with synchronised vector (rather than scalar) hair. However, as was reported recently in Sengo et al. (2023), there are some regions in the solution space of BHs with vector hair that could

still be compatible with the EHT observations of both M87* and Sgr A*, despite containing a significant portion of the mass stored in the hair, e.g., $p \sim 40\%$. This would include solutions just below $p \sim 29\%$, i.e., the thermodynamic upper limit for configurations that might have grown from Kerr via superradiance. Indeed, as we increase the coupling $M m_b$ of the BH solution with vector hair, for a fixed value of p it would become increasingly more difficult for it to be ruled out by EHT (or ngEHT) observations. This is a feature that is in contrast to the scalar case.

4.3.3 Photon ring astrometry for real bosons

We next focus on superradiant clouds made of real bosons. The coherently oscillating features of their wavefunctions generate periodic metric perturbations. On long timescales, these metric perturbations dissipate energy from the cloud in the form of potentially detectable gravitational waves, for example, in the LISA band for a cloud outside Sgr A* (Brito et al., 2015b). On the other hand, locally, these metric perturbations also modify the photon geodesics propagating from the BH horizon scale towards us, providing potential signals for EHT and ngEHT (Chen et al., 2023a).

More explicitly, metric perturbations around a Kerr background $g_{\mu\nu}^K$ can be written as $g_{\mu\nu} \simeq g_{\mu\nu}^K + \epsilon h_{\mu\nu}$, where $\epsilon \ll 1$ controls the perturbative expansion, and $h_{\mu\nu}$ represents the metric perturbations generated from a bosonic cloud. In this metric, photon geodesics also undergo small perturbations compared to the geodesics in a Kerr background $x_{(0)}^\mu$, i.e., $x^\mu \simeq x_{(0)}^\mu + \epsilon x_{(1)}^\mu$, where $x_{(1)}^\mu$ is the deviation to the background geodesic calculated using $h_{\mu\nu}$ and the Kerr metric.

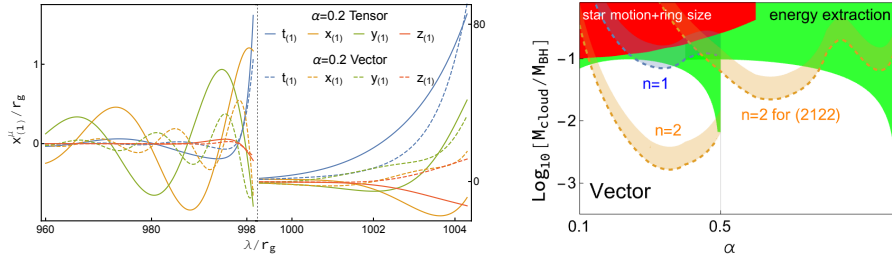


Fig. 15 Left panel: examples of deviations from the Kerr background photon geodesics as a function of the affine parameter, λ , generated by bosonic clouds with $\alpha = 0.2$. The initial values are $\lambda_0 = 0$, $r_0 = 10^3 r_g$, $i = 17^\circ$, and $a_* = 0.94$. The gray vertical line shows the time at which the unperturbed orbit $x_{(0)}^\mu$ crosses the BH equatorial plane for the first time. Right panel: prospects for constraints on the total mass of a vector cloud using photon ring autocorrelations. We show both the ground state $(S, l, m) = (-1, 1, 1)$ with $\alpha < 0.5$ and a higher mode $(S, l, m) = (-1, 2, 2)$. The constraint bands range from a conservative criterium based on ngEHT’s spatial resolution $\sim 10 \mu\text{as}$ to an optimistic criterium based on the intrinsic azimuthal correlation length of the accretion flow $\ell_\phi \approx 4.3^\circ$. Constraints from a joint observation of motion of stars and EHT ring size measurements (Sengo et al., 2023) are shown in red, and theoretical bounds on the maximum superradiant extraction for M_B/M (Herdeiro et al., 2022) are shown in green.

The left panel of Figure 15 shows examples of the deviation $x_{(1)}^\mu$ using Cartesian Kerr-Schild coordinates (t, x, y, z) , for a massive tensor and a vector cloud with $\alpha = 0.2$ in the hydrogenic-like ground state (Chen et al., 2023a). We take the initial point at $i = 17^\circ$ and the BH spin to be $a_* = 0.94$ as benchmark values to be consistent with

M87* (EHT Collaboration, 2019a). The evolution of the deviation can be divided in two stages: an oscillatory stage due to the time-varying energy-momentum tensors of the bosonic clouds and a second stage where the deviation grows exponentially when reaching the nearly-critical orbits of the photon ring. This second stage is caused by the instability of the photon ring orbit and is separated from the oscillatory stage by the time $x_{(0)}^\mu$ it first crosses the BH's equatorial plane. Therefore, the deviation for lensed photons significantly surpasses that of direct emission, along with the local plasma dynamics.

To detect small geodesic deviations, one sensitive probe is to use the photon ring autocorrelation discussed in Sec. 2.2.3, which can measure both the time delay and azimuthal lapse from sources emitting in the BH's equatorial plane. The right panel of Figure 15 shows the prospects to constrain the total mass of a vector cloud as a function of α . The constraint is computed by requiring that the oscillation of the azimuthal lapse generated by the vector cloud is larger than the Gaussian smearing width due to a finite spatial resolution $\sim 10 \mu\text{as}$ or the correlation length of the accretion flow $\ell_\phi \approx 4.3^\circ$ (Hadar et al., 2021). Two other constraints are shown for comparison, including a joint observation of the EHT ring size measurement and motion of stars, as discussed in Sec. 4.3.2, and a theoretical bound on the maximum mass a boson cloud can reach due to superradiance, assuming that there is no angular momentum supplement to the BH (Herdeiro et al., 2022).

For a massive tensor cloud that couples to electromagnetic photons directly, constraints for M_B will be more stringent (Chen et al., 2023a), for which the $n = 1$ photon ring can already constrain a previously unexplored region of the parameter space. In addition, one can also probe their existence if the massive tensor is dark matter and forms a soliton core outside Sgr A*.

On the other hand, a scalar cloud generates time delays more efficiently than spatial deflections, which can in principle also be detected using time domain correlations. Compared to the azimuthal lapse, time delays are more difficult to detect, due to the large correlation time (Hadar et al., 2021). However, a nearby point-like source such as a hotspot or a pulsar can strongly boost these searches with a significantly better time resolution (Chesler et al., 2021). These sources can also play important roles to look for $n = 2$ peaks in the autocorrelation.

The oscillation amplitude of the azimuthal lapse is more significant in the inner region of the critical curve due to a stronger photon ring instability in this region (Chen et al., 2023a). Thus, the improvements in spatial resolution and dynamic range of the ngEHT are crucial to resolve these fine structures in the expected oscillation pattern. Searches for the $n = 2$ ring, which can probe larger regions of the parameter space for both vector and tensor clouds, can also be boosted with an increase in baseline coverage.

4.3.4 Boson and Proca stars

For complex bosons, the hairy BH solutions described in Sec. 4.3.2 connect smoothly to horizonless, self-gravitating structures known as boson or Proca stars, when the field is a massive scalar or vector, respectively. These are interesting BH mimickers and, in the context of EHT observations, the appearance of such solutions has been explored (e.g., Vincent et al., 2016b; Olivares et al., 2020; Herdeiro et al., 2021). While it is shown that under some circumstances these objects produce ring-like structures similar to BH images, in other cases they can produce images with a bright core that are qualitatively

different, and therefore easily distinguishable. These two distinct behaviors, as well as the size of the ring, depend on a number of factors, such as the compactness of the stars, the particular boson field model used to construct the stars, or the inclination angle at which observations are made. In principle, knowledge of these properties could make it possible to set bounds on the star parameters that are compatible with present and future observations (Olivares et al., 2020; Herdeiro et al., 2021). For further details we refer to Sec. 5.2.1 where the capabilities of the ngEHT to discriminate these objects are discussed in the context of horizon physics.

4.3.5 Motion of S-stars

Besides constraints from lensing signals from the Galactic Center by the ngEHT, one should also take into account that observations of S-stars orbiting Sgr A* may impose interesting constraints on putative boson clouds that could be present around Sgr A*. S-stars have been largely monitored and studied in the past decade using both astrometry and spectroscopy, with particular attention paid to the orbit of the star S2. The latter is one of the closest stars to the Galactic Center, reaching a minimum distance of 120 AU (~ 1200 Schwarzschild radius) from the central mass. The high precision of the data collected independently by both the GRAVITY Collaboration (Abuter et al., 2019) and the UCLA Galactic Center group (Ghez et al., 2008) enabled constraint of both the mass of the central object $M \sim 4.3 \times 10^6 M_\odot$ and the Galactic Center distance $D \sim 8.3$ kpc. The hypothesis that Sgr A* is in fact a SMBH has been supported by the direct measurement of both gravitational redshift and the Schwarzschild precession value of $\Delta\omega = 12.1''$ per revolution in the orbit of S2 (Abuter et al., 2018, 2020; Do et al., 2019a). Data collected for S2 have also been used to test the presence of an extended mass within its apocenter, with particular attention paid to spherically symmetric dark matter density distributions (see, e.g., Lacroix, 2018; Bar et al., 2019; Heifsel et al., 2022). The GRAVITY Collaboration (Abuter et al., 2022) provided the current 1σ upper bound of 0.1% of M (equivalent to $\delta M \sim 4000 M_\odot$) on the dark mass around Sgr A* using the motion of four S-stars (S2, S29, S38, S55).

In the context of ultralight scalar fields, a bosonic structure around a SMBH has an impact on stellar orbits (Cardoso et al., 2011; Fujita and Cardoso, 2017; Ferreira et al., 2017; Bošković et al., 2018; Amorim et al., 2019; Della Monica and de Martino, 2023a,b). The presence of a scalar cloud may affect the orbital elements of S2 in a way that is potentially detectable by the GRAVITY interferometer, since the in-plane precession it induces in the orbit is competitive with the first Post-Newtonian (PN) correction, i.e., with the Schwarzschild precession. Describing the scalar cloud by two parameters, the fractional mass $A = M_B/M$ and its dimensionless mass coupling constant α , the largest variations in the orbital elements of S2 (Amorim et al., 2019) are expected for:

$$0.001 \lesssim \alpha \lesssim 0.05, \quad (17)$$

corresponding to an effective scalar field mass of $10^{-20} \text{ eV} \lesssim m_a \lesssim 10^{-18} \text{ eV}$ and an effective peak position of $1.2 \times 10^4 r_g \lesssim R_{\text{peak}} \lesssim 3 \times 10^6 r_g$. The latter is in fact comparable with S2's orbital range of $3 \times 10^3 r_g \lesssim r_{\text{S2}} \lesssim 5 \times 10^4 r_g$, meaning that the scalar cloud has a larger impact on the dynamics of S2 if the star crosses regions of space where the scalar density is higher. We note that for Sgr A* and for ultralight scalar fields with masses in the range (17), the superradiant instability timescale is in

general longer than a Hubble timescale (see Figure 12), except for values of α close to the upper end of that limit, hence the scalar cloud must be formed by means of a different process. A recent analysis of the astrometry and the radial velocity of S2 showed no substantial evidence for a scalar cloud structure with mass coupling roughly in the range (17). The fractional mass of the cloud can be constrained to be $\Lambda \lesssim 10^{-3}$ at the 3σ confidence level, corresponding to 0.1% of the central mass, setting a strong bound on possible bosonic structures around Sgr A* (Foschi et al., 2023).

4.4 Polarimetric measurements for axion-induced birefringence

We have so far focused on bosons that interact only gravitationally or interact only very weakly through possible additional couplings. However, from a particle physics perspective, there are strong reasons to include couplings to all of the Standard Model particles. In fact, the introduction of an axion was originally made specifically in order to couple with gluon sector, so as to explain the smallness of the electric dipole moment of the neutron (Peccei and Quinn, 1977b). More broadly, one could then expect all axion-like particles to have nontrivial couplings to all other fields. In such theories, self-interactions and/or couplings to other particles are generically present and those can change the evolution of the superradiant instability. For example, the superradiance process is expected to be highly suppressed once the self-interactions of the axions become dominant. In the case of axions with a cosine potential $V(a) = m_a^2 f^2 \cos(a/f_a)$ in Equation (11), the self-interactions from the expansion of the potential will lead to emission of scalar radiation towards infinity and transitions into decaying modes. Thus one would expect that in some regimes superradiance and energy loss can balance each other and that the axion cloud enters a coherently oscillating state where the maximum field value of the cloud, a_{\max} , located at the equatorial plane of the Kerr BH at a radius $\sim 2r_g/\alpha^2$, can saturate at around $a_{\max} \sim f_a$ (Yoshino and Kodama, 2012; Baryakhtar et al., 2021). For a_{\max} below 10^{15} GeV, the total mass of the axion cloud is less than 1% of the BH mass for $\alpha > 0.1$. Constraints from spin measurements as discussed in Sec. 4.2 do not apply any more since the extraction of the rotation energy can be considerably slowed down (Baryakhtar et al., 2021). However, one can still expect to see signatures of the ultralight axion if it couples to the visible sector, for example through axionic couplings to photons:

$$\mathcal{L}_{\text{int}} = g_{a\gamma} a F_{\mu\nu} \tilde{F}^{\mu\nu} / 2, \quad (18)$$

where $F^{\mu\nu} \equiv \nabla^\mu A^\nu - \nabla^\nu A^\mu$ is the field strength tensor of photons, $\tilde{F}^{\mu\nu}$ is its dual, and $g_{a\gamma}$ is the axion-photon coupling. Once this coupling is turned on, the oscillating axion field can periodically rotate the EVPA of the linearly polarised emissions (Carroll et al., 1990; Harari and Sikivie, 1992). The period of such oscillations is approximately the inverse of the axion mass and may be written as:

$$T \simeq \frac{2\pi}{m_a} = 4 \times 10^5 \left(\frac{10^{-20} \text{ eV}}{m_a} \right) \text{ seconds}, \quad (19)$$

with small corrections dependent on α (Dolan, 2007; Brito et al., 2015b). Using the equations of covariant radiative transfer in a local frame to take into account the plasma and curved spacetime effects, the axion effect in a local frame is equivalent to adding a term in parallel with the plasma-induced Faraday rotation ρ_V^{FR} , i.e., $\rho_V =$

$\rho_V^{\text{FR}} - 2g_{a\gamma} da/ds$, where s is the proper time and the second term is proportional to the gradient of axion field along the line-of-sight (Chen et al., 2022a,b). The shift of the EVPA is independent of the photon frequency, which can be distinguished from the astrophysical Faraday rotation. Since the superradiantly-grown axion cloud has angular momentum, the variations of the EVPA behave as a propagating wave along the photon ring for a nearly face-on BH (Chen et al., 2020).

An illustration of the EVPA variations around M87* is shown in the left panel of Figure 16, where different colors of the quiver lines represent separate oscillation phases within one period. Using the four days of polarimetric measurements of M87* in 2017 (EHT Collaboration, 2021a), one can already constrain the dimensionless axion-photon coupling $c \equiv 2\pi g_{a\gamma} f_a$ to previously unexplored regions (Chen et al., 2022b), which is shown on the right panel of Figure 16. The upper bound on the axion mass window is determined by the spin of the BH via the superradiant condition and two examples of spins are shown. The lower bound is required to have a superradiant rate timescale much shorter than the age of the Universe.

The fidelity of mm/sub-mm VLBI polarization maps is limited primarily by the ability to reconstruct unknown station-based calibration factors, e.g., complex station gains and polarimetric leakages. Closure traces are polarimetric closure quantities defined on station quadrangles which are (by construction) insensitive to linear station-based corruptions of the coherency matrix, extending the more familiar closure phases and closure amplitudes (Broderick et al., 2020b). Conjugate closure trace products (CCTPs) are combinations of closure traces that are sensitive exclusively to polarization, being unity otherwise, and are therefore providing direct, non-imaging evidence for complex polarization structures (see, e.g., Figure 13 of EHT Collaboration, 2021a). The time-variable EVPA evolution produced by light axion clouds about M87* and Sgr A* results in time-variable excursions of the CCTP phase. Estimates based on the 2017 M87* EHT observations suggest that over a single observing campaign, the EHT can easily constrain the degree of axion-induced EVPA rotations to 2° for $\alpha \simeq 0.4$ (Wang and Broderick, 2023), similar to the limits presented in Chen et al. (2022b). With its considerably larger bandwidth and number of available quadrangles, the ngEHT should be able to improve these limits by nearly two orders of magnitude, detecting EVPA fluctuations as small as 0.05° using CCTP phases alone (Wang and Broderick, 2023).

The robustness of the superradiant phase is essential for the existence of a saturated axion cloud and thus the constraints. The gravitational perturbation is hard to prevent the build-up process since the rotating SMBH dominates the gravitational potential. The parametric instability of the axion to photons (Ikeda et al., 2019; Boskovic et al., 2019; Spijkema et al., 2023) will be kinetically suppressed by the effective photon mass in the presence of plasma that is much higher than the axion mass. The conversion of axion and magnetic fields to electric fields that can heat the plasma is also highly suppressed.

For the ngEHT, one can increase the sensitivity by correlating the different data sets of the EVPA variations by a factor of the square root of the number of data sets (Chen et al., 2022a). Simultaneous correlation of EVPA variations at three different frequencies can increase the statistics or falsify suspicious signals. Correlations of azimuthal EVPA at different radii from the BH center require the angular resolution to be $\sim 10 \mu\text{as}$ and the dynamic range of linear polarization to be above 100. More sequential observations and higher time cadence also bring more statistics. On the other hand, emissions that reach the sky plane simultaneously and originate from different emission points where the axion field oscillates at different phases can potentially wash

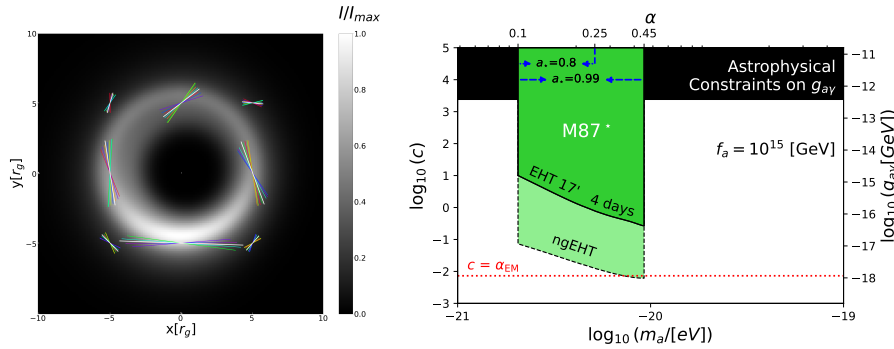


Fig. 16 Left panel: illustration of a covariant radiative transfer simulation (`ipole`) of the polarised emission from a Kerr BH surrounded by an axion cloud. Different colors on the EVPA quivers, which range from red through to purple, represent the time variation of the EVPA in the presence of the axion-photon coupling. White quivers are the EVPAs when the axion field is absent. The intensity scale is normalized so that the brightest pixel is unity. Right panel: the upper limit on the axion-photon coupling (Chen et al., 2022b), characterized by $c \equiv 2\pi g_{a\gamma} f_a$, derived from the EHT polarimetric observations of SMBH M87* (EHT Collaboration, 2021a) and prospect for ngEHT (Chen et al., 2022a). The bounds from other astrophysical observations assuming $f_a = 10^{15}$ GeV are shown for comparison.

out the axion-induced EVPA oscillation, especially for lensed photons that orbit around the BH several times. At 86 GHz these lensed photons contribute less and the amplitude of the EVPA oscillations becomes larger. EVPAs observed at larger radii from the photon ring without the contamination of lensed photons should produce larger and more robust predicted signals.

The time variability of the accretion flow will lead to EVPA variations at each point in the sky plane. To suppress such turbulent behavior, Chen et al. (2022b) introduced the differential EVPA in the time domain, the difference between two sequential observations in the data, in order to test axion-photon couplings. The price to pay is a suppressing factor of $\sin(\omega t_{\text{int}}/2)$, where t_{int} is the interval time between two sequential observations. For longer axion oscillation periods it provides a smaller value, which suppresses the sensitivity at lower axion masses on the right panel of Figure 16. On the other hand, such time variability of the EVPA can be modeled as a kind of noise using GRMHD simulations or extracting from a turbulent field (Lee and Gammie, 2021). Thus one can expect to get rid of the suppression factor in the future with the ngEHT.

In the right panel of Figure 16, we also give the prospective sensitivity of the ngEHT to the axion-photon coupling (Chen et al., 2022a). There are two aspects contributing to the enhancement of the sensitivity: the removal of the suppression factor, $\sin(\omega t_{\text{int}}/2)$, after a more sophisticated understanding of the accretion flow's variations, and an increase in number of data sets. Reasonable expectations include ten times the observation time, five different radii from the BH center for the EVPA, and three different frequencies. We also take into account a larger radial wave-function in the equatorial plane of the BH. In the high mass region, the lowest possible value of $c_{\text{min}} = \alpha_{\text{EM}}$ can potentially be covered, where α_{EM} is the electromagnetic fine-structure constant.

Non-superradiantly-produced axions could also exist around SMBHs as a component of dark matter, contributing to birefringence signals as well. Field profiles of axion

dark matter could be described by soliton cores in the centers of galaxies (Yuan et al., 2021) or gravitational atoms bound to the SMBHs (Gan et al., 2023). The excellent angular resolution of the ngEHT will again help to resolve the coherent oscillating EVPA variations from different points in the sky plane.

4.5 Open issues

In this section we discuss a number of open issues related to other interactions and how astrophysical environments can affect the superradiant instability and affect some of the observables mentioned above.

4.5.1 Other types of interactions

In addition to the axion-photon coupling discussed in Sec. 4.4, various types of ultralight bosons can interact differently with standard model particles, leading to corresponding oscillatory parameters in the standard model. Testing variations of fundamental constants in the strong gravity region, such as near a SMBH, can therefore test the existence of ultralight bosons. A CP-even scalar, often called a dilaton, can couple to the Lagrangian density of the standard model. The two main consequences of this are shifts in α_{EM} from $\phi F_{\mu\nu}F^{\mu\nu}/\Lambda_\gamma$, and in the mass of a fundamental fermion, ψ , from $\phi m_\psi \bar{\psi}\psi/\Lambda_\psi$, where ϕ is the dilaton field, m_ψ is the fermion's rest mass, and Λ_γ and Λ_ψ are the cut-off energy scales of the two couplings.

Measuring the fine-structure constant α_{EM} usually requires spectroscopic observations. For example, comparing absorption lines from S-stars around Sgr A* can test variations of α_{EM} between the star and the Earth (Hees et al., 2020) and constrain the ultralight boson's couplings (Yuan et al., 2022). The fluorescent iron K α line from X-ray observations can also potentially constrain its value near the innermost stable circular orbit (ISCO) (Bambi, 2014). The frequency bands of the EHT and the ngEHT can, in principle, observe molecular lines, but they can only exist far away from the SMBH with lower temperatures compared to the horizon-scale plasma.

Similarly, spectroscopic observations can constrain the ratio between the electron and proton mass (Murphy et al., 2008), which is influenced by the oscillations of the dilaton. In addition, the value of the electron-to-proton mass ratio can be set freely in GRMHD simulations, which could be used to study potential imprints of dilatonic couplings in the plasma.

A vector boson cloud that kinetically mixes with electromagnetic photons through couplings of the form $\epsilon F_{\mu\nu}X^{\mu\nu}$ can heat up the plasma (Caputo et al., 2021), where ϵ is the kinetic mixing coefficient. Predictions of the phenomenological consequences require detailed studies, for example, through GRMHD simulations. In addition, the dense vector cloud may produce time-oscillating electromagnetic signatures, with frequencies much larger than the vector boson mass, arising from Compton-like scattering of photons with the electrons in the plasma (Caputo et al., 2021).

Compared with terrestrial searches for ultralight boson dark matter, the signals from a bosonic cloud can be much more significant due to the large field value that can be attained in the cloud. Using a Newtonian approximation and hydrogenic wavefunctions, the field values for a scalar and a vector cloud at the superradiant ground state

are related to the total cloud mass by

$$\frac{M_B}{M_{\text{BH}}} \approx \begin{cases} 0.5\% \times \left(\frac{\phi_0}{10^{16} \text{ GeV}}\right)^2 \left(\frac{0.4}{\alpha}\right)^4, \\ 0.8\% \times \left(\frac{X_0}{10^{17} \text{ GeV}}\right)^2 \left(\frac{0.4}{\alpha}\right)^4, \end{cases} \quad (20)$$

where ϕ_0 and X_0 are the maximal field values of a scalar and a vector cloud, respectively. Thus a cloud with 10% mass of the BH can have a significant field value up to the grand unification scale. Therefore we expect that the ngEHT could be used to constrain or detect the different couplings mentioned above. However, further work is needed to fully assess the detectability of these type of interactions.

Finally, significant field values and their interactions with matter fields can lead to an enhanced production of matter within a cloud. A pertinent example is the interaction between a scalar cloud and Standard Model neutrinos (Chen et al., 2023b). The substantial scalar field value within the cloud facilitates the generation of a significant number of neutrinos parametrically, akin to the mechanism observed during the pre-heating phase in the early universe (Greene and Kofman, 1999, 2000). Furthermore, spacetime variations in bosonic fields contribute to the acceleration of neutrinos (Chen et al., 2023b). The extended oscillation period of bosons surrounding M87* results in cyclic neutrino fluxes characterized by an angular preference, particularly within the polar angle region. Given the potential of the ngEHT to identify a diverse range of SMBHs and measure their masses and spins, joint observations involving the ngEHT and high-energy neutrino observatories stand to effectively constrain a wider spectrum of scalar masses. Notably, the joint observation approach also enables the identification of astrophysical neutrino backgrounds originating from blazars (Kovalev et al., 2023).

4.5.2 Parametric instability of axion clouds

An important question is whether we understand well enough how couplings of ultra-light bosons with Standard Model particles affect the evolution of the superradiant instability and how taking all the effects into account can affect the observations. For example, Ikeda et al. (2019) considered as a starting point the action (11) with $V(a) = m_a^2 |a|^2/2$, describing a real massive (pseudo)scalar field with axionic couplings to the electromagnetic field in Equation (18). They found that above some critical value for the coupling constant $g_{a\gamma}$, axionic clouds around BHs can transfer an important fraction of their energy to the electromagnetic field due the development of a parametric instability. Their results can be translated into a maximum mass M_B that the cloud can reach:

$$\frac{M_B}{M} \sim \left(\frac{0.1}{M\mu}\right)^4 \left(\frac{2 \times 10^{-17} \text{ GeV}^{-1}}{g_{a\gamma}}\right)^2. \quad (21)$$

An important question is therefore how much of this phenomenology is important and whether plasma couplings can quench the instability due to the modified dispersion of electromagnetic waves in a plasma medium. This was partially studied in Sen (2018) and Boskovic et al. (2019). Considering the case of a cold plasma, the plasma frequency is given by:

$$\omega_p = \sqrt{\frac{4\pi n_e e^2}{m_e}} \approx 10^{-13} \left(\frac{n_e}{10^{-4} \text{ cm}^{-3}}\right)^{1/2} \text{ eV}, \quad (22)$$

with m_e , e and n_e denoting the mass, charge and number density of the free electrons, respectively. Taking $n_e \sim 10^4 - 10^8 \text{ cm}^{-3}$ from EHT observations of M87* (EHT Collaboration, 2021b), photons attain an effective mass of around $10^{-9} - 10^{-7.5} \text{ eV}$, which is much higher than the relevant axion masses $\sim 10^{-21} \text{ eV}$. Thus, one should expect the parametric instability to be highly suppressed.

There are, however, some caveats to this simplistic argument that warrant further study. For example, Sen (2018) showed that there can still be a small instability window at large couplings $g_{a\gamma}$ when m_a is much smaller than the plasma frequency. In addition, these analyses were done using a flat-space approximation and treating the interaction of the electromagnetic field and the plasma as simply giving the photon an effective mass, which might not be a good approximation to describe these systems (see, e.g., Cardoso et al., 2021b; Cannizzaro et al., 2021a,b). It is also known that non-linear plasma effects can open a transmission window in plasmas (Cardoso et al., 2021b) which could therefore allow the parametric instability to develop. Understanding how all these effects affect the superradiant instability is a challenging task, but one which is important to pursue.

4.5.3 Plasma heat-up from axion clouds in a magnetic field

In addition to the parametric instability discussed above, another important question is whether, in the presence of a background magnetic field and axion-photon couplings, the axion cloud can sufficiently heat up electrons/positrons/ions so as to terminate the superradiance process before the BH spins down or the field saturates the self-interaction limit. A similar process happens, for example, due to the kinetic mixing of dark photons with (normal) photons (Caputo et al., 2021).

To understand this problem using a flat-space approximation, it is useful to write the equations of motion for both the transverse electromagnetic field A_T and the axion field a in the presence of a background magnetic field B_0 in terms of Fourier modes:

$$\left\{ \vec{k}^2 - \omega^2 + \begin{pmatrix} \Omega_p^2 & \omega g_{a\gamma} B_0 \\ \omega g_{a\gamma} B_0 & m^2 \end{pmatrix} \right\} \begin{pmatrix} A_T \\ a \end{pmatrix} = 0, \quad (23)$$

where $\Omega_p^2 \equiv \frac{\omega_p^2}{1 + \frac{i\nu}{\omega}}$ and:

$$\nu = \frac{4\sqrt{2}\pi\alpha^2 n_e}{3m_e^{1/2} T_e^{3/2}} \log A_C \approx 3 \times 10^{-21} \text{ eV} \left(\frac{n_e}{0.04 \text{ cm}^{-3}} \right) \left(\frac{8000 \text{ K}}{T_e} \right)^{3/2}, \quad (24)$$

is the electron-ion collision rate contributing to the friction in the plasma. We can then solve Equation (23) to obtain the dissipation rate of the axion field in the plasma:

$$\gamma_a^I = \frac{g_{a\gamma}^2 B_0^2 \nu}{2\omega_p^2}. \quad (25)$$

Again taking EHT observations of M87* as an example, where it was found that $n_e \sim 10^4 - 10^8 \text{ cm}^{-3}$, $B_0 \sim 1 - 30 \text{ G}$ and $T_e \sim (1 - 12) \times 10^{10} \text{ K}$ (EHT Collaboration, 2021b), the dissipation rate of the axion field due to the heating up of the plasma is roughly:

$$\gamma_a^I \sim 10^{-53} \left(\frac{g_{a\gamma}}{10^{-12} \text{ GeV}^{-1}} \right)^2 \text{ eV}, \quad (26)$$

in the non-relativistic limit $|\vec{k}| \ll \omega$ (in this limit the result applies to the longitudinal mode of the photon as well). This is too small to stop superradiance. Whilst we employed a flat-space approximation, one expects that strong gravity effects will not change this picture considerably, although further studies are necessary to assess this.

5 Tests of GR and the Kerr hypothesis with the ngEHT

BHs in GR unavoidably harbor unphysical curvature singularities (Penrose, 1965; Hawking, 1966; Penrose, 1969; Hawking and Penrose, 1970; Penrose, 1972; Hawking and Ellis, 2011; Senovilla, 1998; Senovilla and Garfinkle, 2015). The question is therefore not *if* GR and the Kerr hypothesis break down, but rather *how* and *where* this break down occurs.

There is consensus that trans-Planckian curvature scales are governed by an as of yet unknown quantum theory of gravity which modifies the core of a BH (Ashtekar and Bojowald, 2005; Bojowald, 2007; Ellis et al., 2018). However, quantum-gravity effects may affect the structure of BH spacetimes at much lower curvature scales and even structure outside the horizon (Frolov and Vilkovisky, 1979, 1981; Hájíček, 1987, 2001, 2003; Ambrus and Hájíček, 2005; Almheiri et al., 2013; Barceló et al., 2014; Rovelli and Vidotto, 2014; Barceló et al., 2015; Haggard and Rovelli, 2016; Barceló et al., 2016; Giddings and Psaltis, 2018; Giddings, 2019; Bacchini et al., 2021; Eichhorn and Held, 2022). Furthermore, matter (itself potentially non-minimally coupled) within GR may form exotic compact, supermassive objects which could be found at the cores of galaxies (see Sec. 4). Finally, classical modifications of GR, i.e., so-called modified gravity theories, are being investigated (some motivated by questions in cosmology) and may contain BH solutions that differ from Kerr (see Sec. 5.1.1 as well as Berti et al., 2015; Cardoso and Pani, 2019, for reviews). In view of these many distinct theoretical possibilities, an observational program which pushes as far as possible into the strong-gravity/near-horizon regime is called for, in order to place constraints on theoretical proposals or even discover a deviation from GR.

The astrophysics challenge

A critical challenge for this program is set by the astrophysical environment of a SMBH: the Kerr hypothesis already technically breaks down for astrophysical BHs, since the Kerr solution is strictly a vacuum solution (Kerr, 1963; Newman and Janis, 1965; Newman et al., 1965; Bekenstein, 1972; Robinson, 1975; Chrusciel et al., 2012), yet SMBHs exist within an astrophysical environment typically composed of an accretion disk and relativistic jet outflows. This astrophysical environment is only partially understood, introducing a systematic uncertainty in the comparison between data and theory. Within GR a large body of literature is already devoted to an ever improving understanding of the accretion disk physics and the resulting observational images. Beyond GR it is a key outstanding challenge to achieve a commensurate level of control over the systematic uncertainties introduced by a BH's astrophysical environment.

Searching for a breakdown of GR vs testing modified gravity

There are two questions that we aim to answer with ngEHT observations. First, we ask whether GR fails, and second, we ask whether a modified theory of gravity performs better at explaining the observational data.

Within GR, there are clear predictions for the image of a BH (depending on the accretion disk properties). Exploring whether the observational data agrees with this expectation tests whether or not GR fails for this observation. Knowledge of theoretical predictions beyond GR is unnecessary for such a test.

Beyond GR, predictions for the image of a BH (or a horizonless spacetime) exist in part. Where they exist, it is possible to ask whether the given theory performs better than GR at explaining the data. It is our aim to ask this question as comprehensively

as possible. Controlling the systematic uncertainties arising from a BH’s astrophysical environment is essential to accomplish this task. Thus, we aim at completing the following program.

Confronting ngEHT observations with theoretical predictions

To compare predictions of modified theories of gravity with those of GR, we have to complete the following steps: (i) investigate the theoretical properties of objects/spacetimes beyond GR, in particular their shadows, (ii) examine images of these objects/spacetimes as they appear when illuminated by an accretion disk, and (iii) account for the capabilities of the ngEHT array.

We summarize progress on this program in several scenarios beyond GR in Sec. 5.1 and find that step (i) has already been completed for many objects/spacetimes beyond GR, where the critical curve (shadow boundary) has been calculated. This includes: gravity with Chern-Simons terms (Amarilla et al., 2010; Okounkova et al., 2019), Gauss-Bonnet gravity (Guo and Li, 2020; Konoplya and Zinhailo, 2020; Kumar and Ghosh, 2020; Wei and Liu, 2021), gravity coupled to nonlinear electrodynamics (Allahyari et al., 2020b), scalar-vector-tensor gravity (Moffat, 2015; Wang et al., 2019), tensor-vector gravity (Vetsov et al., 2018), braneworld settings (Amarilla and Eiroa, 2012; Eiroa and Sendra, 2018), Kaluza-Klein BHs (Amarilla and Eiroa, 2013), BHs inspired by asymptotically safe gravity (Held et al., 2019) and Loop Quantum gravity (Liu et al., 2020), regular BHs (Abdujabbarov et al., 2016; Amir and Ghosh, 2016; Tsukamoto, 2018; Stuchlík and Schee, 2019), naked singularities (Abdikamalov et al., 2019; Kumar et al., 2020b) and wormholes (Gyulchev et al., 2018; Brahma et al., 2021; Bouhmadi-López et al., 2021). See also Perlick and Tsupko (2022); Vagnozzi et al. (2023). These constraints have been derived through comparing the diameter of the critical curve obtained from theoretical considerations with the observational measurements of the diameter of the shadow image. We refer to these as *projected constraints*: they provide an estimate of the parameter ranges that an (ng)EHT array may constrain, once simulated images go beyond the critical curve and account for the presence of an accretion disk.

In fact, step (ii) has been partially achieved for some settings beyond GR, where most studies are limited to simple models of accretion disks (Shaikh et al., 2019b; Liu et al., 2021; Zeng et al., 2020; Bauer et al., 2022a; Dong et al., 2022a; Eichhorn and Held, 2021b; Gyulchev et al., 2021; Daas et al., 2022a) and a more limited number of covariant MHD simulations (Mizuno et al., 2018a; Olivares et al., 2020; Röder et al., 2022; Chatterjee et al., 2023b,c) are available. Step (iii) has only been achieved for very few settings (Vincent et al., 2021; Eichhorn et al., 2022a). Therefore, different theoretical scenarios are in different stages of development when it comes to readiness for comparison with actual observational data.

We then take a different approach and condense all these beyond-GR scenarios down to three general signatures which can be parametrically constrained. In Sec. 5.2 we discuss the resulting science cases with respect to the capabilities of the ngEHT.

Relations between ngEHT and other observational constraints

There are several observational programs that are currently making significant progress in constraining deviations from GR, most notably GW measurements (Abbott et al., 2017a,b,c, 2021a,b; The LIGO Scientific Collaboration et al., 2021). Their relation to ngEHT constraints is subject to two considerations. First, because GWs arise in the dynamical regime of a gravity theory, they can be challenging to simulate beyond GR,

such that a waveform catalogue that enables tests of modified-gravity theories is not yet available. In contrast, the ngEHT accesses the (mostly) stationary regime of the spacetime, where one only requires (spinning) stationary solutions of modified-gravity theories. Second, current constraints on deviations from GR from GW observations do not necessarily apply to SMBHs: unless BH uniqueness theorems hold, constraints on the metric of roughly solar-size BHs do not constrain the metric of SMBHs.

5.1 Scenarios for physics beyond GR

In Sec. 5.1.2, we turn to specific spacetimes and compact objects. We discuss various scenarios which: arise from quantum fluctuations, are motivated by quantum gravity, or feature violations of cosmic censorship.

Here, we review physics scenarios beyond GR and the resulting violations of the Kerr hypothesis, according to how it is circumvented. The ngEHT may also provide insight into particle physics beyond the Standard Model. Such new-physics effects typically involve minimally coupled exotic matter, and were discussed separately in Sec. 4. In Sec. 5.1.1 we discuss classical and quantum theories of modified gravity, including non-minimally coupled matter fields and effective field theory. In Sec. 5.1.2 we turn to specific spacetimes and compact objects: we discuss various scenarios which arise from quantum fluctuations, are motivated by quantum gravity, or feature violations of cosmic censorship.

In each subsection, we briefly summarize the theoretical motivation and observational status of the physics scenario beyond GR. We then summarize the state-of-the-art with respect to VLBI imaging, to point out where additional work is necessary to achieve readiness for future comparison with data. This includes, in particular, the question of whether potential ngEHT signatures have been studied in idealized scenarios or in more realistic settings which take into account astrophysical uncertainties and limitations in instrument capabilities.

We remain agnostic as to the theoretical viability of these scenarios. Instead, we take the point of view that observational constraints should guide the search for physics beyond GR.

5.1.1 Modified gravity

The assumption that AGNs are supermassive Kerr BHs rests on the field equations of GR, although the Kerr metric is also a solution of some theories beyond GR, e.g., if the action contains no Riemann invariants (Psaltis et al., 2008; Barausse and Sotiriou, 2008). The EFEs can be taken to follow from a theorem by Lovelock (1971). The theorem, in turn, relies on several assumptions and physics beyond GR, which may lead to alternative paradigms for AGNs and can be classified by how the theorem is circumvented (see, e.g., Pani et al., 2013; Berti et al., 2015). In particular, the theorem assumes: (i) spacetime is a differentiable manifold endowed with a metric, (ii) four spacetime dimensions, (iii) diffeomorphism symmetry, (iv) a local action principle, (v) equations of motion with (at most) second-order time derivatives, (vi) no gravitational degrees of freedom beyond the massless graviton, and (vii) no non-minimal coupling.

Assumption (i) is violated in many (although not all) approaches to quantum gravity. For instance, this gives rise to the fuzzball paradigm, see Sec. 5.1.2 in string theory. Nevertheless, many approaches to quantum gravity work with an effective spacetime

metric, that is constructed at a phenomenological level, e.g., in Loop Quantum Gravity (Ashtekar and Bojowald, 2006), or non-commutative spacetimes⁴. For BHs, this effective metric is typically regular (see Sec. 5.1.2).

In general, it is expected that at sufficiently low curvature scales, quantum effects can be captured in an effective action, even if the UV theory goes beyond the spacetime setting. Within approximations, this effective action is (partially) known, e.g., in string theory (Gibbons and Maeda, 1988; Garfinkle et al., 1991; Sen, 1992), asymptotically safe quantum gravity (e.g., Bonanno et al., 2020) and causal dynamical triangulations (e.g., Loll, 2020). At this level, quantum and classical theories can be treated on the same footing.⁵

In the following, we review how different modifications violate the assumptions of Lovelock’s theorem and discuss the state of maturity of different studies of BH shadows in these various settings.

In settings with extra dimensions, the solutions with an event horizon (see Empanan and Reall, 2008, for a review), can be projected onto four-dimensional spacetime, in which they appear as four-dimensional BHs with a modified line element. Modifications to the critical curve have been investigated (Amarilla and Eiroa, 2012; Papnoi et al., 2014; Singh and Ghosh, 2018; Amir et al., 2018; Long et al., 2019) and *projected constraints* have been obtained using EHT results (Banerjee et al., 2020; Vagnozzi and Visinelli, 2019).

Projected constraints on theories with violations of Lorentz-invariance (or more generally diffeomorphism symmetry, e.g., Barausse et al., 2011) have been obtained in Ding et al. (2020), Khodadi and Saridakis (2021), Vernieri and Sotiriou (2012), and Sotiriou et al. (2014). Moreover, they have been found to exhibit a nested structure for trapping horizons as a function of the frequency of the photons that follow the null geodesics (Carballo-Rubio et al., 2022b). It is an open question as to whether the same statement holds for the photon sphere. If that is indeed the case, tests of achromaticity of the emission ring could constrain violations of Lorentz invariance in gravity. Such Lorentz-invariance violations are already strongly constrained by other observations (e.g., Emir Gümürükçüoğlu et al., 2018; Gupta et al., 2021).

In a four-dimensional diffeomorphism-invariant setting, one can circumvent the Lovelock theorem by modifying the action. A restriction to second-order field equations ensures the absence of potential (Ostrogradski) ghost instabilities and significantly constrains the allowed set of interactions. The converse is not true: if the equations are higher than second order, the theory does not automatically have ghost instabilities.

General theories of ghost-free interactions between gravity and a scalar, so-called scalar-tensor theories (Horndeski, 1974; Deffayet et al., 2011), between gravity and a

⁴ See (Vagnozzi et al., 2023) for *projected constraints* on non-commutativity derived by confronting calculations of the critical curve with observations

⁵ One may expect that quantum-gravity effects are generically tied to higher curvature scales than classical modifications of GR. However, this expectation has been challenged in, e.g., Frolov and Vilkovisky (1979, 1981); Hájíček (1987, 2001, 2003); Ambrus and Hájíček (2005); Almheiri et al. (2013); Barceló et al. (2014); Rovelli and Vidotto (2014); Barceló et al. (2015); Haggard and Rovelli (2016); Barceló et al. (2016); Giddings and Psaltis (2018); Giddings (2019); Bacchini et al. (2021); Eichhorn and Held (2022). Equating the scale of quantum gravity to the Planck scale is, in fact, a simple dimensional estimate which does not use any information whatsoever on the gravitational dynamics. It may thus not do justice to the actual theory of quantum gravity which may, e.g., (i) not follow naturalness arguments and have a scale different from the Planck scale, or (ii) have several dynamical scales.

vector, so-called vector-tensor theories (Heisenberg, 2014; de Rham and Pozsgay, 2020), and between gravity and a second (potentially massive) tensor mode, so-called bimetric or massive gravity theories (de Rham et al., 2011; Hassan and Rosen, 2012), have been constructed with second-order equations of motion. Theories with higher-order equations of motion but without Ostrogradski instability include infinite-derivative gravity (Biswas et al., 2006; Modesto, 2012; Biswas et al., 2012). Theories with higher-order equations of motion include, e.g., Stelle’s higher derivative gravity (Stelle, 1978), in which spherically-symmetric BH solutions have been found numerically (Lu et al., 2015; Podolský et al., 2020). In this theory, BHs with small enough horizon suffer from a classical long-wavelength instability (Brito et al., 2013; Held and Zhang, 2023).

Such theories with higher-order equations of motion can also be interpreted as the leading-order terms in an effective field theory (EFT) (Endlich et al., 2017; Cardoso et al., 2018b; de Rham et al., 2020), which may, for instance, arise from integrating out quantum fluctuations in a quantum theory of gravity. An EFT includes interactions order-by-order and is only valid up to a cutoff scale at which interactions of yet higher order can no longer be neglected. In the EFT (some of) the additional degrees of freedom, associated instabilities, and the new BH branches, may thus be an artefact of extrapolating the EFT beyond its regime of validity.

The existence of a (perturbative) EFT parameter can facilitate the order-by-order extension of some of the properties/theorems of GR to larger classes of modified-gravity theories, e.g., Xie et al. (2021) for the example of circularity. In these settings, more image features are likely to be shared between GR and the beyond-GR theory.

Black-hole uniqueness and ngEHT prospects

Beyond GR, BH uniqueness may be violated (Sotiriou and Faraoni, 2012). Kerr BHs remain a solution of a subclass of these theories (see, e.g., Ben Achour and Liu, 2019; Motohashi and Minamitsuji, 2019). Generically, if curvature invariants built from the Riemann tensor are absent in the action, it is straightforward to show that solutions of GR remain solutions (Psaltis et al., 2008; Barausse and Sotiriou, 2008). This includes a large class of nonlocal theories of gravity (Li et al., 2015). Such theories can therefore be more challenging to constrain with the EHT. Other modifications deform Kerr BHs (Yunes and Pretorius, 2009; Yunes and Stein, 2011; Yagi et al., 2012; Herdeiro and Radu, 2014, 2015b; Silva et al., 2018; Ayzenberg and Yunes, 2018) and/or admit additional BH branches (Lu et al., 2015; Podolský et al., 2020).

If BH uniqueness holds, all astrophysical constraints on modifications of GR at different scales (Yunes and Siemens, 2013; Will, 2014; Berti et al., 2015) should be accounted for. For modifications which are tied to local curvature scales, the EHT and ngEHT probe a regime which is already constrained by GW and Solar System observations (Glampedakis and Pappas, 2021). If BH uniqueness is violated, the ngEHT is uniquely positioned to test modifications of GR on scales associated with AGNs.

Spherically-symmetric black holes and VLBI observations

Most of the known explicit BH solutions in modified gravity are restricted to spherical symmetry. For many of these, spherically-symmetric deviations in the critical curve have been quantified (Ayzenberg and Yunes, 2018; Allahyari et al., 2020b; Konoplya and Zhidenko, 2019; Konoplya et al., 2020; Shaikh, 2019; Zhu et al., 2019; Islam et al., 2020; Khodadi et al., 2020; Konoplya and Zinhailo, 2020; Kumar et al., 2020a; Guo and Li, 2020); see also Perlick and Tsupko (2022) for a recent review.

In spherical symmetry, there is a degeneracy between modified-gravity effects and the mass-to-distance ratio of a given BH (Kocherlakota and Rezzolla, 2022). A second independent mass measurement is required to break this degeneracy. Moreover, all deviations in the critical curve are degenerate across all the different modified theories of gravity (Kocherlakota et al., 2021; Vagnozzi et al., 2023). Breaking at least some of this degeneracy is achievable using finite-order lensing features such as photon rings (e.g., Wielgus, 2021; Kocherlakota et al., 2023).

A much smaller set of theories has been investigated by the use of disk models and resulting photon rings, which includes theories in which a scalar field couples to the Gauss-Bonnet or the Pontryagin invariant (Zeng et al., 2020; Bauer et al., 2022a), as well as Stelle’s higher-derivative gravity (Daas et al., 2022a). Modifications of the emission spectrum and the Blandford-Znajek process have been investigated by Liu et al. (2021) and Dong et al. (2022a), respectively. Even less is known about full (GR)MHD simulations which have been performed for Einstein gravity coupled to additional matter fields in Mizuno et al. (2018a) and Röder et al. (2022). More recent (GR)MHD simulations of spinning (axisymmetric) BHs have been performed in Chatterjee et al. (2023b,c). In general, degeneracy is expected between modifications of the spacetime and properties of the astrophysical environment, making such studies critical. In particular, it may be the case that the *projected constraints* are overly optimistic. Marginalizing over astrophysical parameters may significantly weaken the constraints (Cardenas-Avendano et al., 2019).

Spinning black holes and VLBI observations

Spinning BHs beyond GR have been constructed with the Janis-Newman algorithm (Janis et al., 1968). See Capozziello et al. (2010); Modesto and Nicolini (2010); Bambi and Modesto (2013); Azreg-Aïnou (2014); Toshmatov et al. (2014); Kumar and Ghosh (2020); Wei and Liu (2021) for examples. We note that it is not generally expected that the Janis-Newman algorithm is valid in modified-gravity theories (Drake and Szekeres, 2000; Hansen and Yunes, 2013).

In some theories, BH solutions have been explicitly extended to the case of slow spin (Yunes and Pretorius, 2009; Cano and Ruipérez, 2019). Some axisymmetric solutions have been numerically constructed for arbitrary spin (Kleihaus et al., 2011, 2016; Fernandes and Mulryne, 2022) but full analytical solutions are not yet known. In the few cases in which spin has been explored, there is no hidden (Carter-like) constant of motion (Owen et al., 2021). Moreover, some theories can break reflection symmetry about the equatorial plane (Cardoso et al., 2018b; Cano and Ruipérez, 2019; Chen and Yang, 2022), and others can break circularity (Ben Achour et al., 2020), cf., Sec. 5.2.2. It remains an important open question as to how far (some of) these properties can be tied to generic image features.

Open challenges

The open challenges to further quantify the constraining power of the ngEHT for modified gravity theories are as follows.

- Go beyond spherical symmetry in solutions to modified theories of gravity and account for spin – this will allow breaking of degeneracy in the Kerr mass and potentially even between different modifications.

- Determine which modified-gravity theories break BH uniqueness and admit (stable) non-Kerr BH branches – this identifies a class of theories for which Solar System and GW constraints need not apply.
- Go beyond calculations of the critical curve and instead simulate images, using simple disk models in a first step, and full GRMHD simulations, ideally including polarization and frequency dependence, in a second step.
- Understand degeneracies between modifications of GR and properties of a BH’s astrophysical environment.

5.1.2 Specific spacetimes and compact objects beyond GR

In addition to the explicit BH solutions in modified gravity (see Sec. 5.1.1), several classes of spacetimes have been motivated by theoretical considerations both in and beyond GR.

Exotic compact objects from semi-classical physics

Gravastars (Mazur and Mottola, 2001, 2004; Cattoen et al., 2005; Chirenti and Rezzolla, 2007) are expected to form if quantum fluctuations become so sizable during gravitational collapse that they trigger a phase transition to spacetime regions with an effective stress-energy tensor which violates energy conditions. The viability of such a formation mechanism is debated in the literature (Chen et al., 2018). After formation, the resulting stationary spacetime is effectively described by several radial shells with distinct effective stress-energy tensors.

In the simplest effective gravastar geometries (Visser and Wiltshire, 2004), an exterior asymptotically flat vacuum solution to GR is glued to an interior de-Sitter patch. The interior and the exterior are connected by a thin shell of energy-condition violating matter which facilitates smooth matching. More recently, gravastars with AdS interior have been constructed (Danielsson et al., 2017).

Spinning gravastars have been constructed in the slow-rotation limit by perturbing non-rotating spacetimes (Cardoso et al., 2008; Pani, 2015; Danielsson and Giri, 2018) and are subject to an ergoregion instability (Friedman, 1978).

Semi-classical relativistic stars have also been proposed as a possible endpoint of gravitational collapse, being supported by the most elementary form of quantum pressure provided by gravitational vacuum polarization (Visser et al., 2008; Barceló et al., 2009; Carballo-Rubio, 2018). As with gravastars, proposals for formation mechanisms (Barcelo et al., 2008; Barceló et al., 2016) are only partially understood.

Contrary to gravastars, which have a vacuum core in which the equation of state is $p = -\rho$, semi-classical relativistic stars are formed by a delicate energetic balance between matter and vacuum polarization, and can thus have different equations of state (Ho and Matsuo, 2018; Arrechea et al., 2021, 2022). Due to technical limitations in our knowledge of quantum field theory on rotating backgrounds (Ottewill and Winstanley, 2000; Zilberman et al., 2022a,b), spinning solutions are still to be obtained.

Regular black holes

In some approaches to quantum gravity (Donoghue, 1994; Reuter, 1998), quantum fluctuations have been found to weaken the gravitational force, lead to geodesic defocusing, and thus provide a natural mechanism for singularity resolution. Thus, regular BHs, both spinning (e.g., Reuter and Tuiran, 2011; Bambi and Modesto, 2013; Neves

and Saa, 2014; Toshmatov et al., 2014; Azreg-Aïnou, 2014; Ghosh and Maharaj, 2015; Brahma et al., 2021; Mazza et al., 2021; Eichhorn and Held, 2021a; Franzin et al., 2022) and non-spinning (e.g., Bonanno and Reuter, 2000; Nicolini, 2009; Gambini and Pullin, 2013; Ashtekar et al., 2018; Platania, 2019; Bodendorfer et al., 2019, 2021a,b), have been constructed or motivated in multiple approaches to quantum gravity.⁶

On a more phenomenological level, regular BHs have been put forward in, e.g., Dymnikova (1992) and Hayward (2006), and reviewed in Ansoldi (2008). They also arise as solutions to GR coupled to non-linear electrodynamics (Ayon-Beato and Garcia, 1998). They can also be regarded as a useful paradigm for beyond-GR-spacetimes, given that they resolve one (of several) problematic aspects of BHs in GR, namely the curvature singularity (though not necessarily the Cauchy horizon). There are still open questions regarding their dynamical evolution due to the exponential mass inflation instability (Brown et al., 2011; Frolov and Zelnikov, 2017; Carballo-Rubio et al., 2018a, 2021; Barceló et al., 2022), which is generic but for a specific set of geometries (Carballo-Rubio et al., 2022b).

Generically, regular BHs come with (at least) one free parameter that determines the curvature scale at which deviations from Kerr become sizable (e.g., Held et al., 2019; Contreras et al., 2020; Kumar et al., 2019; Li et al., 2020; Kumar et al., 2020c; Kumar and Ghosh, 2021; Kumar et al., 2020b; Eichhorn et al., 2022b). Parameter values of order 1% in these models lead to $\mathcal{O}(0.1\%)$ effects at the horizon and correspondingly somewhat smaller effects at the photon sphere and on the shadow (see, e.g., Kocherlakota et al., 2021; Eichhorn et al., 2022b). Such parameter values arise if the scale of new physics corresponds to curvature radii of the order of the gravitational radius, and hence to scales far above the Planck scale. This could be, for instance, a consequence of the back-reaction associated with mass inflation (Barceló et al., 2022; Carballo-Rubio et al., 2022).

Key image features of regular BHs (see, e.g., Abdujabbarov et al., 2016; Eichhorn and Held, 2021b,a; Lima et al., 2021; Islam et al., 2021; Eichhorn et al., 2022b) are: (i) at fixed mass, the diameter of the critical curve, as well as all photon rings of regular BHs, is smaller than for a Kerr BH, (ii) the relative photon-ring separation increases, (iii) at finite spin (and non-face-on inclination), the photon-ring shape deviates from Kerr and can, in non-circular⁷ regular BHs, become non-reflection-symmetric about the horizontal image axis and feature cusps and dents.

Property (i) is testable with the ngEHT, if an additional, independent mass measurement is used, e.g., from stellar orbits. In fact, the EHT observation of M87* already provides a first constraint on a regular BH with particularly large deviations from Kerr (Eichhorn et al., 2022b), while other regular BHs remain unconstrained (Kocherlakota et al., 2021). Property (ii) may be testable for some regular BHs (Eichhorn et al., 2022b), where estimates show that the separation between $n = 1$ and $n = 2$ photon rings may reach several μas (for a shadow diameter corresponding to that of M87*), cf., Sec. 5.2.4. Superresolution techniques may be particularly useful to constrain such regular BHs. Properties (iii) and (iv) are likely beyond the reach of ngEHT, although studies accounting for finite resolution have not been conducted yet.

⁶ This is possible within an *effective* metric setting even in quantum-gravity approaches where spacetime is not a smooth manifold at high curvature scales (see, e.g., Ashtekar and Bojowald, 2006; Modesto, 2004, 2006; Hossenfelder et al., 2010; Gambini and Pullin, 2013; Rovelli and Vidotto, 2014; Ashtekar et al., 2018).

⁷ The term “circular” here refers to a technical property of the spacetime.

In addition, the overall lensing structure of these spacetimes differs from Kerr, therefore a spacetime tomography approach (Broderick and Loeb, 2005, 2006; Tiede et al., 2020; Wong, 2021) is also likely to provide constraints on regular BHs. Studies of localized emission regions around regular BHs are, however, currently in their infancy (Eichhorn et al., 2022b). Further, there may be polarization signatures (Liu et al., 2022), which is also not yet well-explored.

Fuzzballs

In string theory, BHs are argued to be replaced by an exotic compact object (ECO), i.e., a fuzzball. Fuzzballs have been motivated by the individual microstates of fluctuating BH geometries in string theory (Mathur, 2005; Hertog and Hartle, 2020; Mayerson, 2020). For a specific class of five-dimensional extremal BHs, the relevant microstates have been shown to successfully reproduce the Bekenstein-Hawking entropy (Strominger and Vafa, 1996; Callan and Maldacena, 1996). Some individual microstate geometries turn out to be regular and horizonless (Balasubramanian et al., 2008). The fuzzball paradigm conjectures that classical BH geometries are the coarse-grained superposition of these individual microstates. In view of classical instabilities (Keir, 2019; Cardoso et al., 2014a; Eperon et al., 2016; Marolf et al., 2017), stability remains an open question. Uncharged, non-supersymmetric, and four-dimensional microstate geometries of direct relevance for astrophysical BHs are challenging to construct (see Bah et al., 2021, for a recent construction of charged, four-dimensional, and non-supersymmetric microstate geometries). The latter break reflection symmetry about the equatorial plane which suggests an asymmetry in their shadows. Moreover, these geometries do not exhibit an ergosphere, which poses a challenge with regard to a viable jet-launching mechanism.

Ray-traced images of the celestial sphere in charged solutions of supergravity interpreted as effective fuzzball geometries have been computed in Bacchini et al. (2021). When a deformation parameter is tuned towards the extremal BH limit, geodesics that enter the interior of the effective fuzzball geometry encounter increasingly large curvature close to timelike surfaces of infinite redshift. The growing redshift (between an emission region at high curvature and an observer at asymptotic infinity) has been argued to increasingly darken the appearance of these effective fuzzball geometries (Bacchini et al., 2021). Quantifying this conjectured darkening could provide a route to constrain the deformation parameter.

Non-hidden wormholes and naked singularities

We refer to non-hidden wormholes as spacetimes with two (or more) asymptotically flat regions which are not separated by a horizon. Similarly, we refer to naked singularities as asymptotically flat spacetimes with a curvature singularity which is not hidden by a horizon. Such objects can even occur as vacuum solutions of GR: for instance, the Kerr solution itself can describe a naked singularity if the spin parameter exceeds its extremal value, i.e., $|a_*| > 1$. Whether or not naked singularities can dynamically form is connected to cosmic censorship (Wald, 1999). Their physical viability is questioned by severe theoretical shortcomings such as geodesic incompleteness and/or closed timelike curves (Morris and Thorne, 1988). Nevertheless, they provide a useful testing ground to understand the capabilities of an ngEHT array. Non-hidden wormholes also arise from regular BHs, at sufficiently large values of the regularization parameter. In the limit of near-critical spin, even Planck-scale modifications of GR can result in a horizonless spacetime (Eichhorn and Held, 2022).

Images of naked singularities strongly depend on whether or not they feature a photon sphere. If they do, they can cast a critical curve that may be similar to that of a BH and the respective deviations in the critical curve have been quantified (Abdikamalov et al., 2019; Kumar et al., 2020b; Nguyen et al., 2023). If they do not possess a photon sphere, there may still be strong-lensing effects, but image features typically appear more distinct from BHs (Shaikh et al., 2019b). Accretion physics around naked singularities has been investigated in Joshi et al. (2011, 2014), finding potentially detectable differences in the high-frequency tail of the emission spectrum. Accretion disks around naked singularities have been investigated in Gylulchev et al. (2019, 2020), Shaikh and Joshi (2019), and Deliyiski et al. (2023).

In distinction to naked singularities, non-hidden wormholes need not contain curvature singularities. In contrast to BHs, they do not feature event horizons, irrespective of whether or not they have a photon sphere. Discriminating between wormholes and BHs via VLBI imaging is still not straightforward, at least at present angular resolutions. Indeed, it has been shown that many wormholes have unstable photon orbits and are able to cast critical curves very similar to BHs, even though in most models the critical curves have a smaller size than those of BHs with the same ADM mass (Bambi, 2013; Gylulchev et al., 2018; Amir et al., 2019; Brahma et al., 2021; Bouhmadi-López et al., 2021). One promising signature to probe wormholes from their images is based on the fact that the observers may see photons falling into the mouth of their side, then reflected either from the throat or from the potential barrier near the photon sphere on the other side of the throat. Even the photons directly from the other side could be detectable. Typically, the combination of these effects would form multiple light rings inside the dark spot of the image (Shaikh et al., 2019a; Wang et al., 2020; Wielgus et al., 2020; Peng et al., 2021), see also Deliyiski et al. (2022) for the effect of polarization. After blurring due to imperfect resolution, these effects appear as an overall enhancement of intensity within the dark spot (Ohgami and Sakai, 2015, 2016; Paul et al., 2020; Vincent et al., 2021; Guerrero et al., 2021; Eichhorn et al., 2022a). This can be used to distinguish the images of wormholes from those of BHs with an ngEHT array, even though the EHT may not achieve this.

5.1.3 *New-physics effects in light propagation and matter dynamics*

Most studies to-date of settings beyond GR account for changes in the spacetime, but use the standard form of the geodesic equation for ray tracing and, where considered, GR dynamics for the accretion disk. Going beyond GR, the geodesic equation can also, in principle, be modified. For instance, it has been known since the seminal work of Drummond and Hathrell (1980) that quantum effects can modify the propagation of light: quantum fluctuations of charged matter fields, most importantly the electron, give rise to the Euler-Heisenberg effective action, which exhibits terms that couple the electromagnetic field strength-tensor to the Ricci scalar, Ricci tensor and Riemann tensor. Even though for GR BHs, the latter term is negligible; for BHs beyond GR, Ricci-flatness need not hold and all three terms may be present. Drummond and Hathrell (1980) found that gravitational lensing in the Schwarzschild metric becomes polarization dependent through such terms, although of an unmeasurably small amount for the Solar System – the case may be different for BHs, although a quick estimate of the type of term, $F^2 R_{\mu\nu\kappa\lambda} R^{\mu\nu\kappa\lambda} \frac{\hbar^2}{m_e^2 c^2}$, indicates that it remains a tiny correction to classical electrodynamics even close to the horizon of a supermassive BH. On the one hand, this particular example, which arises within Quantum Electrodynamics on a

classical GR background, serves as a reminder that quantum effects, may in principle modify the propagation of light through a given geometry. Therefore, working with the standard geodesic equation, as is done in most of the literature, may turn out to be a restriction on the physics beyond GR. On the other hand, the example highlights that within quantum field theory on a GR background, such effects are likely completely negligible. However, there are settings, such as, e.g., regular BHs with large values of the deviation parameter, in which the new-physics scale is rather low. In such settings, the new physics may also affect the propagation of matter. Assuming the standard null geodesic equation when calculating the image of such BHs may thus amount to a certain amount of tuning, in that the new-physics scales in the geometry and the matter sector differ from each other.

Besides quantum effects, classical modifications that involve non-minimal coupling between the electromagnetic field strength and curvature terms may lead to deviations in the geodesic equation. In Bertolami et al. (2008) it has been shown, however, that coupling an arbitrary function of the curvature scalar to the matter Lagrangian only leads to modifications of the massive geodesic equation, not the massless one. Such terms therefore affect the dynamics of the accretion disk, but not the propagation of photons. As a second example, Allahyari et al. (2020a) consider a Horndeski coupling between photons and curvature and perform a parametric estimation of effects on the BH shadow, from which they constrain the corresponding coupling.

To the best of our knowledge, a systematic inclusion of new physics in the propagation of photons and the dynamics of the accretion disk has not yet been attempted. Such investigations must of course also account for experimental and observational constraints from various other settings, including astrophysical observations as well as laboratory tests.

Violations of Lorentz symmetry resulting in a modified dispersion relation for photons could in principle lead to potentially observable signatures when images at different frequencies are available. This can be quantified considering a generic modified dispersion relation (Colladay and Kostelecky, 1998; Liberati and Mattingly, 2016):

$$E^2 = (cp)^2 + f^{(n)} \frac{(cp)^n}{M_{\text{P}}^{n-2}}, \quad n > 2. \quad (27)$$

The group velocity c_{g} is given by:

$$c_{\text{g}} = \frac{\partial E}{\partial p} = c \left(\frac{cp}{E} + \frac{n}{2} \frac{f^{(n)}}{M_{\text{P}}^{n-2}} \frac{(cp)^{n-1}}{E} \right) = c_{\text{p}} \left(1 + \frac{n}{2} f^{(n)} \frac{(cp)^{n-2}}{M_{\text{P}}^{n-2}} \right), \quad (28)$$

where we have defined the phase velocity $c_{\text{p}} = c^2 p / E$. For two values of momenta p_1 and p_2 , there is a displacement of the photon sphere:

$$\Delta r_{\text{ph}} = 3GM \left| \frac{1}{c_{\text{g},1}^2} - \frac{1}{c_{\text{g},2}^2} \right|. \quad (29)$$

We can estimate the order of magnitude of the constraints that can be placed on $|f^{(n)}|$, for a given value of $n > 2$, by equating the displacement above with the angular resolution of ngEHT (there will be a numerical difference between the radius of the photon sphere and the apparent size of the photon ring, but both have the same scaling with the group velocity). For frequencies of 230 and 345 GHz, respectively, the deviation in the speed of propagation from the relativistic speed of light is of the order 10^{-23} ,

which does not lead to a detectable effect in the achromaticity of the photon ring. In fact, such modified dispersion relations for photons are already tightly constrained (with the leading-order term constrained to be transplanckian) with other observations (Addazi et al., 2022).

5.2 Science cases

As summarized above, many of the compact objects motivated in various beyond-GR scenarios share qualitatively common features among each other that distinguish their shadow images from the Kerr case, at least in principle. Here, we delineate a program to test the following generic features.

- First, horizonless objects such as boson stars, gravastars, fuzzballs as well as horizonless regular spacetimes, non-hidden wormholes and naked singularities, may mimic the *central brightness depression* of a BH. However, the central brightness depression is typically less pronounced than for a BH. Accordingly, a high dynamic range enables a better distinction of BHs from these horizonless spacetimes, cf., Sec. 5.2.1.
- Second, BHs beyond GR (both singular ones that may occur in modified-gravity theories and regular ones that may be motivated by quantum gravity) often feature deformations of the $n = 1$ (and higher-order) photon ring, some of which are non-degenerate with the spin. Thus, a high-enough resolution and confident extraction of the lensed emission may constrain *parametric deviations* from Kerr spacetime, cf., Sec. 5.2.2.
- Third, all BHs cast an *inner shadow*⁸, i.e., a central dark image region which is bounded by the direct image of the horizon, cf., Sec. 5.2.3. Just like the photon ring(s), the inner shadow can be deformed in shape and size in scenarios beyond GR.
- Fourth, some alternative spacetimes can lead to a significantly larger separation between different photon rings (in comparison to the Kerr spacetime). This applies to horizonless spacetimes and the respective occurrence of inner photon rings. It also applies to a potential distinction between the $n = 1$ and the $n = 2$ photon rings. Observational searches of *multi-ring structures*, cf., Sec. 5.2.4, can thus constrain deviations from GR, even if the $n = 2$ photon ring of the Kerr spacetime remains unresolvable.

This motivates testing for such image features without theoretical bias and, where possible, in systematic parameterizations beyond GR. Below, we summarize the current status of this effort. It is important to keep in mind that testing GR with spacetime images is a fast-evolving field. Thus, the above list of signatures may not be exhaustive and further promising image features may be added to the ngEHT effort in the future.

5.2.1 Horizonless spacetimes and their central brightness depression

In GR, the defining characteristic of a BH is its horizon, a one-way membrane that can only be crossed inwards. This behavior is a paradigmatic illustration of the strength

⁸ Diffuse foreground emission can obscure the inner shadow.

of the gravitational interaction in its nonlinear regime, and is therefore of essential importance as a test of GR and the Kerr hypothesis.

While this short introduction does not aim at capturing the important technical details in the mathematical definition of horizons, it is important to stress that there are several definitions that have differing motivation and scope. The prevailing definition, both for historical and popularity reasons, is the notion of an event horizon (Penrose, 1969; Hawking, 1976; Hawking and Ellis, 2011). This definition has nevertheless several important drawbacks, which includes its global nature and the associated impossibility of observing an event horizon in any physical experiment (Visser, 2014). This has motivated the search for quasi-local definitions of horizons, such as apparent, dynamical or trapping horizons, which can be coincident depending on the situation (Hayward, 1994; Ashtekar and Krishnan, 2004; Gourgoulhon and Jaramillo, 2008).

In general, any horizonless spacetime can thus be modelled by coefficients that quantify (i) absorption (κ), (ii) reflection (Γ), (iii) re-emission ($\tilde{\Gamma}$), and (iv) transmission (τ) of the central region (cf., Carballo-Rubio et al., 2022a). These coefficients satisfy a sum rule $\kappa + \Gamma + \tilde{\Gamma} + \tau = 1$ coming from energy conservation. In spherical symmetry, we can also define an effective radius R of the central object. These parameters take different values depending on the model being considered, and are associated with different image features as we will discuss in more detail below. We already know from GR that total absorption ($\kappa = 1$) results in a central brightness depression. The more dominant the absorption gets, the closer the horizonless object will mimic a BH. Thus, no experiment can exclude the possibility of horizonless spacetimes. However, the ngEHT will tighten experimental constraints on these coefficients. Such quantitative constraints are crucial since they can exclude beyond-GR scenarios in which the resulting horizonless objects are predicted to exceed these constraints.

In this section, we will describe the image features associated with each of these coefficients Γ , $\tilde{\Gamma}$ and τ , as well as analyzing their observability. The brightness of these features is linearly proportional to the corresponding coefficient, but their characteristics are a function of the effective radius of the horizonless object. The linearity of the problem implies that we can discuss these features independently, focusing on one of them at a time without loss of generality.

- The effective radius R can be constrained to be below $R \lesssim 3 r_g$ if the ngEHT finds clear evidence of a photon ring (see Sec. 2 for a detailed discussion).
- Reflection on a physical surface has been studied, and compared with EHT images for some values of the coefficients R and Γ , in EHT Collaboration (2022d) and Carballo-Rubio et al. (2022a), the latter providing an extensive exploration of the parameter space, and a quantitative analysis of the observability of these features by EHT and a tentative ngEHT configuration based on the corresponding values of angular resolution and dynamic range. The horizonless spacetime metric in that case is a spherically symmetric shell that reflects a fraction Γ of all incoming rays. For ultracompact objects, simulated images show an inner set of photon rings, cf., upper panels in Figure 17, which cannot be resolved by the EHT as the application of a Gaussian filter shows (lower panels). On the other hand, improvements in image dynamic range and angular resolution such as those expected to be achievable by the ngEHT can noticeably change the situation, leading to a constraint $\Gamma \lesssim 10^{-1}$, at least for $i = 0^\circ$ (see Figure 18).
- Re-emission from a physical surface has been also studied in Carballo-Rubio et al. (2022a) within the framework of the same spherically symmetric model and using

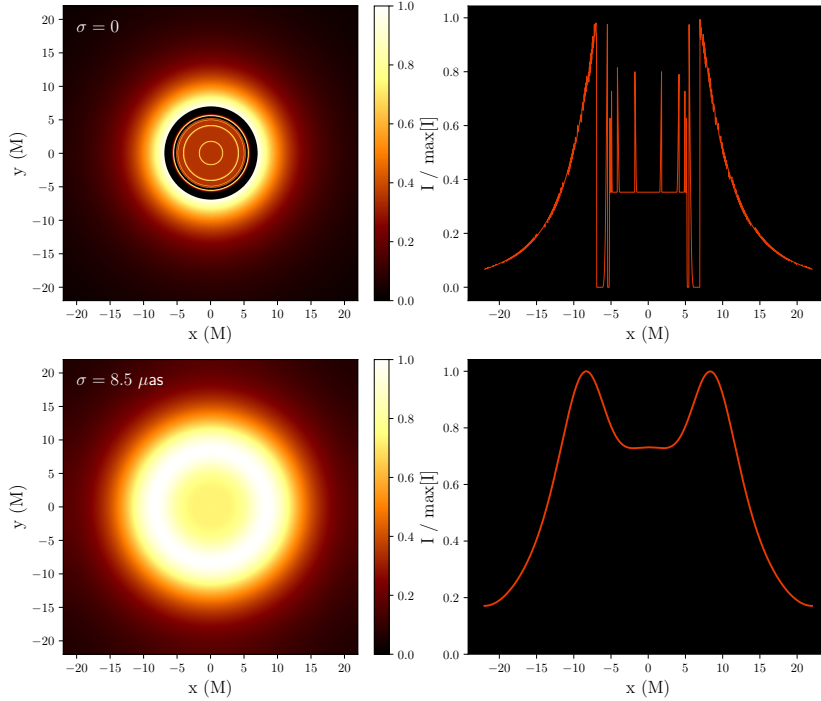


Fig. 17 Images of spacetimes where specular reflection takes place, but with partial absorption ($\Gamma = 0.5$) and an intrinsic brightness ($\eta = 10^{-2}$) included. We take an inclination $i = 0^\circ$, $\epsilon = 10^{-3}$, without filter (top row) and a Gaussian filter with the EHT angular resolution of $20 \mu\text{as}$ (bottom row). We see that these values of η change appreciably the structure of the central depression in brightness.

the same tools to assess the observability of the corresponding features, that take the form of a central region with uniform brightness. As shown in Figure 17, the size of the novel features associated with re-emission can be large enough that even the angular resolution of EHT is enough to pick up these features. In fact, for the ideal situation of $i = 0^\circ$, it is possible to constrain the re-emission channel ($\eta \lesssim 10^{-3}$), but not the specular reflection channel. On the other hand, improvements in image dynamic range and angular resolution such as those expected to be achievable by the ngEHT can greatly improve the situation, leading to more stringent constraints on the re-emission channel ($\eta \lesssim 10^{-4}$) and specular reflection channel ($\Gamma \lesssim 10^{-1}$), at least for $i = 0^\circ$ (see Figure 18).

In addition, infrared observations constrain re-emission from a physical surface. For instance, Sgr A* and M87* cannot have a physical surface that is in equilib-

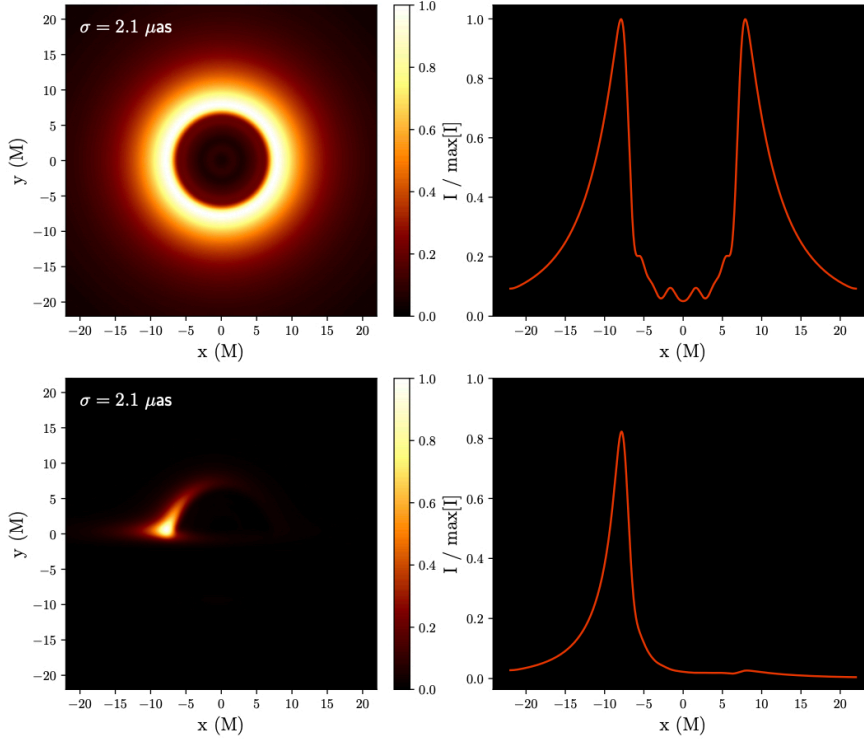


Fig. 18 Results of applying a Gaussian filter with an angular resolution of $5 \mu\text{as}$ for $\epsilon = 10^{-3}$, $\Gamma = 0.5$, $\eta = 10^{-3}$, $i = 0^\circ$ (top row) and $i = 85^\circ$ (bottom row). The optimistic value of angular resolution of $5 \mu\text{as}$ can pick up the innermost structure of the simulated image. However, higher inclination angles make it more difficult to discern the features associated with the existence of a surface.

rium with the surrounding accretion environment (Broderick and Narayan, 2006, 2007; Narayan and McClintock, 2008; Broderick et al., 2009, 2015). However, gravitational lensing may prevent sufficiently compact objects from reaching equilibrium (Lu et al., 2017; Cardoso and Pani, 2017; Cardoso and Pani, 2019). Furthermore, more complete descriptions of the behavior of the surface, including rotation (Zulianello et al., 2021) and absorption (Carballo-Rubio et al., 2018b, 2022a), can have an important impact on the features of the re-emitted radiation and delay reaching equilibrium, respectively. Together with available lower bounds on R (Carballo-Rubio et al., 2018c), such considerations can reduce the allowed parameter space (see also Sec. 4 in EHT Collaboration (2022d) for Sgr A*).

- The case without surface and with full transmission was recently investigated in Eichhorn et al. (2022a), including a quantitative analysis of the capabilities of a tentative ngEHT configuration. The horizonless spacetime metric in that case is an overspun, regular BH with Planck-sized deviations from the Kerr spacetime. Simulated images show an inner set of photon rings (upper panel in Figure 19) which cannot be resolved by the EHT (lower left panel). A ten-telescope extension

of the EHT, specified in the appendix of [Eichhorn et al. \(2022a\)](#), using a multi-frequency reconstruction at 230 GHz and 345 GHz is capable of: (i) distinguishing the horizonless spacetime from the Kerr spacetime with the same disk model by a difference in the central brightness depression by a factor of about 40, (ii) showing non-concentric intensity contours in the shadow region, indicating that the ngEHT may be on the brink of resolving the inner photon rings, see right lower panel in [Figure 19](#). It is an intriguing open question as to whether superresolution techniques could resolve the inner photon rings.

Less compact horizonless objects, in particular boson stars, have been analyzed in [Vincent et al. \(2016b\)](#); [Olivares et al. \(2020\)](#). The enhancement of a central low-density region by gravitational lensing could in principle produce an image with a central brightness depression comparable in size to the shadow of a Kerr BH of the same mass, and with a similar morphology (see [Figure 20](#)). Numerical simulations of accreting boson stars have shown that for the family of solutions with minimal coupling $V(\Phi) \propto |\Phi|^2$ this effect is only present for the unstable members, and that for such cases the predicted size of the dark region is always smaller than that of the shadow of a Kerr BH with the same mass. For the parameters of Sgr A*, this difference is $\gtrsim 15 \mu\text{as}$ and therefore distinguishable with present EHT capabilities ([Olivares et al., 2020](#)). Nevertheless, the distinction could become more challenging for other ECOs. For instance, semi-analytical calculations for the case of Proca stars predict that stable members of the family can produce central brightness depressions which overlap in size with those in Kerr BH images ([Herdeiro et al., 2021](#)) (see [Figure 21](#)). In this case, more precise tests are required to distinguish between a ring produced by MHD effects and a true photon ring produced by the capture of photons by an event horizon. These tests may include looking for deviations from circularity in the shape of the dark region due to the observing angle.

In fact, if lensing is weak (as it is the case for the Proca star shown in [Figure 21](#)), head-on views would produce more circular dark regions, while near-edge-on views would show ellipsoidal, elongated shapes ([Herdeiro et al., 2021](#)). Our ability to distinguish each case would improve with the maximum resolution achievable by the ngEHT, with the possibility of resolving the thin photon ring being of particular importance. Observations at different wavelengths would also play a crucial role. In fact, the apparent location of a true photon ring should be achromatic, while that of a ring of stalled plasma would depend on the optical depth of the accretion flow at different frequencies. Other features which distinguish images of simulated accretion onto boson stars from BH images include a smaller asymmetry due to Doppler beaming and the absence of relativistic jets ([Olivares et al., 2020](#)). In part, the reason for this is that simulations have been performed only for nonrotating mini boson stars, where, for instance, the Blandford-Znajek mechanism cannot operate ([Blandford and Znajek, 1977](#)). Although it has been suggested that rotating boson stars with minimal coupling are likely unstable, this is not necessarily the case for Proca stars or for some cases with self interaction ([Sanchis-Gual et al., 2019](#)). However, GRMHD simulations of surfaceless ECOs are still relatively rare in the literature, and additional studies may be required to explore the conditions and level of confidence with which these objects can be distinguished from BHs.

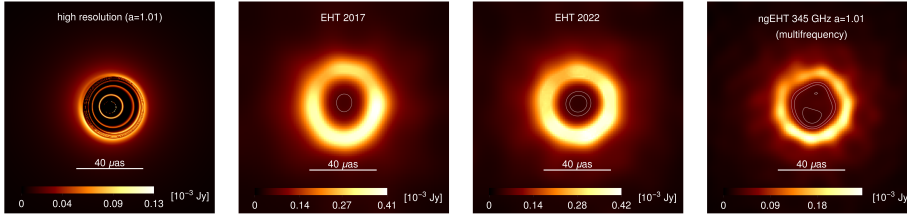


Fig. 19 We compare the simulated high-resolution image (far-left panel) of a horizonless spacetime (generated by overspinning a regular BH to $a_* = 1.01$) and its reconstructions using the ehtim toolkit (Chael et al., 2018), as seen by: (i) the 2017 EHT array (middle-left panel), (ii) the 2022 EHT array (middle-right panel), (iii) a multifrequency observation at 230 GHz and 345 GHz of a potential ngEHT array with ten additional telescopes (far-right panel). We also show (for the three reconstructed images) contour lines at 0.035 Jy, 0.05 Jy, and 0.065 Jy (whenever they exist) to visualize the structure of the central brightness depression. See also Eichhorn et al. (2022a).

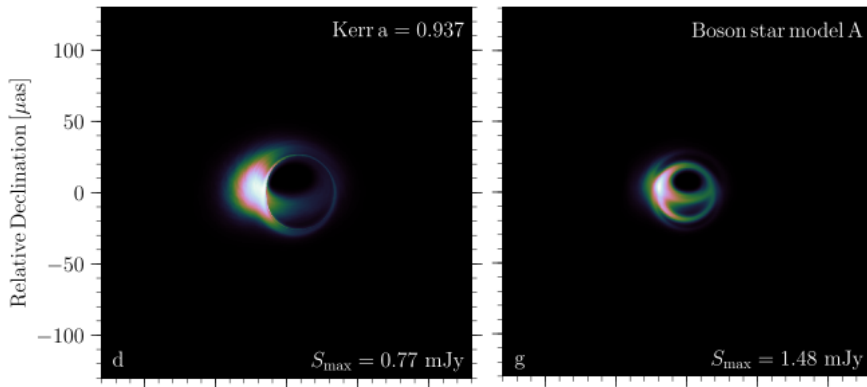


Fig. 20 Ray-traced images from GRMHD simulations of accretion onto a Kerr BH (left) and a boson star (right) with the mass and distance of Sgr A*. Despite the different size, these simulations show that under some circumstances, a horizonless, surfaces ECO can mimic the morphology of a BH image by a combination of GRMHD and lensing effects. Figures taken from Olivares et al. (2020).

5.2.2 Parametric tests of the Kerr paradigm

A complementary approach to the study of specific spacetimes beyond GR is to parameterize deviations from the Kerr spacetime as generally as possible (Benenti and Francaviglia, 1979; Collins and Hughes, 2004; Vigeland and Hughes, 2010; Vigeland et al., 2011; Johannsen and Psaltis, 2011a; Johannsen, 2013; Cardoso et al., 2014b; Konoplya et al., 2016; Ghasemi-Nodehi, 2020; Kocherlakota and Rezzolla, 2020; Delaporte et al., 2022). Because these parameterized spacetimes lack a Lagrangian origin and can be made as general as possible (given assumptions about the symmetries of the spacetime), they in principle provide theory-agnostic tests of the Kerr spacetime, under the assumption that a metric adequately captures all relevant gravitational degrees of freedom. Non-metric theories may thus fall outside the parameterized BH spacetimes in their current form. In practice, a comprehensive test of the underlying parameter spaces is difficult because of their high dimensionality. The most general form of a

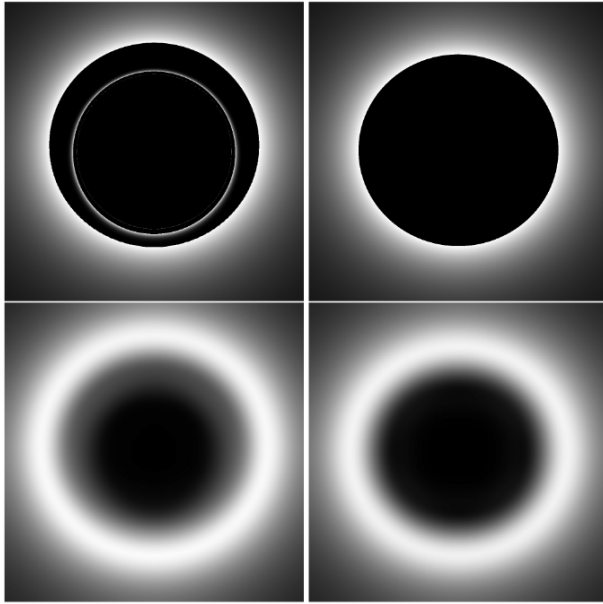


Fig. 21 Ray-traced images of a Schwarzschild BH (left) and a Proca star (right) surrounded by thin accretion disks terminating at the location predicted by the spacetime properties. The lower panels are blurred by a Gaussian kernel, highlighting the possible degeneracy when observing at a single frequency without resolving the thin photon ring. Figure reproduced with permission from [Herdeiro et al. \(2021\)](#).

parameterized spacetime contains several free functions of the spacetime coordinates. Assuming series expansions and truncating at finite order reduces this freedom to a finite set of free parameters. Explicit tests rely on (a) choosing specific functions (e.g., regular BHs can be embedded in parameterizations through specific choices of functions) or (b) working at finite order in the series expansion.

Parameterizations typically make assumptions about the spacetime and its symmetry properties:

- The most general parameterizations to date assume only axisymmetry and stationarity ([Delaporte et al., 2022](#)).
- In addition to axisymmetry and stationarity, one may assume circularity ([Xie et al., 2021](#)), which is an isometry that imposes conditions on the Ricci tensor, resulting in parameterizations with five ([Konoplya et al., 2016](#)) or four free functions ([Papapetrou, 1966](#)).
- In addition to circularity, one may demand the existence of a Killing tensor ([Benenti and Francaviglia, 1979](#); [Vigeland et al., 2011](#); [Johannsen, 2013](#)), which implies a conserved quantity of the geodesic motion, generalizing the Carter constant and guaranteeing integrability. Beyond technical simplicity, there is no fundamental reason why theories beyond GR must satisfy circularity nor admit a generalized Carter constant.
- Reflection symmetry about the equatorial plane can be preserved or broken ([Chen and Yang, 2022](#)). The existence of a Killing tensor guarantees the vertical sym-

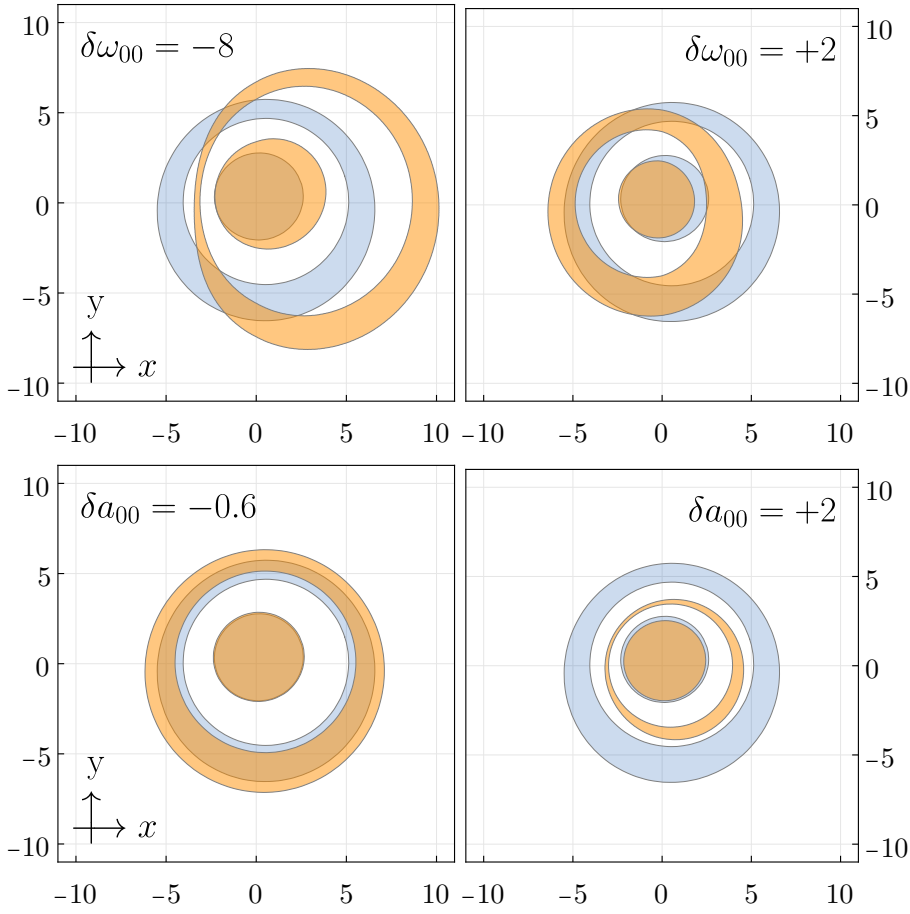


Fig. 22 We show the inner shadow (inner shaded region) and the first lensing band (outer shaded band) of deviations from a Kerr BH with spin $a_* = 0.9$ viewed at near-face-on inclination of 17° . In each panel, we compare the Kerr case (blue-shading and the same throughout all panels) to spacetimes with varying KRZ parameters (Konoplya et al., 2016) (orange-shading) $\delta\omega_{00}$ and δa_{00} . The parameter $\delta\omega_{00}$ relates to deviations of the asymptotic spin parameter. The parameter δa_{00} relates to deviations in the first parameterized post-Newtonian coefficients. See also (Cárdenas-Avendaño and Held, 2023).

metry of the critical curve on the image plane, even if the spacetime is reflection asymmetric (Cunha et al., 2018; Chen, 2020).

One can utilize these spacetimes, model the surrounding accretion flow and then simulate an intensity image to see how these parameterized models can cast shadow images by solving the geodesic equations numerically. There have been various studies utilizing these spacetimes to investigate deviations from the Kerr metric (Psaltis et al., 2020a; Younsi et al., 2016, 2023; Völkel et al., 2021; Mizuno et al., 2018a; Kocherlakota and Rezzolla, 2020, 2022; Nampalliwar and K, 2021; Ayzenberg, 2022; Nampalliwar et al., 2022a; EHT Collaboration, 2022a). Observables which are most relevant to constrain parameterizations of spacetimes with a horizon are likely the photon rings. In

Younsi et al. (2023) and Ayzenberg (2022), photon rings have been used to investigate constraints on parameters of circular metrics with and without Carter-like constants, obtained by analyzing simulated images of spacetimes with accretion disks.

One can also constrain the parameters in these parameterizations with other observations, e.g., GWs (Cardenas-Avendano et al., 2020; Carson and Yagi, 2020; Shashank and Bambi, 2022), or X-ray data (Cardenas-Avendano et al., 2020; Yu et al., 2021), or even Solar System tests. Thus, if uniqueness theorems hold beyond GR, some parameter values are already too small to be further constrained by the ngEHT. However, beyond GR, BH uniqueness theorems do not need to hold and thus SMBHs may well correspond to different solutions from stellar-mass BHs. In this case, only constraints from observing the same object with different techniques are meaningful. In Figure 22 we exemplify how the inner shadow and the first ($n = 1$) lensing band, i.e., the image region in which all lensed (equatorial) emission must occur, deforming when such constraints are set aside (cf., Cárdenas-Avedaño and Held, 2023).

5.2.3 Image signatures of event horizons: the inner shadow

BH can create unique image signatures through their extreme gravitational lensing and event horizon. These signatures are influenced by their surrounding accretion and emission properties. In the high-magnetic-flux MAD state of BH accretion (Igumenshchev et al. (2003); Narayan et al. (2003); Tchekhovskoy et al. (2011); see also Bisnovatyi-Kogan and Ruzmaikin (1974)), which is favored by polarimetric EHT observations of M87* (EHT Collaboration, 2021b), the magnetic pressure exceeds the gas pressure in the disk near the BH. In time-averaged simulation data, the near-horizon material forms a thin, highly magnetized structure in the equatorial plane. This thin equatorial structure is the source of most of the observed 230 GHz emission.

Chael et al. (2021) showed that MAD simulations of M87* naturally exhibit a deep flux depression whose edge is contained well within the photon ring and critical curve (see Figure 23). This darkest region, or *inner shadow*, corresponds to rays that terminate on the event horizon before crossing the equatorial plane even once. This region is bounded by the direct image of the equatorial event horizon. More generally, as long as the emission near a BH is predominantly near the equatorial plane and extends all the way to the horizon, the darkest region in the observed image will correspond to the inner shadow. In addition, because of gravitational redshift, the image brightness falls rapidly near the edge of the inner shadow. As a result, detecting an image feature associated with the inner shadow requires images with high dynamic range.

The inner shadow of a Kerr BH has a significantly different dependence on its parameters than the critical curve (Takahashi, 2004). For instance, the critical curve of a Schwarzschild BH is always a circle with radius $\sqrt{27} r_g$, while the inner shadow of a Kerr BH has a size, shape, and relative displacement that depend sensitively upon the viewing inclination relative to the spin axis and the position angle of the projected spin axis on the sky. The photon ring and inner shadow thus provide complementary information. When considered independently, each is subject to degeneracies in its size and shape as a function of BH mass, spin, and viewing angle: these degeneracies can be broken via simultaneous observations of both features.

In both GRMHD simulations with strong magnetic fields and in semi-analytic, optically thin disk models, the photon ring and the inner shadow are both prominent as observable features. In Figure 23, we investigate the ability of the EHT and ngEHT arrays to recover the inner shadow feature with simulated image reconstructions of a

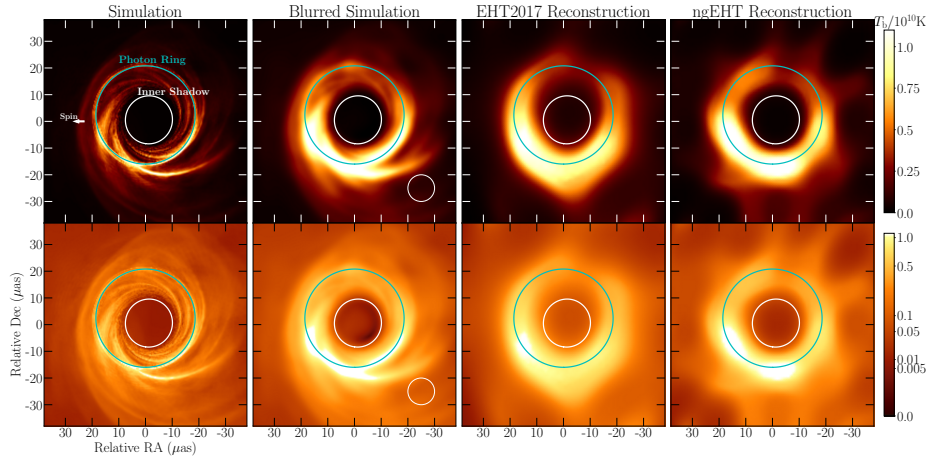


Fig. 23 Left: example GRMHD snapshot image of M87* for a MAD accretion model onto a BH with mass $M = 6.2 \times 10^9 M_{\odot}$ and spin $a_* = 0.9375$ (Chael et al., 2021). Center left: the same GRMHD snapshot image, convolved with a Butterworth filter with a cutoff frequency of $1/10 \mu\text{as}$. Center right: reconstruction of the simulation model from synthetic data generated on EHT2017 baselines. Right: reconstruction of the simulation model from synthetic data generated from a concept ngEHT array. The top row shows images in a linear color scale and the bottom row shows the same images in gamma scale. In all images, the white curve shows the boundary of the inner shadow, while the cyan curve shows the boundary of the shadow. The BH spin vector points to the left (East).

snapshot image from a radiative GRMHD simulation of M87* (Chael et al., 2019). We generate synthetic VLBI data from the 230 GHz simulation image using the EHT baseline coverage on 2017 April 11 (EHT Collaboration, 2019d). We also generate synthetic data using example 230 GHz and 345 GHz ngEHT coverage, assuming a flat spectral index in the underlying source model. This ngEHT concept array used here (Raymond et al., 2021) adds 12 telescopes to the current EHT, substantially improving the EHT’s baseline coverage, angular resolution, and imaging dynamic range. In both cases, we generated synthetic data including thermal noise and completely randomized station phases from atmospheric turbulence, but we did not include the time-variable amplitude gain errors that complicate real EHT imaging (EHT Collaboration, 2019c,d).

The second column of Figure 23 shows the simulation image blurred to half of the nominal ngEHT resolution at 230 GHz (using a circular Gaussian blurring kernel of $10 \mu\text{as}$ FWHM). The remaining columns show the EHT and ngEHT reconstructions using synthetic data. Both reconstructions were performed using the `eht-imaging` library (Chael et al., 2018); the settings used in imaging the 2017 data were the same as those used in `eht-imaging` in the first publication of the M87 results in EHT Collaboration (2019d). While the EHT2017 reconstruction shows a central brightness depression, its size and brightness contrast cannot be strongly constrained or associated with the inner shadow. However, the increased baseline coverage of the ngEHT array significantly increases the dynamic range, and the image reconstruction recovers better the position and size of the high-dynamic-range inner shadow that is visible in the simulation image blurred to the equivalent resolution.

This imaging test is idealized. We neglect realistic station amplitude gains and polarimetric leakage factors that complicate image inversion from EHT data. How-

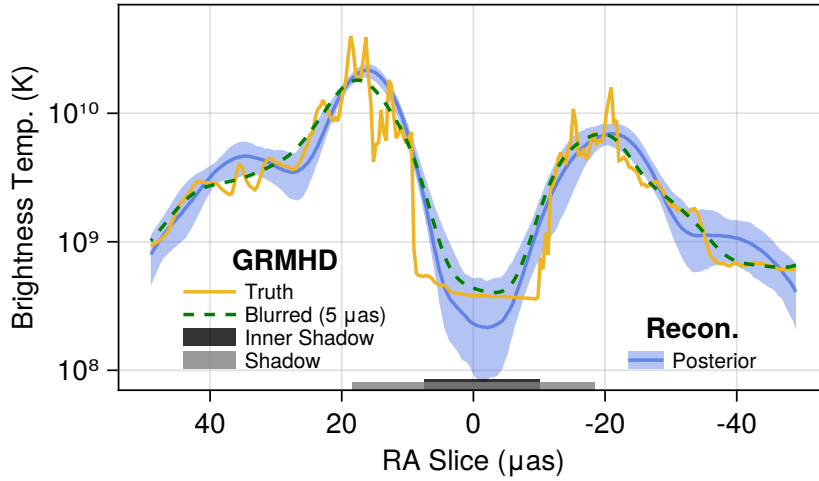


Fig. 24 Simulation and reconstruction brightness cross sections along the East-West axis. The yellow curve shows the 1D brightness profile of the M87* GRMHD simulation snapshot in Figure 23. The dashed green curve shows the 1D brightness profile from the same simulation after convolution with a Gaussian with a FWHM of $5 \mu\text{as}$. The solid blue line shows the median brightness profile extracted from the *Comrade* ngEHT reconstructions. The band shows the 99% posterior credible interval for the 1D brightness profile. The gray band along the bottom shows the region interior to the BH shadow, and the black band shows the inner shadow region.

ever, M87* is weakly polarized, making accurate recovery of the total intensity image possible with no leakage correction (EHT Collaboration, 2019d, 2021a), and image reconstruction of EHT data with even very large amplitude gain factors is possible with a relatively small degradation of the reconstruction quality using *eht-imaging*. In the ngEHT reconstruction, we assume a flat spectral index between 230 GHz and 345 GHz and simply stack the visibility data from simulated ngEHT observations at both frequencies. A more realistic approach would solve for the spectral index between the two frequencies simultaneously with the image during the fit (Chael et al., 2022).

This somewhat idealized example demonstrates that the ngEHT array *could* constrain the presence of an inner shadow in M87* if it is indeed present in the image. In particular, detecting this feature does not require dramatic increases in imaging resolution (which, in the absence of a 230 GHz VLBI satellite, is limited by the size of the Earth) but does require increases in the imaging *dynamic range*, which is limited by the sparse baseline coverage of the EHT array. Once its presence is established via imaging, parametric visibility domain modeling may better recover the size and shape of the inner shadow to higher accuracy than is possible from imaging alone (e.g., EHT Collaboration, 2019f).

In Figure 24, we show cross sections of the simulation and reconstructed images. The reconstructions are from the Julia (Bezanson et al., 2017) Bayesian VLBI imaging package *Comrade* (Tiede, 2022). *Comrade*'s imaging approach is similar to Broderick et al. (2020b); Pesce (2021), and fits a rasterized grid of pixels to the data. For our image model we used a 16×16 raster with a $100 \mu\text{as}$ field of view. A flat Dirichlet prior was chosen for the raster fluxes and we fit to visibility amplitudes and closure phases. The simulation image features faint foreground emission from the approaching

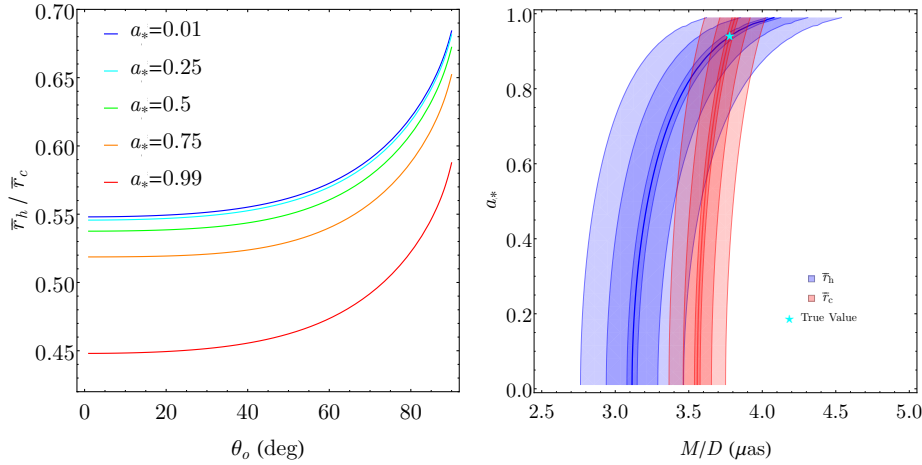


Fig. 25 Left: the ratio of the mean radius of the lensed horizon \bar{r}_h to the mean radius of the critical curve \bar{r}_c . In the low-inclination case, \bar{r}_h/\bar{r}_c shrinks from $\approx 55\%$ at zero spin to $\approx 45\%$ at maximal spin. Right: simultaneous constraints on the BH mass-to-distance ratio M/D and spin a_* enabled by measuring the mean radius of the lensed horizon (blue, \bar{r}_h) and critical curve (red \bar{r}_c), when the inclination is fixed to 17° , as is appropriate for M87* (Mertens et al., 2016; Craig Walker et al., 2018). Without fixing the mass, multiple values of a_* provide the same result for the size of each feature, but combining a measurement of both features breaks this degeneracy. The shaded regions show regions corresponding to 0.1, 0.5, and 1 μas errors on the radius measurement. The input mass scale and spin are $M/D = 3.78 \mu\text{as}$ and $a_* = 0.94$.

relativistic jet, which lies in front of the bulk of the emission in the equatorial plane and provides a finite brightness “floor” inside the inner shadow. With the addition of new sites and short interferometric baselines, the ngEHT achieves the dynamic range necessary to identify the brightness depression associated with the inner shadow, which extends to levels 10^2 dimmer than the peak of the emission for this simulation.

Figure 25 shows how measurements of both the mean radius of the inner shadow (\bar{r}_h) and of the critical curve (\bar{r}_c) could be used to estimate BH parameters. In the low-inclination case, the ratio \bar{r}_h/\bar{r}_c shrinks from $\approx 55\%$ at zero spin to $\approx 45\%$ at maximal spin. For $\theta_o \lesssim 30^\circ$, \bar{r}_h/\bar{r}_c is approximately independent of the inclination, providing a pathway to measuring the BH spin. Importantly, measuring \bar{r}_h/\bar{r}_c for an astrophysical BH would *not* require accurate measurements of the BH mass M or distance D .

Figure 25 demonstrates how a simultaneous measurement of the radius of the critical curve and the lensed horizon could be used to constrain the mass and spin in M87* when the inclination is fixed at $\theta_o = 17^\circ$ (Mertens et al., 2016). These simultaneous constraints are analogous to those discussed in Broderick et al. (2022), which considers constraints from measuring multiple lensed images from a single face-on emitting ring. The blue line shows the space of mass-to-distance ratios M/D and spins a_* that give the same mean lensed horizon radius for an image of M87*; the red line shows the same for the critical curve. The red and blue lines intersect in only one location corresponding to the input BH mass $M/D = 3.78 \mu\text{as}$ and spin $a_* = 0.94$. The shaded bands around the intersecting lines show absolute errors in the radius measurements of 0.1, 0.5, and 1 μas . Given a reported EHT radius measurement uncertainty of 1.5 μas from geometric modeling of the EHT 2017 data in EHT Collaboration (2019f), measurements of the ring and inner shadow radius and centroid locations at $\lesssim 1 \mu\text{as}$ precision may be

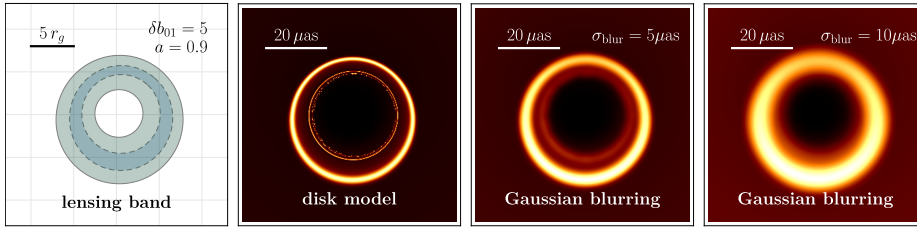


Fig. 26 Multi-ring structures for specific circular deviations of Kerr spacetime ($b_{01} = 5$ in the KRZ parameterization (Konoplya et al., 2016)) at fixed spin parameter of $a_* = 0.9 M$ and viewed at the inclination of M87*. From left to right we show (i) the $n = 1$ lensing band (for Kerr spacetime in blue-dashed and with deviation in green-continuous), cf. Cárdenas-Avedaño and Held (2023); (ii) the resulting image in this spacetime assuming a specific disk model, cf. Eichhorn et al. (2022a); (iii) the same image but blurred with a Gaussian kernel with $\sigma_{\text{blur}} = 5 \mu\text{as}$; and (iv) with $\sigma_{\text{blur}} = 10 \mu\text{as}$. (For the translation of $r_g = M$ to the overall image scale in μas , we determine the maximum diameter of the convex hull of all image pixels with at least half of the average intensity per pixel.)

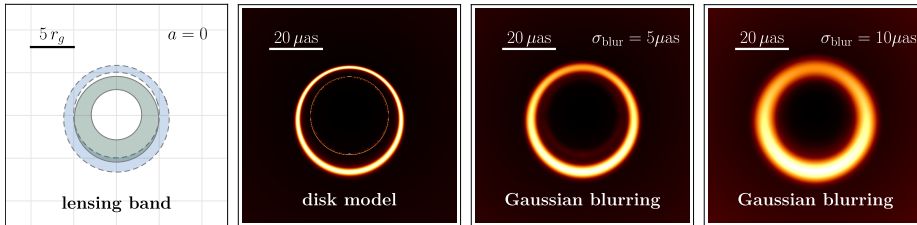


Fig. 27 As in Figure 26 but for a non-spinning ($a_* = 0$) regular BH with exponential falloff in the mass function as in (Simpson and Visser, 2019). The deviation is chosen near-critical such that if it is further increased, the regular spacetime would transition from a BH to a horizonless object.

feasible with the ngEHT. In addition to reducing uncertainty in the image size measurement itself, precisely constraining both features will depend on reducing systematic uncertainty in the relationship between the gravitational features and images from a set of plausible astrophysical models (e.g., EHT Collaboration, 2019f).

5.2.4 Resolvable multi-ring structures

In any given spacetime, the n^{th} -order photon rings (for $n > 0$) necessarily lie within finite lensing-band regions in the image plane, irrespective of the radial location of the emission region. With astrophysical priors on the emission region, these finite lensing-band regions can only become more restrictive. Moreover, each lensing-band region of order n contains all higher-order ($m > n$) ones and thus provides a theoretical upper limit on the maximum radial separation of successive photon rings in the image plane (cf., Sec. 2 for a discussion of the ngEHT capabilities of resolving photon rings in the Kerr spacetime).

Some of the possible deviations from Kerr (Sec. 5.2.2) can significantly broaden the $n = 1$ lensing-band region (see Cárdenas-Avedaño and Held, 2023, and Figure 26 for an example). For any such deviations, higher-order photon rings could become resolv-

able at an appreciably lower resolution than for the Kerr spacetime. This entails that the respective scenarios for new physics could be constrained by the non-observation of such multi-ring structures, even if the ngEHT resolution is insufficient to resolve multiple photon rings in Kerr spacetime. One such scenario to be constrained by multi-ring structures are regular BHs with an exponential falloff function (see Figure 27).

Constraints on new physics from searches for multi-ring structures naturally benefit from increased (effective) resolution. However, they also benefit from an increase in dynamic range. This is because higher-order rings are less bright, as can be seen in the middle-right panels in Figures 26–27, where the secondary ring appears far lower in intensity than the primary one.

5.3 ngEHT challenges for numerical simulations

Numerical simulations played a crucial role in interpreting the observations of M87* and Sgr A* obtained during the 2017 EHT campaign (EHT Collaboration, 2022c). Libraries of synthetic images from GRMHD models have enabled constraints on parameters of the accretion flow and the BH spacetime with increasing accuracy. These include the BH mass, accretion rate, and inclination angle. Under a few additional assumptions, they also provide information on the magnitude of the BH spin and the typical ratios between electron and ion temperatures (e.g., Roelofs et al., 2023; Chatterjee et al., 2023a).

From the point of view of testing of GR and the Kerr hypothesis, GRMHD simulations can be used to understand the extent to which deviations from a model can be attributed to the spacetime, as opposed to those attributable to the accretion flow model (Bronzwaer et al., 2020). In fact, insights obtained from simulation-based modeling, such as the deviation of the size of the bright ring with respect to the actual BH shadow, have been used by the EHT Collaboration to test the Kerr hypothesis and to study a few specific BH alternatives (Psaltis et al., 2020b; Kocherlakota et al., 2021; EHT Collaboration, 2022d; Younsi et al., 2023). One of the most interesting prospects of the ngEHT is the possibility of probing the spacetime around supermassive compact objects in even greater detail. In light of this, we list here what we consider to be some of the most interesting research avenues that should be addressed using numerical simulations (not necessarily in order of importance).

GRMHD-informed semi-analytic models

Synthetic images created from semi-analytic models of the accretion flow are much faster to generate as compared to those from GRMHD models, offering clear advantages when fitting images by sampling over large regions of the parameter space (Palumbo et al., 2022). This is especially important when considering alternatives to Kerr BHs, for which the size of the parameter space increases considerably. Semi-analytic models have been used to explore emission from fluid configurations around non-Kerr BHs and other compact objects (see e.g. Vincent et al., 2016b, 2021; Kocherlakota and Rezzolla, 2022; Bauer et al., 2022b; Daas et al., 2022b; Özel et al., 2022; Younsi et al., 2023). However, in many cases these are limited to spherically or axisymmetric static configurations, and leave out much of the physics present in simulations, e.g., turbulence and temporal variability. With increasingly detailed observations enabled through the ngEHT, more detailed models will help to better constrain the properties of the spacetime and the accretion flow.

Work to characterize variability in GRMHD simulations has been performed previously (Georgiev and et al., 2022). This characterization becomes increasingly relevant in light of the difficulties of GRMHD models within the EHT library to match the observed variability of Sgr A*, which could point to the necessity of considering different accretion models or including additional physical processes (EHT Collaboration, 2022c).

Alternatives to Kerr BHs may come with additional features in the accretion flow that are essential to include in realistic semi-analytic models. For instance, models in which the event horizon is replaced by a surface that exchanges momentum with electromagnetic radiation (EHT Collaboration, 2022d) may be incomplete without considering a similar exchange of momentum with matter. It is to be expected that the interaction of the relativistically-infalling plasma with a hard surface would produce strong shock waves that could be detectable (notwithstanding redshift of subsequent emission) even when the surface itself has a very large heat capacity and produces almost no thermal emission.

Another issue to consider is the possibility of images with ring-like features that do not originate from a BH shadow. This situation occurs even in several SANE (Narayan et al., 2012) Kerr models of the EHT simulation library, where the radius of maximum emission appears to be related to the position of the ISCO (Bronzwaer et al., 2020), and for models where there is strong emission coming from the jet base (EHT Collaboration, 2022c). In non-Kerr spacetimes with a maximum in the rotation velocity profile of circular geodesics, very clear ring structures may appear as a result of the suppression of the magnetorotational instability (MRI) (see Olivares et al., 2020, and Sec. 4.3.4). This latter effect has already been considered in semi-analytic models of horizonless compact objects (Herdeiro et al., 2021) However, there are several questions that need to be answered, as its robustness, or whether there are mechanisms other than the suppression of the MRI that could produce similar ring-like structures. A better understanding of these features would aid in constructing semi-analytic models of accretion onto alternative compact objects with the correct emission geometry.

Perturbative deviations from the Kerr metric

General-relativistic hydrodynamic and GRMHD simulations of accretion in alternative spacetimes are still relatively uncommon. Examples include non-BH objects such as boson stars (Meliani et al., 2016, 2017a; Olivares et al., 2020; Teodoro et al., 2021), BHs in specific alternative theories of gravity (Mizuno et al., 2018b; Fromm et al., 2021; Röder et al., 2022, 2023; Chatterjee et al., 2023b) and BHs in theory-agnostic parameterized metrics (Nampalliwar et al., 2022b; Chatterjee et al., 2023c). Some of these examples were conceived mainly as proofs of principle, and are either extreme cases that exhibit properties that are easily distinguishable from those of Kerr BHs, or consider accretion regimes distinct from that expected around the main EHT targets.

However, observations of M87* and Sgr A* during the EHT 2017 campaign show a remarkable agreement with the Kerr hypothesis. This indicates that deviations with respect to the Kerr geometry are likely small and can be treated as perturbations using the existing parameterized expansions (see Sec. 5.2.2). The search for such deviations would benefit from a systematic study of the effects that varying the leading order deviation parameters have on the accretion flow properties and subsequent synthetic images.

Although the different deviation parameters span a large parameter space, the regions to explore could be reduced by exploring near to the Kerr models most favored

by the EHT scoring (EHT Collaboration, 2022c), and by making informed choices that account for existing degeneracies, as was done by (Nampalliwar et al., 2022b) for the degeneracy between the spin and the size of the ISCO. The parameter space exploration would also benefit from the use of informed semi-analytic models as described above.

The structure of the accretion flow onto SMBHs

All of the simulations used for the interpretation of the EHT M87* observations and most of those used for Sgr A* are variations of the same physical scenario: a rotation-supported torus in hydrodynamic equilibrium is initialized at a distance of a few r_g from the SMBH, a weak poloidal magnetic loop is added inside the torus, and the system is slightly perturbed. Subsequently, the MRI (Balbus and Hawley, 1991) produces turbulence, which amplifies the magnetic field and facilitates angular momentum transport. Depending on the dynamical importance of the magnetic field in the saturated state, models are classified as SANE (less magnetized) or MAD (more magnetized).

However, large scale simulations of accretion onto Sgr A* fed by stellar winds show flow patterns that differ from this scenario in several aspects. Most notably, they show that the MRI is relatively unimportant at several scales. While at large scales the magnetic fields are weak and passively advected (Ressler et al., 2020a), at horizon scales they accumulate and become dynamically, regulating accretion in a way similar to MADs (Ressler et al., 2020b). Due to computational limitations, however, few works have treated the problem using GRMHD (Ressler et al., 2020b; Lalakos et al., 2022).

For a correct interpretation of the ngEHT observations, it is essential to understand in which regime the accretion flow pattern can be represented by typical tori simulations and whether this regime is realized by in the environment of the ngEHT targets, or if a change in the simulation paradigm is needed. Of course, this consideration also applies to alternative spacetime geometries and compact objects, for which uncertainties associated with the accretion flow need to be sufficiently understood before drawing conclusions regarding the spacetime properties or the presence of new fundamental physics.

Beyond ideal MHD

In general, models based on GRMHD simulations show an excess in variability when compared to observations at 230 GHz (EHT Collaboration, 2022c). However, it is expected that non-ideal effects like viscosity and thermal conduction will lead to a decrease in variability. Their inclusion is motivated by the fact that plasma in the vicinity of Sgr A* and M87* is practically collisionless, and these can be used in GRMHD simulations to describe leading order corrections due to kinetic effects (Chandra et al., 2015; Foucart et al., 2017). The consequences of these and other non-ideal effects like resistivity (Ripperda et al., 2019) for the source variability and other observable properties still needs to be investigated.

Another research direction that requires physics beyond ideal MHD is the study of BH magnetospheres. These regions are difficult to simulate using GRMHD and are more readily described using force-free electrodynamics (FFE). This commonly leads to the choice of ignoring regions with very high magnetizations when producing ray-traced images from GRMHD data. However, general relativistic simulations combining the physics of GRMHD and FFE have already been performed in the context of accretion onto millisecond pulsars (Parfrey and Tchekhovskoy, 2017). These kinds of simulations may become increasingly important in light of accretion scenarios such as

those described in [Blandford and Globus \(2022a,b\)](#), in which magnetospheres play a crucial role in the dynamics and overall flow pattern.

Similar to the discussion regarding the structure of the accretion flow, any attempt to probe gravity and new fundamental physics in the vicinity of BHs must take into account the limitations of the plasma model, and the pursuit of research lines such as those outlined above is expected to contribute towards helping alleviate these current uncertainties.

5.4 Outlook

Many of the known beyond-GR scenarios, (cf., [Sec. 5.1](#)) result in similar signatures for VLBI observations of SMBHs. Amongst these signatures, we have identified as promising science cases for the ngEHT: (i) a less pronounced central brightness depression (cf., [Sec. 5.2.1](#)), (ii) deformations of the $n = 1$ photon ring (cf., [Sec. 5.2.2](#)), and (iii) potentially resolvable multi-ring structures (cf., [Sec. 5.2.4](#)). There may well be further relevant science cases in the future, given the field of testing GR and other theories of gravity with BH images is now evolving quickly.

We highlight the key role of BH uniqueness theorems: in GR, BH uniqueness holds and implies that the Kerr spacetime can be constrained by a range of different observations of distinct BHs, namely with electromagnetic signals, GWs, and with PN constraints. Beyond GR, the assumption of BH uniqueness is a very strong constraint on the theory. For instance, even in one of the simplest extensions of GR, curvature-squared gravity ([Stelle, 1978](#)), there are several spherically-symmetric BH solutions at any given value of the asymptotic mass, albeit only one stable one ([Brito et al., 2013](#); [Held and Zhang, 2023](#)). There are therefore two distinct possibilities regarding the constraints that the ngEHT may impose.

- If BH uniqueness holds beyond GR, then many beyond-GR spacetimes are already constrained by other observations. Possible ngEHT signatures are then in many cases small and difficult to detect.
- If BH uniqueness does not hold beyond GR, then the ngEHT has the potential to constrain the strong-field regime of SMBHs. Then, ngEHT signatures may be large enough to be detected.

There is by now a considerable body of theoretical work on images of spacetimes beyond GR. However, many of these are limited to determining the critical curve, which in itself is not observable. Images with disks have been generated for some spacetimes and enable us to better assess whether these spacetimes may be distinguished from the Kerr spacetime with the ngEHT.

By moving beyond static images, it is likely that much can be learned from a spacetime-tomography approach to spacetimes beyond GR. There is currently a gap in the literature in the sense that systematic investigations of how informative, e.g., time-dependent emission, hot spots and similar features can be, have not yet been conducted.

A further critical gap in the literature concerns the power of superresolution techniques. In [Broderick et al. \(2022\)](#), it has been demonstrated that, under additional assumptions, superresolution techniques allow one to reconstruct the $n = 1$ photon ring. Beyond GR, these techniques may be invaluable in imposing meaningful constraints.

From the phenomenological side, there are several observables for which little is known beyond their Kerr signature. This includes polarization, which is poorly investigated in spacetimes beyond GR. Similarly, the achromaticity of the ring could be a strong way to distinguish the Kerr spacetime from at least some settings beyond GR. However, studies of images at several frequencies are so far mostly lacking in settings beyond GR.

6 Exploring binary black holes with ngEHT

In our dark energy, dark matter driven Universe, structures are expected to build up hierarchically from the merger of smaller scale collapsed haloes, suggesting that larger galaxies assemble by via mergers over cosmic time, potentially also involving primordial BHs as seeds of collapse. Since the growth of SMBHs hosted in galactic nuclei is understood to be driven by both accretion and BH-BH mergers, supermassive BH binaries (SMBHBs) are believed to be the natural outcome of galaxy mergers. In particular, mergers are expected to be the dominant growth channel for BHs hosted in galaxies that reside in dense environments, especially at high BH masses, the range that is accessible to ngEHT observations (Kulier et al., 2015; Weinberger et al., 2018; Ricarte and Natarajan, 2018; Pacucci and Loeb, 2020). Binary BH mergers, or other strongly dynamical spacetimes such as collapsing configurations, may probe the strong-curvature regime of GR (Cardoso et al., 2023). SMBHBs in the GW-driven regime are the critical missing piece to the assembly of supermassive BHs. The ngEHT can probe the most astrophysically relevant parameter space (total masses of order $10^8 - 10^9 M_\odot$) that are challenging for both Pulsar Timing Arrays (PTAs) or LISA. Furthermore, multiple detections of binaries at different redshifts (especially with a fortunate simultaneous GW detection) probe cosmology. SMBHBs would be very efficient natural multimessenger laboratories for addressing ngEHT science goals, especially those described in Secs. 3, 5, & 6.3.

During SMBH mergers, dynamical friction and interactions with the stellar contents and accreting materials draws the two SMBHs to the nucleus of the newly created merger remnant (Merritt and Milosavljević, 2005). The evolution and fate of the SMBHB is dictated by a range of physical processes that operate to cause it to shrink via the loss of angular momentum in the orbit. The environmental interactions that drive the binary down to separations of $\sim 0.1-10$ pc are well understood, but the detailed mechanism(s) implicated in causing continued inspiral beyond this point, and in particular down to the sub-parsec scale regime in which GW emission takes over to shrink the binary orbit, still remain unclear (e.g., Begelman et al., 1980a). A number of viable solutions to this long-standing and so-called “final parsec problem” (Armitage and Natarajan, 2002; Milosavljević and Merritt, 2003) have been proposed. For instance, interactions with gas in a circumbinary disk and three-body interactions with stars in the innermost regions could all contribute to, and have a significant influence on, the evolutionary timescale for the binary. Uncovering the details of the physics during this last parsec of evolution and final merger informs the science cases of ongoing and future GW detectors such as PTAs, space-based GW interferometry (e.g., LISA), and other future advanced GW facilities.

Dynamically speaking, the formation and evolution of SMBHBs evolves through three main phases after galaxy mergers (Begelman et al., 1980b; Armitage and Natarajan, 2002; Colpi, 2014): the pairing stage, the hardening stage, and the gravitational radiation dominated final coalescence phase. During the pairing phase, the binary separation is of the order of several kpc, and the two SMBHs migrate inwards towards the center through dynamical friction with gas until a compact binary is formed at separations of a few pc (Armitage and Natarajan, 2002). The second hardening phase involves interaction with the stellar population in the innermost regions and could also be modulated by the presence and availability of gas in the vicinity. It is not clear how long it is likely to take SMBHBs to reach the critical separation where angular momentum loss via GW emission starts taking over. The presence of gas in the inner

regions has been demonstrated to facilitate this stage [Armitage and Natarajan \(2002\)](#). In idealized simulations, it appears that mergers and final coalescence can occur within a Hubble time, in agreement with theoretical work modeling the mass assembly history of SMBHs over cosmic time that requires BH mergers to explain the mass distribution of SMBHs as observed today. The recent observational detection of a SMBHB in UGC 4211 with a 230 pc separation by ALMA opens up a new window into potential detection for candidates in the transition phase between the pairing and hardening stage [Koss et al. \(2023\)](#). The lack of even indirect observational evidence for SMBHBs at the sub-parsec separation phase is impeding progress in this field and it is in this domain that the ngEHT stands to be transformative.

The remnant evolution of SMBH binaries at the gravitational radiation phase is determined by their emitted GWs. The frequency of GWs emitted by SMBHBs at this phase enters into the PTA band, which is about 1 per year to 1 per decade. Simultaneously, their angular separation assuming they are located at Gpc distances is roughly a few to several tens of μas , which is within the reach of the ngEHT. The combination of multi-band electromagnetic observations and PTA observations forms a multi-band and multi-messenger astrophysical era of SMBHBs. For smaller binary separations and shorter orbital periods the orbital decay is GW-driven and may outpace the viscous time scale in the disk, leading to a decoupling of the binary from the disk (see, e.g., [Gold, 2019](#)). The transition where this decoupling occurs is obtained by equating the GW time scale with the viscous time scale of the disk, which depends strongly on the geometric thickness. For thin disks the decoupling could occur at separations relevant for the ngEHT. For geometrically thicker disks, accretion may proceed until smaller separations with mini-disk formation ([Paschalidis et al., 2021](#)).

Much like the study of binary stars, which are generally described by their method of discovery and observation, SMBHBs are apt to be found by the ngEHT in one of the following ways: transiting binaries, astrometric binaries, and telescopic binaries. We discuss these techniques and the candidates detected by each of these methodologies in more detail later in this section. A wide range of SMBHB candidates are detected via multiple techniques and these include periodically variable quasars ([D’Orazio et al., 2015](#); [Charisi et al., 2016](#)) and quasars exhibiting broad emission lines that indicate high recoil velocities ($\geq 1000 \text{ km s}^{-1}$) ([Eracleous et al., 2012](#)). Among the periodically variable AGN, the low-luminosity AGN exhibit shorter mm-wavelength variation timescales and may be superior targets for the ngEHT as these SMBHBs may be resolved with relative astrometry ([D’Orazio and Loeb, 2018a](#)). Recently, the search for SMBHBs amongst quasars with offset broad lines using very long baseline arrays was conducted by [Breiding et al. \(2021\)](#), however, no double radio sources were found to be resolved. One possible reason for their non-detection is that the projected orbital separation lies within the limit of the current observing resolution ([Breiding et al., 2021](#)). The ngEHT with significantly better resolution has the capacity to resolve potential candidates.

The ngEHT will have a nominal angular resolution of $\sim 15 \mu\text{as}$, which translates to a spatial resolution of $\leq 0.13 \text{ pc}$ across redshifts. Additionally the adoption of super-resolution techniques might help improve this further, by factor of a few for imaging ([Chael et al. 2016](#), [Akiyama et al. 2017](#), [Broderick et al. 2020c](#)) or substantially more for geometric modeling of simple structures such as displaced but individually unresolved emission regions. This means that the ngEHT can therefore *spatially resolve* SMBHBs that have entered their steady-state GW emission phase. The orbital period at this stage is typically short (ranging from months to years), which makes it acces-

sible to multi-epoch observations with the ngEHT. Furthermore, [D’Orazio and Loeb \(2018b\)](#) estimate that between 1 and 30 sub-parsec SMBHBs should have millimeter flux densities in the $\gtrsim 1$ mJy regime and will hence also be accessible with the ngEHT.

The current best studied candidate SMBHB is the radio source OJ287 ($z = 0.306$). This source has been observed for over 120 years and is a quasi-periodic flaring source. There is a well observed double flare structure with ~ 12 year periodicity (as measured from Earth), or ~ 9.2 years in the source proper time. This difference has been attributed to the presence of an as of yet unseen secondary BH with mass $1.5 \times 10^8 M_\odot$ passing through the accretion disk of a much more massive primary, with an estimated mass of $\sim 1.835 \times 10^{10} M_\odot$ (e.g., [Sillanpaa et al., 1988](#); [Lehto and Valtonen, 1996](#); [Dey et al., 2018](#)). The mass and period of OJ287 imply a Newtonian semi-major axis of 1.16×10^4 AU, corresponding to $12.4 \mu\text{as}$ at the source redshift, and with the estimated eccentricity of ~ 0.65 , a maximum primary-secondary separation at apoapsis of $\sim 20.3 \mu\text{as}$. This renders it directly resolvable by the ngEHT at its highest frequency. At periapse, the secondary would move at a proper (local) circular velocity of $\sim 8.11 \times 10^4 \text{ km s}^{-1}$, or $0.271 c$, corresponding to $\sim 14 \mu\text{as yr}^{-1}$ as seen from Earth, slowing down to $1.72 \times 10^4 \text{ km s}^{-1}$, or $0.057 c$ ($\sim 3 \mu\text{as yr}^{-1}$) at apoapse. If the secondary BH in OJ287 were visible at 345 GHz, the ngEHT should be able to easily detect its absolute astrometric motion, while the motion of the primary would be ~ 20 times smaller, and likely not detectable even with a decade-long observing campaign. The ISCO radius for OJ287 is ~ 1100 AU or $\sim 1.2 \mu\text{as}$, and therefore unresolvable by the ngEHT.

An alternate explanation for OJ287 has also been proposed. Detailed investigation of 120 epochs of VLBA observations of this source reveal that viewing angle changes due to a putative precessing (and nutating) jet could cause the morphological changes of the pc-scale jet as well as the radio variability that is observed ([Britzen et al., 2018](#)). The jet would complete a full orbit in projection in about 22 years, twice the dominant time scale observed in the optical waveband. It is likely that the optical emission is also produced by the jet. While a binary BH model or the Lense-Thirring (LT) effect is required to explain jet precession, the piercing of the accretion disk by a secondary BH is not required in this scenario. By contrast, the obvious stability of the jet and jet motion do not support the plunging SMBHB interpretation, as it is incompatible with regular disturbances of the accretion disk. [Britzen et al. \(2023\)](#) show that the phase of the precession relates to the variability of the Spectral Energy Distribution (SED). The precession model for OJ287 is further supported by other, independent observations. [Komossa et al. \(2023\)](#) failed to detect the 2022 outburst predicted by the “plunging”-model. Instead, OJ287 was at low optical–UV emission levels, declining further into November. The predicted thermal bremsstrahlung spectrum was not observed either, at any epoch. Furthermore, the authors estimate a SMBH mass of $10^8 M_\odot$ for OJ287 and confirm the mass estimate by [Britzen et al. \(2018\)](#) based on the precession model. [Yuan et al. \(2023\)](#) validate the plausible predictions of a jet with precession characteristics in OJ287 based on an archival study of VLBI observations at 2.3, 8.6, 15, and 43 GHz. The first GMVA plus ALMA observations reveal a compact and twisted jet extending along the northwest direction, with two bends within the inner $200 \mu\text{as}$, resembling a precessing jet in projection ([Zhao et al., 2022](#)). Recent Space VLBI observations with RadioAstron at 22 GHz with an angular resolution of $\sim 150 \mu\text{as}$, or $\sim 40 r_g$ spatial resolution, add to this physical picture a high brightness temperature, qualitatively confirming violent processes in the inner part of the source ([Kim et al., 2023](#)). VHE flaring emission in OJ287 has been investigated by, e.g., [Lico et al. \(2022\)](#).

ngEHT observations could resolve the question of which of these clearly conflicting and competing models for OJ287 provide a proper description of the source. While OJ287 may be the favorite SMBHB in our own backyard for the ngEHT, our current understanding of the assembly history of BHs suggests that multiple resolvable sources ought to exist. At present, there is an ongoing effort to find and characterize additional viable SMBHB candidates besides OJ287.

We briefly review the possibilities for the detection of SMBHBs via a range of observational techniques. As we have noted above, the ngEHT will have sufficient angular resolution to identify sub-parsec SMBHBs at any redshift, providing a powerful complement to GW observations of galaxy mergers from PTAs and future planned facilities like LISA. At the present time there are several theoretical uncertainties with predictions of the merger rates stemming from our incomplete understanding of the astrophysical processes that effect coalescence, as well our lack of knowledge about the abundance and masses of initial BH seeds. This translates directly into a lack of secure predictions for the separation distribution for SMBHBs. This is once again where data from the ngEHT could significantly alter and constrain theoretical models, permitting better-calibrated subsequent predictions. While the ngEHT is not a survey instrument, it will nevertheless be able to observe many binary candidate sources by utilizing sub arrays. In addition, key synergies with the next-generation VLA (ngVLA) can effectively address the limited field of view of the ngEHT.

6.1 Multiple supermassive black hole systems

Studies of binary and multiple stellar systems and their evolution have revealed that a significant proportion of stars are in multiples [Tokovinin \(1997\)](#), with substantial evidence that some binary stellar systems were likely former triple systems ([Eggleton and Yakut, 2017](#)). It is known from planetary systems and close binary stars that therein a third body orbiting the binary impacts the orbit of the inner binary. This astrophysical coupling process is referred to as the von Zeipel, Kozai and Lidov mechanism ([von Zeipel, 1910](#); [Kozai, 1962](#); [Lidov, 1962](#)), and it explains a variety of phenomena ([Naoz, 2016](#)). The mechanism is effective in the merger processes with the changes it can create in the inner orbit under certain conditions ([Antonini et al., 2017](#); [Stephan et al., 2016](#)).

A few candidates for multiple SMBH triple systems have been identified in recent years, e.g., SDSS J0849+111 ([Pfeifle et al., 2019](#); [Liu et al., 2019](#)), J150243.09+111557.3 ([Deane et al., 2014](#)), NGC 7733-7734 ([Yadav et al., 2021](#)), and SDSS J1056+5516 ([Kalfountzou et al., 2017](#)). The presence of another SMBH sufficiently close to, and in orbit around, a SMBHB system can affect the orbit of the binary SMBH and accelerate the merger process significantly. As a result of the existence of a third SMBH in the vicinity, an oscillation will occur between the orbital eccentricity of the SMBHB in the inner orbit and the angle between the orbital planes of this and the outer SMBH. This complex interaction will play a crucial role in the convergence and merging of paired SMBHBs and may shorten the merging times significantly. Of course, when examining this mechanism we note that some SMBHBs observed today could potentially be residuals of former triple systems. Simulations suggest that such tiered mergers could play an essential role in the evolution of galaxies ([Begelman et al., 1980b](#); [Khan et al., 2016a](#); [Hopkins et al., 2008](#)).

In this context, such sufficiently close triple SMBH systems, whilst observationally rare, if and when detected would provide an extraordinary opportunity to study a distinct set of astrophysical processes which serve to catalyze SMBHB mergers. While SMBH mergers are an essential ingredient in galaxy evolution, close triple SMBHs offer a unique opportunity for studying the dynamics of three-body interactions in GR. In a hierarchical triple SMBH system, the orbital eccentricity of the binary system in the inner orbit will exhibit variations over time, allowing it to grow to very large values (e.g., $e > 0.9$). The effect of the impact of a third SMBH seems likely to be detectable with low-frequency GW observations, especially at the periphery (Merritt, 2013). Any direct evidence that can be provided from low-frequency GW observations for ngEHT triple candidates will in turn provide us with new information concerning binary SMBH coalescence.

6.2 Taxonomy of SMBHBs

Table 3 Selected SMBHB candidates. We list the estimated masses for both objects in the SMBHB. In some cases, only the total mass of the potential binary system is known. We also include below the first confirmed triple system. References are: (1) Hu et al. (2020), (2) Britzen et al. (2019b), (3) Britzen et al. (2018), (4) Dey et al. (2018), (5) Bhatta (2019), (6) Sarkar et al. (2021), (7) O’Neill et al. (2022), (8) Rodriguez et al. (2006), (9) Bansal et al. (2017), (10) Kharb et al. (2017), (11) Liu et al. (2019).

Type of signal	AGN	z	Angular separation	Masses (M_{\odot})	References
<i>Transiting Binaries</i>					
Self-lensing signal	“Spiky” KIC 11606854	0.918		$10^{7.4}, 10^{6.7}$	(1)
<i>Astrometric Binaries</i>					
Jet precession	3C 84	0.0176	?	$\lesssim 8 \times 10^8$	(2)
Jet precession	OJ 287	0.306	0.001/0.01 pc	$3.96/2.96 \times 10^8, 4 \times 10^6/1.04 \times 10^8$	(3)
Optical flaring	OJ 287	0.306	$\sim 20.3 \mu\text{as}$	$1.5 \times 10^8, 1.835 \times 10^{10}$	(4)
QPOs	Mrk 501	0.0337	5 millipc	$7 \times 10^8 - 10^9$	(5)
QPOs	3C 454.3	0.859		$7 \times 10^9 - 5.7 \times 10^{10}$	(6)
QPOs	PKS 2131-021	1.285	0.001-0.01 pc		
<i>Telescopic binaries</i>					
	4C +37.11 (B2 0402+37)	0.055	7.3 pc	15×10^9	(8), (9)
	NGC 7674 (Mrk 533)	0.028924	0.35 pc	3.63×10^7	(10)
<i>Apparent Binaries</i>	1038+52{A,B}		33 ³⁷		
Triple System	SDSS J0849+111	0.078	within 5 kpc radius	$\sim 10^{7.5}, 10^{8.4}, 10^{6.7}$	(11)

These objects are mostly selected by their observed signatures, which could in principle overlap. At 1 mm wavelengths a 25-meter radio telescope has a beam width of ~ 8 arcseconds. In this instance the primary systems of interest are pairs of objects that could be observed simultaneously within the same beam-width. Most of these correspond to classical astronomical binaries, but the relativistic nature of the orbiting objects introduces new effects and additional sets of observable quantities that are not available with main sequence stars. We list the best candidate sources in Table 3.

For some of these classes of binary candidates there may be degeneracies with regard to the physical origin of the observed periodic signal. Jet precession as well as periodic light-curve flaring can also be caused by the LT effect due to the frame-dragging of the rotating Kerr BH (Thirring, 1918; Lense and Thirring, 1918).

6.2.1 Telescopic binaries

In telescopic binaries the primary and secondary can both be seen directly and their motion measured. For the ngEHT, this would require both SMBHs to be radio-loud.

- Image or visibility stacking with source frequency phase referencing (SFPR), e.g., Rioja et al. (2011), which could improve the detectability of weaker targets. This would help to reveal the secondaries in some sources, especially if there are ngEHT or other independent estimates of the orbital parameters.
- If observable they would represent the “gold standard” in SMBHBs.
- Large separation binaries are likely to be easily resolvable by the ngEHT out to cosmological distances, but their periods will be $\gg 1$ per decade and their motions will therefore be harder to detect.

The ngEHT with a nominal angular resolution in the range of 5–15 μas and monitoring duration ranging from weeks to ~ 10 years will be able to study telescopic SMBHBs within a broad range of masses and orbital geometries, at various redshifts inaccessible to other existing and prospective observatories.

6.2.2 Astrometric binaries

With an astrometric binary only one source is typically visible, and the binary is detected through a periodic “wobble” in the positions of its radio-loud jets, jet components, core, or BH shadow. From a detected periodic occurrence one can infer that the perturbation occurs due to the gravitational influence of an unseen companion. At least one BH within the binary system is required to be radio-loud, which means it is required to have a radio-loud jet. For this reason the expectation is that more ngEHT binaries will fall into this category than telescopic binaries. The best candidates are those AGN where the jet precesses (e.g., OJ287, 3C 84) or/and where periodic flux-density changes are observed (e.g., Mrk 501, 3C 454.3), and where the model parameters predict close separations (see Table 3). Astrometric binary candidates have been proposed for, e.g., 3C 279 (Abraham and Carrara, 1998), 3C 273 (Abraham and Romero, 1999), PKS 0735+178 (Britzen et al., 2010), 2200+420 (BL Lac) (Caproni et al., 2013), PG 1553+113 (Caproni et al., 2017), 3C 345 (Caproni and Abraham, 2004b), 3C 120 (Caproni and Abraham, 2004a), 1308+326 (Britzen et al., 2017), TXS 0506+056 (Britzen et al., 2019a), PKS 1502+106 (Britzen et al., 2021). Recently, a candidate SMBHB J2102+6015 has been identified on the basis of astrometric VLBI

monitoring (Titov et al., 2023). If confirmed as a SMBHB, this source would become an example of a synergistic multimessenger bridge between ngEHT and prospective GW facilities (Gurvits et al., 2023). All cases of astrometric SMBHB candidates need to demonstrate noticeable motion in order to be detected, and thus will observationally be selected by both the period and the angular separation of the binary. Long-term VLBI monitoring can resolve the orbital motion of a binary (D’Orazio and Loeb, 2018a) and this can be achieved both in the image and visibility domains.

We note two practical features of potential applications of the ngEHT for studies of astrometric binaries.

- An extra factor of $(1 + z)$ between the proper motion distance and the better determined angular diameter distance should be taken into account. The same factor results in the “time dilation” of the observed period of the binary over the actual period in its rest frame.
- As opposed to the case of telescopic binaries considered in Sec. 6.2.1, detection of an astrometric SMBHB by the ngEHT would require only one component of the binary to be a sufficiently strong radio emitter. In this case, the SMBHB observational signature would be a peculiar astrometric behavior or “wobbles” on an angular scale smaller than the nominal array resolution. An example of such an “astrometric” detection of a potential SMBHB is offered by the source J2102+6015 (Titov et al., 2023).

Astrometric signatures of precession in AGN jets persist on long time-scales and are comparable to clocks or metronomes. Britzen et al. (2023) argue that most of the blazar variability (morphology as well as light-curve) may be due to precession-induced phenomena (except for M87, Sgr A* and TeV blazars). These signals should not be confused with other interesting fluctuations due to plasma instabilities (current-driven or kink) of the flow which develop and disappear on shorter time scales and are lower energy phenomena which do not dominate the observational data.

6.2.3 Spectroscopic binaries

Spectroscopic binaries are detected as either “single-peaked” sources (with spectral emission from only one source) through the detection of periodically varying spectral line frequencies, or as “double-peaked” sources with two sets of spectral lines, one from each source.

- Single-peaked sources can in practice only be detected if the orbital period is short enough to see periodic variations in spectral frequencies.
- Double-peaked spectral source lines would have frequency separations changing with the orbital phase, but could be detected as binaries even for very long orbital periods. Rubinur et al. (2019) surveyed 20 double-peaked AGN in [O III] at ~ 500 nm with the VLA whilst searching for telescopic binaries and found that “one of them is a dual AGN (DAGN), while the other two could be either DAGN or AGN+star-forming nuclei pairs.” An imaging snapshot ngEHT survey of double-peaked radio sources with indications of compact cores might be an extremely efficient detection strategy to find additional binary candidates for further study.
- The large spectral shifts that would be found with sources approaching inspiral (at ~ 0.3 c) suggests that this method should be utilized as a means of finding candidate multi-messenger binaries.

- An optical search for broad absorption line (BAL) quasars with periodically changing line frequencies might also be an efficient way to find binaries nearing inspiral.

We note that “discoverability” of spectroscopic binaries with the ngEHT might be problematic due to the likely long orbital periods (thousands of years). However, a potential ngEHT role in studies of spectroscopic binaries discovered by other facilities/techniques is warranted by the unique resolving power of ngEHT imaging in the otherwise unreachable range of angular scales.

6.2.4 Relativistic transiting binaries

Transiting binaries would appear superficially as photometric binaries, with quasi-periodic flaring. However, the changes in brightness would be because of “self-imaging”, one component imaging the photon orbit region of the other (Davelaar and Haiman, 2022; Davelaar and Haiman, 2022; Kelley et al., 2021).

- The photon orbit region of one component would be magnified by the other during the transit due to lensing. If the transit was exact, this would include a central drop, as the focal point passed over the shadow itself.
- Transiting binaries would make it possible to accurately estimate the mass, orbital phase, and the non-Keplerian variations of the system’s orbital parameters, and also permit super-resolving the shadow region of each component. A transiting binary with two visible sources (i.e., one that is also an optical binary) would offer a very sensitive laboratory for the study of fundamental gravitational physics.

6.2.5 Reverberation binaries

SMBHs act as omni-directional mirrors, reflecting some part of incoming light from any direction to any other direction, possibly after multiple orbits around the BH. These multiple orbits impose delays and thus temporal correlations on radiation received by a remote observer (Chesler et al., 2021; Andrianov et al., 2022). Such binaries could be detected in the time domain, through the study of time delays due to photon orbits around the two photon spheres in a binary system. This section assumes Schwarzschild BHs, and approximation which does not change the qualitative nature of the BH reverberations.

No radiation is received from the BH shadow itself, but around the shadow there is a series of increasingly sharp sub-rings, produced by photons that travel around the BH multiple times near the bound photon orbit (see Chesler et al., 2021, and Sec. 2). Suppose there is a flare in the accretion disk of a solitary SMBH: a distant observer would first see a primary burst from the direct light ($n = 0$), then a delayed lensed burst coming from light partially orbiting the BH, delayed by a time $< T$ ($n = 1$), followed by a series of $n > 1$ successively delayed light echoes, each separated by T . In the Schwarzschild approximation, for Sgr A* the scale is $T \sim 668$ s (11.1 minutes), while for M87* the scale is $T \sim 1.03 \times 10^6$ s (~ 12.0 days).

There are several different ways that reverberation binaries may be detected and studied. Denoting the two binary components by “1” and “2”, we start with the assumption that only component 1 is directly visible from the Earth.

- A simple reverberation binary could be detected through the presence of two sets of autocorrelations in the source photometry. If the components have very different

masses the two correlation trains would be well separated in delay space (e.g., 44 days versus 9 hours for the red shifted components of OJ287) and thus could be separated even for a one pixel source.

- If both components 1 and 2 are visible from Earth, the physical separation between 1 and 2 will introduce yet another delay due to path length differences in the time correlations. For example, for OJ287 the $T = 44$ day delay for one photon orbit of the primary is comparable to the one-way propagation delay between the components, which varies between ~ 22 days and 132 days with the orbital phase. Observing a reflection of one component at another would therefore provide a direct determination of the distance between the primary and secondary, and thus a novel way of determining the inclination of the orbit.
- Suppose the component 2 jet is not bright enough to be seen directly from Earth, but its jet is pointed directly at component 1 during its orbit (this would happen twice during each orbit, due to the dual sided nature of SMBH jets). This could then cause multiple quasi-periodic flares: from where the photon flux from the component 2 jet reaches component 1, the charged particle flux from component 2's jet reaches component 1 and excites its jet, alongside the various delays of the component 1 echos.
- The delay of these secondary echos (the light travel time plus the partial photon orbit echo) will vary with the orbital phase of the two components, both because the orbital distance can be changing, and because the length of the $n = 1$ photon orbit will change with orbital phase. If the SMBH orbit is circular but not aligned with component 1's equatorial rotation plane, it may be possible to use the variation in this total delay to determine the spin of component 1.

6.3 Multi-messenger detection of supermassive black hole binaries

SMBHB systems must emit GWs accompanied by electromagnetic counterparts, especially when they are in gas-rich environments (Schnittman, 2011; Dotti et al., 2012; Burke-Spolaor, 2013; Kocsis et al., 2008a) which could be a result of galaxy mergers (Sanders et al., 1988; Mayer et al., 2007).

We anticipate scientific synergies between the ngEHT and several key multi-messenger facilities that are already operational, as well as those that will become operational concurrently with the ngEHT.

- The EHT (EHT Collaboration, 2019a) is already probing the SMBHB candidate OJ287 with highest resolution at 230 GHz. Quasars exhibiting broad emission lines with $\geq 1000 \text{ km s}^{-1}$ velocity offsets with respect to the host galaxy rest frame have been discovered. These velocity-offset broad lines could be due to the dynamics of a SMBHB (e.g., Breiding et al., 2021).
- The ngVLA will be able to probe these system at angular scales as small as $\sim 3 \text{ mas}$ – $80 \mu\text{as}$ for the respective frequency range of 2.4–93 GHz (Astronomical Society of the Pacific Conference Series, 2018).
- While Gaia observations use a novel technique to search for binary quasars at previously unreachable sub-kpc scales (e.g., Shen et al., 2021), the unprecedented near-IR sensitivity, spatial resolution, and spectral coverage of the James Webb

Space Telescope (JWST) will enable detailed study of the gas dynamics in binary quasars at high redshifts (Ishikawa et al., 2021).

- The Athena (Advanced Telescope for High ENergy Astrophysics) mission has the broad aim of understanding the hot and energetic universe and will help unravel accretion processes and jet physics in SMBHBs (Piro et al., 2022).
- The Cherenkov Telescope Array (CTA), a next generation ground-based very-high-energy gamma-ray observatory, will be a key instrument for multi-messenger astrophysics in the very-high energy (VHE, i.e., > 100 GeV) range (Cherenkov Telescope Array Consortium et al., 2019). Due to its unprecedented sensitivity, rapid response, and capability to monitor a large sky area via a scanning mode of operation, SMBHBs might be detectable by their specific flaring properties.
- On-going PTA projects aim at detecting GWs in the nanohertz band, dominated by the gravitational radiation emitted by SMBH binaries with masses in the range 10^8 – $10^{10} M_{\odot}$ inspiraling at sub-parsec separations (~ 0.01 pc).
- Future space-based GW detectors such as LISA (Amaro-Seoane and et al, 2017), Tianqin (Luo and et al, 2016), and Taiji (Hu and Wu, 2017) are designed to detect the millihertz GWs of SMBH binaries with masses in the range 10^5 – $10^7 M_{\odot}$, emitting during their late inspiral and merger phases.

There are many proposed channels through which SMBHBs could emit EM counterparts, either simultaneously with their GW emission phase or afterward. The interaction between a SMBH binary with the gaseous disc in a gas-rich environment is likely to be the primary mechanism for the dissipation of orbital angular momentum by a SMBH binary in its final parsec stage (i.e., shrinking down from several parsec to sub-parsec separations, or, during the GW-emitting stage), effecting the merger within a Hubble time (see, e.g., Khan et al., 2016b). If one or both components of the SMBHB continue to accrete gas the coalescing binary may emit electromagnetic counterparts with a periodic variability that would be detectable both in the PTA band (see e.g., Kelley et al., 2019, for reviews) and in the LISA band (Kocsis et al., 2006; Armitage and Natarajan, 2002). Some of the SMBHB candidates detected with electromagnetic counterparts are listed in Table 3, and the proposed emission models are discussed in Sec. 6.4.

The joint detection of SMBHBs with GWs and electromagnetic counterparts stands to fundamentally transform our understanding of the important role played by astrophysics, and will offer cosmological probes via a new class of standard sirens while also revealing fundamental aspects of gravity (see Schnittman, 2011; Kelley et al., 2019; Mangiagli et al., 2020, for reviews).

6.3.1 Multi-messengers with pulsar timing arrays

A stochastic isotropic GW background (GWB) is predicted from the GWs emitted by the population of SMBHBs at sub-parsec separations across the whole universe. The GWB detected by PTAs will be characterized by a common spectrum and interpulsar spatial correlations: the Hellings & Downs, or HD correlations (Hellings and Downs, 1983), which is the ‘smoking gun’ signature for GWB signals (Tiburzi et al., 2015). Recently, evidence for a spatially uncorrelated common-spectrum process was detected in the 12.5 yr NANOGrav data set (Arzoumanian et al., 2020), and later confirmed by the Parkes PTA (Goncharov and et al, 2021), the European PTA (Chen et al., 2021),

and International PTA (Antoniadis et al., 2022) in their corresponding data releases. The GWB production process is modelled as an additional time-correlated term with a similar power spectrum with GWB in all of the pulsars. While evidence is currently lacking in support of the existence of spatial HD correlations (Arzoumanian et al., 2020; Goncharov et al., 2021; Chen et al., 2021; Antoniadis et al., 2022), we cannot yet declare a detection of GWB. The reported signal offers a hint of the existence of a GWB from SMBHBs, but on-going analysis of the 15 yr data is likely to improve matters (Middleton et al., 2021; Mingarelli, 2019). The current non-detection is already providing interesting constraints on both SMBH binary populations (Graham et al., 2015; Kelley et al., 2019) as well as on individual candidates (Jenet et al., 2004). With monitoring by the SKA, even a small number (~ 20) of high-quality millisecond pulsars will be able to deliver valuable information about the redshift evolution of SMBHBs. Calculations show that within 30 years of operation, about 60 individual SMBHB detections with $z < 0.05$ and more than 104 with $z < 1$ can be expected (Feng et al., 2020).

6.3.2 Multi-messengers with LISA

Contrary to PTAs detecting GWs of individual SMBHBs in the local Universe ($z < 0.5$), LISA, with its high GW detection sensitivity, could reach to the highest redshifts over a large mass range (Amaro-Seoane et al., 2017). Additionally, the detection of the full chirping signal of LISA sources will help to break the degeneracy between the chirp mass and luminosity distance for SMBHBs. The ability to measure the luminosity distance and sky-position of SMBHBs with the full inspiral-merger-ringdown waveform means LISA could make a relatively precise prediction of the source locations (Cutler, 1998; Barack and Cutler, 2004; Vecchio, 2004; Berti et al., 2005; Holz and Hughes, 2005; Kocsis et al., 2008b; Mangiagli et al., 2020). Parameter estimation from the inspiral waveform could provide an early warning system for upcoming merger events, on the order of a week to up to a month in advance of the merger itself (Holz and Hughes, 2005; Lang and Hughes, 2008; Kocsis et al., 2008b; Mangiagli et al., 2020), thereby enabling monitoring and detection of any associated electromagnetic counterparts. The predicted merger events of SMBH binaries detectable by LISA is uncertain at present and stands between about 5–100 per year (Klein et al., 2016) as it is closely related to the poorly determined galaxy merger rates and the ill-determined dynamical evolution time scales of SMBHBs in their post-merger environments.

6.3.3 The role of VLBI in multi-messenger studies

Despite the various multi-band detections of SMBHB candidates at separations close to or larger than a parsec, sub-parsec scale-bound SMBHBs can only be spatially resolved with radio VLBI. The array size and observing frequency sets a fundamental limit on the ability of a VLBI network to resolve a telescopic binary. For a well distributed network, VLBI image resolutions primarily depend on the size of the network, and are thus expected to be ~ 50 , 20 and 15 μas at the proposed observing frequencies of 86, 230 and 345 GHz, respectively. For a source at a redshift of $z = 1$, these correspond to 0.41, 0.16 and 0.12 pc, respectively. These resolution limits are all smaller than the radius where dynamical accretion disk drag is thought to become ineffective (leading to the so-called “final parsec” problem), but much larger than the ISCO of ~ 0.3 milliparsec

for a $10^9 M_\odot$ SMBHB at that redshift. A SMBHB of that mass would therefore need to be at $z \lesssim 0.03$ in order for its ISCO to be resolveable by the ngEHT.

The array size and observing frequency also sets a limit on the astrometric accuracy of even in-beam SMBHB astrometry. The candidate binary source 0402+379 ($z = 0.055$) was observed by the VLBA over 12 years and at frequencies between 5 and 22 GHz, revealing a motion consistent with a binary orbit with an orbital velocity of $0.0054 c \pm 0.0003 c$ and an orbital period of 3×10^4 yr, implying a total binary mass of $1.5 \times 10^{10} M_\odot$ (Bansal et al., 2017). This source is likely an astrometric binary with a separation of ~ 7.5 pc. Astrometry of this source or other parsec-scale candidate sources with the ngEHT could be significantly more precise, but it would likely be impossible to observe non-linear motions (and thus fit an orbit) with the planned duration of the ngEHT program.

The enhanced resolution of the ngEHT is promising to resolve SMBHBs at sub-parsec separation through relative astrometry (D’Orazio and Loeb, 2018a; Fang and Yang, 2022). By fitting the time-varying visibility function of point-like emitters, one can in principle recover the orbital parameters of SMBHBs (Fang and Yang, 2022). The joint detection of SMBHBs with VLBI and PTAs will help to break the degeneracy between characteristic parameters (Fang and Yang, 2022). In the future, multi-messenger and/or multi-band detections of SMBHBs will enable us to confirm or rule out candidate sources.

6.4 Emission models of supermassive binary black holes

The ngEHT as a VLBI array will measure complex visibilities in the Fourier domain depending on their mutual separation and its orientation with respect to the source (i.e., Earth aperture synthesis). Any theoretical model must make predictions for these or derived data products. We discuss several distinct modeling routes for the emission from a binary BH source and discuss prospects for detection and characterization of the source parameters.

6.4.1 Hybrid modeling

A critical and unavoidable complication for the ngEHT will be that any binary source will produce other emission components that are not directly related to the orbital motion of the BH binary. This will in general cause a mismatch between data and model that must be investigated and where possible mitigated. With a hybrid imaging+modeling technique (see Broderick et al., 2020b) the ngEHT will be able to harness its exquisite signal-to-noise ratio to search for even faint binary components buried in diffuse emission beyond the nominal resolution.

6.4.2 Model selection: binary vs Lense-Thirring

A Bayesian framework like Themis allows for a statistically meaningful way to select models based on fit quality and degrees of freedom via the Bayesian evidence or standard information criteria (BIC, AIC, etc.). More concretely, given two competing emission models, both can be fit to the ngEHT or simulated data and the statistically preferred model can be inferred.

6.4.3 Simple emission models

A simple but effective emission model that is implemented in Themis (Broderick et al., 2020a) is a double Gaussian source on a circular orbit. Obvious extensions to eccentric and PN orbits are planned. For any given value of the free parameters the model can generate the set of complex visibilities as a function of observing time and uv coordinate. These simple emission models do not rely on the detailed physical properties of the source and instead utilize a simple representation of a physical scenario via a geometric approach.

6.5 Simplified physical models: approximate, semi-analytic emission models

In moving towards more realistic modelling approaches one can develop phenomenological models utilising semi-analytic schemes, e.g., by considering a SMBBH system orbiting within semi-analytic accretion disk model of the surrounding circumbinary disk.

The simplest model of a binary BH is an analytic spacetime metric which is a superposition of two stationary Kerr BHs, with a binary separation large enough to ensure that the spacetime is approximately Minkowskian at the centre of mass of the system and tidal and secular effects induced between the binary pair are negligible. Whilst such a metric does not formally satisfy the EFEs, we are only concerned with mildly relativistic orbital velocities and the spins of the BHs are anti-aligned such that precession is formally zero and the binary orbit is confined to a two-dimensional plane (adiabatic approximation). Since ngEHT binary targets will have to contain SMBHs with orbital separations sufficient large that the distinct BHs can be spatially resolved, the above assumptions are appropriate. Furthermore, this spacetime metric accurately incorporates the effects of gravitational self-lensing of the binary pair, which is a key observable from synchrotron-emitting plasmas in future ngEHT images. The morphologies of self-lensing flares (SLFs) using a superimposed binary BH metric have been studied by Davelaar and Haiman (2022). In the case where the binary orbit is observed nearly edge-on, a distinct feature in the light curve is imprinted by the shadow around the larger of the two BHs. This method of SLF measurement could make it possible to infer and extract BH shadows that are spatially unresolvable by high-resolution VLBI.

6.5.1 Physical models: GRMHD simulations of accreting SMBH binaries

GRMHD simulations in combination with general-relativistic radiative transfer (GRRT) codes (e.g., Dexter and Agol, 2009; Younsi et al., 2012; Chan et al., 2013; Younsi and Wu, 2015; Pu et al., 2016; Dexter, 2016; Mościbrodzka and Gammie, 2018; Chan et al., 2018; Bronzwaer et al., 2018) are another approach for modeling emission from SMBHBs. In contrast to geometric and semi-analytic modeling, they aim to model the observable phenomenology from ‘first principles’ by directly solving the equations that describe the behavior of plasma, magnetic fields, and radiation, in the vicinity of BHs. While this is desirable from the point of view of physical accuracy, their main disadvantage is their computational cost, which makes it impossible to sample the parameter space as efficiently as the aforementioned approaches. This comes in large part from the necessity of simulating small length and time scales, such

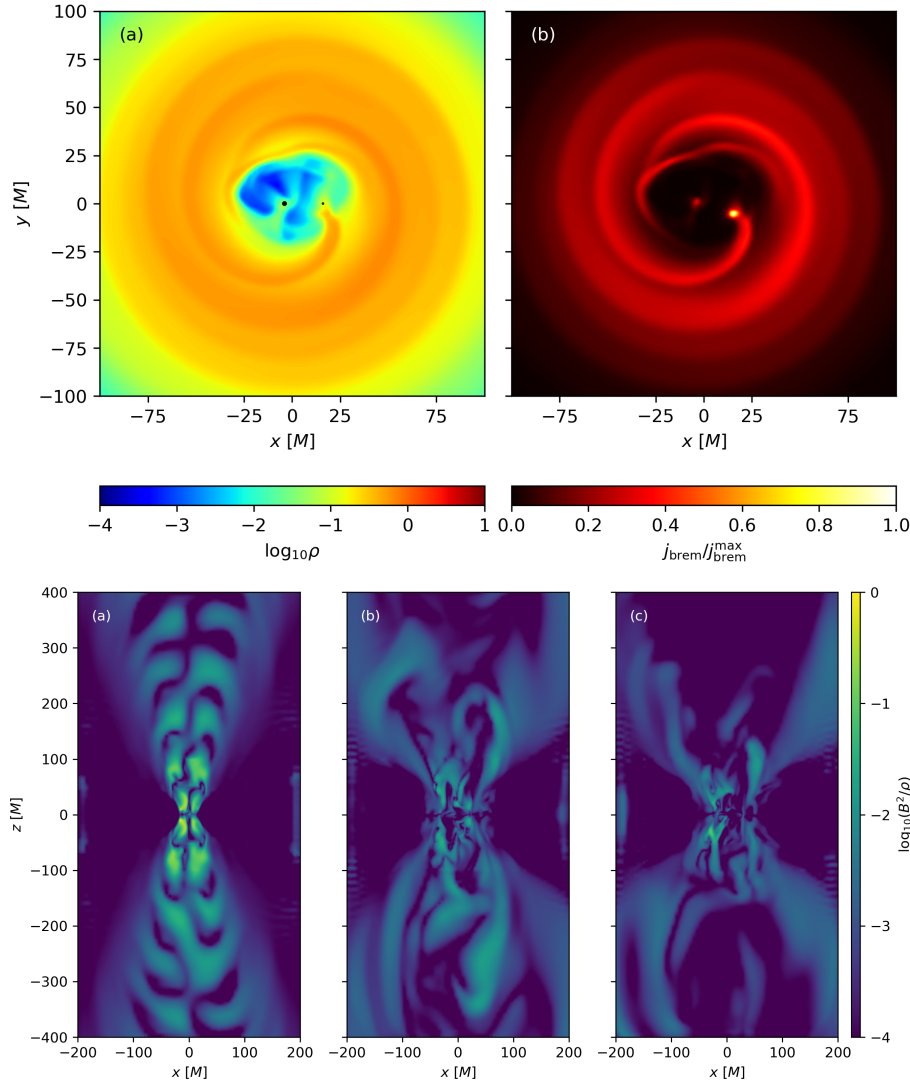


Fig. 28 GRMHD simulations of SMBHBs. Top: simulation viewed in the equatorial plane for a binary with mass ratio 1:4, colored by logarithm (base 10) of plasma rest mass density (left) and normalized bremsstrahlung emissivity (j_{brem} , right). A spiral shock is produced by the smaller mass secondary, increasing j_{brem} . Bottom: the structure of the jet (colored by magnetization of the plasma) for three cases with different mass ratios: (a) 1:1 with zero spin, (b) 1:4 with zero spin, and (c) 1:4 with spin $a_* = 0.7$ for both BHs. The jets form a “braid” structure for the 1:1 case, while the other cases show a more disordered structure (Olivares et al., 2023, in prep.).

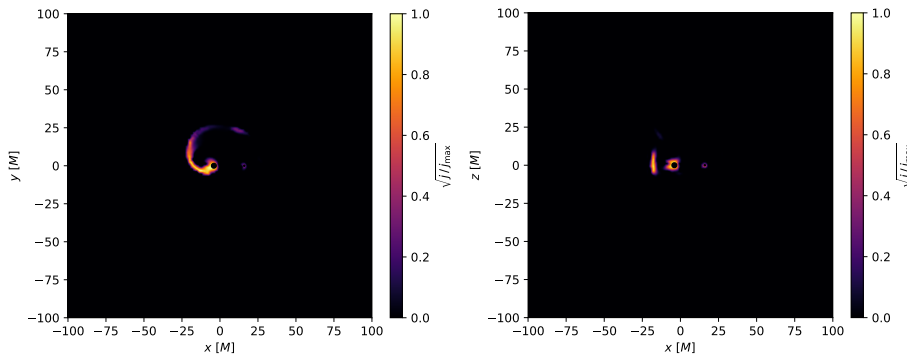


Fig. 29 Proxy for synchrotron emissivity at 230 GHz (equation (18) of Porth et al., 2019) for a GRMHD simulation of accretion onto a binary with mass ratio 1:4 and aligned spins with $a_* = 0.7$, viewed in the equatorial plane (*left*) and meridional plane (*right*). It is possible to observe emission from the spiral shock, and contrary to the Bremsstrahlung case (c.f., Figure 28), the primary appears brighter than the secondary (Olivares et al., 2023, in prep.).

as those required to resolve the MRI turbulence on horizon-scales, alongside the much larger scales of the system such as those governing the dynamics of the binary.

While GRMHD simulations become prohibitive for binaries with large separations, where semi-analytic modeling can be sufficiently accurate, they can yield more detailed information at smaller separations, where the timescales of the accretion flow and the binary dynamics become comparable. This makes the two approaches complementary. GRMHD simulations can also provide information on the connection between large scale features observed in SMBHB candidates and the physical processes originating from within them, which is very difficult to establish using semi-analytic models.

In addition to considering the plasma as a test fluid which does not back react on the metric, GRMHD simulations of SMBHBs in the literature use different approximations that are valid at different separations and evolutionary stages of the binary.

At large binary separations, a metric constructed from the superposition of two boosted Kerr BH spacetimes approximates sufficiently well the corresponding solution to the EFEs. GRMHD simulations on spacetimes constructed in this way have been performed by Combi (2021) and explored in a series of papers (Armengol et al., 2021; Combi et al., 2022; Gutiérrez et al., 2022; Noble et al., 2021). The approximation is shown to be accurate up to separations as small as $\sim 10 r_g$, when the BHs are moving with trajectories prescribed by PN equations. From the observational point of view, among the most interesting predictions is a periodic modulation in lightcurves caused by an asymmetric accretion disk, which in principle could be used to detect SMBHBs and constrain their masses (Noble et al., 2021).

In order to obtain higher accuracy for the spacetime in a regime where gravitational radiation can still be neglected, another approach is to use a conformal thin sandwich approximation (Gold et al., 2014; Olivares et al., 2023, in prep.). This enables finding a SMBHB spacetime that fulfills the Einstein constraints and is stationary in a reference frame co-rotating with the binary. Consequently, standard techniques used for GRMHD simulations in stationary spacetimes can be used. Figure 28 displays snapshots of simulations of binaries performed this way for different values of the mass ratio and spin, reproduced from Olivares et al. (2023, in prep.). They show some of the

features that are expected in accretion onto SMBHBs, such as spiral shocks producing bremsstrahlung radiation (top panels), and helical jets that appear more ordered for the equal mass case (bottom panels). The spiral shock may also be detectable in synchrotron emission at 230 GHz, as shown in Figure 28, which employs a proxy for synchrotron emission described in Porth et al. (2019).

When gravitational radiation becomes dominant as a mechanism for decreasing the orbital separation, the spacetime needs to be evolved using full numerical relativity. Besides being more physically accurate, this permits simultaneous retrieval of the GW signal and the electromagnetic counterpart, e.g., as done in Gold et al. (2014).

After the merger, the spacetime settles down to that of a Kerr BH. The spacetime is stationary again in a frame where the BH is at rest. However, the accretion flow will likely still show signatures of the recent merger. It has been shown that after the release of linear momentum in the form of GWs, the resulting BH can have a residual recoil velocity from hundreds to thousands of kilometers per second (Baker et al., 2007). This can produce spiral shocks emitting Bremsstrahlung radiation, indicating a recent merger. Simulations of these electromagnetic counterparts have been performed by Zanotti et al. (2010) and Meliani et al. (2017b).

The ngEHT will bring the possibility to refine theoretical models of circumbinary accretion flows by allowing comparison of simulations with higher precision observations. Possible directions for simulation-based modeling of these systems in the near future are to specialize to the parameters of the most promising SMBHB candidates, and to refine predictions of observational signatures that enable identification at different stages in their evolution.

6.6 Summary of prospects of probing SMBH binaries with the ngEHT

Supermassive BH binaries in sub-parsec separation phase evolution located at Gpc distances typically have angular separations of $1\text{--}10\mu\text{as}$. This close separation is beyond the current resolution of most telescopes. The ngEHT, with its higher resolution, promises to resolve these supermassive BH binaries through relative astrometry (D’Orazio and Loeb, 2018a; Fang and Yang, 2022).

To track the orbital path of the components in the binary, both individual SMBHBs are required to be bright enough to be detectable independently, or if one component is bright, then a calibrator nearby is necessary, as it will be required for successful relative astrometry. The orbital period could be inferred from the regularity of the periodic variations, which is possible when the orbital period is shorter than the detection duration of the ngEHT lifetime. The upper limit on the detection duration is the designed lifetime of ngEHT, which is 10 years. Furthermore, the validity of the second criterion requires that the mm-wavelength emission region (roughly the light-travel distance within the duration of the shortest mm-variability timescales) should be smaller than the binary separation. It is suggested that the low-luminosity AGN (LLAGN) with mm-emission regions comparable to the size of the event horizon meet the requirement of the variation timescale in the emission region (D’Orazio and Loeb, 2018a). By modeling the fraction of SMBHBs in the distribution function of LLAGN, D’Orazio and Loeb (2018a) predict that the abundance of SMBHBs resolvable by ngEHT at redshift $z \leq 0.5$ is about 100, assuming the orbital period is less than the ten-year lifetime ngEHT.

The quantity measured by EHT is the visibility function, which is the Fourier transformation of the intensity function of the image, realized by the technology of VLBI. In the LLAGN scenario of SMBHB candidates, the emission region of the individual sources is small compared to the binary separation. The simplest assumption for the intensity function of the components is to model them with point-like luminosities. In this point-like luminosity approximation, the amplitude of the visibility function is proportional to $\sqrt{I_1^2 + I_2^2 + 2I_1I_2 \cos 2\pi \mathbf{u} \cdot \boldsymbol{\theta}}$, where I_1 and I_2 are the intensity amplitudes for the two components, and \mathbf{u} and $\boldsymbol{\theta}$ are the baseline vector and angular separation vector of the binary in the sky plane, respectively. Due to the orbital motion of the binary, the projected relative position vector $\boldsymbol{\theta}$ changes its direction with respect to the baseline \mathbf{u} , and varies in amplitude if there is eccentricity or inclination in the binary orbit. Thus the variation of the visibility function is modulated by the binary orbital motion with the same period. By considering the binary intensities as point-like emitters, Fang and Yang (2022) make a proof-of-concept estimate that the orbital motion of the SMBHB could be traced and recovered by fitting the time-varying visibility function. They report that orbital tomography of the binary orbital motion is possible even if the binary orbital period is larger than the lifetime of ngEHT (Fang and Yang, 2022). This could greatly increase the orbital period or semi-major axis of SMBHBs resolvable by ngEHT, and as a consequence increase the source abundance from ~ 100 up to several 1000s, as inferred from the LLAGN scenario modeled by D’Orazio and Loeb (2018a).

6.7 Challenges & future prospects

To prepare for future detections and monitoring of SMBHBs with the ngEHT, further detailed simulations are required.

- The preparation of simulations testing the imaging quality of different ngEHT-arrays (e.g., number of telescopes) using different geometric models will be pivotal. In particular, emission blobs with various parameters (e.g., different intensities, angular separation, sizes, field of view) and their reconstructed images will need to be probed and studied in detail.
- Orbital and light curve tomographies will need to be ray-traced whilst taking additional physical effects and interactions into account.
- Modeling of different types of binary systems, i.e., two radio-loud objects versus a combination of a radio-loud and a radio-quiet object, will be essential. The role of jets, circumbinary accretion disk, and other radiating material media for specific candidate sources will need to be prepared. In this context, inspecting the specific signatures and time scales of LT-precession and helical magnetic fields will be important.
- Simulation of lensing signatures will be of crucial importance, i.e., if the accretion disk has (spiral) structure visible in the radio/synchrotron emission, the ngEHT may be able to see that structure lensed in the BH shadow (i.e., the emission is a gravitationally-lensed image of the accretion disk, which would have a spiral structure here). Further self-lensing effects with the ngEHT need to be studied.
- The influence of GW emission on the closest pairs and their appearance in ngEHT imaging also needs to be explored further.

Conclusions

The past four years have been a short yet exciting time for BH physicists, first with the EHT measurement of the M87* SMBH shadow in 2019, and shortly thereafter with the measurement of Sgr A*'s shadow in 2022. These pioneering measurements heralded the start of a new era in BH research and have enabled, for the first time, direct imaging of matter in the vicinity of event horizons. In the years ahead, improvements will be made in the instrument specifications of telescopes within the interferometric array, which will in turn open several new avenues for exploring physical phenomena around BHs. This review provides an overview of the major fundamental physics themes and current status of BH imaging observations which will guide the development of a future ngEHT array and enable significantly more sensitive studies of SMBHs.

In the context of these future improvements we have summarised the current status of several key science topics underpinning BH imaging studies: studies of the photon ring, measurement of BH mass and spin, searches for ultralight fields, tests of GR and Kerr, and potential studies of binary SMBHs. In the years to come, advances will be made in both the sensitivity of measurements, and in the data analysis techniques which are applied to these data, which will further advance our understanding of BHs and their environments. This review presents an overview of the exciting scientific potential of future BH imaging studies, and is intended to be useful as a reference for researchers interested in utilising the ngEHT as a distinct new tool for probing BHs and studying fundamental physics.

Acknowledgments

We are grateful to Kfir Blum, Sam Gralla, Paolo Pani, Odele Straub and Nico Yunes for useful discussions and important feedback. We express our thanks to the EHT Collaboration's Publication Committee and the three anonymous internal referees.

References

- Abbott BP, et al. (2017a) Gravitational Waves and Gamma-rays from a Binary Neutron Star Merger: GW170817 and GRB 170817A. *Astrophys J Lett* 848(2):L13. <https://doi.org/10.3847/2041-8213/aa920c>. [arXiv:1710.05834](https://arxiv.org/abs/1710.05834) [astro-ph.HE]
- Abbott BP, et al. (2017b) GW170104: Observation of a 50-Solar-Mass Binary Black Hole Coalescence at Redshift 0.2. *Phys Rev Lett* 118(22):221101. <https://doi.org/10.1103/PhysRevLett.118.221101>, [Erratum: *Phys.Rev.Lett.* 121, 129901 (2018)]. [arXiv:1706.01812](https://arxiv.org/abs/1706.01812) [gr-qc]
- Abbott BP, et al. (2017c) GW170817: Observation of Gravitational Waves from a Binary Neutron Star Inspiral. *Phys Rev Lett* 119(16):161101. <https://doi.org/10.1103/PhysRevLett.119.161101>. [arXiv:1710.05832](https://arxiv.org/abs/1710.05832) [gr-qc]
- Abbott BP, et al. (2021a) A Gravitational-wave Measurement of the Hubble Constant Following the Second Observing Run of Advanced LIGO and Virgo. *Astrophys J* 909(2):218. <https://doi.org/10.3847/1538-4357/abdcb7>. [arXiv:1908.06060](https://arxiv.org/abs/1908.06060) [astro-ph.CO]
- Abbott LF, Sikivie P (1983) A Cosmological Bound on the Invisible Axion. *Phys Lett B* 120:133–136. [https://doi.org/10.1016/0370-2693\(83\)90638-X](https://doi.org/10.1016/0370-2693(83)90638-X)
- Abbott R, et al. (2021b) Constraints on Cosmic Strings Using Data from the Third Advanced LIGO–Virgo Observing Run. *Phys Rev Lett* 126(24):241102. <https://doi.org/10.1103/PhysRevLett.126.241102>. [arXiv:2101.12248](https://arxiv.org/abs/2101.12248) [gr-qc]
- Abdikamalov AB, Abdujabbarov AA, Ayzenberg D, Malafarina D, Bambi C, Ahmedov B (2019) Black hole mimicker hiding in the shadow: Optical properties of the γ metric. *Phys Rev D* 100(2):024014. <https://doi.org/10.1103/PhysRevD.100.024014>. [arXiv:1904.06207](https://arxiv.org/abs/1904.06207) [gr-qc]
- Abdujabbarov A, Amir M, Ahmedov B, Ghosh SG (2016) Shadow of rotating regular black holes. *Phys Rev D* 93(10):104004. <https://doi.org/10.1103/PhysRevD.93.104004>. [arXiv:1604.03809](https://arxiv.org/abs/1604.03809) [gr-qc]
- Abel SA, Goodsell MD, Jaeckel J, Khoze VV, Ringwald A (2008) Kinetic Mixing of the Photon with Hidden U(1)s in String Phenomenology. *JHEP* 07:124. <https://doi.org/10.1088/1126-6708/2008/07/124>. [arXiv:0803.1449](https://arxiv.org/abs/0803.1449) [hep-ph]
- Abraham Z, Carrara EA (1998) The Precessing Jet in 3C 279. *ApJ* 496(1):172–176. <https://doi.org/10.1086/305387>
- Abraham Z, Romero GE (1999) Beaming and precession in the inner jet of 3C 273. *A&A* 344:61–67
- Abuter R, Accardo M, Amorim A, Anugu N, Ávila G, et al. (2017) First light for GRAVITY: Phase referencing optical interferometry for the Very Large Telescope Interferometer. *Astronomy and Astrophysics* 602:A94. <https://doi.org/10.1051/0004-6361/201730838>. [arXiv:1705.02345](https://arxiv.org/abs/1705.02345) [astro-ph.IM]
- Abuter R, Amorim A, Bauböck M, Berger JP, Bonnet H, et al. (2018) Detection of orbital motions near the last stable circular orbit of the massive black hole SgrA*. *Astronomy and Astrophysics* 618:L10. <https://doi.org/10.1051/0004-6361/201834294>. [arXiv:1810.12641](https://arxiv.org/abs/1810.12641) [astro-ph.GA]
- Abuter R, Alarcon P, Allouche F, Amorim A, Bailet C, et al. (2022) The GRAVITY+ Project: Towards All-sky, Faint-Science, High-Contrast Near-Infrared Interferometry at the VLTI. *The Messenger* 189:17–22. <https://doi.org/10.18727/0722-6691/5285>
- Abuter R, et al. (2018) Detection of the gravitational redshift in the orbit of the star S2 near the Galactic centre massive black hole. *Astron Astrophys* 615:L15. <https://doi.org/10.1051/0004-6361/201833718>. [arXiv:1807.09409](https://arxiv.org/abs/1807.09409) [astro-ph.GA]

- Abuter R, et al. (2019) A geometric distance measurement to the galactic center black hole with 0.3% uncertainty. *A&A* 625:L10. <https://doi.org/10.1051/0004-6361/201935656>
- Abuter R, et al. (2020) Detection of the Schwarzschild precession in the orbit of the star S2 near the Galactic centre massive black hole. *Astron Astrophys* 636:L5. <https://doi.org/10.1051/0004-6361/202037813>. [arXiv:2004.07187](https://arxiv.org/abs/2004.07187) [astro-ph.GA]
- Abuter R, et al. (2022) Mass distribution in the Galactic Center based on interferometric astrometry of multiple stellar orbits. *Astron Astrophys* 657:L12. <https://doi.org/10.1051/0004-6361/202142465>. [arXiv:2112.07478](https://arxiv.org/abs/2112.07478) [astro-ph.GA]
- Addazi A, et al. (2022) Quantum gravity phenomenology at the dawn of the multi-messenger era—A review. *Prog Part Nucl Phys* 125:103948. <https://doi.org/10.1016/j.ppnp.2022.103948>. [arXiv:2111.05659](https://arxiv.org/abs/2111.05659) [hep-ph]
- Akiyama K, Ikeda S, Pleau M, Fish VL, Tazaki F, Kuramochi K, Broderick AE, Dexter J, Mościbrodzka M, Gowanlock M, Honma M, Doeleman SS (2017) Superresolution Full-polarimetric Imaging for Radio Interferometry with Sparse Modeling. *Astrrophys. J.*153(4):159. <https://doi.org/10.3847/1538-3881/aa6302>. [arXiv:1702.00424](https://arxiv.org/abs/1702.00424) [astro-ph.IM]
- Alexander T, Hopman C (2009) Strong mass segregation around a massive black hole. *Astrophys J* 697:1861–1869. <https://doi.org/10.1088/0004-637X/697/2/1861>. [arXiv:0808.3150](https://arxiv.org/abs/0808.3150) [astro-ph]
- Allahyari A, Gorji MA, Mukohyama S (2020a) Bounds on the Horndeski Gauge-Gravity Coupling. *JCAP* 05:013. <https://doi.org/10.1088/1475-7516/2020/05/013>, [Erratum: *JCAP* 05, E02 (2021)]. [arXiv:2002.11932](https://arxiv.org/abs/2002.11932) [astro-ph.CO]
- Allahyari A, Khodadi M, Vagnozzi S, Mota DF (2020b) Magnetically charged black holes from non-linear electrodynamics and the Event Horizon Telescope. *JCAP* 02:003. <https://doi.org/10.1088/1475-7516/2020/02/003>. [arXiv:1912.08231](https://arxiv.org/abs/1912.08231) [gr-qc]
- Almheiri A, Marolf D, Polchinski J, Sully J (2013) Black Holes: Complementarity or Firewalls? *JHEP* 02:062. [https://doi.org/10.1007/JHEP02\(2013\)062](https://doi.org/10.1007/JHEP02(2013)062). [arXiv:1207.3123](https://arxiv.org/abs/1207.3123) [hep-th]
- Amarilla L, Eiroa EF (2012) Shadow of a rotating braneworld black hole. *Phys Rev D* 85:064019. <https://doi.org/10.1103/PhysRevD.85.064019>. [arXiv:1112.6349](https://arxiv.org/abs/1112.6349) [gr-qc]
- Amarilla L, Eiroa EF (2013) Shadow of a Kaluza-Klein rotating dilaton black hole. *Phys Rev D* 87(4):044057. <https://doi.org/10.1103/PhysRevD.87.044057>. [arXiv:1301.0532](https://arxiv.org/abs/1301.0532) [gr-qc]
- Amarilla L, Eiroa EF, Giribet G (2010) Null geodesics and shadow of a rotating black hole in extended Chern-Simons modified gravity. *Phys Rev D* 81:124045. <https://doi.org/10.1103/PhysRevD.81.124045>. [arXiv:1005.0607](https://arxiv.org/abs/1005.0607) [gr-qc]
- Amaro-Seoane P, et al (2017) Laser Interferometer Space Antenna. [arXiv e-prints arXiv:1702.00786](https://arxiv.org/abs/1702.00786). [arXiv:1702.00786](https://arxiv.org/abs/1702.00786) [astro-ph.IM]
- Amaro-Seoane P, Audley H, Babak S, Baker J, Barausse E, Bender P, Berti E, Binétruy P, Born M, Bortoluzzi D, Camp J, Caprini C, Cardoso V, Colpi M, Conklin J, Cornish N, Cutler C, Danzmann K, Dolesi R, Ferraioli L, Ferroni V, Fitzsimons E, Gair J, Gesa Bote L, Giardini D, Gibert F, Grigani C, Hallain H, Heinzel G, Hertog T, Hewitson M, Holley-Bockelmann K, Hollington D, Hueller M, Inchauspe H, Jetzer P, Karnesis N, Killow C, Klein A, Klipstein B, Korsakova N, Larson SL, Livas J, Lloro I, Man N, Mance D, Martino J, Mateos I, McKenzie K, McWilliams ST, Miller C, Mueller G, Nardini G, Nelemans G, Nofrarias M, Petiteau A, Pivato P, Plagnol E, Porter E, Reiche J, Robertson D, Robertson N, Rossi E, Russano G, Schutz B, Sesana A, Shoemaker D, Slutsky J, Sopuerta CF, Sumner T, Tamanini N, Thorpe

- I, Troebs M, Vallisneri M, Vecchio A, Vetrugno D, Vitale S, Volonteri M, Wanner G, Ward H, Wass P, Weber W, Ziemer J, Zweifel P (2017) Laser Interferometer Space Antenna. arXiv e-prints arXiv:1702.00786. <https://doi.org/10.48550/arXiv.1702.00786>. arXiv:1702.00786 [astro-ph.IM]
- Ambrus M, Hájíček P (2005) Quantum superposition principle and gravitational collapse: Scattering times for spherical shells. *Phys Rev D* 72:064025. <https://doi.org/10.1103/PhysRevD.72.064025>. arXiv:gr-qc/0507017
- Ames WL, Thorne KS (1968) The Optical Appearance of a Star that is Collapsing Through its Gravitational Radius. *Astrophys. J.*151:659. <https://doi.org/10.1086/149465>
- Amir M, Ghosh SG (2016) Shapes of rotating nonsingular black hole shadows. *Phys Rev D* 94(2):024054. <https://doi.org/10.1103/PhysRevD.94.024054>. arXiv:1603.06382 [gr-qc]
- Amir M, Singh BP, Ghosh SG (2018) Shadows of rotating five-dimensional charged EMCS black holes. *Eur Phys J C* 78(5):399. <https://doi.org/10.1140/epjc/s10052-018-5872-3>. arXiv:1707.09521 [gr-qc]
- Amir M, Jusufi K, Banerjee A, Hansraj S (2019) Shadow images of Kerr-like wormholes. *Class Quant Grav* 36(21):215007. <https://doi.org/10.1088/1361-6382/ab42be>. arXiv:1806.07782 [gr-qc]
- Amorim A, et al. (2019) Scalar field effects on the orbit of S2 star. *Mon Not Roy Astron Soc* 489(4):4606–4621. <https://doi.org/10.1093/mnras/stz2300>. arXiv:1908.06681 [astro-ph.GA]
- Andrianov A, Chernov S, Girin I, Likhachev S, Lyakhovets A, Shchekinov Y (2022) Flares and their echoes can help distinguish photon rings from black holes with space-Earth very long baseline interferometry. *Phys Rev D* 105(6):063015. <https://doi.org/10.1103/PhysRevD.105.063015>. arXiv:2203.00577 [astro-ph.HE]
- Ansoldi S (2008) Spherical black holes with regular center: A Review of existing models including a recent realization with Gaussian sources. In: Conference on Black Holes and Naked Singularities. arXiv:0802.0330 [gr-qc]
- Antoniadis J, et al. (2022) The International Pulsar Timing Array second data release: Search for an isotropic gravitational wave background. *Mon Not Roy Astron Soc* 510(4):4873–4887. <https://doi.org/10.1093/mnras/stab3418>. arXiv:2201.03980 [astro-ph.HE]
- Antonini F, Toonen S, Hamers AS (2017) Binary Black Hole Mergers from Field Triples: Properties, Rates, and the Impact of Stellar Evolution. *Astrophys. J.*841(2):77. <https://doi.org/10.3847/1538-4357/aa6f5e>. arXiv:1703.06614 [astro-ph.GA]
- Armengol FGL, Combi L, Campanelli M, Noble SC, Krolik JH, Bowen DB, Avara MJ, Mewes V, Nakano H (2021) Circumbinary Disk Accretion into Spinning Black Hole Binaries. *The Astrophysical Journal* 913(1):16. <https://doi.org/10.3847/1538-4357/abf0af>, URL <https://dx.doi.org/10.3847/1538-4357/abf0af>, publisher: The American Astronomical Society
- Armitage PJ, Natarajan P (2002) Accretion during the Merger of Supermassive Black Holes. *Astrophys. J. Lett.*567(1):L9–L12. <https://doi.org/10.1086/339770>. arXiv:astro-ph/0201318 [astro-ph]
- Armitage PJ, Natarajan P (2002) Accretion during the merger of supermassive black holes. *The Astrophysical Journal* 567(1):L9
- Arrechea J, Barceló C, Carballo-Rubio R, Garay LJ (2021) Semiclassical constant-density spheres in a regularized Polyakov approximation. *Phys Rev D* 104(8):084071. <https://doi.org/10.1103/PhysRevD.104.084071>. arXiv:2105.11261 [gr-qc]

- Arrechea J, Barceló C, Carballo-Rubio R, Garay LJ (2022) Semiclassical relativistic stars. *Sci Rep* 12(1):15958. <https://doi.org/10.1038/s41598-022-19836-8>. [arXiv:2110.15808](https://arxiv.org/abs/2110.15808) [gr-qc]
- Arvanitaki A, Dimopoulos S, Dubovsky S, Kaloper N, March-Russell J (2010) String Axiverse. *Phys Rev D* 81:123530. <https://doi.org/10.1103/PhysRevD.81.123530>. [arXiv:0905.4720](https://arxiv.org/abs/0905.4720) [hep-th]
- Arvanitaki A, Baryakhtar M, Dimopoulos S, Dubovsky S, Lasenby R (2017) Black Hole Mergers and the QCD Axion at Advanced LIGO. *Phys Rev D* 95(4):043001. <https://doi.org/10.1103/PhysRevD.95.043001>. [arXiv:1604.03958](https://arxiv.org/abs/1604.03958) [hep-ph]
- Arzoumanian Z, et al. (2020) The NANOGrav 12.5 yr Data Set: Search for an Isotropic Stochastic Gravitational-wave Background. *Astrophys J Lett* 905(2):L34. <https://doi.org/10.3847/2041-8213/abd401>. [arXiv:2009.04496](https://arxiv.org/abs/2009.04496) [astro-ph.HE]
- Asada K, Kino M, Honma M, Hirota T, Lu RS, Inoue M, Sohn BW, Shen ZQ, Ho PTP, Akiyama K, Algaba JC, An T, Bower G, Byun DY, Dodson R, Doi A, Edwards PG, Fujisawa K, Gu MF, Hada K, Hagiwara Y, Jaroenjittichai P, Jung T, Kawashima T, Koyama S, Lee SS, Matsushita S, Nagai H, Nakamura M, Niinuma K, Phillips C, Park JH, Pu HY, Ro HW, Stevens J, Trippe S, Wajima K, Zhao GY (2017) White Paper on East Asian Vision for mm/submm VLBI: Toward Black Hole Astrophysics down to Angular Resolution of $1 R_S$. *arXiv e-prints arXiv:1705.04776*. [arXiv:1705.04776](https://arxiv.org/abs/1705.04776) [astro-ph.HE]
- Ashtekar A, Bojowald M (2005) Black hole evaporation: A Paradigm. *Class Quant Grav* 22:3349–3362. <https://doi.org/10.1088/0264-9381/22/16/014>. [arXiv:gr-qc/0504029](https://arxiv.org/abs/gr-qc/0504029)
- Ashtekar A, Bojowald M (2006) Quantum geometry and the Schwarzschild singularity. *Class Quant Grav* 23:391–411. <https://doi.org/10.1088/0264-9381/23/2/008>. [arXiv:gr-qc/0509075](https://arxiv.org/abs/gr-qc/0509075)
- Ashtekar A, Krishnan B (2004) Isolated and dynamical horizons and their applications. *Living Rev Rel* 7:10. <https://doi.org/10.12942/lrr-2004-10>. [arXiv:gr-qc/0407042](https://arxiv.org/abs/gr-qc/0407042)
- Ashtekar A, Olmedo J, Singh P (2018) Quantum Transfiguration of Kruskal Black Holes. *Phys Rev Lett* 121(24):241301. <https://doi.org/10.1103/PhysRevLett.121.241301>. [arXiv:1806.00648](https://arxiv.org/abs/1806.00648) [gr-qc]
- Astronomical Society of the Pacific Conference Series (2018) Science with a Next Generation Very Large Array. *Astronomical Society of the Pacific Conference Series*, vol 517
- Ayon-Beato E, Garcia A (1998) Regular black hole in general relativity coupled to nonlinear electrodynamics. *Phys Rev Lett* 80:5056–5059. <https://doi.org/10.1103/PhysRevLett.80.5056>. [arXiv:gr-qc/9911046](https://arxiv.org/abs/gr-qc/9911046)
- Ayzenberg D (2022) Testing Gravity with Black Hole Shadow Subrings. *arXiv e-prints arXiv:2202.02355* [gr-qc]
- Ayzenberg D, Yunes N (2018) Black Hole Shadow as a Test of General Relativity: Quadratic Gravity. *Class Quant Grav* 35(23):235002. <https://doi.org/10.1088/1361-6382/aae87b>. [arXiv:1807.08422](https://arxiv.org/abs/1807.08422) [gr-qc]
- Azreg-Aïnou M (2014) Generating rotating regular black hole solutions without complexification. *Phys Rev D* 90(6):064041. <https://doi.org/10.1103/PhysRevD.90.064041>. [arXiv:1405.2569](https://arxiv.org/abs/1405.2569) [gr-qc]
- Babak S, et al. (2010) The Mock LISA Data Challenges: From Challenge 3 to Challenge 4. *Class Quant Grav* 27:084009. <https://doi.org/10.1088/0264-9381/27/8/084009>. [arXiv:0912.0548](https://arxiv.org/abs/0912.0548) [gr-qc]
- Bacchini F, Mayerson DR, Ripperda B, Davelaar J, Olivares H, Hertog T, Vercnocke B (2021) Fuzzball Shadows: Emergent Horizons from Microstructure.

- Phys Rev Lett 127(17):171601. <https://doi.org/10.1103/PhysRevLett.127.171601>. [arXiv:2103.12075](https://arxiv.org/abs/2103.12075) [hep-th]
- Backes M, Müller C, Conway JE, Deane R, Evans R, Falcke H, Fraga-Encinas R, Goddi C, Klein Wolt M, Krichbaum TP, MacLeod G, Ribeiro VARM, Roelofs F, Shen ZQ, van Langevelde HJ (2016) The Africa Millimetre Telescope. In: The 4th Annual Conference on High Energy Astrophysics in Southern Africa (HEASA 2016). p 29. <https://doi.org/10.22323/1.275.0029>
- Bah I, Bena I, Heidmann P, Li Y, Mayerson DR (2021) Gravitational footprints of black holes and their microstate geometries. JHEP 10:138. [https://doi.org/10.1007/JHEP10\(2021\)138](https://doi.org/10.1007/JHEP10(2021)138). [arXiv:2104.10686](https://arxiv.org/abs/2104.10686) [hep-th]
- Baker JG, Boggs WD, Centrella J, Kelly BJ, McWilliams ST, Miller MC, van Meter JR (2007) Modeling Kicks from the Merger of Nonprecessing Black Hole Binaries. The Astrophysical Journal 668:1140–1144. <https://doi.org/10.1086/521330>, URL <https://ui.adsabs.harvard.edu/abs/2007ApJ...668.1140B>, aDS Bibcode: 2007ApJ...668.1140B
- Balasubramanian V, de Boer J, El-Showk S, Messamah I (2008) Black Holes as Effective Geometries. Class Quant Grav 25:214004. <https://doi.org/10.1088/0264-9381/25/21/214004>. [arXiv:0811.0263](https://arxiv.org/abs/0811.0263) [hep-th]
- Balbus SA, Hawley JF (1991) A powerful local shear instability in weakly magnetized disks. I - Linear analysis. II - Nonlinear evolution. Astrophys J 376:214. <https://doi.org/10.1086/170270>, URL <http://adsabs.harvard.edu/doi/10.1086/170270>
- Ball D, Sironi L, Özel F (2019) The Mechanism of Electron Injection and Acceleration in Transrelativistic Reconnection. Astrophys. J.884(1):57. <https://doi.org/10.3847/1538-4357/ab3f2e>. [arXiv:1908.05866](https://arxiv.org/abs/1908.05866) [astro-ph.HE]
- Bambi C (2013) Can the supermassive objects at the centers of galaxies be traversable wormholes? The first test of strong gravity for mm/sub-mm very long baseline interferometry facilities. Phys Rev D 87:107501. <https://doi.org/10.1103/PhysRevD.87.107501>. [arXiv:1304.5691](https://arxiv.org/abs/1304.5691) [gr-qc]
- Bambi C (2014) Constraining possible variations of the fine structure constant in strong gravitational fields with the $K\alpha$ iron line. JCAP 03:034. <https://doi.org/10.1088/1475-7516/2014/03/034>. [arXiv:1308.2470](https://arxiv.org/abs/1308.2470) [gr-qc]
- Bambi C, Modesto L (2013) Rotating regular black holes. Phys Lett B 721:329–334. <https://doi.org/10.1016/j.physletb.2013.03.025>. [arXiv:1302.6075](https://arxiv.org/abs/1302.6075) [gr-qc]
- Banerjee I, Chakraborty S, SenGupta S (2020) Silhouette of M87*: A New Window to Peek into the World of Hidden Dimensions. Phys Rev D 101(4):041301. <https://doi.org/10.1103/PhysRevD.101.041301>. [arXiv:1909.09385](https://arxiv.org/abs/1909.09385) [gr-qc]
- Bansal K, Taylor GB, Peck AB, Zavala RT, Romani RW (2017) Constraining the Orbit of the Supermassive Black Hole Binary 0402+379. Astrophys J 843(1):14. <https://doi.org/10.3847/1538-4357/aa74e1>. [arXiv:1705.08556](https://arxiv.org/abs/1705.08556) [astro-ph.GA]
- Bar N, Blas D, Blum K, Sibiriyakov S (2018) Galactic rotation curves versus ultralight dark matter: Implications of the soliton-host halo relation. Phys Rev D 98(8):083027. <https://doi.org/10.1103/PhysRevD.98.083027>. [arXiv:1805.00122](https://arxiv.org/abs/1805.00122) [astro-ph.CO]
- Bar N, Blum K, Lacroix T, Panci P (2019) Looking for ultralight dark matter near supermassive black holes. JCAP 07:045. <https://doi.org/10.1088/1475-7516/2019/07/045>. [arXiv:1905.11745](https://arxiv.org/abs/1905.11745) [astro-ph.CO]
- Barack L, Cutler C (2004) Lisa capture sources: Approximate waveforms, signal-to-noise ratios, and parameter estimation accuracy. Phys Rev D 69:082005. <https://doi.org/10.1103/PhysRevD.69.082005>, URL <https://link.aps.org/doi/10.1103/PhysRevD.69.082005>

- Barausse E, Sotiriou TP (2008) Perturbed Kerr Black Holes can probe deviations from General Relativity. *Phys Rev Lett* 101:099001. <https://doi.org/10.1103/PhysRevLett.101.099001>. [arXiv:0803.3433](https://arxiv.org/abs/0803.3433) [gr-qc]
- Barausse E, Jacobson T, Sotiriou TP (2011) Black holes in Einstein-aether and Horava-Lifshitz gravity. *Phys Rev D* 83:124043. <https://doi.org/10.1103/PhysRevD.83.124043>. [arXiv:1104.2889](https://arxiv.org/abs/1104.2889) [gr-qc]
- Barcelo C, Liberati S, Sonogo S, Visser M (2008) Fate of gravitational collapse in semiclassical gravity. *Phys Rev D* 77:044032. <https://doi.org/10.1103/PhysRevD.77.044032>. [arXiv:0712.1130](https://arxiv.org/abs/0712.1130) [gr-qc]
- Barceló C, Liberati S, Sonogo S, Visser M (2009) Black Stars, Not Holes. *Sci Am* 301(4):38–45. <https://doi.org/10.1038/scientificamerican1009-38>
- Barceló C, Carballo-Rubio R, Garay LJ (2014) Mutiny at the white-hole district. *Int J Mod Phys D* 23(12):1442022. <https://doi.org/10.1142/S021827181442022X>. [arXiv:1407.1391](https://arxiv.org/abs/1407.1391) [gr-qc]
- Barceló C, Carballo-Rubio R, Garay LJ, Jannes G (2015) The lifetime problem of evaporating black holes: mutiny or resignation. *Class Quant Grav* 32(3):035012. <https://doi.org/10.1088/0264-9381/32/3/035012>. [arXiv:1409.1501](https://arxiv.org/abs/1409.1501) [gr-qc]
- Barceló C, Carballo-Rubio R, Garay LJ (2016) Where does the physics of extreme gravitational collapse reside? *Universe* 2(2):7. <https://doi.org/10.3390/universe2020007>. [arXiv:1510.04957](https://arxiv.org/abs/1510.04957) [gr-qc]
- Barceló C, Boyanov V, Carballo-Rubio R, Garay LJ (2022) Classical mass inflation versus semiclassical inner horizon inflation. *Phys Rev D* 106(12):124006. <https://doi.org/10.1103/PhysRevD.106.124006>. [arXiv:2203.13539](https://arxiv.org/abs/2203.13539) [gr-qc]
- Bardeen JM (1973) Timelike and null geodesics in the Kerr metric. In: *Les Houches Summer School of Theoretical Physics: Black Holes*. pp 215–240
- Bardeen JM, Press WH, Teukolsky SA (1972) Rotating Black Holes: Locally Non-rotating Frames, Energy Extraction, and Scalar Synchrotron Radiation. *Astrophys J* 178:347–370. <https://doi.org/10.1086/151796>
- Baryakhtar M, Lasenby R, Teo M (2017) Black Hole Superradiance Signatures of Ultralight Vectors. *Phys Rev D* 96(3):035019. <https://doi.org/10.1103/PhysRevD.96.035019>. [arXiv:1704.05081](https://arxiv.org/abs/1704.05081) [hep-ph]
- Baryakhtar M, Galanis M, Lasenby R, Simon O (2021) Black hole superradiance of self-interacting scalar fields. *Phys Rev D* 103(9):095019. <https://doi.org/10.1103/PhysRevD.103.095019>. [arXiv:2011.11646](https://arxiv.org/abs/2011.11646) [hep-ph]
- Bauer AM, Cárdenas-Avenidaño A, Gammie CF, Yunes N (2022a) Spherical Accretion in Alternative Theories of Gravity. *Astrophys J* 925(2):119. <https://doi.org/10.3847/1538-4357/ac3a03>. [arXiv:2111.02178](https://arxiv.org/abs/2111.02178) [gr-qc]
- Bauer AM, Cárdenas-Avenidaño A, Gammie CF, Yunes N (2022b) Spherical Accretion in Alternative Theories of Gravity. *The Astrophysical Journal* 925(2):119. <https://doi.org/10.3847/1538-4357/ac3a03>, URL <https://dx.doi.org/10.3847/1538-4357/ac3a03>, publisher: The American Astronomical Society
- Baumann D, Chia HS, Stout J, ter Haar L (2019) The Spectra of Gravitational Atoms. *JCAP* 12:006. <https://doi.org/10.1088/1475-7516/2019/12/006>. [arXiv:1908.10370](https://arxiv.org/abs/1908.10370) [gr-qc]
- Begelman MC, Blandford RD, Rees MJ (1980a) Massive black hole binaries in active galactic nuclei. *Nature* 287(5780):307–309. <https://doi.org/10.1038/287307a0>
- Begelman MC, Blandford RD, Rees MJ (1980b) Massive black hole binaries in active galactic nuclei. *Nature* 287(5780):307–309. <https://doi.org/10.1038/287307a0>

- Bekenstein JD (1972) Nonexistence of baryon number for static black holes. *Phys Rev D* 5:1239–1246. <https://doi.org/10.1103/PhysRevD.5.1239>
- Ben Achour J, Liu H (2019) Hairy Schwarzschild-(A)dS black hole solutions in degenerate higher order scalar-tensor theories beyond shift symmetry. *Phys Rev D* 99(6):064042. <https://doi.org/10.1103/PhysRevD.99.064042>. [arXiv:1811.05369](https://arxiv.org/abs/1811.05369) [gr-qc]
- Ben Achour J, Liu H, Motohashi H, Mukohyama S, Noui K (2020) On rotating black holes in DHOST theories. *JCAP* 11:001. <https://doi.org/10.1088/1475-7516/2020/11/001>. [arXiv:2006.07245](https://arxiv.org/abs/2006.07245) [gr-qc]
- Benenti S, Francaviglia M (1979) Remarks on certain separability structures and their applications to general relativity. *General Relativity and Gravitation* 10(1):79–92. <https://doi.org/10.1007/BF00757025>
- Berti E, Buonanno A, Will CM (2005) Estimating spinning binary parameters and testing alternative theories of gravity with lisa. *Phys Rev D* 71:084025. <https://doi.org/10.1103/PhysRevD.71.084025>, URL <https://link.aps.org/doi/10.1103/PhysRevD.71.084025>
- Berti E, et al. (2015) Testing General Relativity with Present and Future Astrophysical Observations. *Class Quant Grav* 32:243001. <https://doi.org/10.1088/0264-9381/32/24/243001>. [arXiv:1501.07274](https://arxiv.org/abs/1501.07274) [gr-qc]
- Bertolami O, Paramos J, Harko T, Lobo FSN (2008) Non-minimal curvature-matter couplings in modified gravity. *arXiv e-prints* [arXiv:0811.2876](https://arxiv.org/abs/0811.2876) [gr-qc]
- Bezanson J, Edelman A, Karpinski S, Shah VB (2017) Julia: A fresh approach to numerical computing. *SIAM Review* 59(1):65–98. <https://doi.org/10.1137/141000671>, URL <https://epubs.siam.org/doi/10.1137/141000671>
- Bhatta G (2019) Blazar Mrk 501 shows rhythmic oscillations in its γ -ray emission. *Mon. Not. R. Astron. Soc.* 487(3):3990–3997. <https://doi.org/10.1093/mnras/stz1482>. [arXiv:1808.06067](https://arxiv.org/abs/1808.06067) [astro-ph.HE]
- Binney J, Tremaine S (2011) *Galactic dynamics*, vol 20. Princeton university press
- Bisnovatyi-Kogan GS, Ruzmaikin AA (1974) The Accretion of Matter by a Collapsing Star in the Presence of a Magnetic Field. *Astrophysics and Space Science* 28(1):45–59. <https://doi.org/10.1007/BF00642237>
- Biswas T, Mazumdar A, Siegel W (2006) Bouncing universes in string-inspired gravity. *JCAP* 03:009. <https://doi.org/10.1088/1475-7516/2006/03/009>. [arXiv:hep-th/0508194](https://arxiv.org/abs/hep-th/0508194)
- Biswas T, Gerwick E, Koivisto T, Mazumdar A (2012) Towards singularity and ghost free theories of gravity. *Phys Rev Lett* 108:031101. <https://doi.org/10.1103/PhysRevLett.108.031101>. [arXiv:1110.5249](https://arxiv.org/abs/1110.5249) [gr-qc]
- Blandford R, Globus N (2022a) Ergomagnetosphere, ejection disc, magnetopause in M87 – I. Global flow of mass, angular momentum, energy, and current. *Mon Not R Astron Soc* 514(4):5141–5158. <https://doi.org/10.1093/MNRAS/STAC1682>, URL <https://academic.oup.com/mnras/article/514/4/5141/6609931>. [arXiv:2204.11995](https://arxiv.org/abs/2204.11995)
- Blandford R, Globus N (2022b) Jets, Disks and Winds from Spinning Black Holes: Nature or Nurture? *Galaxies* 2022, Vol 10, Page 89 10(4):89. <https://doi.org/10.3390/GALAXIES10040089>, URL <https://www.mdpi.com/2075-4434/10/4/89/html><https://www.mdpi.com/2075-4434/10/4/89>. [arXiv:2207.05839](https://arxiv.org/abs/2207.05839)
- Blandford R, Znajek R (1977) Electromagnetic extractions of energy from Kerr black holes. *MonNotRoyAstronSoc* 179:433–456
- Bodendorfer N, Mele FM, Münch J (2019) Effective Quantum Extended Spacetime of Polymer Schwarzschild Black Hole. *Class Quant Grav* 36(19):195015. <https://doi.org/10.1088/1361-6382/ab9000>

- [org/10.1088/1361-6382/ab3f16](https://doi.org/10.1088/1361-6382/ab3f16). [arXiv:1902.04542](https://arxiv.org/abs/1902.04542) [gr-qc]
- Bodendorfer N, Mele FM, Münch J (2021a) (b,v)-type variables for black to white hole transitions in effective loop quantum gravity. *Phys Lett B* 819:136390. <https://doi.org/10.1016/j.physletb.2021.136390>. [arXiv:1911.12646](https://arxiv.org/abs/1911.12646) [gr-qc]
- Bodendorfer N, Mele FM, Münch J (2021b) Mass and Horizon Dirac Observables in Effective Models of Quantum Black-to-White Hole Transition. *Class Quant Grav* 38(9):095002. <https://doi.org/10.1088/1361-6382/abe05d>. [arXiv:1912.00774](https://arxiv.org/abs/1912.00774) [gr-qc]
- Bojowald M (2007) Singularities and Quantum Gravity. *AIP Conf Proc* 910(1):294–333. <https://doi.org/10.1063/1.2752483>. [arXiv:gr-qc/0702144](https://arxiv.org/abs/gr-qc/0702144)
- Bonanno A, Reuter M (2000) Renormalization group improved black hole space-times. *Phys Rev D* 62:043008. <https://doi.org/10.1103/PhysRevD.62.043008>. [arXiv:hep-th/0002196](https://arxiv.org/abs/hep-th/0002196)
- Bonanno A, Eichhorn A, Gies H, Pawłowski JM, Percacci R, Reuter M, Saueressig F, Vacca GP (2020) Critical reflections on asymptotically safe gravity. *Front in Phys* 8:269. <https://doi.org/10.3389/fphy.2020.00269>. [arXiv:2004.06810](https://arxiv.org/abs/2004.06810) [gr-qc]
- Boskovic M, Brito R, Cardoso V, Ikeda T, Witek H (2019) Axionic instabilities and new black hole solutions. *Phys Rev D* 99(3):035006. <https://doi.org/10.1103/PhysRevD.99.035006>. [arXiv:1811.04945](https://arxiv.org/abs/1811.04945) [gr-qc]
- Bouhmadi-López M, Chen CY, Chew XY, Ong YC, Yeom Dh (2021) Traversable wormhole in Einstein 3-form theory with self-interacting potential. *JCAP* 10:059. <https://doi.org/10.1088/1475-7516/2021/10/059>. [arXiv:2108.07302](https://arxiv.org/abs/2108.07302) [gr-qc]
- Bošković M, Duque F, Ferreira MC, Miguel FS, Cardoso V (2018) Motion in time-periodic backgrounds with applications to ultralight dark matter haloes at galactic centers. *Phys Rev D* 98:024037. <https://doi.org/10.1103/PhysRevD.98.024037>. [arXiv:1806.07331](https://arxiv.org/abs/1806.07331) [gr-qc]
- Bower GC, et al. (2018) Galactic Center Pulsars with the ngVLA. *ASP Conf Ser* 517:793. [arXiv:1810.06623](https://arxiv.org/abs/1810.06623) [astro-ph.HE]
- Bower GC, et al. (2019) Fundamental Physics with Galactic Center Pulsars. *Bulletin of the American Astronomical Society* 51(3):438
- Boyce H, Haggard D, Witzel G, Willner SP, Nielsen J, Hora JL, Markoff S, Ponti G, Baganoff F, Becklin EE, Fazio GG, Lowrance P, Morris MR, Smith HA (2019) Simultaneous X-Ray and Infrared Observations of Sagittarius A*’s Variability. *Astrophys. J.* 871(2):161. <https://doi.org/10.3847/1538-4357/aaf71f>. [arXiv:1812.05764](https://arxiv.org/abs/1812.05764) [astro-ph.HE]
- Boyer RH, Lindquist RW (1967) Maximal Analytic Extension of the Kerr Metric. *Journal of Mathematical Physics* 8(2):265–281. <https://doi.org/10.1063/1.1705193>
- Brahma S, Chen CY, Yeom Dh (2021) Testing Loop Quantum Gravity from Observational Consequences of Nonsingular Rotating Black Holes. *Phys Rev Lett* 126(18):181301. <https://doi.org/10.1103/PhysRevLett.126.181301>. [arXiv:2012.08785](https://arxiv.org/abs/2012.08785) [gr-qc]
- Breiding P, Burke-Spolaor S, Eracleous M, Bogdanović T, Lazio TJW, Runnoe J, Sigurdsson S (2021) The Search for Binary Supermassive Black Holes among Quasars with Offset Broad Lines Using the Very Long Baseline Array. *The Astrophysical Journal* 914(1):37. <https://doi.org/10.3847/1538-4357/abfa9a>. [arXiv:2103.14176](https://arxiv.org/abs/2103.14176) [astro-ph.GA]
- Brill DR, Chrzanowski PL, Martin Pereira C, Fackerell ED, Ipser JR (1972) Solution of the scalar wave equation in a kerr background by separation of variables. *Phys Rev D* 5:1913–1915. <https://doi.org/10.1103/PhysRevD.5.1913>

- Brink J, Geyer M, Hinderer T (2015) Astrophysics of resonant orbits in the Kerr metric. *Phys. Rev. D* 91(8):083001. <https://doi.org/10.1103/PhysRevD.91.083001>. [arXiv:1501.07728](https://arxiv.org/abs/1501.07728) [gr-qc]
- Brito R, Cardoso V, Pani P (2013) Massive spin-2 fields on black hole spacetimes: Instability of the Schwarzschild and Kerr solutions and bounds on the graviton mass. *Phys Rev D* 88(2):023514. <https://doi.org/10.1103/PhysRevD.88.023514>. [arXiv:1304.6725](https://arxiv.org/abs/1304.6725) [gr-qc]
- Brito R, Cardoso V, Pani P (2015a) Black holes as particle detectors: evolution of superradiant instabilities. *Class Quant Grav* 32(13):134001. <https://doi.org/10.1088/0264-9381/32/13/134001>. [arXiv:1411.0686](https://arxiv.org/abs/1411.0686) [gr-qc]
- Brito R, Cardoso V, Pani P (2015b) Superradiance: New Frontiers in Black Hole Physics. *Lect Notes Phys* 906:pp.1–237. <https://doi.org/10.1007/978-3-319-19000-6>. [arXiv:1501.06570](https://arxiv.org/abs/1501.06570) [gr-qc]
- Brito R, Ghosh S, Barausse E, Berti E, Cardoso V, Dvorkin I, Klein A, Pani P (2017) Gravitational wave searches for ultralight bosons with LIGO and LISA. *Phys Rev D* 96(6):064050. <https://doi.org/10.1103/PhysRevD.96.064050>. [arXiv:1706.06311](https://arxiv.org/abs/1706.06311) [gr-qc]
- Brito R, Grillo S, Pani P (2020) Black Hole Superradiant Instability from Ultralight Spin-2 Fields. *Phys Rev Lett* 124(21):211101. <https://doi.org/10.1103/PhysRevLett.124.211101>. [arXiv:2002.04055](https://arxiv.org/abs/2002.04055) [gr-qc]
- Britzen S, Witzel A, Gong BP, Zhang JW, Gopal-Krishna, Goyal A, Aller MF, Aller HD, Zensus JA (2010) Understanding BL Lacertae objects. Structural and kinematic mode changes in the BL Lac object PKS 0735+178. *aap* 515:A105. <https://doi.org/10.1051/0004-6361/200913685>. [arXiv:1002.3531](https://arxiv.org/abs/1002.3531) [astro-ph.CO]
- Britzen S, Qian SJ, Steffen W, Kun E, Karouzos M, Gergely L, Schmidt J, Aller M, Aller H, Krause M, Fendt C, Böttcher M, Witzel A, Eckart A, Moser L (2017) A swirling jet in the quasar 1308+326. *aap* 602:A29. <https://doi.org/10.1051/0004-6361/201629999>
- Britzen S, Fendt C, Witzel G, Qian SJ, Pashchenko IN, Kurtanidze O, Zajacek M, Martinez G, Karas V, Aller M, Aller H, Eckart A, Nilsson K, Arévalo P, Cuadra J, Subroweit M, Witzel A (2018) OJ287: deciphering the ‘Rosetta stone of blazars. *Mon. Not. R. Astron. Soc.* 478(3):3199–3219. <https://doi.org/10.1093/mnras/sty1026>
- Britzen S, Fendt C, Böttcher M, Zajaček M, Jaron F, Pashchenko IN, Araudo A, Karas V, Kurtanidze O (2019a) A cosmic collider: Was the IceCube neutrino generated in a precessing jet-jet interaction in TXS 0506+056? *aap* 630:A103. <https://doi.org/10.1051/0004-6361/201935422>
- Britzen S, Fendt C, Zajaček M, Jaron F, Pashchenko I, Aller MF, Aller HD (2019b) 3C 84: Observational Evidence for Precession and a Possible Relation to TeV Emission. *Galaxies* 7(3):72. <https://doi.org/10.3390/galaxies7030072>
- Britzen S, Zajaček M, Popović LČ, Fendt C, Tramacere A, Pashchenko IN, Jaron F, Pánis R, Petrov L, Aller MF, Aller HD (2021) A ring accelerator? Unusual jet dynamics in the IceCube candidate PKS 1502+106. *mnras* 503(3):3145–3178. <https://doi.org/10.1093/mnras/stab589>. [arXiv:2103.00292](https://arxiv.org/abs/2103.00292) [astro-ph.HE]
- Britzen S, Zajaček M, Gopal-Krishna, Fendt C, Kun E, Jaron F, Sillanpää A, Eckart A (2023) Precession-induced Variability in AGN Jets and OJ 287. *Astrophys. J.* 951(2):106. <https://doi.org/10.3847/1538-4357/acbbbc>. [arXiv:2307.05838](https://arxiv.org/abs/2307.05838) [astro-ph.HE]
- Broadhurst T, de Martino I, Luu HN, Smoot GF, Tye SHH (2020) Ghostly Galaxies as Solitons of Bose-Einstein Dark Matter. *Phys Rev D* 101(8):083012. <https://doi.org/10.1103/PhysRevD.101.083012>

- [org/10.1103/PhysRevD.101.083012](https://doi.org/10.1103/PhysRevD.101.083012). [arXiv:1902.10488](https://arxiv.org/abs/1902.10488) [astro-ph.CO]
- Broderick AE, Loeb A (2005) Imaging bright spots in the accretion flow near the black hole horizon of Sgr A*. *Mon Not Roy Astron Soc* 363:353–362. <https://doi.org/10.1111/j.1365-2966.2005.09458.x>. [arXiv:astro-ph/0506433](https://arxiv.org/abs/astro-ph/0506433)
- Broderick AE, Loeb A (2006) Imaging optically-thin hot spots near the black hole horizon of sgr a* at radio and near-infrared wavelengths. *Mon Not Roy Astron Soc* 367:905–916. <https://doi.org/10.1111/j.1365-2966.2006.10152.x>. [arXiv:astro-ph/0509237](https://arxiv.org/abs/astro-ph/0509237)
- Broderick AE, Narayan R (2006) On the nature of the compact dark mass at the galactic center. *Astrophys J Lett* 638:L21–L24. <https://doi.org/10.1086/500930>. [arXiv:astro-ph/0512211](https://arxiv.org/abs/astro-ph/0512211)
- Broderick AE, Narayan R (2007) Where are all the gravastars? Limits upon the gravastar model from accreting black holes. *Class Quant Grav* 24:659–666. <https://doi.org/10.1088/0264-9381/24/3/009>. [arXiv:gr-qc/0701154](https://arxiv.org/abs/gr-qc/0701154)
- Broderick AE, Fish VL, Doeleman SS, Loeb A (2009) Estimating the Parameters of Sagittarius A*'s Accretion Flow Via Millimeter VLBI. *Astrophys. J.*697(1):45–54. <https://doi.org/10.1088/0004-637X/697/1/45>. [arXiv:0809.4490](https://arxiv.org/abs/0809.4490) [astro-ph]
- Broderick AE, Loeb A, Narayan R (2009) The Event Horizon of Sagittarius A*. *Astrophys J* 701:1357–1366. <https://doi.org/10.1088/0004-637X/701/2/1357>. [arXiv:0903.1105](https://arxiv.org/abs/0903.1105) [astro-ph.HE]
- Broderick AE, Fish VL, Doeleman SS, Loeb A (2011) Evidence for Low Black Hole Spin and Physically Motivated Accretion Models from Millimeter-VLBI Observations of Sagittarius A*. *Astrophys. J.*735(2):110. <https://doi.org/10.1088/0004-637X/735/2/110>. [arXiv:1011.2770](https://arxiv.org/abs/1011.2770) [astro-ph.HE]
- Broderick AE, Johannsen T, Loeb A, Psaltis D (2014) Testing the No-hair Theorem with Event Horizon Telescope Observations of Sagittarius A*. *Astrophys. J.*784(1):7. <https://doi.org/10.1088/0004-637X/784/1/7>. [arXiv:1311.5564](https://arxiv.org/abs/1311.5564) [astro-ph.HE]
- Broderick AE, Narayan R, Kormendy J, Perlman ES, Rieke MJ, Doeleman SS (2015) The Event Horizon of M87. *Astrophys J* 805(2):179. <https://doi.org/10.1088/0004-637X/805/2/179>. [arXiv:1503.03873](https://arxiv.org/abs/1503.03873) [astro-ph.HE]
- Broderick AE, Gold R, Karami M, et al (2020a) THEMIS: A Parameter Estimation Framework for the Event Horizon Telescope. *Astrophys. J.*897(2):139. <https://doi.org/10.3847/1538-4357/ab91a4>
- Broderick AE, Pesce DW, Tiede P, Pu HY, Gold R (2020b) Hybrid Very Long Baseline Interferometry Imaging and Modeling with THEMIS. *Astrophys. J.*898(1):9. <https://doi.org/10.3847/1538-4357/ab9c1f>
- Broderick AE, Pesce DW, Tiede P, Pu HY, Gold R (2020c) Hybrid Very Long Baseline Interferometry Imaging and Modeling with THEMIS. *Astrophys. J.*898(1):9. <https://doi.org/10.3847/1538-4357/ab9c1f>. [arXiv:2208.09003](https://arxiv.org/abs/2208.09003) [astro-ph.IM]
- Broderick AE, Tiede P, Pesce DW, Gold R (2022) Measuring Spin from Relative Photon-ring Sizes. *Astrophys. J.*927(1):6. <https://doi.org/10.3847/1538-4357/ac4970>. [arXiv:2105.09962](https://arxiv.org/abs/2105.09962) [astro-ph.HE]
- Broderick AE, et al. (2022) The Photon Ring in M87*. *Astrophys J* 935:61. <https://doi.org/10.3847/1538-4357/ac7c1d>. [arXiv:2208.09004](https://arxiv.org/abs/2208.09004) [astro-ph.HE]
- Bronzwaer T, Davelaar J, Younsi Z, Mościbrodzka M, Falcke H, Kramer M, Rezzolla L (2018) RAPTOR. I. Time-dependent radiative transfer in arbitrary space-times. *Astron. Astrophys.*613:A2. <https://doi.org/10.1051/0004-6361/201732149>. [arXiv:1801.10452](https://arxiv.org/abs/1801.10452) [astro-ph.HE]

- Bronzwaer T, Davelaar J, Younsi Z, Mościbrodzka M, Olivares H, Mizuno Y, Vos J, Falcke H (2020) Visibility of Black Hole Shadows in Low-luminosity AGN. *Mon Not R Astron Soc* <https://doi.org/10.1093/mnras/staa3430>, URL <https://academic.oup.com/mnras/advance-article/doi/10.1093/mnras/staa3430/5960176>. [arXiv:2011.00069](https://arxiv.org/abs/2011.00069)
- Brown EG, Mann RB, Modesto L (2011) Mass Inflation in the Loop Black Hole. *Phys Rev D* 84:104041. <https://doi.org/10.1103/PhysRevD.84.104041>. [arXiv:1104.3126](https://arxiv.org/abs/1104.3126) [gr-qc]
- Burke-Spolaor S (2013) Multi-messenger approaches to binary supermassive black holes in the ‘continuous-wave’ regime. *Class Quant Grav* 30:224013. <https://doi.org/10.1088/0264-9381/30/22/224013>. [arXiv:1308.4408](https://arxiv.org/abs/1308.4408) [astro-ph.CO]
- Callan CG, Maldacena JM (1996) D-brane approach to black hole quantum mechanics. *Nucl Phys B* 472:591–610. [https://doi.org/10.1016/0550-3213\(96\)00225-8](https://doi.org/10.1016/0550-3213(96)00225-8). [arXiv:hep-th/9602043](https://arxiv.org/abs/hep-th/9602043)
- Cannizzaro E, Caputo A, Sberna L, Pani P (2021a) Plasma-photon interaction in curved spacetime I: formalism and quasibound states around nonspinning black holes. *Phys Rev D* 103:124018. <https://doi.org/10.1103/PhysRevD.103.124018>. [arXiv:2012.05114](https://arxiv.org/abs/2012.05114) [gr-qc]
- Cannizzaro E, Caputo A, Sberna L, Pani P (2021b) Plasma-photon interaction in curved spacetime. II. Collisions, thermal corrections, and superradiant instabilities. *Phys Rev D* 104(10):104048. <https://doi.org/10.1103/PhysRevD.104.104048>. [arXiv:2107.01174](https://arxiv.org/abs/2107.01174) [gr-qc]
- Cano PA, Ruipérez A (2019) Leading higher-derivative corrections to Kerr geometry. *JHEP* 05:189. [https://doi.org/10.1007/JHEP05\(2019\)189](https://doi.org/10.1007/JHEP05(2019)189), [Erratum: *JHEP* 03, 187 (2020)]. [arXiv:1901.01315](https://arxiv.org/abs/1901.01315) [gr-qc]
- Capozziello S, De Laurentis M, Stabile A (2010) Axially symmetric solutions in $f(R)$ -gravity. *Class Quant Grav* 27:165008. <https://doi.org/10.1088/0264-9381/27/16/165008>. [arXiv:0912.5286](https://arxiv.org/abs/0912.5286) [gr-qc]
- Caproni A, Abraham Z (2004a) Can long-term periodic variability and jet helicity in 3C 120 be explained by jet precession? *mnras* 349(4):1218–1226. <https://doi.org/10.1111/j.1365-2966.2004.07550.x>. [arXiv:astro-ph/0312407](https://arxiv.org/abs/astro-ph/0312407) [astro-ph]
- Caproni A, Abraham Z (2004b) Precession in the Inner Jet of 3C 345. *apj* 602(2):625–634. <https://doi.org/10.1086/381195>. [arXiv:astro-ph/0311137](https://arxiv.org/abs/astro-ph/0311137) [astro-ph]
- Caproni A, Abraham Z, Monteiro H (2013) Parsec-scale jet precession in BL Lacertae (2200+420). *mnras* 428(1):280–290. <https://doi.org/10.1093/mnras/sts014>. [arXiv:1210.2286](https://arxiv.org/abs/1210.2286) [astro-ph.HE]
- Caproni A, Abraham Z, Motter JC, Monteiro H (2017) Jet Precession Driven by a Supermassive Black Hole Binary System in the BL Lac Object PG 1553+113. *ApJL* 851(2):L39. <https://doi.org/10.3847/2041-8213/aa9fea>. [arXiv:1712.06881](https://arxiv.org/abs/1712.06881) [astro-ph.GA]
- Caputo A, Witte SJ, Blas D, Pani P (2021) Electromagnetic signatures of dark photon superradiance. *Phys Rev D* 104(4):043006. <https://doi.org/10.1103/PhysRevD.104.043006>. [arXiv:2102.11280](https://arxiv.org/abs/2102.11280) [hep-ph]
- Carballo-Rubio R (2018) Stellar equilibrium in semiclassical gravity. *Phys Rev Lett* 120(6):061102. <https://doi.org/10.1103/PhysRevLett.120.061102>. [arXiv:1706.05379](https://arxiv.org/abs/1706.05379) [gr-qc]
- Carballo-Rubio R, Di Filippo F, Liberati S, Pacilio C, Visser M (2018a) On the viability of regular black holes. *JHEP* 07:023. [https://doi.org/10.1007/JHEP07\(2018\)023](https://doi.org/10.1007/JHEP07(2018)023). [arXiv:1805.02675](https://arxiv.org/abs/1805.02675) [gr-qc]

- Carballo-Rubio R, Di Filippo F, Liberati S, Visser M (2018b) Phenomenological aspects of black holes beyond general relativity. *Phys Rev D* 98(12):124009. <https://doi.org/10.1103/PhysRevD.98.124009>. [arXiv:1809.08238](https://arxiv.org/abs/1809.08238) [gr-qc]
- Carballo-Rubio R, Kumar P, Lu W (2018c) Seeking observational evidence for the formation of trapping horizons in astrophysical black holes. *Phys Rev D* 97(12):123012. <https://doi.org/10.1103/PhysRevD.97.123012>. [arXiv:1804.00663](https://arxiv.org/abs/1804.00663) [gr-qc]
- Carballo-Rubio R, Di Filippo F, Liberati S, Pacilio C, Visser M (2021) Inner horizon instability and the unstable cores of regular black holes. *JHEP* 05:132. [https://doi.org/10.1007/JHEP05\(2021\)132](https://doi.org/10.1007/JHEP05(2021)132). [arXiv:2101.05006](https://arxiv.org/abs/2101.05006) [gr-qc]
- Carballo-Rubio R, Cardoso V, Younsi Z (2022a) Towards VLBI Observations of Black Hole Structure. *arXiv e-prints* [arXiv:2208.00704](https://arxiv.org/abs/2208.00704) [gr-qc]
- Carballo-Rubio R, Di Filippo F, Liberati S, Pacilio C, Visser M (2022b) Regular black holes without mass inflation instability. *JHEP* 09:118. [https://doi.org/10.1007/JHEP09\(2022\)118](https://doi.org/10.1007/JHEP09(2022)118). [arXiv:2205.13556](https://arxiv.org/abs/2205.13556) [gr-qc]
- Carballo-Rubio R, Di Filippo F, Liberati S, Visser M (2022) A connection between regular black holes and horizonless ultracompact stars. *arXiv e-prints* [arXiv:2211.05817](https://arxiv.org/abs/2211.05817). <https://doi.org/10.48550/arXiv.2211.05817>. [arXiv:2211.05817](https://arxiv.org/abs/2211.05817) [gr-qc]
- Carballo-Rubio R, Di Filippo F, Liberati S, Visser M (2022a) Constraints on horizonless objects after the EHT observation of Sagittarius A*. *JCAP* 08(08):055. <https://doi.org/10.1088/1475-7516/2022/08/055>. [arXiv:2205.13555](https://arxiv.org/abs/2205.13555) [astro-ph.HE]
- Carballo-Rubio R, Di Filippo F, Liberati S, Visser M (2022b) Geodesically complete black holes in Lorentz-violating gravity. *JHEP* 02:122. [https://doi.org/10.1007/JHEP02\(2022\)122](https://doi.org/10.1007/JHEP02(2022)122). [arXiv:2111.03113](https://arxiv.org/abs/2111.03113) [gr-qc]
- Cárdenas-Avenidaño A, Held A (2023) Lensing-band constraints on black-hole uniqueness
- Cardenas-Avendano A, Godfrey J, Yunes N, Lohfink A (2019) Experimental Relativity with Accretion Disk Observations. *Phys Rev D* 100(2):024039. <https://doi.org/10.1103/PhysRevD.100.024039>. [arXiv:1903.04356](https://arxiv.org/abs/1903.04356) [gr-qc]
- Cardenas-Avendano A, Nampalliwar S, Yunes N (2020) Gravitational-wave versus X-ray tests of strong-field gravity. *Class Quant Grav* 37(13):135008. <https://doi.org/10.1088/1361-6382/ab8f64>. [arXiv:1912.08062](https://arxiv.org/abs/1912.08062) [gr-qc]
- Cardoso V, Gualtieri L (2016) Testing the black hole ‘no-hair’ hypothesis. *Class Quant Grav* 33(17):174001. <https://doi.org/10.1088/0264-9381/33/17/174001>. [arXiv:1607.03133](https://arxiv.org/abs/1607.03133) [gr-qc]
- Cardoso V, Pani P (2017) Tests for the existence of black holes through gravitational wave echoes. *Nature Astronomy* 1:586–591. <https://doi.org/10.1038/s41550-017-0225-y>. [arXiv:1707.03021](https://arxiv.org/abs/1707.03021) [gr-qc]
- Cardoso V, Pani P (2019) Testing the nature of dark compact objects: a status report. *Living Rev Rel* 22(1):4. <https://doi.org/10.1007/s41114-019-0020-4>. [arXiv:1904.05363](https://arxiv.org/abs/1904.05363) [gr-qc]
- Cardoso V, Yoshida S (2005) Superradiant instabilities of rotating black branes and strings. *JHEP* 07:009. <https://doi.org/10.1088/1126-6708/2005/07/009>. [arXiv:hep-th/0502206](https://arxiv.org/abs/hep-th/0502206)
- Cardoso V, Pani P, Cadoni M, Cavaglia M (2008) Ergoregion instability of ultracompact astrophysical objects. *Phys Rev D* 77:124044. <https://doi.org/10.1103/PhysRevD.77.124044>. [arXiv:0709.0532](https://arxiv.org/abs/0709.0532) [gr-qc]
- Cardoso V, Miranda AS, Berti E, Witek H, Zanchin VT (2009) Geodesic stability, Lyapunov exponents and quasinormal modes. *Phys Rev D* 79(6):064016. <https://doi.org/10.1103/PhysRevD.79.064016>. [arXiv:0812.1806](https://arxiv.org/abs/0812.1806) [hep-th]

- Cardoso V, Chakrabarti S, Pani P, Berti E, Gualtieri L (2011) Floating and sinking: The Imprint of massive scalars around rotating black holes. *Phys Rev Lett* 107:241101. <https://doi.org/10.1103/PhysRevLett.107.241101>. [arXiv:1109.6021](https://arxiv.org/abs/1109.6021) [gr-qc]
- Cardoso V, Crispino LCB, Macedo CFB, Okawa H, Pani P (2014a) Light rings as observational evidence for event horizons: long-lived modes, ergoregions and nonlinear instabilities of ultracompact objects. *Phys Rev D* 90(4):044069. <https://doi.org/10.1103/PhysRevD.90.044069>. [arXiv:1406.5510](https://arxiv.org/abs/1406.5510) [gr-qc]
- Cardoso V, Pani P, Rico J (2014b) On generic parametrizations of spinning black-hole geometries. *Phys Rev D* 89:064007. <https://doi.org/10.1103/PhysRevD.89.064007>. [arXiv:1401.0528](https://arxiv.org/abs/1401.0528) [gr-qc]
- Cardoso V, Dias OJC, Hartnett GS, Middleton M, Pani P, Santos JE (2018a) Constraining the mass of dark photons and axion-like particles through black-hole superradiance. *JCAP* 03:043. <https://doi.org/10.1088/1475-7516/2018/03/043>. [arXiv:1801.01420](https://arxiv.org/abs/1801.01420) [gr-qc]
- Cardoso V, Kimura M, Maselli A, Senatore L (2018b) Black Holes in an Effective Field Theory Extension of General Relativity. *Phys Rev Lett* 121(25):251105. <https://doi.org/10.1103/PhysRevLett.121.251105>. [arXiv:1808.08962](https://arxiv.org/abs/1808.08962) [gr-qc]
- Cardoso V, Duque F, Foschi A (2021a) Light ring and the appearance of matter accreted by black holes. *Phys Rev D* 103(10):104044. <https://doi.org/10.1103/PhysRevD.103.104044>. [arXiv:2102.07784](https://arxiv.org/abs/2102.07784) [gr-qc]
- Cardoso V, Guo WD, Macedo CFB, Pani P (2021b) The tune of the Universe: the role of plasma in tests of strong-field gravity. *Mon Not Roy Astron Soc* 503(1):563–573. <https://doi.org/10.1093/mnras/stab404>. [arXiv:2009.07287](https://arxiv.org/abs/2009.07287) [gr-qc]
- Cardoso V, Hilditch D, Marouda K, Natário J, Sperhake U (2023) Curvature and dynamical spacetimes: can we peer into the quantum regime? *Classical and Quantum Gravity* 40(6):065008. <https://doi.org/10.1088/1361-6382/acb9cd>. [arXiv:2209.12589](https://arxiv.org/abs/2209.12589) [gr-qc]
- Carroll SM, Field GB, Jackiw R (1990) Limits on a Lorentz and Parity Violating Modification of Electrodynamics. *Phys Rev D* 41:1231. <https://doi.org/10.1103/PhysRevD.41.1231>
- Carson Z, Yagi K (2020) Probing beyond-Kerr spacetimes with inspiral-ringdown corrections to gravitational waves. *Phys Rev D* 101:084050. <https://doi.org/10.1103/PhysRevD.101.084050>. [arXiv:2003.02374](https://arxiv.org/abs/2003.02374) [gr-qc]
- Carter B (1968) Global structure of the kerr family of gravitational fields. *Phys Rev* 174:1559–1571. <https://doi.org/10.1103/PhysRev.174.1559>, URL <https://link.aps.org/doi/10.1103/PhysRev.174.1559>
- Cattoen C, Faber T, Visser M (2005) Gravastars must have anisotropic pressures. *Class Quant Grav* 22:4189–4202. <https://doi.org/10.1088/0264-9381/22/20/002>. [arXiv:gr-qc/0505137](https://arxiv.org/abs/gr-qc/0505137)
- Chael A, Narayan R, Johnson MD (2019) Two-temperature, Magnetically Arrested Disc simulations of the jet from the supermassive black hole in M87. *Mon. Not. R. Astron. Soc.* 486(2):2873–2895. <https://doi.org/10.1093/mnras/stz988>. [arXiv:1810.01983](https://arxiv.org/abs/1810.01983) [astro-ph.HE]
- Chael A, Johnson MD, Lupsasca A (2021) Observing the Inner Shadow of a Black Hole: A Direct View of the Event Horizon. *Astrophys. J.* 918(1):6. <https://doi.org/10.3847/1538-4357/ac09ee>. [arXiv:2106.00683](https://arxiv.org/abs/2106.00683) [astro-ph.HE]
- Chael A, et al. (2022) Multi-frequency Black Hole Imaging for the Next-Generation Event Horizon Telescope. in prep

- Chael AA, Johnson MD, Narayan R, Doeleman SS, Wardle JFC, Bouman KL (2016) High-resolution Linear Polarimetric Imaging for the Event Horizon Telescope. *Astrophys. J.* 829(1):11. <https://doi.org/10.3847/0004-637X/829/1/11>. [arXiv:1605.06156](https://arxiv.org/abs/1605.06156) [astro-ph.IM]
- Chael AA, Johnson MD, Bouman KL, Blackburn LL, Akiyama K, Narayan R (2018) Interferometric Imaging Directly with Closure Phases and Closure Amplitudes. *Astrophys J* 857(1):23. <https://doi.org/10.3847/1538-4357/aab6a8>. [arXiv:1803.07088](https://arxiv.org/abs/1803.07088) [astro-ph.IM]
- Chan Ck, Psaltis D, Özel F (2013) GRay: A Massively Parallel GPU-based Code for Ray Tracing in Relativistic Spacetimes. *Astrophys. J.* 777(1):13. <https://doi.org/10.1088/0004-637X/777/1/13>. [arXiv:1303.5057](https://arxiv.org/abs/1303.5057) [astro-ph.IM]
- Chan Ck, Medeiros L, Özel F, Psaltis D (2018) GRay2: A General Purpose Geodesic Integrator for Kerr Spacetimes. *Astrophys. J.* 867(1):59. <https://doi.org/10.3847/1538-4357/aadfe5>. [arXiv:1706.07062](https://arxiv.org/abs/1706.07062) [astro-ph.HE]
- Chandra M, Gammie CF, Foucart F, Quataert E (2015) An Extended Magnetohydrodynamics Model for Relativistic Weakly Collisional Plasmas. *The Astrophysical Journal* 810:162. <https://doi.org/10.1088/0004-637X/810/2/162>, URL <https://ui.adsabs.harvard.edu/abs/2015ApJ...810..162C>, aDS Bibcode: 2015ApJ...810..162C
- Chandrasekhar S (1983) *The Mathematical Theory of Black Holes*. Oxford University Press, New York
- Charisi M, Bartos I, Haiman Z, Price-Whelan AM, Graham MJ, Bellm EC, Laher RR, Marka S (2016) A Population of Short-Period Variable Quasars from PTF as Supermassive Black Hole Binary Candidates. *Mon Not Roy Astron Soc* 463(2):2145–2171. <https://doi.org/10.1093/mnras/stw1838>. [arXiv:1604.01020](https://arxiv.org/abs/1604.01020) [astro-ph.GA]
- Chatterjee K, Younsi Z, Liska M, Tchekhovskoy A, Markoff SB, Yoon D, van Eijnatten D, Hesp C, Ingram A, van der Klis MBM (2020) Observational signatures of disc and jet misalignment in images of accreting black holes. *Mon. Not. R. Astron. Soc.* 499(1):362–378. <https://doi.org/10.1093/mnras/staa2718>. [arXiv:2002.08386](https://arxiv.org/abs/2002.08386) [astro-ph.GA]
- Chatterjee K, Chael A, Tiede P, Mizuno Y, Emami R, Fromm C, Ricarte A, Blackburn L, Roelofs F, Johnson MD, Doeleman SS, Arras P, Fuentes A, Knollmüller J, Kosogorov N, Lindahl G, Müller H, Patel N, Raymond A, Traianou E, Vega J (2023a) Accretion Flow Morphology in Numerical Simulations of Black Holes from the ngEHT Model Library: The Impact of Radiation Physics. *Galaxies* 11(2):38. <https://doi.org/10.3390/galaxies11020038>. [arXiv:2212.01804](https://arxiv.org/abs/2212.01804) [astro-ph.HE]
- Chatterjee K, Kocherlakota P, Younsi Z, Narayan R (2023b) Energy Extraction from Spinning Stringy Black Holes. *arXiv e-prints arXiv:2310.20040*. <https://doi.org/10.48550/arXiv.2310.20040>. [arXiv:2310.20040](https://arxiv.org/abs/2310.20040) [gr-qc]
- Chatterjee K, Younsi Z, Kocherlakota P, Narayan R (2023c) On the Universality of Energy Extraction from Black Hole Spacetimes. *arXiv e-prints arXiv:2310.20043*. <https://doi.org/10.48550/arXiv.2310.20043>. [arXiv:2310.20043](https://arxiv.org/abs/2310.20043) [gr-qc]
- Chen CY (2020) Rotating black holes without \mathbb{Z}_2 symmetry and their shadow images. *JCAP* 05:040. <https://doi.org/10.1088/1475-7516/2020/05/040>. [arXiv:2004.01440](https://arxiv.org/abs/2004.01440) [gr-qc]
- Chen CY, Yang HYK (2022) Curved accretion disks around rotating black holes without reflection symmetry. *Eur Phys J C* 82(4):307. <https://doi.org/10.1140/epjc/s10052-022-10263-7>. [arXiv:2109.00564](https://arxiv.org/abs/2109.00564) [gr-qc]
- Chen P, Unruh WG, Wu CH, Yeom DH (2018) Pre-Hawking radiation cannot prevent the formation of apparent horizon. *Phys Rev D* 97(6):064045. <https://doi.org/10.1103/PhysRevD.97.064045>

- 1103/PhysRevD.97.064045. arXiv:1710.01533 [gr-qc]
- Chen S, et al. (2021) Common-red-signal analysis with 24-yr high-precision timing of the European Pulsar Timing Array: inferences in the stochastic gravitational-wave background search. *Mon Not Roy Astron Soc* 508(4):4970–4993. <https://doi.org/10.1093/mnras/stab2833>. arXiv:2110.13184 [astro-ph.HE]
- Chen Y, Shu J, Xue X, Yuan Q, Zhao Y (2020) Probing Axions with Event Horizon Telescope Polarimetric Measurements. *Phys Rev Lett* 124(6):061102. <https://doi.org/10.1103/PhysRevLett.124.061102>. arXiv:1905.02213 [hep-ph]
- Chen Y, Li C, Mizuno Y, Shu J, Xue X, Yuan Q, Zhao Y, Zhou Z (2022a) Birefringence tomography for axion cloud. *JCAP* 09:073. <https://doi.org/10.1088/1475-7516/2022/09/073>. arXiv:2208.05724 [hep-ph]
- Chen Y, Liu Y, Lu RS, Mizuno Y, Shu J, Xue X, Yuan Q, Zhao Y (2022b) Stringent axion constraints with Event Horizon Telescope polarimetric measurements of M87*. *Nature Astron* 6(5):592–598. <https://doi.org/10.1038/s41550-022-01620-3>. arXiv:2105.04572 [hep-ph]
- Chen Y, Roy R, Vagnozzi S, Visinelli L (2022c) Superradiant evolution of the shadow and photon ring of Sgr A*. *Phys Rev D* 106(4):043021. <https://doi.org/10.1103/PhysRevD.106.043021>. arXiv:2205.06238 [astro-ph.HE]
- Chen Y, Xue X, Brito R, Cardoso V (2023a) Photon Ring Astrometry for Superradiant Clouds. *Phys Rev Lett* 130(11):111401. <https://doi.org/10.1103/PhysRevLett.130.111401>. arXiv:2211.03794 [gr-qc]
- Chen Y, Xue X, Cardoso V (2023b) Black Holes as Neutrino Factories. arXiv e-prints arXiv:2308.00741 [hep-ph]
- Cherenkov Telescope Array Consortium, Acharya BS, et al (2019) Science with the Cherenkov Telescope Array. *World Scientific*. <https://doi.org/10.1142/10986>
- Chesler PM, Blackburn L, Doeleman SS, Johnson MD, Moran JM, Narayan R, Wielgus M (2021) Light echos and coherent autocorrelations in a black hole space-time. *Class Quant Grav* 38(12):125006. <https://doi.org/10.1088/1361-6382/abeae4>. arXiv:2012.11778 [gr-qc]
- Chirenti CBMH, Rezzolla L (2007) How to tell a gravastar from a black hole. *Class Quant Grav* 24:4191–4206. <https://doi.org/10.1088/0264-9381/24/16/013>. arXiv:0706.1513 [gr-qc]
- Chrusciel PT, Lopes Costa J, Heusler M (2012) Stationary Black Holes: Uniqueness and Beyond. *Living Rev Rel* 15:7. <https://doi.org/10.12942/lrr-2012-7>. arXiv:1205.6112 [gr-qc]
- Colladay D, Kostelecky VA (1998) Lorentz violating extension of the standard model. *Phys Rev D* 58:116002. <https://doi.org/10.1103/PhysRevD.58.116002>. arXiv:hep-ph/9809521
- Collins NA, Hughes SA (2004) Towards a formalism for mapping the space-times of massive compact objects: Bumpy black holes and their orbits. *Phys Rev D* 69:124022. <https://doi.org/10.1103/PhysRevD.69.124022>. arXiv:gr-qc/0402063
- Colpi M (2014) Massive Binary Black Holes in Galactic Nuclei and Their Path to Coalescence. *Space Sci. Rev.* 183(1-4):189–221. <https://doi.org/10.1007/s11214-014-0067-1>. arXiv:1407.3102 [astro-ph.GA]
- Combi L (2021) Superposed metric for spinning black hole binaries approaching merger. *Physical Review D* 104(4). <https://doi.org/10.1103/PhysRevD.104.044041>
- Combi L, Armengol FGL, Campanelli M, Noble SC, Avara M, Krolik JH, Bowen D (2022) Minidisk Accretion onto Spinning Black Hole Binaries: Quasi-periodicities and Outflows. *The Astrophysical Journal* 928(2):187. <https://doi.org/10.3847/>

- 1538-4357/ac532a, URL <https://dx.doi.org/10.3847/1538-4357/ac532a>, publisher: The American Astronomical Society
- Conroy NS, Bauböck M, Dhruv V, Lee D, Broderick AE, Chan Ck, Georgiev B, Joshi AV, Prather B, Gammie CF (2023) Rotation in Event Horizon Telescope Movies. *Astrophys. J.* 951(1):46. <https://doi.org/10.3847/1538-4357/acd2c8>. arXiv:2304.03826 [astro-ph.HE]
- Contreras E, Rincón A, Panotopoulos G, Bargueño P, Koch B (2020) Black hole shadow of a rotating scale-dependent black hole. *Phys Rev D* 101(6):064053. <https://doi.org/10.1103/PhysRevD.101.064053>. arXiv:1906.06990 [gr-qc]
- Craig Walker R, Hardee PE, Davies FB, Ly C, Junor W (2018) The Structure and Dynamics of the Subparsec Jet in M87 Based on 50 VLBA Observations over 17 Years at 43 GHz. *Astrophys J* 855(2):128. <https://doi.org/10.3847/1538-4357/aaafcc>. arXiv:1802.06166 [astro-ph.HE]
- Creci G, Vandoren S, Witek H (2020) Evolution of black hole shadows from superradiance. *Phys Rev D* 101(12):124051. <https://doi.org/10.1103/PhysRevD.101.124051>. arXiv:2004.05178 [gr-qc]
- Crew GB, Goddi C, Matthews LD, Rottmann H, Saez A, Martí-Vidal I (2023) A Characterization of the ALMA Phasing System at 345 GHz. *Publ. Astron. Soc. Pac* 135(1044):025002. <https://doi.org/10.1088/1538-3873/acb348>. arXiv:2301.04543 [astro-ph.IM]
- Crispino LCB, Kennefick D (2019) 100 years of the first experimental test of General Relativity. *Nature Phys* 15:416. <https://doi.org/10.1038/s41567-019-0519-3>. arXiv:1907.10687 [physics.hist-ph]
- Cruz-Orsorio A, Fromm CM, Mizuno Y, Nathanail A, Younsi Z, Porth O, Davelaar J, Falcke H, Kramer M, Rezzolla L (2022) State-of-the-art energetic and morphological modelling of the launching site of the M87 jet. *Nature Astron* 6(1):103–108. <https://doi.org/10.1038/s41550-021-01506-w>. arXiv:2111.02517 [astro-ph.HE]
- Cunha PVP, Herdeiro CAR (2018) Shadows and strong gravitational lensing: a brief review. *Gen Rel Grav* 50(4):42. <https://doi.org/10.1007/s10714-018-2361-9>. arXiv:1801.00860 [gr-qc]
- Cunha PVP, Herdeiro CAR, Radu E, Runarsson HF (2015) Shadows of Kerr black holes with scalar hair. *Phys Rev Lett* 115(21):211102. <https://doi.org/10.1103/PhysRevLett.115.211102>. arXiv:1509.00021 [gr-qc]
- Cunha PVP, Herdeiro CAR, Radu E (2018) Isolated black holes without \mathbb{Z}_2 isometry. *Phys Rev D* 98(10):104060. <https://doi.org/10.1103/PhysRevD.98.104060>. arXiv:1808.06692 [gr-qc]
- Cunha PVP, Herdeiro CAR, Radu E (2019) EHT constraint on the ultralight scalar hair of the M87 supermassive black hole. *Universe* 5(12):220. <https://doi.org/10.3390/universe5120220>. arXiv:1909.08039 [gr-qc]
- Cutler C (1998) Angular resolution of the lisa gravitational wave detector. *Phys Rev D* 57:7089–7102. <https://doi.org/10.1103/PhysRevD.57.7089>, URL <https://link.aps.org/doi/10.1103/PhysRevD.57.7089>
- Daas J, Kuijpers K, Saueressig F, Wondrak MF, Falcke H (2022a) Probing Quadratic Gravity with the Event Horizon Telescope. arXiv e-prints arXiv:2204.08480 [gr-qc]
- Daas J, Kuijpers K, Saueressig F, Wondrak MF, Falcke H (2022b) Probing Quadratic Gravity with the Event Horizon Telescope. URL <https://ui.adsabs.harvard.edu/abs/2022arXiv220408480D>, publication Title: arXiv e-prints ADS Bibcode: 2022arXiv220408480D Type: article

- Danielsson U, Giri S (2018) Observational signatures from horizonless black shells imitating rotating black holes. *JHEP* 07:070. [https://doi.org/10.1007/JHEP07\(2018\)070](https://doi.org/10.1007/JHEP07(2018)070). [arXiv:1712.00511](https://arxiv.org/abs/1712.00511) [hep-th]
- Danielsson UH, Dibitetto G, Giri S (2017) Black holes as bubbles of AdS. *JHEP* 10:171. [https://doi.org/10.1007/JHEP10\(2017\)171](https://doi.org/10.1007/JHEP10(2017)171). [arXiv:1705.10172](https://arxiv.org/abs/1705.10172) [hep-th]
- Darwin C (1959) The Gravity Field of a Particle. *Proceedings of the Royal Society of London Series A* 249(1257):180–194. <https://doi.org/10.1098/rspa.1959.0015>
- Davelaar J, Haiman Z (2022) Self-lensing flares from black hole binaries: General-relativistic ray tracing of black hole binaries. *Phys. Rev. D* 105(10):103010. <https://doi.org/10.1103/PhysRevD.105.103010>. [arXiv:2112.05828](https://arxiv.org/abs/2112.05828) [astro-ph.HE]
- Davelaar J, Haiman Z (2022) Self-Lensing Flares from Black Hole Binaries: Observing Black Hole Shadows via Light Curve Tomography. *Phys Rev Lett* 128(19):191101. <https://doi.org/10.1103/PhysRevLett.128.191101>. [arXiv:2112.05829](https://arxiv.org/abs/2112.05829) [astro-ph.HE]
- Davoudiasl H, Denton PB (2019) Ultralight Boson Dark Matter and Event Horizon Telescope Observations of M87*. *Phys Rev Lett* 123(2):021102. <https://doi.org/10.1103/PhysRevLett.123.021102>. [arXiv:1904.09242](https://arxiv.org/abs/1904.09242) [astro-ph.CO]
- De Martino I, Broadhurst T, Tye SHH, Chiueh T, Schive HY (2020) Dynamical Evidence of a Solitonic Core of $10^9 M_\odot$ in the Milky Way. *Phys Dark Univ* 28:100503. <https://doi.org/10.1016/j.dark.2020.100503>. [arXiv:1807.08153](https://arxiv.org/abs/1807.08153) [astro-ph.GA]
- Deane RP, Paragi Z, Jarvis MJ, Coriat M, Bernardi G, Fender RP, Frey S, Heywood I, Klöckner HR, Grainge K, Rumsey C (2014) A close-pair binary in a distant triple supermassive black hole system. *Nature* 511(7507):57–60. <https://doi.org/10.1038/nature13454>. [arXiv:1406.6365](https://arxiv.org/abs/1406.6365) [astro-ph.GA]
- Deffayet C, Gao X, Steer DA, Zahariade G (2011) From k-essence to generalised Galileons. *Phys Rev D* 84:064039. <https://doi.org/10.1103/PhysRevD.84.064039>. [arXiv:1103.3260](https://arxiv.org/abs/1103.3260) [hep-th]
- Degollado JC, Herdeiro CAR, Radu E (2018) Effective stability against superradiance of Kerr black holes with synchronised hair. *Phys Lett B* 781:651–655. <https://doi.org/10.1016/j.physletb.2018.04.052>. [arXiv:1802.07266](https://arxiv.org/abs/1802.07266) [gr-qc]
- Delaporte H, Eichhorn A, Held A (2022) Parameterizations of black-hole spacetimes beyond circularity. *arXiv e-prints* [arXiv:2203.00105](https://arxiv.org/abs/2203.00105) [gr-qc]
- Delgado JFM, Herdeiro CAR, Radu E (2019) Kerr black holes with synchronised scalar hair and higher azimuthal harmonic index. *Phys Lett B* 792:436–444. <https://doi.org/10.1016/j.physletb.2019.04.009>. [arXiv:1903.01488](https://arxiv.org/abs/1903.01488) [gr-qc]
- Delgado JFM, Herdeiro CAR, Radu E (2021) Kerr black holes with synchronized axionic hair. *Phys Rev D* 103(10):104029. <https://doi.org/10.1103/PhysRevD.103.104029>. [arXiv:2012.03952](https://arxiv.org/abs/2012.03952) [gr-qc]
- Delijski V, Gyulchev G, Nedkova P, Yazadjiev S (2022) Polarized image of equatorial emission in horizonless spacetimes: Traversable wormholes. *Phys Rev D* 106(10):104024. <https://doi.org/10.1103/PhysRevD.106.104024>. [arXiv:2206.09455](https://arxiv.org/abs/2206.09455) [gr-qc]
- Delijski V, Gyulchev G, Nedkova P, Yazadjiev S (2023) Polarized image of equatorial emission in horizonless spacetimes: naked singularities. *arXiv e-prints* [arXiv:2303.14756](https://arxiv.org/abs/2303.14756). <https://doi.org/10.48550/arXiv.2303.14756>. [arXiv:2303.14756](https://arxiv.org/abs/2303.14756) [gr-qc]
- Della Monica R, de Martino I (2023a) Bounding the mass of ultralight bosonic Dark Matter particles with the motion of the S2 star around Sgr A*. *arXiv e-prints* [arXiv:2305.10242](https://arxiv.org/abs/2305.10242) [gr-qc]

- Della Monica R, de Martino I (2023b) Narrowing the allowed mass range of ultra-light bosons with the S2 star. *Astron Astrophys* 670:L4. <https://doi.org/10.1051/0004-6361/202245150>. [arXiv:2206.03980](https://arxiv.org/abs/2206.03980) [gr-qc]
- Della Monica R, De Martino I, De Laurentis M (2023) Testing space-time geometries and theories of gravity at the Galactic centre with pulsar's time delay. *Mon. Not. R. Astron. Soc.*524(3):3782–3796. <https://doi.org/10.1093/mnras/stad2125>. [arXiv:2305.18178](https://arxiv.org/abs/2305.18178) [gr-qc]
- Detweiler SL (1980) KLEIN-GORDON EQUATION AND ROTATING BLACK HOLES. *Phys Rev D* 22:2323–2326. <https://doi.org/10.1103/PhysRevD.22.2323>
- Dexter J (2016) A public code for general relativistic, polarised radiative transfer around spinning black holes. *Mon. Not. R. Astron. Soc.*462(1):115–136. <https://doi.org/10.1093/mnras/stw1526>. [arXiv:1602.03184](https://arxiv.org/abs/1602.03184) [astro-ph.HE]
- Dexter J, Agol E (2009) A Fast New Public Code for Computing Photon Orbits in a Kerr Spacetime. *Astrophys. J.*696(2):1616–1629. <https://doi.org/10.1088/0004-637X/696/2/1616>. [arXiv:0903.0620](https://arxiv.org/abs/0903.0620) [astro-ph.HE]
- Dexter J, O'Leary RM (2014) The Peculiar Pulsar Population of the Central Parsec. *The Astrophysical Journal* 783(1):L7. <https://doi.org/10.1088/2041-8205/783/1/L7>. [arXiv:1310.7022](https://arxiv.org/abs/1310.7022) [astro-ph.GA]
- Dey L, Valtonen MJ, Gopakumar A, et al (2018) Authenticating the Presence of a Relativistic Massive Black Hole Binary in OJ 287 Using Its General Relativity Centenary Flare: Improved Orbital Parameters. *Ap J* 866(1):11. <https://doi.org/10.3847/1538-4357/aadd95>. [arXiv:1808.09309](https://arxiv.org/abs/1808.09309) [astro-ph.HE]
- Dias OJC, Lingetti G, Pani P, Santos JE (2023) Black hole superradiant instability for massive spin-2 fields. *arXiv e-prints* arXiv:2304.01265. <https://doi.org/10.48550/arXiv.2304.01265> [gr-qc]
- Dine M, Fischler W (1983) The Not So Harmless Axion. *Phys Lett B* 120:137–141. [https://doi.org/10.1016/0370-2693\(83\)90639-1](https://doi.org/10.1016/0370-2693(83)90639-1)
- Ding C, Liu C, Casana R, Cavalcante A (2020) Exact Kerr-like solution and its shadow in a gravity model with spontaneous Lorentz symmetry breaking. *Eur Phys J C* 80(3):178. <https://doi.org/10.1140/epjc/s10052-020-7743-y>. [arXiv:1910.02674](https://arxiv.org/abs/1910.02674) [gr-qc]
- Do T, et al (2019) Relativistic redshift of the star s0-2 orbiting the galactic center supermassive black hole. *Science* 365:664 – 668
- Do T, et al. (2019a) Relativistic redshift of the star S0-2 orbiting the Galactic center supermassive black hole. *Science* 365(6454):664–668. <https://doi.org/10.1126/science.aav8137>. [arXiv:1907.10731](https://arxiv.org/abs/1907.10731) [astro-ph.GA]
- Do T, et al. (2019b) Relativistic redshift of the star S0-2 orbiting the Galactic center supermassive black hole. *Science* 365(6454):664–668. <https://doi.org/10.1126/science.aav8137>. [arXiv:1907.10731](https://arxiv.org/abs/1907.10731) [astro-ph.GA]
- Dodds-Eden K, et al. (2009) Evidence for X-ray synchrotron emission from simultaneous mid-IR to X-ray observations of a strong Sgr A* flare. *Astrophys J* 698:676–692. <https://doi.org/10.1088/0004-637X/698/1/676>. [arXiv:0903.3416](https://arxiv.org/abs/0903.3416) [astro-ph.GA]
- Doeleman S, Agol E, Backer D, Baganoff F, Bower GC, Broderick A, Fabian A, Fish V, Gammie C, Ho P, Honman M, Krichbaum T, Loeb A, Marrone D, Reid M, Rogers A, Shapiro I, Strittmatter P, Tilanus R, Weintroub J, Whitney A, Wright M, Ziurys L (2009a) Imaging an Event Horizon: submm-VLBI of a Super Massive Black Hole. In: *astro2010: The Astronomy and Astrophysics Decadal Survey*. vol 2010. p 68. <https://doi.org/10.48550/arXiv.0906.3899>. [arXiv:0906.3899](https://arxiv.org/abs/0906.3899) [astro-ph.CO]

- Doeleman S, et al. (2019) Studying Black Holes on Horizon Scales with VLBI Ground Arrays. *Bull AAS* 51(7). URL <https://baas.aas.org/pub/2020n7i256>
- Doeleman SS, Weintroub J, Rogers AEE, Plambeck R, Freund R, Tilanus RPJ, Friberg P, Ziurys LM, Moran JM, Corey B, Young KH, Smythe DL, Titus M, Marrone DP, Cappallo RJ, Bock DCJ, Bower GC, Chamberlin R, Davis GR, Krichbaum TP, Lamb J, Maness H, Niell AE, Roy A, Strittmatter P, Werthimer D, Whitney AR, Woody D (2008) Event-horizon-scale structure in the supermassive black hole candidate at the Galactic Centre. *Nature* 455(7209):78–80. <https://doi.org/10.1038/nature07245>. [arXiv:0809.2442](https://arxiv.org/abs/0809.2442) [astro-ph]
- Doeleman SS, Fish VL, Broderick AE, Loeb A, Rogers AEE (2009b) Detecting Flaring Structures in Sagittarius A* with High-Frequency VLBI. *Astrophys. J.* 695(1):59–74. <https://doi.org/10.1088/0004-637X/695/1/59>. [arXiv:0809.3424](https://arxiv.org/abs/0809.3424) [astro-ph]
- Doeleman SS, Fish VL, Schenck DE, Beaudoin C, Blundell R, Bower GC, Broderick AE, Chamberlin R, Freund R, Friberg P, Gurwell MA, Ho PTP, Honma M, Inoue M, Krichbaum TP, Lamb J, Loeb A, Lonsdale C, Marrone DP, Moran JM, Oyama T, Plambeck R, Primiani RA, Rogers AEE, Smythe DL, SooHoo J, Strittmatter P, Tilanus RPJ, Titus M, Weintroub J, Wright M, Young KH, Ziurys LM (2012) Jet-Launching Structure Resolved Near the Supermassive Black Hole in M87. *Science* 338(6105):355. <https://doi.org/10.1126/science.1224768>. [arXiv:1210.6132](https://arxiv.org/abs/1210.6132) [astro-ph.HE]
- Doeleman SS, Barrett J, Blackburn L, Bouman KL, Broderick AE, Chaves R, Fish VL, Fitzpatrick G, Freeman M, Fuentes A, Gómez JL, Haworth K, Houston J, Issaoun S, Johnson MD, Kettenis M, Loinard L, Nagar N, Narayanan G, Oppenheimer A, Palumbo DCM, Patel N, Pesce DW, Raymond AW, Roelofs F, Srinivasan R, Tiede P, Weintroub J, Wielgus M (2023) Reference Array and Design Consideration for the Next-Generation Event Horizon Telescope. *Galaxies* 11(5):107. <https://doi.org/10.3390/galaxies11050107>. [arXiv:2306.08787](https://arxiv.org/abs/2306.08787) [astro-ph.IM]
- Dokuchaev VI (2014) Spin and mass of the nearest supermassive black hole. *General Relativity and Gravitation* 46:1832. <https://doi.org/10.1007/s10714-014-1832-x>. [arXiv:1306.2033](https://arxiv.org/abs/1306.2033) [astro-ph.HE]
- Dolan SR (2007) Instability of the massive Klein-Gordon field on the Kerr spacetime. *Phys Rev D* 76:084001. <https://doi.org/10.1103/PhysRevD.76.084001>. [arXiv:0705.2880](https://arxiv.org/abs/0705.2880) [gr-qc]
- Dolan SR (2018) Instability of the Proca field on Kerr spacetime. *Phys Rev D* 98(10):104006. <https://doi.org/10.1103/PhysRevD.98.104006>. [arXiv:1806.01604](https://arxiv.org/abs/1806.01604) [gr-qc]
- Dolence JC, Gammie CF, Shiokawa H, Noble SC (2012) Near-infrared and X-Ray Quasi-periodic Oscillations in Numerical Models of Sgr A*. *Astrophys. J. Lett.* 746(1):L10. <https://doi.org/10.1088/2041-8205/746/1/L10>. [arXiv:1201.1917](https://arxiv.org/abs/1201.1917) [astro-ph.HE]
- Dong J, Patiño N, Xie Y, Cárdenas-Avendaño A, Gammie CF, Yunes N (2022a) Blandford-Znajek process in quadratic gravity. *Phys Rev D* 105(4):044008. <https://doi.org/10.1103/PhysRevD.105.044008>. [arXiv:2111.08758](https://arxiv.org/abs/2111.08758) [gr-qc]
- Dong Y, Shao L, Hu Z, Miao X, Wang Z (2022b) Prospects for constraining the Yukawa gravity with pulsars around Sagittarius A*. *JCAP* 11:051. <https://doi.org/10.1088/1475-7516/2022/11/051>. [arXiv:2210.16130](https://arxiv.org/abs/2210.16130) [astro-ph.HE]
- Donoghue JF (1994) Leading quantum correction to the Newtonian potential. *Phys Rev Lett* 72:2996–2999. <https://doi.org/10.1103/PhysRevLett.72.2996>. [arXiv:gr-qc/9310024](https://arxiv.org/abs/gr-qc/9310024)

- D’Orazio DJ, Loeb A (2018a) Repeated imaging of massive black hole binary orbits with millimeter interferometry: Measuring black hole masses and the hubble constant. *The Astrophysical Journal* 863(2):185. <https://doi.org/10.3847/1538-4357/aad413>, URL <https://doi.org/10.3847/1538-4357/aad413>
- D’Orazio DJ, Loeb A (2018b) Repeated imaging of massive black hole binary orbits with millimeter interferometry: Measuring black hole masses and the hubble constant. *The Astrophysical Journal* 863(2):185. <https://doi.org/10.3847/1538-4357/aad413>, URL <https://doi.org/10.3847/1538-4357/aad413>
- D’Orazio DJ, Haiman Z, Duffell P, Farris BD, MacFadyen AI (2015) A reduced orbital period for the supermassive black hole binary candidate in the quasar PG 1302-102? *Monthly Notices of the Royal Astronomical Society* 452(3):2540–2545. <https://doi.org/10.1093/mnras/stv1457>, URL <https://doi.org/10.1093/mnras/stv1457>. <https://academic.oup.com/mnras/article-pdf/452/3/2540/4921183/stv1457.pdf>
- Dotti M, Sesana A, Decarli R (2012) Massive Black Hole Binaries: Dynamical Evolution and Observational Signatures. *Advances in Astronomy* 2012:940568. <https://doi.org/10.1155/2012/940568>. arXiv:1111.0664 [astro-ph.CO]
- Drake SP, Szekeres P (2000) Uniqueness of the Newman-Janis algorithm in generating the Kerr-Newman metric. *Gen Rel Grav* 32:445–458. <https://doi.org/10.1023/A:1001920232180>. arXiv:gr-qc/9807001
- Drummond IT, Hathrell SJ (1980) QED Vacuum Polarization in a Background Gravitational Field and Its Effect on the Velocity of Photons. *Phys Rev D* 22:343. <https://doi.org/10.1103/PhysRevD.22.343>
- Dymnikova I (1992) Vacuum nonsingular black hole. *Gen Rel Grav* 24:235–242. <https://doi.org/10.1007/BF00760226>
- East WE (2022) Vortex String Formation in Black Hole Superradiance of a Dark Photon with the Higgs Mechanism. *Phys Rev Lett* 129(14):141103. <https://doi.org/10.1103/PhysRevLett.129.141103>. arXiv:2205.03417 [hep-ph]
- East WE, Pretorius F (2017) Superradiant Instability and Backreaction of Massive Vector Fields around Kerr Black Holes. *Phys Rev Lett* 119(4):041101. <https://doi.org/10.1103/PhysRevLett.119.041101>. arXiv:1704.04791 [gr-qc]
- Eggleton PP, Yakut K (2017) Models for 60 double-lined binaries containing giants. *Mon. Not. R. Astron. Soc.* 468(3):3533–3556. <https://doi.org/10.1093/mnras/stx598>. arXiv:1611.05041 [astro-ph.SR]
- EHT Collaboration (2019a) First M87 Event Horizon Telescope Results. I. The Shadow of the Supermassive Black Hole. *Astrophys. J. Lett.* 875(1):L1. <https://doi.org/10.3847/2041-8213/ab0ec7>. arXiv:1906.11238 [astro-ph.GA]
- EHT Collaboration (2019b) First M87 Event Horizon Telescope Results. II. Array and Instrumentation. *Astrophys. J. Lett.* 875(1):L2. <https://doi.org/10.3847/2041-8213/ab0c96>. arXiv:1906.11239 [astro-ph.IM]
- EHT Collaboration (2019c) First M87 Event Horizon Telescope Results. III. Data Processing and Calibration. *Astrophys. J. Lett.* 875(1):L3. <https://doi.org/10.3847/2041-8213/ab0c57>. arXiv:1906.11240 [astro-ph.GA]
- EHT Collaboration (2019d) First M87 Event Horizon Telescope Results. IV. Imaging the Central Supermassive Black Hole. *Astrophys. J. Lett.* 875(1):L4. <https://doi.org/10.3847/2041-8213/ab0e85>. arXiv:1906.11241 [astro-ph.GA]
- EHT Collaboration (2019e) First M87 Event Horizon Telescope Results. V. Physical Origin of the Asymmetric Ring. *Astrophys. J. Lett.* 875(1):L5. <https://doi.org/10.3847/2041-8213/ab0f43>. arXiv:1906.11242 [astro-ph.GA]

- EHT Collaboration (2019f) First M87 Event Horizon Telescope Results. VI. The Shadow and Mass of the Central Black Hole. *Astrophys. J. Lett.*875(1):L6. <https://doi.org/10.3847/2041-8213/ab1141>. [arXiv:1906.11243](https://arxiv.org/abs/1906.11243) [astro-ph.GA]
- EHT Collaboration (2021a) First M87 Event Horizon Telescope Results. VII. Polarization of the Ring. *Astrophys. J. Lett.*910(1):L12. <https://doi.org/10.3847/2041-8213/abe71d>. [arXiv:2105.01169](https://arxiv.org/abs/2105.01169) [astro-ph.HE]
- EHT Collaboration (2021b) First M87 Event Horizon Telescope Results. VIII. Magnetic Field Structure near The Event Horizon. *Astrophys. J. Lett.*910(1):L13. <https://doi.org/10.3847/2041-8213/abe4de>. [arXiv:2105.01173](https://arxiv.org/abs/2105.01173) [astro-ph.HE]
- EHT Collaboration (2022a) First Sagittarius A* Event Horizon Telescope Results. I. The Shadow of the Supermassive Black Hole in the Center of the Milky Way. *Astrophys. J. Lett.*930(2):L12. <https://doi.org/10.3847/2041-8213/ac6674>
- EHT Collaboration (2022b) First Sagittarius A* Event Horizon Telescope Results. IV. Variability, Morphology, and Black Hole Mass. *Astrophys. J. Lett.*930(2):L15. <https://doi.org/10.3847/2041-8213/ac6736>
- EHT Collaboration (2022c) First Sagittarius A* Event Horizon Telescope Results. V. Testing Astrophysical Models of the Galactic Center Black Hole. *Astrophys. J. Lett.*930(2):L16. <https://doi.org/10.3847/2041-8213/ac6672>
- EHT Collaboration (2022d) First Sagittarius A* Event Horizon Telescope Results. VI. Testing the Black Hole Metric. *Astrophys. J. Lett.*930(2):L17. <https://doi.org/10.3847/2041-8213/ac6756>
- Eichhorn A, Held A (2021a) From a locality-principle for new physics to image features of regular spinning black holes with disks. *JCAP* 05:073. <https://doi.org/10.1088/1475-7516/2021/05/073>. [arXiv:2103.13163](https://arxiv.org/abs/2103.13163) [gr-qc]
- Eichhorn A, Held A (2021b) Image features of spinning regular black holes based on a locality principle. *Eur Phys J C* 81(10):933. <https://doi.org/10.1140/epjc/s10052-021-09716-2>. [arXiv:2103.07473](https://arxiv.org/abs/2103.07473) [gr-qc]
- Eichhorn A, Held A (2022) Quantum gravity lights up spinning black holes. *arXiv e-prints* [arXiv:2206.11152](https://arxiv.org/abs/2206.11152) [gr-qc]
- Eichhorn A, Gold R, Held A (2022a) Horizonless spacetimes as seen by present and next-generation Event Horizon Telescope arrays. *arXiv e-prints* [arXiv:2205.14883](https://arxiv.org/abs/2205.14883) [astro-ph.HE]
- Eichhorn A, Held A, Johannsen PV (2022b) Universal signatures of singularity-resolving physics in photon rings of black holes and horizonless objects. *arXiv e-prints* [arXiv:2204.02429](https://arxiv.org/abs/2204.02429) [gr-qc]
- Eiroa EF, Sendra CM (2018) Shadow cast by rotating braneworld black holes with a cosmological constant. *Eur Phys J C* 78(2):91. <https://doi.org/10.1140/epjc/s10052-018-5586-6>. [arXiv:1711.08380](https://arxiv.org/abs/1711.08380) [gr-qc]
- Ellis GFR, Meissner KA, Nicolai H (2018) The physics of infinity. *Nature Physics* 14(8):770–772. <https://doi.org/10.1038/s41567-018-0238-1>
- Emami R, Loeb A (2020) Observational signatures of the black hole mass distribution in the galactic center. *JCAP* 02:021. <https://doi.org/10.1088/1475-7516/2020/02/021>. [arXiv:1903.02578](https://arxiv.org/abs/1903.02578) [astro-ph.HE]
- Emami R, Loeb A (2021) Detectability of gravitational waves from a population of inspiralling black holes in Milky Way-mass galaxies. *Mon Not Roy Astron Soc* 502(3):3932–3941. <https://doi.org/10.1093/mnras/stab290>. [arXiv:1903.02579](https://arxiv.org/abs/1903.02579) [astro-ph.HE]
- Emami R, Ricarte A, Wong GN, Palumbo D, Chang D, Doeleman SS, Broderick AE, Narayan R, Wielgus M, Blackburn L, Prather BS, Chael AA, Anantua R, Chatterjee

- K, Marti-Vidal I, Gómez JL, Akiyama K, Liska M, Hernquist L, Tremblay G, Vogelsberger M, Alcock C, Smith R, Steiner J, Tiede P, Roelofs F (2023) Unraveling Twisty Linear Polarization Morphologies in Black Hole Images. *Astrophys. J.*950(1):38. <https://doi.org/10.3847/1538-4357/acc8cd>. [arXiv:2210.01218](https://arxiv.org/abs/2210.01218) [astro-ph.GA]
- Emir Gümürükçüoğlu A, Saravani M, Sotiriou TP (2018) Hořava gravity after GW170817. *Phys Rev D* 97(2):024032. <https://doi.org/10.1103/PhysRevD.97.024032>. [arXiv:1711.08845](https://arxiv.org/abs/1711.08845) [gr-qc]
- Emparan R, Reall HS (2008) Black Holes in Higher Dimensions. *Living Rev Rel* 11:6. <https://doi.org/10.12942/lrr-2008-6>. [arXiv:0801.3471](https://arxiv.org/abs/0801.3471) [hep-th]
- Endlich S, Gorbenko V, Huang J, Senatore L (2017) An effective formalism for testing extensions to General Relativity with gravitational waves. *JHEP* 09:122. [https://doi.org/10.1007/JHEP09\(2017\)122](https://doi.org/10.1007/JHEP09(2017)122). [arXiv:1704.01590](https://arxiv.org/abs/1704.01590) [gr-qc]
- Eperon FC, Reall HS, Santos JE (2016) Instability of supersymmetric microstate geometries. *JHEP* 10:031. [https://doi.org/10.1007/JHEP10\(2016\)031](https://doi.org/10.1007/JHEP10(2016)031). [arXiv:1607.06828](https://arxiv.org/abs/1607.06828) [hep-th]
- Eracleous M, Boroson TA, Halpern JP, Liu J (2012) A LARGE SYSTEMATIC SEARCH FOR CLOSE SUPERMASSIVE BINARY AND RAPIDLY RECOILING BLACK HOLES. *The Astrophysical Journal Supplement Series* 201(2):23. <https://doi.org/10.1088/0067-0049/201/2/23>, URL <https://doi.org/10.1088/0067-0049/201/2/23>
- Evans C, Puech M, Afonso J, Almaini O, Amram P, Aussel H, Barbuy B, Basden A, Bastian N, Battaglia G, et al. (2015) The science case for multi-object spectroscopy on the european elt. *arXiv preprint arXiv:150104726*
- Falcke H, Melia F, Agol E (2000) Viewing the shadow of the black hole at the galactic center. *Astrophys J* 528:L13. <https://doi.org/10.1086/312423>. [arXiv:astro-ph/9912263](https://arxiv.org/abs/astro-ph/9912263) [astro-ph]
- Fang Y, Yang H (2022) Orbit Tomography of Binary Supermassive Black Holes with Very Long Baseline Interferometry. *Astrophys J* 927(1):93. <https://doi.org/10.3847/1538-4357/ac4bd7>. [arXiv:2111.00368](https://arxiv.org/abs/2111.00368) [gr-qc]
- Fazio GG, Hora JL, Witzel G, Willner SP, Ashby MLN, Baganoff F, Becklin E, Carey S, Haggard D, Gammie C, Ghez A, Gurwell MA, Ingalls J, Marrone D, Morris MR, Smith HA (2018) Multiwavelength Light Curves of Two Remarkable Sagittarius A* Flares. *Astrophys. J.*864(1):58. <https://doi.org/10.3847/1538-4357/aad4a2>. [arXiv:1807.07599](https://arxiv.org/abs/1807.07599) [astro-ph.HE]
- von Fellenberg SD, et al. (2022) The Young Stars in the Galactic Center. *Astrophys J Lett* 932(1):L6. <https://doi.org/10.3847/2041-8213/ac68ef>. [arXiv:2205.07595](https://arxiv.org/abs/2205.07595) [astro-ph.GA]
- Feng Y, Li D, Zheng Z, Tsai CW (2020) Supermassive binary black hole evolution can be traced by a small ska pulsar timing array. *Phys Rev D* 102:023014. <https://doi.org/10.1103/PhysRevD.102.023014>, URL <https://link.aps.org/doi/10.1103/PhysRevD.102.023014>
- Fernandes PGS, Mulryne DJ (2022) A new approach and code for spinning black holes in modified gravity. *arXiv e-prints arXiv:2212.07293*. <https://doi.org/10.48550/arXiv.2212.07293>. [arXiv:2212.07293](https://arxiv.org/abs/2212.07293) [gr-qc]
- Ferrari V, Mashhoon B (1984) New approach to the quasinormal modes of a black hole. *Phys Rev D* 30:295–304. <https://doi.org/10.1103/PhysRevD.30.295>
- Ferreira EGM (2021) Ultra-light dark matter. *Astron Astrophys Rev* 29(1):7. <https://doi.org/10.1007/s00159-021-00135-6>. [arXiv:2005.03254](https://arxiv.org/abs/2005.03254) [astro-ph.CO]

- Ferreira MC, Macedo CFB, Cardoso V (2017) Orbital fingerprints of ultralight scalar fields around black holes. *Phys Rev D* 96(8):083017. <https://doi.org/10.1103/PhysRevD.96.083017>. [arXiv:1710.00830](https://arxiv.org/abs/1710.00830) [gr-qc]
- Foschi A, et al. (2023) Using the motion of S2 to constrain scalar clouds around Sgr A*. *Mon Not Roy Astron Soc* 524(1):1075–1086. <https://doi.org/10.1093/mnras/stad1939>. [arXiv:2306.17215](https://arxiv.org/abs/2306.17215) [astro-ph.GA]
- Foucart F, Chandra M, Gammie CF, Quataert E, Tchekhovskoy A (2017) How important is non-ideal physics in simulations of sub-Eddington accretion on to spinning black holes? *Monthly Notices of the Royal Astronomical Society* 470(2):2240–2252. <https://doi.org/10.1093/mnras/stx1368>, URL <https://doi.org/10.1093/mnras/stx1368>
- Franzin E, Liberati S, Mazza J, Vellucci V (2022) Stable rotating regular black holes. *Phys Rev D* 106(10):104060. <https://doi.org/10.1103/PhysRevD.106.104060>. [arXiv:2207.08864](https://arxiv.org/abs/2207.08864) [gr-qc]
- Freitas FF, Herdeiro CAR, Morais AP, Onofre A, Pasechnik R, Radu E, Sanchis-Gual N, Santos R (2021) Ultralight bosons for strong gravity applications from simple Standard Model extensions. *JCAP* 12(12):047. <https://doi.org/10.1088/1475-7516/2021/12/047>. [arXiv:2107.09493](https://arxiv.org/abs/2107.09493) [hep-ph]
- Friedman JL (1978) Generic instability of rotating relativistic stars. *Commun Math Phys* 62(3):247–278. <https://doi.org/10.1007/BF01202527>
- Frolov VP, Vilkovisky GA (1979) Quantum gravity removes classical singularities and shortens the life of black holes. In: *The Second Marcel Grossmann Meeting on the Recent Developments of General Relativity (In Honor of Albert Einstein)*
- Frolov VP, Vilkovisky GA (1981) Spherically Symmetric Collapse in Quantum Gravity. *Phys Lett B* 106:307–313. [https://doi.org/10.1016/0370-2693\(81\)90542-6](https://doi.org/10.1016/0370-2693(81)90542-6)
- Frolov VP, Zelnikov A (2017) Quantum radiation from an evaporating nonsingular black hole. *Phys Rev D* 95(12):124028. <https://doi.org/10.1103/PhysRevD.95.124028>. [arXiv:1704.03043](https://arxiv.org/abs/1704.03043) [hep-th]
- Frolov VP, Krtouš P, Kubizňák D, Santos JE (2018) Massive Vector Fields in Rotating Black-Hole Spacetimes: Separability and Quasinormal Modes. *Phys Rev Lett* 120:231103. <https://doi.org/10.1103/PhysRevLett.120.231103>. [arXiv:1804.00030](https://arxiv.org/abs/1804.00030) [hep-th]
- Fromm CM, Mizuno Y, Younsi Z, Olivares H, Porth O, De Laurentis M, Falcke H, Kramer M, Rezzolla L (2021) Using space-VLBI to probe gravity around Sgr A*. *Astron. Astrophys.*649:A116. <https://doi.org/10.1051/0004-6361/201937335>. [arXiv:2101.08618](https://arxiv.org/abs/2101.08618) [astro-ph.HE]
- Fujita R, Cardoso V (2017) Ultralight scalars and resonances in black-hole physics. *Phys Rev D* 95(4):044016. <https://doi.org/10.1103/PhysRevD.95.044016>. [arXiv:1612.00978](https://arxiv.org/abs/1612.00978) [gr-qc]
- Fukuda H, Nakayama K (2020) Aspects of Nonlinear Effect on Black Hole Superradiance. *JHEP* 01:128. [https://doi.org/10.1007/JHEP01\(2020\)128](https://doi.org/10.1007/JHEP01(2020)128). [arXiv:1910.06308](https://arxiv.org/abs/1910.06308) [hep-ph]
- Gambini R, Pullin J (2013) Loop quantization of the Schwarzschild black hole. *Phys Rev Lett* 110(21):211301. <https://doi.org/10.1103/PhysRevLett.110.211301>. [arXiv:1302.5265](https://arxiv.org/abs/1302.5265) [gr-qc]
- Gammie CF, McKinney JC, Tóth G (2003) HARM: A Numerical Scheme for General Relativistic Magnetohydrodynamics. *Astrophys. J.*589:444–457. <https://doi.org/10.1086/374594>. [astro-ph/0301509](https://arxiv.org/abs/astro-ph/0301509)

- Gan X, Wang LT, Xiao H (2023) Detecting Axion Dark Matter with Black Hole Polarimetry. arXiv e-prints [arXiv:2311.02149](https://arxiv.org/abs/2311.02149) [hep-ph]
- Ganchev B, Santos JE (2018) Scalar Hairy Black Holes in Four Dimensions are Unstable. *Phys Rev Lett* 120(17):171101. <https://doi.org/10.1103/PhysRevLett.120.171101>. [arXiv:1711.08464](https://arxiv.org/abs/1711.08464) [gr-qc]
- Garfinkle D, Horowitz GT, Strominger A (1991) Charged black holes in string theory. *Phys. Rev. D* 43(10):3140–3143. <https://doi.org/10.1103/PhysRevD.43.3140>
- Gelles Z, Himwich E, Johnson MD, Palumbo DCM (2021a) Polarized image of equatorial emission in the Kerr geometry. *Phys. Rev. D* 104(4):044060. <https://doi.org/10.1103/PhysRevD.104.044060>. [arXiv:2105.09440](https://arxiv.org/abs/2105.09440) [gr-qc]
- Gelles Z, Himwich E, Palumbo DCM, Johnson MD (2021b) Polarized Image of Equatorial Emission in the Kerr Geometry. arXiv e-prints [arXiv:2105.09440](https://arxiv.org/abs/2105.09440). [arXiv:2105.09440](https://arxiv.org/abs/2105.09440) [gr-qc]
- Genzel R, Schödel R, Ott T, Eckart A, Alexander T, Lacombe F, Rouan D, Aschenbach B (2003) Near-infrared flares from accreting gas around the supermassive black hole at the Galactic Centre. *Nature* 425(6961):934–937. <https://doi.org/10.1038/nature02065>. [arXiv:astro-ph/0310821](https://arxiv.org/abs/astro-ph/0310821) [astro-ph]
- Genzel R, Schödel R, Ott T, Eckart A, Alexander T, Lacombe F, Rouan D, Aschenbach B (2003) Near-infrared flares from accreting gas around the supermassive black hole at the galactic centre. *Nature* 425:934–937. <https://doi.org/10.1038/nature02065>. [arXiv:astro-ph/0310821](https://arxiv.org/abs/astro-ph/0310821)
- Georgiev B, et al (2022) A Universal Power-law Prescription for Variability from Synthetic Images of Black Hole Accretion Flows. *The Astrophysical Journal Letters* 930(2):L20. <https://doi.org/10.3847/2041-8213/AC65EB>, URL <https://iopscience.iop.org/article/10.3847/2041-8213/ac65eb>, publisher: IOP Publishing
- Ghasemi-Nodehi M (2020) Testing Ghasemi-Nodehi-Bambi spacetime with continuum-fitting method. *European Physical Journal C* 80(5):405. <https://doi.org/10.1140/epjc/s10052-020-7916-8>. [arXiv:2006.13628](https://arxiv.org/abs/2006.13628) [gr-qc]
- Ghez AM, et al. (2008) Measuring Distance and Properties of the Milky Way’s Central Supermassive Black Hole with Stellar Orbits. *Astrophys J* 689:1044–1062. <https://doi.org/10.1086/592738>. [arXiv:0808.2870](https://arxiv.org/abs/0808.2870) [astro-ph]
- Ghosh SG, Maharaj SD (2015) Radiating Kerr-like regular black hole. *Eur Phys J C* 75:7. <https://doi.org/10.1140/epjc/s10052-014-3222-7>. [arXiv:1410.4043](https://arxiv.org/abs/1410.4043) [gr-qc]
- Gibbons G (1975) Vacuum Polarization and the Spontaneous Loss of Charge by Black Holes. *CommunMathPhys* 44:245–264. <https://doi.org/10.1007/BF01609829>
- Gibbons GW, Maeda KI (1988) Black holes and membranes in higher-dimensional theories with dilaton fields. *Nuclear Physics B* 298(4):741–775. [https://doi.org/10.1016/0550-3213\(88\)90006-5](https://doi.org/10.1016/0550-3213(88)90006-5)
- Giddings SB (2019) Searching for quantum black hole structure with the Event Horizon Telescope. *Universe* 5(9):201. <https://doi.org/10.3390/universe5090201>. [arXiv:1904.05287](https://arxiv.org/abs/1904.05287) [gr-qc]
- Giddings SB, Psaltis D (2018) Event Horizon Telescope Observations as Probes for Quantum Structure of Astrophysical Black Holes. *Phys Rev D* 97(8):084035. <https://doi.org/10.1103/PhysRevD.97.084035>. [arXiv:1606.07814](https://arxiv.org/abs/1606.07814) [astro-ph.HE]
- Gillessen S, Eisenhauer F, Quataert E, Genzel R, Paumard T, Trippe S, Ott T, Abuter R, Eckart A, Lagage PO, Lehnert MD, Tacconi LJ, Martins F (2006) Variations in the spectral slope of Sgr A* during a NIR flare. In: *Journal of Physics Conference Series*. *Journal of Physics Conference Series*, vol 54. pp 411–419. <https://doi.org/10.1088/1742-6596/54/1/065>

- Glampedakis K, Pappas G (2021) Can supermassive black hole shadows test the Kerr metric? *Phys Rev D* 104(8):L081503. <https://doi.org/10.1103/PhysRevD.104.L081503>. [arXiv:2102.13573](https://arxiv.org/abs/2102.13573) [gr-qc]
- Goddi C, et al. (2016) BlackHoleCam: Fundamental physics of the galactic center. *Int J Mod Phys D* 26(02):1730001. https://doi.org/10.1142/9789813226609_0046. [arXiv:1606.08879](https://arxiv.org/abs/1606.08879) [astro-ph.HE]
- Gold R (2019) Relativistic aspects of accreting supermassive black hole binaries in their natural habitat: A review. *Galaxies* 7:63
- Gold R, Paschalidis V, Etienne ZB, Shapiro SL, Pfeiffer HP (2014) Accretion disks around binary black holes of unequal mass: General relativistic magnetohydrodynamic simulations near decoupling. *Physical Review D* 89(6):064060. <https://doi.org/10.1103/PhysRevD.89.064060>, URL <https://link.aps.org/doi/10.1103/PhysRevD.89.064060>, publisher: American Physical Society
- Goldreich P, Julian WH (1969) Pulsar Electrodynamics. *Astrophys. J.*157:869. <https://doi.org/10.1086/150119>
- Goncharov B, et al (2021) On the evidence for a common-spectrum process in the search for the nanohertz gravitational-wave background with the parkes pulsar timing array. *The Astrophysical Journal Letters* 917(2):L19. <https://doi.org/10.3847/2041-8213/ac17f4>, URL <https://doi.org/10.3847/2041-8213/ac17f4>
- Goodsell M, Jaeckel J, Redondo J, Ringwald A (2009) Naturally Light Hidden Photons in LARGE Volume String Compactifications. *JHEP* 11:027. <https://doi.org/10.1088/1126-6708/2009/11/027>. [arXiv:0909.0515](https://arxiv.org/abs/0909.0515) [hep-ph]
- Gourgoulhon E, Jaramillo JL (2008) New theoretical approaches to black holes. *New Astron Rev* 51:791–798. <https://doi.org/10.1016/j.newar.2008.03.026>. [arXiv:0803.2944](https://arxiv.org/abs/0803.2944) [astro-ph]
- Gourgoulhon E, Le Tiec A, Vincent FH, Warburton N (2019) Gravitational waves from bodies orbiting the Galactic Center black hole and their detectability by LISA. *Astron Astrophys* 627:A92. <https://doi.org/10.1051/0004-6361/201935406>. [arXiv:1903.02049](https://arxiv.org/abs/1903.02049) [gr-qc]
- Graham MJ, Djorgovski SG, Stern D, Drake AJ, Mahabal AA, Donalek C, Glikman E, Larson S, Christensen E (2015) A systematic search for close supermassive black hole binaries in the Catalina Real-time Transient Survey. *Monthly Notices of the Royal Astronomical Society* 453(2):1562–1576. <https://doi.org/10.1093/mnras/stv1726>, URL <https://doi.org/10.1093/mnras/stv1726>. <https://academic.oup.com/mnras/article-pdf/453/2/1562/13770995/stv1726.pdf>
- Gralla SE, Lupsasca A (2020a) Lensing by Kerr Black Holes. *Phys Rev D* 101(4):044031. <https://doi.org/10.1103/PhysRevD.101.044031>. [arXiv:1910.12873](https://arxiv.org/abs/1910.12873) [gr-qc]
- Gralla SE, Lupsasca A (2020b) Null geodesics of the Kerr exterior. *Phys Rev D* 101(4):044032. <https://doi.org/10.1103/PhysRevD.101.044032>. [arXiv:1910.12881](https://arxiv.org/abs/1910.12881) [gr-qc]
- Gralla SE, Zimmerman P (2018) Scaling and Universality in Extremal Black Hole Perturbations. *JHEP* 06:061. [https://doi.org/10.1007/JHEP06\(2018\)061](https://doi.org/10.1007/JHEP06(2018)061). [arXiv:1804.04753](https://arxiv.org/abs/1804.04753) [gr-qc]
- Gralla SE, Lupsasca A, Strominger A (2018) Observational Signature of High Spin at the Event Horizon Telescope. *Mon Not Roy Astron Soc* 475(3):3829–3853. <https://doi.org/10.1093/mnras/sty039>. [arXiv:1710.11112](https://arxiv.org/abs/1710.11112) [astro-ph.HE]
- Gralla SE, Holz DE, Wald RM (2019) Black Hole Shadows, Photon Rings, and Lensing Rings. *Phys Rev D* 100(2):024018. <https://doi.org/10.1103/PhysRevD.100.024018>.

- [arXiv:1906.00873](https://arxiv.org/abs/1906.00873) [astro-ph.HE]
- GRAVITY Collaboration, Bauböck M, et al (2020) Modeling the orbital motion of Sgr A*’s near-infrared flares. *Astron. Astrophys.*635:A143. <https://doi.org/10.1051/0004-6361/201937233>. [arXiv:2002.08374](https://arxiv.org/abs/2002.08374) [astro-ph.HE]
- Gravity Collaboration, Jiménez-Rosales A, et al (2020) Dynamically important magnetic fields near the event horizon of Sgr A*. *Astron. Astrophys.*643:A56. <https://doi.org/10.1051/0004-6361/202038283>. [arXiv:2009.01859](https://arxiv.org/abs/2009.01859) [astro-ph.HE]
- Gravity Collaboration, Abuter R, et al (2022) Deep images of the Galactic center with GRAVITY. *Astronomy and Astrophysics* 657:A82. <https://doi.org/10.1051/0004-6361/202142459>. [arXiv:2112.07477](https://arxiv.org/abs/2112.07477) [astro-ph.GA]
- Greene PB, Kofman L (1999) Preheating of fermions. *Phys Lett B* 448:6–12. [https://doi.org/10.1016/S0370-2693\(99\)00020-9](https://doi.org/10.1016/S0370-2693(99)00020-9). [arXiv:hep-ph/9807339](https://arxiv.org/abs/hep-ph/9807339)
- Greene PB, Kofman L (2000) On the theory of fermionic preheating. *Phys Rev D* 62:123516. <https://doi.org/10.1103/PhysRevD.62.123516>. [arXiv:hep-ph/0003018](https://arxiv.org/abs/hep-ph/0003018)
- Guerrero M, Olmo GJ, Rubiera-García D, Gómez DSC (2021) Shadows and optical appearance of black bounces illuminated by a thin accretion disk. *JCAP* 08:036. <https://doi.org/10.1088/1475-7516/2021/08/036>. [arXiv:2105.15073](https://arxiv.org/abs/2105.15073) [gr-qc]
- Guica M, Hartman T, Song W, Strominger A (2009) The Kerr/CFT Correspondence. *Phys Rev D* 80:124008. <https://doi.org/10.1103/PhysRevD.80.124008>. [arXiv:0809.4266](https://arxiv.org/abs/hep-th/0809.4266) [hep-th]
- Guo M, Li PC (2020) Innermost stable circular orbit and shadow of the 4D Einstein–Gauss–Bonnet black hole. *Eur Phys J C* 80(6):588. <https://doi.org/10.1140/epjc/s10052-020-8164-7>. [arXiv:2003.02523](https://arxiv.org/abs/2003.02523) [gr-qc]
- Gupta T, Herrero-Valea M, Blas D, Barausse E, Cornish N, Yagi K, Yunes N (2021) New binary pulsar constraints on Einstein-æther theory after GW170817. *Class Quant Grav* 38(19):195003. <https://doi.org/10.1088/1361-6382/ac1a69>. [arXiv:2104.04596](https://arxiv.org/abs/2104.04596) [gr-qc]
- Gurvits LI, Frey S, Krezinger M, Titov O, An T, Zhang Y, Polnarev AG, Gabányi KÉ, Perger K, Melnikov A (2023) J2102+6015: a potential distant multimessenger? In: Liodakis I, Aller MF, Krawczynski H, Lähteenmäki A, Pearson TJ (eds) *The Multimessenger Chakra of Blazar Jets*. vol 375. pp 86–90. <https://doi.org/10.1017/S1743921323001151>. [arXiv:2301.12283](https://arxiv.org/abs/2301.12283) [astro-ph.CO]
- Gutiérrez EM, Combi L, Noble SC, Campanelli M, Krolik JH, Armengol FL, García F (2022) Electromagnetic Signatures from Supermassive Binary Black Holes Approaching Merger. *The Astrophysical Journal* 928(2):137. <https://doi.org/10.3847/1538-4357/ac56de>, URL <https://dx.doi.org/10.3847/1538-4357/ac56de>, publisher: The American Astronomical Society
- Gyulchev G, Nedkova P, Tinchev V, Yazadjiev S (2018) On the shadow of rotating traversable wormholes. *Eur Phys J C* 78(7):544. <https://doi.org/10.1140/epjc/s10052-018-6012-9>. [arXiv:1805.11591](https://arxiv.org/abs/1805.11591) [gr-qc]
- Gyulchev G, Nedkova P, Vetsov T, Yazadjiev S (2019) Image of the Janis-Newman–Winicour naked singularity with a thin accretion disk. *Phys Rev D* 100(2):024055. <https://doi.org/10.1103/PhysRevD.100.024055>. [arXiv:1905.05273](https://arxiv.org/abs/1905.05273) [gr-qc]
- Gyulchev G, Kunz J, Nedkova P, Vetsov T, Yazadjiev S (2020) Observational signatures of strongly naked singularities: image of the thin accretion disk. *Eur Phys J C* 80(11):1017. <https://doi.org/10.1140/epjc/s10052-020-08575-7>. [arXiv:2003.06943](https://arxiv.org/abs/2003.06943) [gr-qc]
- Gyulchev G, Nedkova P, Vetsov T, Yazadjiev S (2021) Image of the thin accretion disk around compact objects in the Einstein–Gauss–Bonnet gravity. *Eur Phys J C*

- 81(10):885. <https://doi.org/10.1140/epjc/s10052-021-09624-5>. arXiv:2106.14697 [gr-qc]
- Hackmann E, Lammerzahl C, Kagramanova V, Kunz J (2010) Analytical solution of the geodesic equation in Kerr-(anti) de Sitter space-times. *Phys Rev D* 81:044020. <https://doi.org/10.1103/PhysRevD.81.044020>. arXiv:1009.6117 [gr-qc]
- Hada K, Kino M, Doi A, Nagai H, Honma M, Akiyama K, Tazaki F, Lico R, Giroletti M, Giovannini G, Orienti M, Hagiwara Y (2016) High-sensitivity 86 GHz (3.5 mm) VLBI Observations of M87: Deep Imaging of the Jet Base at a Resolution of 10 Schwarzschild Radii. *Astrophys. J.* 817(2):131. <https://doi.org/10.3847/0004-637X/817/2/131>. arXiv:1512.03783 [astro-ph.HE]
- Hadar S, Johnson MD, Lupsasca A, Wong GN (2021) Photon Ring Autocorrelations. *Phys Rev D* 103(10):104038. <https://doi.org/10.1103/PhysRevD.103.104038>. arXiv:2010.03683 [gr-qc]
- Haggard HM, Rovelli C (2016) Quantum Gravity Effects around Sagittarius A*. *Int J Mod Phys D* 25(12):1644021. <https://doi.org/10.1142/S0218271816440211>. arXiv:1607.00364 [gr-qc]
- Hájíček P (1987) On the Origin of Hawking Radiation. *Phys Rev D* 36:1065. <https://doi.org/10.1103/PhysRevD.36.1065>
- Hájíček P (2001) Unitary dynamics of spherical null gravitating shells. *Nucl Phys B* 603:555–577. [https://doi.org/10.1016/S0550-3213\(01\)00140-7](https://doi.org/10.1016/S0550-3213(01)00140-7). arXiv:hep-th/0007005
- Hájíček P (2003) Quantum theory of gravitational collapse: (Lecture notes on quantum conchology). *Lect Notes Phys* 631:255–299. https://doi.org/10.1007/978-3-540-45230-0_6. arXiv:gr-qc/0204049
- Hamaus N, Paumard T, Müller T, Gillessen S, Eisenhauer F, Trippe S, Genzel R (2009) Prospects for testing the nature of Sgr A*'s NIR flares on the basis of current VLT- and future VLTI-observations. *Astrophys J* 692:902–916. <https://doi.org/10.1088/0004-637X/692/1/902>. arXiv:0810.4947 [astro-ph]
- Hansen D, Yunes N (2013) Applicability of the Newman-Janis Algorithm to Black Hole Solutions of Modified Gravity Theories. *Phys Rev D* 88(10):104020. <https://doi.org/10.1103/PhysRevD.88.104020>. arXiv:1308.6631 [gr-qc]
- Harari D, Sikivie P (1992) Effects of a Nambu-Goldstone boson on the polarization of radio galaxies and the cosmic microwave background. *Phys Lett B* 289:67–72. [https://doi.org/10.1016/0370-2693\(92\)91363-E](https://doi.org/10.1016/0370-2693(92)91363-E)
- Hassan SF, Rosen RA (2012) Bimetric Gravity from Ghost-free Massive Gravity. *JHEP* 02:126. [https://doi.org/10.1007/JHEP02\(2012\)126](https://doi.org/10.1007/JHEP02(2012)126). arXiv:1109.3515 [hep-th]
- Hawking SW (1966) The Occurrence of Singularities in Cosmology. *Proceedings of the Royal Society of London Series A* 294(1439):511–521. <https://doi.org/10.1098/rspa.1966.0221>
- Hawking SW (1976) Breakdown of Predictability in Gravitational Collapse. *Phys Rev D* 14:2460–2473. <https://doi.org/10.1103/PhysRevD.14.2460>
- Hawking SW, Ellis GFR (2011) *The Large Scale Structure of Space-Time*. Cambridge Monographs on Mathematical Physics, Cambridge University Press. <https://doi.org/10.1017/CBO9780511524646>
- Hawking SW, Penrose R (1970) The Singularities of gravitational collapse and cosmology. *Proc Roy Soc Lond A* 314:529–548. <https://doi.org/10.1098/rspa.1970.0021>
- Hayward SA (1994) General laws of black hole dynamics. *Phys Rev D* 49:6467–6474. <https://doi.org/10.1103/PhysRevD.49.6467>

- Hayward SA (2006) Formation and evaporation of regular black holes. *Phys Rev Lett* 96:031103. <https://doi.org/10.1103/PhysRevLett.96.031103>. [arXiv:gr-qc/0506126](https://arxiv.org/abs/gr-qc/0506126)
- Hees A, et al. (2020) Search for a Variation of the Fine Structure Constant around the Supermassive Black Hole in Our Galactic Center. *Phys Rev Lett* 124(8):081101. <https://doi.org/10.1103/PhysRevLett.124.081101>. [arXiv:2002.11567](https://arxiv.org/abs/2002.11567) [astro-ph.GA]
- Heisenberg L (2014) Generalization of the Proca Action. *JCAP* 05:015. <https://doi.org/10.1088/1475-7516/2014/05/015>. [arXiv:1402.7026](https://arxiv.org/abs/1402.7026) [hep-th]
- Heißel G, Paumard T, Perrin G, Vincent F (2022) The dark mass signature in the orbit of S2. *Astron Astrophys* 660:A13. <https://doi.org/10.1051/0004-6361/202142114>. [arXiv:2112.07778](https://arxiv.org/abs/2112.07778) [astro-ph.GA]
- Held A, Zhang J (2023) Instability of spherically symmetric black holes in quadratic gravity. *Phys. Rev. D* 107(6):064060. <https://doi.org/10.1103/PhysRevD.107.064060>. [arXiv:2209.01867](https://arxiv.org/abs/2209.01867) [gr-qc]
- Held A, Gold R, Eichhorn A (2019) Asymptotic safety casts its shadow. *JCAP* 06:029. <https://doi.org/10.1088/1475-7516/2019/06/029>. [arXiv:1904.07133](https://arxiv.org/abs/1904.07133) [gr-qc]
- Hellings RW, Downs GS (1983) Upper limits on the isotropic gravitational radiation background from pulsar timing analysis. *Astrophys. J. Lett.* 265:L39–L42. <https://doi.org/10.1086/183954>
- Herdeiro C, Radu E (2015a) Construction and physical properties of Kerr black holes with scalar hair. *Class Quant Grav* 32(14):144001. <https://doi.org/10.1088/0264-9381/32/14/144001>. [arXiv:1501.04319](https://arxiv.org/abs/1501.04319) [gr-qc]
- Herdeiro C, Radu E, Rúnarsson H (2016) Kerr black holes with Proca hair. *Class Quant Grav* 33(15):154001. <https://doi.org/10.1088/0264-9381/33/15/154001>. [arXiv:1603.02687](https://arxiv.org/abs/1603.02687) [gr-qc]
- Herdeiro CAR, Radu E (2014) Kerr black holes with scalar hair. *Phys Rev Lett* 112:221101. <https://doi.org/10.1103/PhysRevLett.112.221101>. [arXiv:1403.2757](https://arxiv.org/abs/1403.2757) [gr-qc]
- Herdeiro CAR, Radu E (2015b) Asymptotically flat black holes with scalar hair: a review. *Int J Mod Phys D* 24(09):1542014. <https://doi.org/10.1142/S0218271815420146>. [arXiv:1504.08209](https://arxiv.org/abs/1504.08209) [gr-qc]
- Herdeiro CAR, Radu E (2017) Dynamical Formation of Kerr Black Holes with Synchronized Hair: An Analytic Model. *Phys Rev Lett* 119(26):261101. <https://doi.org/10.1103/PhysRevLett.119.261101>. [arXiv:1706.06597](https://arxiv.org/abs/1706.06597) [gr-qc]
- Herdeiro CAR, Radu E, Rúnarsson H (2015) Kerr black holes with self-interacting scalar hair: hairier but not heavier. *Phys Rev D* 92(8):084059. <https://doi.org/10.1103/PhysRevD.92.084059>. [arXiv:1509.02923](https://arxiv.org/abs/1509.02923) [gr-qc]
- Herdeiro CAR, Pombo AM, Radu E, Cunha PVP, Sanchis-Gual N (2021) The imitation game: Proca stars that can mimic the Schwarzschild shadow. *JCAP* 04:051. <https://doi.org/10.1088/1475-7516/2021/04/051>. [arXiv:2102.01703](https://arxiv.org/abs/2102.01703) [gr-qc]
- Herdeiro CAR, Radu E, Santos NM (2022) A bound on energy extraction (and hairiness) from superradiance. *Phys Lett B* 824:136835. <https://doi.org/10.1016/j.physletb.2021.136835>. [arXiv:2111.03667](https://arxiv.org/abs/2111.03667) [gr-qc]
- Hertog T, Hartle J (2020) Observational Implications of Fuzzball Formation. *Gen Rel Grav* 52(7):67. <https://doi.org/10.1007/s10714-020-02720-z>. [arXiv:1704.02123](https://arxiv.org/abs/1704.02123) [hep-th]
- Hilbert D (1917) *Nachrichten von der königlichen gesellschaft der wissenschaften zu göttingen—mathematisch-physikalische klasse, chapter die grundlagen der physik—zweite mitteilung*. Weidmannsche Buchhandlung, Berlin pp 53–76

- Himwich E, Johnson MD, Lupsasca Ar, Strominger A (2020) Universal polarimetric signatures of the black hole photon ring. *Phys. Rev. D*101(8):084020. <https://doi.org/10.1103/PhysRevD.101.084020>. [arXiv:2001.08750](https://arxiv.org/abs/2001.08750) [gr-qc]
- Ho PM, Matsuo Y (2018) Static Black Hole and Vacuum Energy: Thin Shell and Incompressible Fluid. *JHEP* 03:096. [https://doi.org/10.1007/JHEP03\(2018\)096](https://doi.org/10.1007/JHEP03(2018)096). [arXiv:1710.10390](https://arxiv.org/abs/1710.10390) [hep-th]
- Holz DE, Hughes SA (2005) Using gravitational-wave standard sirens. *The Astrophysical Journal* 629(1):15
- Hopkins PF, Hernquist L, Cox TJ, Kereš D (2008) A Cosmological Framework for the Co-Evolution of Quasars, Supermassive Black Holes, and Elliptical Galaxies. I. Galaxy Mergers and Quasar Activity. *Astrophys. J. Suppl.*175(2):356–389. <https://doi.org/10.1086/524362>. [arXiv:0706.1243](https://arxiv.org/abs/0706.1243) [astro-ph]
- Horndeski GW (1974) Second-order scalar-tensor field equations in a four-dimensional space. *Int J Theor Phys* 10:363–384. <https://doi.org/10.1007/BF01807638>
- Hossenfelder S, Modesto L, Premont-Schwarz I (2010) A Model for non-singular black hole collapse and evaporation. *Phys Rev D* 81:044036. <https://doi.org/10.1103/PhysRevD.81.044036>. [arXiv:0912.1823](https://arxiv.org/abs/0912.1823) [gr-qc]
- Hu BX, D’Orazio DJ, Haiman Z, Smith KL, Snios B, Charisi M, Di Stefano R (2020) Spikey: self-lensing flares from eccentric SMBH binaries. *Mon. Not. R. Astron. Soc.*495(4):4061–4070. <https://doi.org/10.1093/mnras/staa1312>. [arXiv:1910.05348](https://arxiv.org/abs/1910.05348) [astro-ph.HE]
- Hu W, Barkana R, Gruzinov A (2000) Cold and fuzzy dark matter. *Phys Rev Lett* 85:1158–1161. <https://doi.org/10.1103/PhysRevLett.85.1158>. [arXiv:astro-ph/0003365](https://arxiv.org/abs/hep-ph/0003365)
- Hu WR, Wu YL (2017) The Taiji Program in Space for gravitational wave physics and the nature of gravity. *National Science Review* 4(5):685–686. <https://doi.org/10.1093/nsr/nwx116>, URL <https://doi.org/10.1093/nsr/nwx116>. <https://academic.oup.com/nsr/article-pdf/4/5/685/31566708/nwx116.pdf>
- Hui L, Ostriker JP, Tremaine S, Witten E (2017) Ultralight scalars as cosmological dark matter. *Phys Rev D* 95(4):043541. <https://doi.org/10.1103/PhysRevD.95.043541>. [arXiv:1610.08297](https://arxiv.org/abs/1610.08297) [astro-ph.CO]
- Igumenshchev IV, Narayan R, Abramowicz MA (2003) Three-dimensional Magnetohydrodynamic Simulations of Radiatively Inefficient Accretion Flows. *Astrophys. J.*592(2):1042–1059. <https://doi.org/10.1086/375769>. [arXiv:astro-ph/0301402](https://arxiv.org/abs/astro-ph/0301402) [astro-ph]
- Ikeda T, Brito R, Cardoso V (2019) Blasts of Light from Axions. *Phys Rev Lett* 122(8):081101. <https://doi.org/10.1103/PhysRevLett.122.081101>. [arXiv:1811.04950](https://arxiv.org/abs/1811.04950) [gr-qc]
- Iorio L (2020) The Short-period S-stars S4711, S62, S4714 and the Lense–Thirring Effect due to the Spin of Sgr A*. *Astrophys J* 904(2):186. <https://doi.org/10.3847/1538-4357/abbfb5>. [arXiv:2009.01158](https://arxiv.org/abs/2009.01158) [gr-qc]
- Ishikawa Y, Liu X, Shen Y, Zakamska NL, Chen YC, Hwang HC (2021) Kpc-scale dual supermassive black holes and their impact on galaxy formation at cosmic noon. *JWST Proposal. Cycle 1, ID. #2654*
- Islam SU, Kumar R, Ghosh SG (2020) Gravitational lensing by black holes in the 4D Einstein-Gauss-Bonnet gravity. *JCAP* 09:030. <https://doi.org/10.1088/1475-7516/2020/09/030>. [arXiv:2004.01038](https://arxiv.org/abs/2004.01038) [gr-qc]
- Islam SU, Kumar J, Ghosh SG (2021) Strong gravitational lensing by rotating Simpson–Visser black holes. *JCAP* 10:013. <https://doi.org/10.1088/1475-7516/2021/10/013>.

- [arXiv:2104.00696](#) [gr-qc]
- Issaoun S, Pesce DW, Roelofs F, Chael A, Dodson R, Rioja MJ, Akiyama K, Aran R, Blackburn L, Doeleman SS, Fish VL, Fitzpatrick G, Johnson MD, Narayanan G, Raymond AW, Tilanus RPJ (2023) Enabling Transformational ngEHT Science via the Inclusion of 86 GHz Capabilities. *Galaxies* 11(1):28. <https://doi.org/10.3390/galaxies11010028>. [arXiv:2302.05415](#) [astro-ph.IM]
- Janis AI, Newman ET, Winicour J (1968) Reality of the Schwarzschild Singularity. *Phys Rev Lett* 20:878–880. <https://doi.org/10.1103/PhysRevLett.20.878>
- Jenet FA, Lommen A, Larson SL, Wen L (2004) Constraining the properties of supermassive black hole systems using pulsar timing: Application to 3c 66b. *The Astrophysical Journal* 606(2):799–803. <https://doi.org/10.1086/383020>, URL <https://doi.org/10.1086/383020>
- Jeter B, Broderick AE, Gold R (2020) Differentiating disc and black hole-driven jets with EHT images of variability in M87. *Mon. Not. R. Astron. Soc.* 493(4):5606–5616. <https://doi.org/10.1093/mnras/staa679>. [arXiv:1804.05861](#) [astro-ph.HE]
- Jiménez-Rosales A, Dexter J, Ressler SM, Tchekhovskoy A, Bauböck M, Dallilar Y, de Zeeuw PT, Drescher A, Eisenhauer F, von Fellenberg S, Gao F, Genzel R, Gillessen S, Habibi M, Ott T, Stadler J, Straub O, Widmann F (2021) Relative depolarization of the black hole photon ring in GRMHD models of Sgr A* and M87*. *Mon. Not. R. Astron. Soc.* 503(3):4563–4575. <https://doi.org/10.1093/mnras/stab784>. [arXiv:2103.06292](#) [astro-ph.HE]
- Johannsen T (2013) Regular black hole metric with three constants of motion. *Phys. Rev. D* 88(4):044002. <https://doi.org/10.1103/PhysRevD.88.044002>. [arXiv:1501.02809](#) [gr-qc]
- Johannsen T, Psaltis D (2010) Testing the No-Hair Theorem with Observations in the Electromagnetic Spectrum: II. Black-Hole Images. *Astrophys J* 718:446–454. <https://doi.org/10.1088/0004-637X/718/1/446>. [arXiv:1005.1931](#) [astro-ph.HE]
- Johannsen T, Psaltis D (2011a) Metric for rapidly spinning black holes suitable for strong-field tests of the no-hair theorem. *Phys. Rev. D* 83(12):124015. <https://doi.org/10.1103/PhysRevD.83.124015>. [arXiv:1105.3191](#) [gr-qc]
- Johannsen T, Psaltis D (2011b) Testing the No-hair Theorem with Observations in the Electromagnetic Spectrum. III. Quasi-periodic Variability. *Astrophys. J.* 726(1):11. <https://doi.org/10.1088/0004-637X/726/1/11>. [arXiv:1010.1000](#) [astro-ph.HE]
- Johnson MD, Akiyama K, Blackburn L, Bouman KL, Broderick AE, Cardoso V, Fender RP, Fromm CM, Galison P, Gómez JL, Haggard D, Lister ML, Lobanov AP, Markoff S, Narayan R, Natarajan P, Nichols T, Pesce DW, Younsi Z, Chael A, Chatterjee K, Chaves R, Doboszewski J, Dodson R, Doeleman SS, Elder J, Fitzpatrick G, Haworth K, Houston J, Issaoun S, Kovalev YY, Levis A, Lico R, Marcoci A, Martens NCM, Nagar NM, Oppenheimer A, Palumbo DCM, Ricarte A, Rioja MJ, Roelofs F, Thresher AC, Tiede P, Weintroub J, Wielgus M (2023) Key Science Goals for the Next-Generation Event Horizon Telescope. *Galaxies* 11(3):61. <https://doi.org/10.3390/galaxies11030061>. [arXiv:2304.11188](#) [astro-ph.HE]
- Johnson MD, et al. (2020) Universal interferometric signatures of a black hole’s photon ring. *Sci Adv* 6(12):eaaz1310. <https://doi.org/10.1126/sciadv.aaz1310>. [arXiv:1907.04329](#) [astro-ph.IM]
- Joshi PS, Malafarina D, Narayan R (2011) Equilibrium configurations from gravitational collapse. *Class Quant Grav* 28:235018. <https://doi.org/10.1088/0264-9381/28/23/235018>. [arXiv:1106.5438](#) [gr-qc]

- Joshi PS, Malafarina D, Narayan R (2014) Distinguishing black holes from naked singularities through their accretion disc properties. *Class Quant Grav* 31:015002. <https://doi.org/10.1088/0264-9381/31/1/015002>. arXiv:1304.7331 [gr-qc]
- Kalfountzou E, Santos Lleo M, Trichas M (2017) SDSS J1056+5516: A Triple AGN or an SMBH Recoil Candidate? *Astrophys. J. Lett.*851(1):L15. <https://doi.org/10.3847/2041-8213/aa9b2d>. arXiv:1712.03909 [astro-ph.GA]
- Kato Y, Miyoshi M, Takahashi R, Negoro H, Matsumoto R (2010) Measuring spin of a supermassive black hole at the Galactic centre - implications for a unique spin. *Mon. Not. R. Astron. Soc.*403(1):L74–L78. <https://doi.org/10.1111/j.1745-3933.2010.00818.x>. arXiv:0906.5423 [astro-ph.GA]
- Kauffmann J, Rajagopalan G, Akiyama K, Fish V, Lonsdale C, Matthews LD, Pillai TG (2023) The haystack telescope as an astronomical instrument. *Galaxies* 11(1). <https://doi.org/10.3390/galaxies11010009>, URL <https://www.mdpi.com/2075-4434/11/1/9>
- Keir J (2019) Wave propagation on microstate geometries. *Annales Henri Poincaré* 21(3):705–760. <https://doi.org/10.1007/s00023-019-00874-4>. arXiv:1609.01733 [gr-qc]
- Kelley L, Charisi M, Burke-Spolaor S, et al (2019) Multi-Messenger Astrophysics With Pulsar Timing Arrays. *Bulletin of the American Astronomical Society* 51(3):490. arXiv:1903.07644 [astro-ph.HE]
- Kelley LZ, D’Orazio DJ, Di Stefano R (2021) Gravitational self-lensing in populations of massive black hole binaries. *Mon. Not. R. Astron. Soc.*508(2):2524–2536. <https://doi.org/10.1093/mnras/stab2776>. arXiv:2107.07522 [astro-ph.HE]
- Kerr RP (1963) Gravitational field of a spinning mass as an example of algebraically special metrics. *Phys Rev Lett* 11:237–238. <https://doi.org/10.1103/PhysRevLett.11.237>
- Khan FM, Fiacconi D, Mayer L, Berczik P, Just A (2016a) Swift Coalescence of Supermassive Black Holes in Cosmological Mergers of Massive Galaxies. *Astrophys. J.*828(2):73. <https://doi.org/10.3847/0004-637X/828/2/73>. arXiv:1604.00015 [astro-ph.GA]
- Khan FM, Fiacconi D, Mayer L, Berczik P, Just A (2016b) Swift Coalescence of Supermassive Black Holes in Cosmological Mergers of Massive Galaxies. *Astrophys. J.*828(2):73. <https://doi.org/10.3847/0004-637X/828/2/73>. arXiv:1604.00015 [astro-ph.GA]
- Kharb P, Lal DV, Merritt D (2017) A candidate sub-parsec binary black hole in the Seyfert galaxy NGC 7674. *Nature Astronomy* 1:727–733. <https://doi.org/10.1038/s41550-017-0256-4>. arXiv:1709.06258 [astro-ph.GA]
- Khodadi M, Saridakis EN (2021) Einstein-Æther gravity in the light of event horizon telescope observations of M87*. *Phys Dark Univ* 32:100835. <https://doi.org/10.1016/j.dark.2021.100835>. arXiv:2012.05186 [gr-qc]
- Khodadi M, Allahyari A, Vagnozzi S, Mota DF (2020) Black holes with scalar hair in light of the Event Horizon Telescope. *JCAP* 09:026. <https://doi.org/10.1088/1475-7516/2020/09/026>. arXiv:2005.05992 [gr-qc]
- Kim JY, Savolainen T, Voitsik P, Kravchenko EV, Lisakov MM, Kovalev YY, Müller H, Lobanov AP, Sokolovsky KV, Bruni G, Edwards PG, Reynolds C, Bach U, Gurvits LI, Krichbaum TP, Hada K, Giroletti M, Orienti M, Anderson JM, Lee SS, Sohn BW, Zensus JA (2023) RadioAstron Space VLBI Imaging of the Jet in M87. I. Detection of High Brightness Temperature at 22 GHz. *Astrophys. J.*952(1):34. <https://doi.org/10.3847/1538-4357/acf17>. arXiv:2304.09816 [astro-ph.GA]

- Kleihaus B, Kunz J, Radu E (2011) Rotating Black Holes in Dilatonic Einstein–Gauss–Bonnet Theory. *Phys Rev Lett* 106:151104. <https://doi.org/10.1103/PhysRevLett.106.151104>. [arXiv:1101.2868](https://arxiv.org/abs/1101.2868) [gr-qc]
- Kleihaus B, Kunz J, Mojica S, Radu E (2016) Spinning black holes in Einstein–Gauss–Bonnet–dilaton theory: Nonperturbative solutions. *Phys Rev D* 93(4):044047. <https://doi.org/10.1103/PhysRevD.93.044047>. [arXiv:1511.05513](https://arxiv.org/abs/1511.05513) [gr-qc]
- Klein A, et al. (2016) Science with the space-based interferometer eLISA: Supermassive black hole binaries. *Phys Rev D* 93(2):024003. <https://doi.org/10.1103/PhysRevD.93.024003>. [arXiv:1511.05581](https://arxiv.org/abs/1511.05581) [gr-qc]
- Kobayashi T, Murgia R, De Simone A, Iršič V, Viel M (2017) Lyman- α constraints on ultralight scalar dark matter: Implications for the early and late universe. *Phys Rev D* 96(12):123514. <https://doi.org/10.1103/PhysRevD.96.123514>. [arXiv:1708.00015](https://arxiv.org/abs/1708.00015) [astro-ph.CO]
- Kocherlakota P, Rezzolla L (2020) Accurate mapping of spherically symmetric black holes in a parametrized framework. *Phys. Rev. D* 102(6):064058. <https://doi.org/10.1103/PhysRevD.102.064058>. [arXiv:2007.15593](https://arxiv.org/abs/2007.15593) [gr-qc]
- Kocherlakota P, Rezzolla L (2022) Distinguishing gravitational and emission physics in black hole imaging: spherical symmetry. *Mon Not Roy Astron Soc* 513(1):1229–1243. <https://doi.org/10.1093/mnras/stac891>. [arXiv:2201.05641](https://arxiv.org/abs/2201.05641) [gr-qc]
- Kocherlakota P, Rezzolla L (2022) Distinguishing gravitational and emission physics in black hole imaging: spherical symmetry. *Mon. Not. R. Astron. Soc.* 513(1):1229–1243. <https://doi.org/10.1093/mnras/stac891>. [arXiv:2201.05641](https://arxiv.org/abs/2201.05641) [gr-qc]
- Kocherlakota P, Rezzolla L, Roy R, Wielgus M (2023) Extreme Light Bending in Spherically-Symmetric Black Hole Spacetimes: Universal Characteristics and Strong-Field Tests of Gravity. *arXiv e-prints* arXiv:2307.16841. <https://doi.org/10.48550/arXiv.2307.16841>. [arXiv:2307.16841](https://arxiv.org/abs/2307.16841) [gr-qc]
- Kocherlakota P, et al. (2021) Constraints on black-hole charges with the 2017 EHT observations of M87*. *Phys Rev D* 103(10):104047. <https://doi.org/10.1103/PhysRevD.103.104047>. [arXiv:2105.09343](https://arxiv.org/abs/2105.09343) [gr-qc]
- Kocsis B, Frei Z, Haiman Z, Menou K (2006) Finding the electromagnetic counterparts of cosmological standard sirens. *The Astrophysical Journal* 637(1):27–37. <https://doi.org/10.1086/498236>, URL <https://doi.org/10.1086/498236>
- Kocsis B, Haiman Z, Menou K (2008a) Pre-Merger Localization of Gravitational-Wave Standard Sirens With LISA: Triggered Search for an Electromagnetic Counterpart. *Astrophys J* 684:870–888. <https://doi.org/10.1086/590230>. [arXiv:0712.1144](https://arxiv.org/abs/0712.1144) [astro-ph]
- Kocsis B, Haiman Z, Menou K (2008b) Premerger localization of gravitational wave standard sirens with lisa: Triggered search for an electromagnetic counterpart. *The Astrophysical Journal* 684(2):870–887. <https://doi.org/10.1086/590230>, URL <https://doi.org/10.1086/590230>
- Komossa S, Grupe D, Kraus A, Gurwell MA, Haiman Z, Liu FK, Tchekhovskoy A, Gallo LC, Berton M, Blandford R, Gómez JL, Gonzalez AG (2023) Absence of the predicted 2022 October outburst of OJ 287 and implications for binary SMBH scenarios. *Mon. Not. R. Astron. Soc.* <https://doi.org/10.1093/mnras/slad016>. [arXiv:2302.11646](https://arxiv.org/abs/2302.11646) [astro-ph.HE]
- Konoplya R, Rezzolla L, Zhidenko A (2016) General parametrization of axisymmetric black holes in metric theories of gravity. *Phys. Rev. D* 93(6):064015. <https://doi.org/10.1103/PhysRevD.93.064015>. [arXiv:1602.02378](https://arxiv.org/abs/1602.02378) [gr-qc]

- Konoplya R, Rezzolla L, Zhidenko A (2016) General parametrization of axisymmetric black holes in metric theories of gravity. *Phys Rev D* 93(6):064015. <https://doi.org/10.1103/PhysRevD.93.064015>. [arXiv:1602.02378](https://arxiv.org/abs/1602.02378) [gr-qc]
- Konoplya RA, Zhidenko A (2019) Analytical representation for metrics of scalarized Einstein-Maxwell black holes and their shadows. *Phys Rev D* 100(4):044015. <https://doi.org/10.1103/PhysRevD.100.044015>. [arXiv:1907.05551](https://arxiv.org/abs/1907.05551) [gr-qc]
- Konoplya RA, Zinhailo AF (2020) Quasinormal modes, stability and shadows of a black hole in the 4D Einstein–Gauss–Bonnet gravity. *Eur Phys J C* 80(11):1049. <https://doi.org/10.1140/epjc/s10052-020-08639-8>. [arXiv:2003.01188](https://arxiv.org/abs/2003.01188) [gr-qc]
- Konoplya RA, Pappas T, Zhidenko A (2020) Einstein-scalar–Gauss-Bonnet black holes: Analytical approximation for the metric and applications to calculations of shadows. *Phys Rev D* 101(4):044054. <https://doi.org/10.1103/PhysRevD.101.044054>. [arXiv:1907.10112](https://arxiv.org/abs/1907.10112) [gr-qc]
- Koss MJ, Treister E, Kakkad D, Casey-Clyde JA, Kawamuro T, Williams J, Foord A, Trakhtenbrot B, Bauer FE, Privon GC, Ricci C, Mushotzky R, Barcos-Munoz L, Blecha L, Connor T, Harrison F, Liu T, Magno M, Mingarelli CMF, Muller-Sanchez F, Oh K, Shimizu TT, Smith KL, Stern D, Tello MP, Urry CM (2023) Ugc 4211: A confirmed dual active galactic nucleus in the local universe at 230 pc nuclear separation. *The Astrophysical Journal Letters* 942(1):L24. <https://doi.org/10.3847/2041-8213/aca8f0>, URL <https://dx.doi.org/10.3847/2041-8213/aca8f0>
- Kovalev YY, Plavin AV, Pushkarev AB, Troitsky SV (2023) Probing neutrino production in blazars by millimeter VLBI. *Galaxies* 11:84. <https://doi.org/10.3390/galaxies11040084>. [arXiv:2307.02267](https://arxiv.org/abs/2307.02267) [astro-ph.HE]
- Kozai Y (1962) Secular perturbations of asteroids with high inclination and eccentricity. *The Astronomical Journal* 67:591–598. <https://doi.org/10.1086/108790>
- Kramer M, Backer DC, Cordes JM, Lazio TJW, Stappers BW, Johnston S (2004) Strong-field tests of gravity using pulsars and black holes. *New Astron Rev* 48:993–1002. <https://doi.org/10.1016/j.newar.2004.09.020>. [arXiv:astro-ph/0409379](https://arxiv.org/abs/astro-ph/0409379)
- Kulier A, Ostriker JP, Natarajan P, Lackner CN, Cen R (2015) Understanding Black Hole Mass Assembly via Accretion and Mergers at Late Times in Cosmological Simulations. *Astrophys. J.* 799(2):178. <https://doi.org/10.1088/0004-637X/799/2/178>. [arXiv:1307.3684](https://arxiv.org/abs/1307.3684) [astro-ph.CO]
- Kumar R, Ghosh SG (2020) Rotating black holes in 4D Einstein-Gauss-Bonnet gravity and its shadow. *JCAP* 07:053. <https://doi.org/10.1088/1475-7516/2020/07/053>. [arXiv:2003.08927](https://arxiv.org/abs/2003.08927) [gr-qc]
- Kumar R, Ghosh SG (2021) Photon ring structure of rotating regular black holes and no-horizon spacetimes. *Class Quant Grav* 38(8):8. <https://doi.org/10.1088/1361-6382/abdd48>. [arXiv:2004.07501](https://arxiv.org/abs/2004.07501) [gr-qc]
- Kumar R, Ghosh SG, Wang A (2019) Shadow cast and deflection of light by charged rotating regular black holes. *Phys Rev D* 100(12):124024. <https://doi.org/10.1103/PhysRevD.100.124024>. [arXiv:1912.05154](https://arxiv.org/abs/1912.05154) [gr-qc]
- Kumar R, Islam SU, Ghosh SG (2020a) Gravitational lensing by charged black hole in regularized 4D Einstein–Gauss–Bonnet gravity. *Eur Phys J C* 80(12):1128. <https://doi.org/10.1140/epjc/s10052-020-08606-3>. [arXiv:2004.12970](https://arxiv.org/abs/2004.12970) [gr-qc]
- Kumar R, Kumar A, Ghosh SG (2020b) Testing Rotating Regular Metrics as Candidates for Astrophysical Black Holes. *Astrophys J* 896(1):89. <https://doi.org/10.3847/1538-4357/ab8c4a>. [arXiv:2006.09869](https://arxiv.org/abs/2006.09869) [gr-qc]
- Kumar R, Singh BP, Ghosh SG (2020c) Shadow and deflection angle of rotating black hole in asymptotically safe gravity. *Annals Phys* 420:168252. <https://doi.org/10.1016/j.aip.2020.168252>

- 1016/j.aop.2020.168252. arXiv:1904.07652 [gr-qc]
- Kuo CY, et al. (2014) Measuring Mass Accretion Rate onto the Supermassive Black Hole in M87 Using Faraday Rotation Measure with the Submillimeter Array. *Astrophys J Lett* 783:L33. <https://doi.org/10.1088/2041-8205/783/2/L33>. arXiv:1402.5238 [astro-ph.GA]
- Lacroix T (2018) Dynamical constraints on a dark matter spike at the Galactic Centre from stellar orbits. *Astron Astrophys* 619:A46. <https://doi.org/10.1051/0004-6361/201832652>. arXiv:1801.01308 [astro-ph.GA]
- Lalakos A, Gottlieb O, Kaaz N, Chatterjee K, Liska M, Christie IM, Tchekhovskoy A, Zhuravleva I, Nokhrina E (2022) Bridging the Bondi and Event Horizon Scales: 3D GRMHD Simulations Reveal X-shaped Radio Galaxy Morphology. *The Astrophysical Journal Letters* 936(1):L5. <https://doi.org/10.3847/2041-8213/AC7BED>, URL <https://iopscience.iop.org/article/10.3847/2041-8213/ac7bed>, arXiv: 2202.08281 Publisher: IOP Publishing
- Lang RN, Hughes SA (2008) Localizing coalescing massive black hole binaries with gravitational waves. *The Astrophysical Journal* 677(2):1184–1200. <https://doi.org/10.1086/528953>, URL <https://doi.org/10.1086/528953>
- Lee D, Gammie CF (2021) Disks as Inhomogeneous, Anisotropic Gaussian Random Fields. *Astrophys J* 906(1):39. <https://doi.org/10.3847/1538-4357/abc8f3>. arXiv:2011.07151 [astro-ph.IM]
- Lehto HJ, Valtonen MJ (1996) OJ 287 Outburst Structure and a Binary Black Hole Model. *Astrophys. J.*460:207. <https://doi.org/10.1086/176962>
- Lense J, Thirring H (1918) Über den Einfluß der Eigenrotation der Zentralkörper auf die Bewegung der Planeten und Monde nach der Einsteinschen Gravitationstheorie. *Physikalische Zeitschrift* 19:156
- Levis A, Srinivasan PP, Chael AA, Ng R, Bouman KL (2022) Gravitationally lensed black hole emission tomography. arXiv <https://doi.org/10.48550/ARXIV.2204.03715>, URL <https://arxiv.org/abs/2204.03715>
- Li PC, Guo M, Chen B (2020) Shadow of a Spinning Black Hole in an Expanding Universe. *Phys Rev D* 101(8):084041. <https://doi.org/10.1103/PhysRevD.101.084041>. arXiv:2001.04231 [gr-qc]
- Li YD, Modesto L, Rachwał L (2015) Exact solutions and spacetime singularities in nonlocal gravity. *JHEP* 12:173. [https://doi.org/10.1007/JHEP12\(2015\)173](https://doi.org/10.1007/JHEP12(2015)173). arXiv:1506.08619 [hep-th]
- Liberati S, Mattingly D (2016) Lorentz breaking effective field theory models for matter and gravity: theory and observational constraints, Springer, pp 367–417. https://doi.org/10.1007/978-3-319-20224-2_11. arXiv:1208.1071 [gr-qc]
- Lico R, Casadio C, Jorstad SG, Gómez JL, Marscher AP, Traianou E, Kim JY, Zhao GY, Fuentes A, Cho I, Krichbaum TP, Hervet O, O'Brien S, Boccardi B, Myserlis I, Agudo I, Alberdi A, Weaver ZR, Zensus JA (2022) New jet feature in the parsec-scale jet of the blazar OJ 287 connected to the 2017 teraelectronvolt flaring activity. *Astron. Astrophys.*658:L10. <https://doi.org/10.1051/0004-6361/202142948>. arXiv:2202.02523 [astro-ph.HE]
- Lidov ML (1962) The evolution of orbits of artificial satellites of planets under the action of gravitational perturbations of external bodies. *Planetary and Space Science* 9(10):719–759. [https://doi.org/10.1016/0032-0633\(62\)90129-0](https://doi.org/10.1016/0032-0633(62)90129-0)
- Liebling SL, Palenzuela C (2023) Dynamical Boson Stars. *Living Rev Rel* 26:1. <https://doi.org/10.1007/s41114-023-00043-4>. arXiv:1202.5809 [gr-qc]

- Lima HCD Junior, Crispino LCB, Cunha PVP, Herdeiro CAR (2021) Can different black holes cast the same shadow? *Phys Rev D* 103(8):084040. <https://doi.org/10.1103/PhysRevD.103.084040>. [arXiv:2102.07034](https://arxiv.org/abs/2102.07034) [gr-qc]
- Linial I, Sari R (2022) Stellar Distributions around a Supermassive Black Hole: Strong-segregation Regime Revisited. *Astrophys J* 940(2):101. <https://doi.org/10.3847/1538-4357/ac9bfd>. [arXiv:2206.14817](https://arxiv.org/abs/2206.14817) [astro-ph.GA]
- Liu C, Zhu T, Wu Q, Jusufi K, Jamil M, Azreg-Ainou M, Wang A (2020) Shadow and quasinormal modes of a rotating loop quantum black hole. *Phys Rev D* 101(8):084001. <https://doi.org/10.1103/PhysRevD.101.084001>, [Erratum: *Phys.Rev.D* 103, 089902 (2021)]. [arXiv:2003.00477](https://arxiv.org/abs/2003.00477) [gr-qc]
- Liu C, Zhu T, Wu Q (2021) Thin Accretion Disk around a four-dimensional Einstein-Gauss-Bonnet Black Hole. *Chin Phys C* 45(1):015105. <https://doi.org/10.1088/1674-1137/abc16c>. [arXiv:2004.01662](https://arxiv.org/abs/2004.01662) [gr-qc]
- Liu K, Wex N, Kramer M, Cordes JM, Lazio TJW (2012) Prospects for Probing the Spacetime of Sgr A* with Pulsars. *Astrophys J* 747:1. <https://doi.org/10.1088/0004-637X/747/1/1>. [arXiv:1112.2151](https://arxiv.org/abs/1112.2151) [astro-ph.HE]
- Liu X, Hou M, Li Z, Nyland K, Guo H, Kong M, Shen Y, Wrobel JM, Peng S (2019) A Trio of Massive Black Holes Caught in the Act of Merging. *Astrophys. J.* 887(1):90. <https://doi.org/10.3847/1538-4357/ab54c3>. [arXiv:1907.10639](https://arxiv.org/abs/1907.10639) [astro-ph.GA]
- Liu X, Chen S, Jing J (2022) Polarization distribution in the image of a synchrotron emitting ring around a regular black hole. *Science China Physics, Mechanics, and Astronomy* 65(12):120411. <https://doi.org/10.1007/s11433-022-1946-2>. [arXiv:2205.00391](https://arxiv.org/abs/2205.00391) [gr-qc]
- Lockhart W, Gralla SE (2022) How narrow is the M87* ring - II. A new geometric model. *Mon. Not. R. Astron. Soc.* 517(2):2462–2470. <https://doi.org/10.1093/mnras/stac2743>. [arXiv:2208.09989](https://arxiv.org/abs/2208.09989) [astro-ph.HE]
- Loll R (2020) Quantum Gravity from Causal Dynamical Triangulations: A Review. *Class Quant Grav* 37(1):013002. <https://doi.org/10.1088/1361-6382/ab57c7>. [arXiv:1905.08669](https://arxiv.org/abs/1905.08669) [hep-th]
- Long F, Wang J, Chen S, Jing J (2019) Shadow of a rotating squashed Kaluza-Klein black hole. *JHEP* 10:269. [https://doi.org/10.1007/JHEP10\(2019\)269](https://doi.org/10.1007/JHEP10(2019)269). [arXiv:1906.04456](https://arxiv.org/abs/1906.04456) [gr-qc]
- Lovelock D (1971) The Einstein tensor and its generalizations. *J Math Phys* 12:498–501. <https://doi.org/10.1063/1.1665613>
- Lu H, Perkins A, Pope CN, Stelle KS (2015) Black Holes in Higher-Derivative Gravity. *Phys Rev Lett* 114(17):171601. <https://doi.org/10.1103/PhysRevLett.114.171601>. [arXiv:1502.01028](https://arxiv.org/abs/1502.01028) [hep-th]
- Lu JR, Ghez AM, Hornstein SD, Morris MR, Becklin EE, Matthews K (2009) A Disk of Young Stars at the Galactic Center as Determined by Individual Stellar Orbits. *Astrophys J* 690:1463–1487. <https://doi.org/10.1088/0004-637X/690/2/1463>. [arXiv:0808.3818](https://arxiv.org/abs/0808.3818) [astro-ph]
- Lu W, Kumar P, Narayan R (2017) Stellar disruption events support the existence of the black hole event horizon. *Mon Not Roy Astron Soc* 468(1):910–919. <https://doi.org/10.1093/mnras/stx542>. [arXiv:1703.00023](https://arxiv.org/abs/1703.00023) [astro-ph.HE]
- Luminet JP (1979) Image of a spherical black hole with thin accretion disk. *Astron. Astrophys.* 75:228–235
- Luo J, et al (2016) TianQin: a space-borne gravitational wave detector. *Classical and Quantum Gravity* 33(3):035010. <https://doi.org/10.1088/0264-9381/33/3/035010>, URL <https://doi.org/10.1088/0264-9381/33/3/035010>

- Ly C, Walker RC, Junor W (2007) High-Frequency VLBI Imaging of the Jet Base of M87. *Astrophys. J.*660(1):200–205. <https://doi.org/10.1086/512846>. [arXiv:astro-ph/0701511](https://arxiv.org/abs/astro-ph/0701511) [astro-ph]
- Mangiagli A, Klein A, Bonetti M, Katz ML, Sesana A, Volonteri M, Colpi M, Marsat S, Babak S (2020) On the inspiral of coalescing massive black hole binaries with LISA in the era of Multi-Messenger Astrophysics. *Phys Rev D* 102:084056. <https://doi.org/10.1103/PhysRevD.102.084056>. [arXiv:2006.12513](https://arxiv.org/abs/2006.12513) [astro-ph.HE]
- Marolf D, Michel B, Puhm A (2017) A rough end for smooth microstate geometries. *JHEP* 05:021. [https://doi.org/10.1007/JHEP05\(2017\)021](https://doi.org/10.1007/JHEP05(2017)021). [arXiv:1612.05235](https://arxiv.org/abs/1612.05235) [hep-th]
- Marsh DJE (2016) Axion Cosmology. *Phys Rept* 643:1–79. <https://doi.org/10.1016/j.physrep.2016.06.005>. [arXiv:1510.07633](https://arxiv.org/abs/1510.07633) [astro-ph.CO]
- Mathur SD (2005) The Fuzzball proposal for black holes: An Elementary review. *Fortsch Phys* 53:793–827. <https://doi.org/10.1002/prop.200410203>. [arXiv:hep-th/0502050](https://arxiv.org/abs/hep-th/0502050)
- Matsumoto T, Chan CH, Piran T (2020) The origin of hotspots around Sgr A*: orbital or pattern motion? *Mon. Not. R. Astron. Soc.*497(2):2385–2392. <https://doi.org/10.1093/mnras/staa2095>. [arXiv:2004.13029](https://arxiv.org/abs/2004.13029) [astro-ph.HE]
- Mayer L, Kazantzidis S, Madau P, Colpi M, Quinn TR, Wadsley J (2007) Rapid Formation of Supermassive Black Hole Binaries in Galaxy Mergers with Gas. *Science* 316:1874–1877. <https://doi.org/10.1126/science.1141858>. [arXiv:0706.1562](https://arxiv.org/abs/0706.1562) [astro-ph]
- Mayerson DR (2020) Fuzzballs and Observations. *Gen Rel Grav* 52(12):115. <https://doi.org/10.1007/s10714-020-02769-w>. [arXiv:2010.09736](https://arxiv.org/abs/2010.09736) [hep-th]
- Mazur PO, Mottola E (2001) Gravitational condensate stars: An alternative to black holes. *arXiv e-prints* [arXiv:gr-qc/0109035](https://arxiv.org/abs/gr-qc/0109035)
- Mazur PO, Mottola E (2004) Gravitational vacuum condensate stars. *Proc Natl Acad Sci* 101:9545–9550. <https://doi.org/10.1073/pnas.0402717101>. [arXiv:gr-qc/0407075](https://arxiv.org/abs/gr-qc/0407075)
- Mazza J, Franzin E, Liberati S (2021) A novel family of rotating black hole mimickers. *JCAP* 04:082. <https://doi.org/10.1088/1475-7516/2021/04/082>. [arXiv:2102.01105](https://arxiv.org/abs/2102.01105) [gr-qc]
- Medeiros L, Psaltis D, Özel F (2020) A Parametric Model for the Shapes of Black Hole Shadows in Non-Kerr Spacetimes. *Astrophys. J.*896(1):7. <https://doi.org/10.3847/1538-4357/ab8bd1>. [arXiv:1907.12575](https://arxiv.org/abs/1907.12575) [astro-ph.HE]
- Meliani Z, Grandclément P, Casse F, Vincent FH, Straub O, Dauvergne F (2016) GR-AMRVAC code applications: accretion onto compact objects, boson stars versus black holes. *Classical and Quantum Gravity* 33(15):155010. <https://doi.org/10.1088/0264-9381/33/15/155010>, URL <http://stacks.iop.org/0264-9381/33/i=15/a=155010?key=crossref.29dc10715e8c2c21f6f281c0c416fe01>, publisher: IOP Publishing
- Meliani Z, Casse F, Grandclément P, Gourgoulhon E, Dauvergne F (2017a) On tidal disruption of clouds and disk formation near boson stars. *Classical and Quantum Gravity* 34(22):225003. <https://doi.org/10.1088/1361-6382/aa8fb5>, URL <http://stacks.iop.org/0264-9381/34/i=22/a=225003?key=crossref.a3b6c61cdc459d2c434c6349a6a707d3>, publisher: IOP Publishing
- Meliani Z, Mizuno Y, Olivares H, Porth O, Rezzolla L, Younsi Z (2017b) Simulations of recoiling black holes: adaptive mesh refinement and radiative transfer. *Astronomy & Astrophysics* 598:A38. <https://doi.org/10.1051/0004-6361/201629191>, URL <http://www.aanda.org/10.1051/0004-6361/201629191>, publisher: EDP Sciences
- Merritt D (2013) Dynamics and Evolution of Galactic Nuclei, vol 23. Princeton University Press. URL <http://www.jstor.org/stable/j.ctv1nxcw93>

- Merritt D, Milosavljević M (2005) Massive Black Hole Binary Evolution. *Living Reviews in Relativity* 8:8. <https://doi.org/10.12942/lrr-2005-8>. [arXiv:astro-ph/0410364](https://arxiv.org/abs/astro-ph/0410364) [astro-ph]
- Merritt D, Alexander T, Mikkola S, Will CM (2010) Testing Properties of the Galactic Center Black Hole Using Stellar Orbits. *Phys Rev D* 81:062002. <https://doi.org/10.1103/PhysRevD.81.062002>. [arXiv:0911.4718](https://arxiv.org/abs/astro-ph.GA/09114718) [astro-ph.GA]
- Mertens F, Lobanov AP, Walker RC, Hardee PE (2016) Kinematics of the jet in M 87 on scales of 100-1000 Schwarzschild radii. *Astron. Astrophys.*595:A54. <https://doi.org/10.1051/0004-6361/201628829>
- Meyer L, Ghez AM, Schödel R, Yelda S, Boehle A, Lu JR, Do T, Morris MR, Becklin EE, Matthews K (2012) The Shortest-Known-Period Star Orbiting Our Galaxy's Supermassive Black Hole. *Science* 338(6103):84. <https://doi.org/10.1126/science.1225506>. [arXiv:1210.1294](https://arxiv.org/abs/1210.1294) [astro-ph.GA]
- Middleton H, Sesana A, Chen S, Vecchio A, Del Pozzo W, Rosado PA (2021) Massive black hole binary systems and the NANOGrav 12.5 yr results. *Mon Not Roy Astron Soc* 502(1):L99–L103. <https://doi.org/10.1093/mnras/502.1/L99>. [arXiv:2011.01246](https://arxiv.org/abs/2011.01246) [astro-ph.HE]
- Milosavljević M, Merritt D (2003) Long-Term Evolution of Massive Black Hole Binaries. *Astrophys. J.*596(2):860–878. <https://doi.org/10.1086/378086>. [arXiv:astro-ph/0212459](https://arxiv.org/abs/astro-ph/0212459) [astro-ph]
- Mingarelli CMF (2019) Probing supermassive black hole binaries with pulsar timing. *Nature Astronomy* 3:8–10. <https://doi.org/10.1038/s41550-018-0666-y>. [arXiv:1901.06785](https://arxiv.org/abs/1901.06785) [gr-qc]
- Miyoshi M, Shen ZQ, Oyama T, Takahashi R, Kato Y (2011) Oscillation Phenomena in the Disk around the Massive Black Hole Sagittarius A*. *Publ. Astron. Soc. Jpn*63:1093–1116. <https://doi.org/10.1093/pasj/63.5.1093>
- Mizuno Y, Younsi Z, Fromm CM, Porth O, De Laurentis M, Olivares H, Falcke H, Kramer M, Rezzolla L (2018a) The Current Ability to Test Theories of Gravity with Black Hole Shadows. *Nature Astron* 2(7):585–590. <https://doi.org/10.1038/s41550-018-0449-5>. [arXiv:1804.05812](https://arxiv.org/abs/1804.05812) [astro-ph.GA]
- Mizuno Y, Younsi Z, Fromm CM, Porth O, De Laurentis M, Olivares H, Falcke H, Kramer M, Rezzolla L (2018b) The current ability to test theories of gravity with black hole shadows. *Nat Astron* 2(7):585–590. <https://doi.org/10.1038/s41550-018-0449-5>, URL <http://www.nature.com/articles/s41550-018-0449-5>
- Modesto L (2004) Disappearance of black hole singularity in quantum gravity. *Phys Rev D* 70:124009. <https://doi.org/10.1103/PhysRevD.70.124009>. [arXiv:gr-qc/0407097](https://arxiv.org/abs/gr-qc/0407097)
- Modesto L (2006) Loop quantum black hole. *Class Quant Grav* 23:5587–5602. <https://doi.org/10.1088/0264-9381/23/18/006>. [arXiv:gr-qc/0509078](https://arxiv.org/abs/gr-qc/0509078)
- Modesto L (2012) Super-renormalizable Quantum Gravity. *Phys Rev D* 86:044005. <https://doi.org/10.1103/PhysRevD.86.044005>. [arXiv:1107.2403](https://arxiv.org/abs/1107.2403) [hep-th]
- Modesto L, Nicolini P (2010) Charged rotating noncommutative black holes. *Phys Rev D* 82:104035. <https://doi.org/10.1103/PhysRevD.82.104035>. [arXiv:1005.5605](https://arxiv.org/abs/1005.5605) [gr-qc]
- Moffat JW (2015) Modified Gravity Black Holes and their Observable Shadows. *Eur Phys J C* 75(3):130. <https://doi.org/10.1140/epjc/s10052-015-3352-6>. [arXiv:1502.01677](https://arxiv.org/abs/1502.01677) [gr-qc]
- Moriyama K, Mineshige S (2015) New method for black-hole spin measurement based on flux variation from an infalling gas ring. *Publ. Astron. Soc. Jpn*67(6):106. <https://doi.org/10.1093/pasj/psv074>. [arXiv:1508.03334](https://arxiv.org/abs/1508.03334) [astro-ph.HE]

- Moriyama K, Mineshige S, Honma M, Akiyama K (2019) Black Hole Spin Measurement Based on Time-domain VLBI Observations of Infalling Gas Clouds. *Astrophys. J.*887(2):227. <https://doi.org/10.3847/1538-4357/ab505b>. [arXiv:1910.10713](https://arxiv.org/abs/1910.10713) [astro-ph.HE]
- Morris MS, Thorne KS (1988) Wormholes in space-time and their use for interstellar travel: A tool for teaching general relativity. *Am J Phys* 56:395–412. <https://doi.org/10.1119/1.15620>
- Mościbrodzka M, Gammie CF (2018) IPOLE - semi-analytic scheme for relativistic polarized radiative transport. *Mon. Not. R. Astron. Soc.*475:43–54. <https://doi.org/10.1093/mnras/stx3162>. [arXiv:1712.03057](https://arxiv.org/abs/1712.03057) [astro-ph.HE]
- Mościbrodzka M, Falcke H, Shikawa H (2016) General relativistic magnetohydrodynamical simulations of the jet in M 87. *Astron. Astrophys.*586:A38. <https://doi.org/10.1051/0004-6361/201526630>. [arXiv:1510.07243](https://arxiv.org/abs/1510.07243) [astro-ph.HE]
- Mościbrodzka M, Janiuk A, De Laurentis M (2021) Unraveling circular polarimetric images of magnetically arrested accretion flows near event horizon of a black hole. *Mon. Not. R. Astron. Soc.*508(3):4282–4296. <https://doi.org/10.1093/mnras/stab2790>. [arXiv:2103.00267](https://arxiv.org/abs/2103.00267) [astro-ph.HE]
- Motohashi H, Minamitsuji M (2019) Exact black hole solutions in shift-symmetric quadratic degenerate higher-order scalar-tensor theories. *Phys Rev D* 99(6):064040. <https://doi.org/10.1103/PhysRevD.99.064040>. [arXiv:1901.04658](https://arxiv.org/abs/1901.04658) [gr-qc]
- Murphy MT, Flambaum VV, Muller S, Henkel C (2008) Strong Limit on a Variable Proton-to-Electron Mass Ratio from Molecules in the Distant Universe. *Science* 320:1611–1613. <https://doi.org/10.1126/science.1156352>. [arXiv:0806.3081](https://arxiv.org/abs/0806.3081) [astro-ph]
- Nampalliwar S, K S (2021) Theory-agnostic tests of gravity with black hole shadows. *arXiv e-prints* [arXiv:2108.01190](https://arxiv.org/abs/2108.01190). <https://doi.org/10.48550/arXiv.2108.01190>. [arXiv:2108.01190](https://arxiv.org/abs/2108.01190) [gr-qc]
- Nampalliwar S, Yfantis AI, Kokkotas KD (2022a) Extending GRMHD for thin disks to non-Kerr spacetimes. *Phys Rev D* 106(6):063009. <https://doi.org/10.1103/PhysRevD.106.063009>
- Nampalliwar S, Yfantis AI, Kokkotas KD (2022b) Extending GRMHD for thin disks to non-Kerr spacetimes. *Phys Rev D* 106(6):063009. <https://doi.org/10.1103/PhysRevD.106.063009>, URL <https://journals.aps.org/prd/abstract/10.1103/PhysRevD.106.063009>
- Naoz S (2016) The Eccentric Kozai-Lidov Effect and Its Applications. *Annu. Rev. Astron. Astrophys.*54:441–489. <https://doi.org/10.1146/annurev-astro-081915-023315>. [arXiv:1601.07175](https://arxiv.org/abs/1601.07175) [astro-ph.EP]
- Naoz S, Will CM, Ramirez-Ruiz E, Hees A, Ghez AM, Do T (2020) A hidden friend for the galactic center black hole, Sgr A*. *Astrophys J Lett* 888(1):L8. <https://doi.org/10.3847/2041-8213/ab5e3b>. [arXiv:1912.04910](https://arxiv.org/abs/1912.04910) [astro-ph.GA]
- Narayan R, McClintock JE (2008) Advection-Dominated Accretion and the Black Hole Event Horizon. *New Astron Rev* 51:733–751. <https://doi.org/10.1016/j.newar.2008.03.002>. [arXiv:0803.0322](https://arxiv.org/abs/0803.0322) [astro-ph]
- Narayan R, Igumenshchev IV, Abramowicz MA (2003) Magnetically Arrested Disk: an Energetically Efficient Accretion Flow. *Publ. Astron. Soc. Jpn*55:L69–L72. <https://doi.org/10.1093/pasj/55.6.L69>. [arXiv:astro-ph/0305029](https://arxiv.org/abs/astro-ph/0305029) [astro-ph]
- Narayan R, Sądowski A, Penna RF, Kulkarni AK (2012) GRMHD simulations of magnetized advection-dominated accretion on a non-spinning black hole: role of outflows. *Mon. Not. R. Astron. Soc.*426(4):3241–3259. <https://doi.org/10.1111/j.1365-2966.2012.22002.x>. [arXiv:1206.1213](https://arxiv.org/abs/1206.1213) [astro-ph.HE]

- Narayan R, Palumbo DCM, Johnson MD, Gelles Z, et al (2021) The Polarized Image of a Synchrotron-emitting Ring of Gas Orbiting a Black Hole. *Astrophys. J.*912(1):35. <https://doi.org/10.3847/1538-4357/abf117>. [arXiv:2105.01804](https://arxiv.org/abs/2105.01804) [astro-ph.HE]
- Neilsen J, Nowak MA, Gammie C, Dexter J, Markoff S, Haggard D, Nayakshin S, Wang QD, Grosso N, Porquet D, Tomsick JA, Degenaar N, Fragile PC, Houck JC, Wijnands R, Miller JM, Baganoff FK (2013) A Chandra/HETGS Census of X-Ray Variability from Sgr A* during 2012. *Astrophys. J.*774(1):42. <https://doi.org/10.1088/0004-637X/774/1/42>. [arXiv:1307.5843](https://arxiv.org/abs/1307.5843) [astro-ph.HE]
- Neves JCS, Saa A (2014) Regular rotating black holes and the weak energy condition. *Phys Lett B* 734:44–48. <https://doi.org/10.1016/j.physletb.2014.05.026>. [arXiv:1402.2694](https://arxiv.org/abs/1402.2694) [gr-qc]
- Newman ET, Janis AI (1965) Note on the Kerr spinning particle metric. *J Math Phys* 6:915–917. <https://doi.org/10.1063/1.1704350>
- Newman ET, Couch R, Chinnapared K, Exton A, Prakash A, Torrence R (1965) Metric of a Rotating, Charged Mass. *J Math Phys* 6:918–919. <https://doi.org/10.1063/1.1704351>
- Ng KKY, Hannuksela OA, Vitale S, Li TGF (2021) Searching for ultralight bosons within spin measurements of a population of binary black hole mergers. *Phys Rev D* 103(6):063010. <https://doi.org/10.1103/PhysRevD.103.063010>. [arXiv:1908.02312](https://arxiv.org/abs/1908.02312) [gr-qc]
- Nguyen B, Christian P, Chan Ck (2023) Shadow Geometry of Kerr Naked Singularities. *Astrophys. J.*954(1):78. <https://doi.org/10.3847/1538-4357/ace697>. [arXiv:2302.08094](https://arxiv.org/abs/2302.08094) [astro-ph.HE]
- Nicolini P (2009) Noncommutative Black Holes, The Final Appeal To Quantum Gravity: A Review. *Int J Mod Phys A* 24:1229–1308. <https://doi.org/10.1142/S0217751X09043353>. [arXiv:0807.1939](https://arxiv.org/abs/0807.1939) [hep-th]
- Noble SC, Krolik JH, Campanelli M, Zlochower Y, Mundim BC, Nakano H, Zilhão M (2021) Mass-ratio and Magnetic Flux Dependence of Modulated Accretion from Circumbinary Disks. *The Astrophysical Journal* 922(2):175. <https://doi.org/10.3847/1538-4357/ac2229>, URL <https://dx.doi.org/10.3847/1538-4357/ac2229>, publisher: The American Astronomical Society
- Ohgami T, Sakai N (2015) Wormhole shadows. *Phys Rev D* 91(12):124020. <https://doi.org/10.1103/PhysRevD.91.124020>. [arXiv:1704.07065](https://arxiv.org/abs/1704.07065) [gr-qc]
- Ohgami T, Sakai N (2016) Wormhole shadows in rotating dust. *Phys Rev D* 94(6):064071. <https://doi.org/10.1103/PhysRevD.94.064071>. [arXiv:1704.07093](https://arxiv.org/abs/1704.07093) [gr-qc]
- Okounkova M, Scheel MA, Teukolsky SA (2019) Numerical black hole initial data and shadows in dynamical Chern-Simons gravity. *Class Quant Grav* 36(5):054001. <https://doi.org/10.1088/1361-6382/aafcdf>. [arXiv:1810.05306](https://arxiv.org/abs/1810.05306) [gr-qc]
- Olivares H, Younsi Z, Fromm CM, De Laurentis M, Porth O, Mizuno Y, Faleke H, Kramer M, Rezzolla L (2020) How to tell an accreting boson star from a black hole. *Mon Not Roy Astron Soc* 497(1):521–535. <https://doi.org/10.1093/mnras/staa1878>. [arXiv:1809.08682](https://arxiv.org/abs/1809.08682) [gr-qc]
- Olivares H, Gold R, Tootle S (2023, in prep.) In preparation.
- Omiya H, Takahashi T, Tanaka T, Yoshino H (2023) Impact of multiple modes on the evolution of self-interacting axion condensate around rotating black holes. *J. Cosmol. Astropart. Phys.*2023(6):016. <https://doi.org/10.1088/1475-7516/2023/06/016>. [arXiv:2211.01949](https://arxiv.org/abs/2211.01949) [gr-qc]

- O'Neill S, Kiehlmann S, Readhead ACS, Aller MF, Blandford RD, Liidakis I, Lister ML, Mróz P, O'Dea CP, Pearson TJ, Ravi V, Vallisneri M, Cleary KA, Graham MJ, Grainge KJB, Hodges MW, Hovatta T, Lähteenmäki A, Lamb JW, Lazio TJW, Max-Moerbeck W, Pavlidou V, Prince TA, Reeves RA, Tornikoski M, Vergara de la Parra P, Zensus JA (2022) The Unanticipated Phenomenology of the Blazar PKS 2131-021: A Unique Supermassive Black Hole Binary Candidate. *Astrophys. J. Lett.* 926(2):L35. <https://doi.org/10.3847/2041-8213/ac504b>. [arXiv:2111.02436](https://arxiv.org/abs/2111.02436) [astro-ph.HE]
- Ottewill AC, Winstanley E (2000) The Renormalized stress tensor in Kerr spacetime: general results. *Phys Rev D* 62:084018. <https://doi.org/10.1103/PhysRevD.62.084018>. [arXiv:gr-qc/0004022](https://arxiv.org/abs/gr-qc/0004022)
- Owen CB, Yunes N, Witek H (2021) Petrov type, principal null directions, and Killing tensors of slowly rotating black holes in quadratic gravity. *Phys Rev D* 103(12):124057. <https://doi.org/10.1103/PhysRevD.103.124057>. [arXiv:2103.15891](https://arxiv.org/abs/2103.15891) [gr-qc]
- Özel F, Psaltis D, Younsi Z (2022) Black Hole Images as Tests of General Relativity: Effects of Plasma Physics. *Astrophys. J.* 941(1):88. <https://doi.org/10.3847/1538-4357/ac9fcb>. [arXiv:2111.01123](https://arxiv.org/abs/2111.01123) [astro-ph.HE]
- Pacucci F, Loeb A (2020) Separating accretion and mergers in the cosmic growth of black holes with x-ray and gravitational-wave observations. *The Astrophysical Journal* 895(2):95. <https://doi.org/10.3847/1538-4357/ab886e>, URL <https://dx.doi.org/10.3847/1538-4357/ab886e>
- Palumbo DCM, Wong GN (2022) Photon Ring Symmetries in Simulated Linear Polarization Images of Messier 87*. *Astrophys. J.* 929(1):49. <https://doi.org/10.3847/1538-4357/ac59b4>. [arXiv:2203.00844](https://arxiv.org/abs/2203.00844) [astro-ph.HE]
- Palumbo DCM, Wong GN, Prather BS (2020) Discriminating Accretion States via Rotational Symmetry in Simulated Polarimetric Images of M87. *Astrophys. J.* 894(2):156. <https://doi.org/10.3847/1538-4357/ab86ac>. [arXiv:2004.01751](https://arxiv.org/abs/2004.01751) [astro-ph.HE]
- Palumbo DCM, Gelles Z, Tiede P, Chang DO, Pesce DW, Chael A, Johnson MD (2022) Bayesian Accretion Modeling: Axisymmetric Equatorial Emission in the Kerr Spacetime. *Astrophys. J.* 939(2):107. <https://doi.org/10.3847/1538-4357/ac9ab7>. [arXiv:2210.07108](https://arxiv.org/abs/2210.07108) [astro-ph.HE]
- Palumbo DCM, Wong GN, Chael A, Johnson MD (2023) Demonstrating Photon Ring Existence with Single-baseline Polarimetry. *Astrophys. J. Lett.* 952(2):L31. <https://doi.org/10.3847/2041-8213/ace630>. [arXiv:2307.05293](https://arxiv.org/abs/2307.05293) [astro-ph.HE]
- Palumbo DCM, Wong GN, Chael AA, Johnson MD (2023) Demonstrating Photon Ring Existence with Single-baseline Polarimetry. *Astrophys J Lett* 952(2):L31. <https://doi.org/10.3847/2041-8213/ace630>. [arXiv:2307.05293](https://arxiv.org/abs/2307.05293) [astro-ph.HE]
- Pan Z, Yang H (2021a) Formation Rate of Extreme Mass Ratio Inspirals in Active Galactic Nuclei. *Phys Rev D* 103(10):103018. <https://doi.org/10.1103/PhysRevD.103.103018>. [arXiv:2101.09146](https://arxiv.org/abs/2101.09146) [astro-ph.HE]
- Pan Z, Yang H (2021b) Supercritical Accretion of Stellar-mass Compact Objects in Active Galactic Nuclei. *Astrophys J* 923(2):173. <https://doi.org/10.3847/1538-4357/ac249c>. [arXiv:2108.00267](https://arxiv.org/abs/2108.00267) [astro-ph.HE]
- Pan Z, Lyu Z, Yang H (2022) Mass-gap extreme mass ratio inspirals. *Phys Rev D* 105(8):083005. <https://doi.org/10.1103/PhysRevD.105.083005>. [arXiv:2112.10237](https://arxiv.org/abs/2112.10237) [astro-ph.HE]
- Pani P (2015) I-Love-Q relations for gravastars and the approach to the black-hole limit. *Phys Rev D* 92(12):124030. <https://doi.org/10.1103/PhysRevD.92.124030>, [Erra-

- tum: Phys.Rev.D 95, 049902 (2017)]. [arXiv:1506.06050](https://arxiv.org/abs/1506.06050) [gr-qc]
- Pani P, Cardoso V, Gualtieri L, Berti E, Ishibashi A (2012) Perturbations of slowly rotating black holes: massive vector fields in the Kerr metric. Phys Rev D 86:104017. <https://doi.org/10.1103/PhysRevD.86.104017>. [arXiv:1209.0773](https://arxiv.org/abs/1209.0773) [gr-qc]
- Pani P, Sotiriou TP, Vernieri D (2013) Gravity with auxiliary fields. Phys. Rev. D88(12):121502. <https://doi.org/10.1103/PhysRevD.88.121502>. [arXiv:1306.1835](https://arxiv.org/abs/1306.1835) [gr-qc]
- Papapetrou A (1966) Champs gravitationnels stationnaires a symetrie axiale. Ann Inst H Poincare Phys Theor 4:83–105
- Papnoi U, Atamurotov F, Ghosh SG, Ahmedov B (2014) Shadow of five-dimensional rotating Myers-Perry black hole. Phys Rev D 90(2):024073. <https://doi.org/10.1103/PhysRevD.90.024073>. [arXiv:1407.0834](https://arxiv.org/abs/1407.0834) [gr-qc]
- Parfrey K, Tchekhovskoy A (2017) General-relativistic Simulations of Four States of Accretion onto Millisecond Pulsars. The Astrophysical Journal Letters 851(2):L34. <https://doi.org/10.3847/2041-8213/aa9c85>, URL <https://dx.doi.org/10.3847/2041-8213/aa9c85>, publisher: The American Astronomical Society
- Paschalidis V, Bright J, Ruiz M, Gold R (2021) Minidisk Dynamics in Accreting, Spinning Black Hole Binaries: Simulations in Full General Relativity. Astrophys. J. Lett.910(2):L26. <https://doi.org/10.3847/2041-8213/abee21>. [arXiv:2102.06712](https://arxiv.org/abs/2102.06712) [astro-ph.HE]
- Paul S, Shaikh R, Banerjee P, Sarkar T (2020) Observational signatures of wormholes with thin accretion disks. JCAP 03:055. <https://doi.org/10.1088/1475-7516/2020/03/055>. [arXiv:1911.05525](https://arxiv.org/abs/1911.05525) [gr-qc]
- Paumard T, et al. (2006) The two young star disks in the central parsec of the galaxy: properties, dynamics and formation. Astrophys J 643:1011–1035. <https://doi.org/10.1086/503273>. [arXiv:astro-ph/0601268](https://arxiv.org/abs/astro-ph/0601268)
- Peccei RD, Quinn HR (1977a) Constraints Imposed by CP Conservation in the Presence of Instantons. Phys Rev D 16:1791–1797. <https://doi.org/10.1103/PhysRevD.16.1791>
- Peccei RD, Quinn HR (1977b) CP Conservation in the Presence of Instantons. Phys Rev Lett 38:1440–1443. <https://doi.org/10.1103/PhysRevLett.38.1440>
- Peng J, Guo M, Feng XH (2021) Observational signature and additional photon rings of an asymmetric thin-shell wormhole. Phys Rev D 104(12):124010. <https://doi.org/10.1103/PhysRevD.104.124010>. [arXiv:2102.05488](https://arxiv.org/abs/2102.05488) [gr-qc]
- Penrose R (1965) Gravitational collapse and space-time singularities. Phys Rev Lett 14:57–59. <https://doi.org/10.1103/PhysRevLett.14.57>
- Penrose R (1969) Gravitational collapse: The role of general relativity. Riv Nuovo Cim 1:252–276. <https://doi.org/10.1023/A:1016578408204>
- Penrose R (1972) Techniques of differential topology in relativity. In: CBMS-NSF Regional Conference Series in Applied Mathematics, Vol. 7. Society for Industrial & Applied Mathematics, Philadelphia
- Penrose R, Floyd RM (1971) Extraction of rotational energy from a black hole. Nature 229:177–179. <https://doi.org/10.1038/physci229177a0>
- Perlick V (2004) Gravitational Lensing from a Spacetime Perspective. Living Rev Relativ 7(9). <https://doi.org/10.12942/lrr-2004-9>
- Perlick V, Tsupko OY (2022) Calculating black hole shadows: Review of analytical studies. Phys Rept 947:1–39. <https://doi.org/10.1016/j.physrep.2021.10.004>. [arXiv:2105.07101](https://arxiv.org/abs/2105.07101) [gr-qc]

- Pesce DW (2021) A D-term Modeling Code (DMC) for Simultaneous Calibration and Full-Stokes Imaging of Very Long Baseline Interferometric Data. *The Astronomical Journal* 161(4):178. <https://doi.org/10.3847/1538-3881/abe3f8>. [arXiv:2102.03328](https://arxiv.org/abs/2102.03328) [astro-ph.IM]
- Pfeifle RW, Satyapal S, Manzano-King C, Cann J, Sexton RO, Rothberg B, Canalizo G, Ricci C, Blecha L, Ellison SL, Gliozzi M, Secret NJ, Constantin A, Harvey JB (2019) A Triple AGN in a Mid-infrared Selected Late-stage Galaxy Merger. *Astrophys. J.* 883(2):167. <https://doi.org/10.3847/1538-4357/ab3a9b>. [arXiv:1908.01732](https://arxiv.org/abs/1908.01732) [astro-ph.GA]
- Piro L, Ahlers M, Coleiro A, Colpi M, de Oña Wilhelmi E, Guainazzi M, Jonker PG, Namara PM, Nichols DA, O'Brien P, Troja E, Vink J, Aird J, Amati L, Anand S, Bozzo E, Carrera FJ, Fabian AC, Fryer C, Hall E, Korobkin O, Korol V, Mangiagli A, Martínez-Núñez S, Nissanke S, Osborne J, Padovani P, Rossi EM, Ryan G, Sesana A, Stratta G, Tanvir N, van Eerten H (2022) Athena synergies in the multi-messenger and transient universe. *Experimental Astronomy* 54(1):23–117. <https://doi.org/10.1007/s10686-022-09865-6>. [arXiv:2110.15677](https://arxiv.org/abs/2110.15677) [astro-ph.HE]
- Platania A (2019) Dynamical renormalization of black-hole spacetimes. *Eur Phys J C* 79(6):470. <https://doi.org/10.1140/epjc/s10052-019-6990-2>. [arXiv:1903.10411](https://arxiv.org/abs/1903.10411) [gr-qc]
- Podolský J, Švarc R, Pravda V, Pravdova A (2020) Black holes and other exact spherical solutions in Quadratic Gravity. *Phys Rev D* 101(2):024027. <https://doi.org/10.1103/PhysRevD.101.024027>. [arXiv:1907.00046](https://arxiv.org/abs/1907.00046) [gr-qc]
- Podurets MA (1965) Asymptotic Behavior of the Optical Luminosity of a Star in Gravitational Collapse. *Soviet Ast* 8:868
- Ponti G, et al. (2017) A powerful flare from Sgr A* confirms the synchrotron nature of the X-ray emission. *Mon Not Roy Astron Soc* 468(2):2447–2468. <https://doi.org/10.1093/mnras/stx596>. [arXiv:1703.03410](https://arxiv.org/abs/1703.03410) [astro-ph.HE]
- Porth O, et al. (2019) The Event Horizon General Relativistic Magnetohydrodynamic Code Comparison Project. *Astrophys J Suppl* 243(2):26. <https://doi.org/10.3847/1538-4365/ab29fd>. [arXiv:1904.04923](https://arxiv.org/abs/1904.04923) [astro-ph.HE]
- Pozo A, Broadhurst T, De Martino I, Luu HN, Smoot GF, Lim J, Neyrinck M (2021) Wave dark matter and ultra-diffuse galaxies. *Mon Not Roy Astron Soc* 504(2):2868–2876. <https://doi.org/10.1093/mnras/stab855>. [arXiv:2003.08313](https://arxiv.org/abs/2003.08313) [astro-ph.GA]
- Preskill J, Wise MB, Wilczek F (1983) Cosmology of the Invisible Axion. *Phys Lett B* 120:127–132. [https://doi.org/10.1016/0370-2693\(83\)90637-8](https://doi.org/10.1016/0370-2693(83)90637-8)
- Psaltis D, Perrodin D, Dienes KR, Mocioiu I (2008) Kerr Black Holes are Not Unique to General Relativity. *Phys Rev Lett* 100:091101. <https://doi.org/10.1103/PhysRevLett.100.091101>. [arXiv:0710.4564](https://arxiv.org/abs/0710.4564) [astro-ph]
- Psaltis D, Wex N, Kramer M (2016) A Quantitative Test of the No-Hair Theorem with Sgr A* using stars, pulsars, and the Event Horizon Telescope. *Astrophys J* 818(2):121. <https://doi.org/10.3847/0004-637X/818/2/121>. [arXiv:1510.00394](https://arxiv.org/abs/1510.00394) [astro-ph.HE]
- Psaltis D, et al. (2020a) Gravitational Test Beyond the First Post-Newtonian Order with the Shadow of the M87 Black Hole. *Phys Rev Lett* 125(14):141104. <https://doi.org/10.1103/PhysRevLett.125.141104>. [arXiv:2010.01055](https://arxiv.org/abs/2010.01055) [gr-qc]
- Psaltis D, et al. (2020b) Gravitational Test beyond the First Post-Newtonian Order with the Shadow of the M87 Black Hole. *Phys Rev Lett* 125(14):141104. <https://doi.org/10.1103/PhysRevLett.125.141104>, URL <https://link.aps.org/doi/10.1103/PhysRevLett.125.141104>

- Pu HY, Yun K, Younsi Z, Yoon SJ (2016) Odyssey: A Public GPU-based Code for General Relativistic Radiative Transfer in Kerr Spacetime. *Astrophys. J.* 820(2):105. <https://doi.org/10.3847/0004-637X/820/2/105>. arXiv:1601.02063 [astro-ph.HE]
- Raymond AW, Palumbo D, Paine SN, Blackburn L, Córdova Rosado R, Doelman SS, Farah JR, Johnson MD, Roelofs F, Tilanus RPJ, Weintroub J (2021) Evaluation of New Submillimeter VLBI Sites for the Event Horizon Telescope. *Astrophys. J. Suppl.* 253(1):5. <https://doi.org/10.3847/1538-3881/abc3c3>. arXiv:2102.05482 [astro-ph.IM]
- Ressler SM, Quataert E, Stone JM (2018) Hydrodynamic simulations of the inner accretion flow of Sagittarius A* fuelled by stellar winds. *Mon Not Roy Astron Soc* 478(3):3544–3563. <https://doi.org/10.1093/mnras/sty1146>. arXiv:1805.00474 [astro-ph.HE]
- Ressler SM, Quataert E, Stone JM (2020a) The Surprisingly Small Impact of Magnetic Fields On The Inner Accretion Flow of Sagittarius A* Fueled By Stellar Winds. *Mon Not Roy Astron Soc* 492(3):3272–3293. <https://doi.org/10.1093/mnras/stz3605>. arXiv:2001.04469 [astro-ph.HE]
- Ressler SM, White CJ, Quataert E, Stone JM (2020b) Ab Initio Horizon-scale Simulations of Magnetically Arrested Accretion in Sagittarius A* Fed by Stellar Winds. *Astrophys J* 896(1):L6. <https://doi.org/10.3847/2041-8213/ab9532>, URL <https://iopscience.iop.org/article/10.3847/2041-8213/ab9532https://iopscience.iop.org/article/10.3847/2041-8213/ab9532/meta>. arXiv:2006.00005
- Reuter M (1998) Nonperturbative evolution equation for quantum gravity. *Phys Rev D* 57:971–985. <https://doi.org/10.1103/PhysRevD.57.971>. arXiv:hep-th/9605030
- Reuter M, Tuiran E (2011) Quantum Gravity Effects in the Kerr Spacetime. *Phys Rev D* 83:044041. <https://doi.org/10.1103/PhysRevD.83.044041>. arXiv:1009.3528 [hep-th]
- de Rham C, Pozsgay V (2020) New class of Proca interactions. *Phys Rev D* 102(8):083508. <https://doi.org/10.1103/PhysRevD.102.083508>. arXiv:2003.13773 [hep-th]
- de Rham C, Gabadadze G, Tolley AJ (2011) Resummation of Massive Gravity. *Phys Rev Lett* 106:231101. <https://doi.org/10.1103/PhysRevLett.106.231101>. arXiv:1011.1232 [hep-th]
- de Rham C, Francfort J, Zhang J (2020) Black Hole Gravitational Waves in the Effective Field Theory of Gravity. *Phys Rev D* 102(2):024079. <https://doi.org/10.1103/PhysRevD.102.024079>. arXiv:2005.13923 [hep-th]
- Ricarte A, Natarajan P (2018) The observational signatures of supermassive black hole seeds. *Mon. Not. R. Astron. Soc.* 481(3):3278–3292. <https://doi.org/10.1093/mnras/sty2448>. arXiv:1809.01177 [astro-ph.GA]
- Ricarte A, Qiu R, Narayan R (2021) Black hole magnetic fields and their imprint on circular polarization images. *Mon. Not. R. Astron. Soc.* 505(1):523–539. <https://doi.org/10.1093/mnras/stab1289>. arXiv:2104.11301 [astro-ph.HE]
- Ricarte A, Palumbo DCM, Narayan R, Roelofs F, Emami R (2022) Observational Signatures of Frame Dragging in Strong Gravity. *Astrophys. J. Lett.* 941(1):L12. <https://doi.org/10.3847/2041-8213/aca087>. arXiv:2211.01810 [gr-qc]
- Rioja M, Dodson R, Malarecki J, Asaki Y (2011) EXPLORATION OF SOURCE FREQUENCY PHASE REFERENCING TECHNIQUES FOR ASTROMETRY AND OBSERVATIONS OF WEAK SOURCES WITH HIGH FREQUENCY SPACE VERY LONG BASELINE INTERFEROMETRY. *The Astronomical Journal* 142(5):157. <https://doi.org/10.1088/0004-6256/142/5/157>, URL <https://doi.org/10.1088/0004-6256/142/5/157>

- [org/10.1088%2F0004-6256%2F142%2F5%2F157](https://doi.org/10.1088%2F0004-6256%2F142%2F5%2F157)
- Rioja MJ, Dodson R, Asaki Y (2023) The transformational power of frequency phase transfer methods for ngeht. *Galaxies* 11(1). <https://doi.org/10.3390/galaxies11010016>, URL <https://www.mdpi.com/2075-4434/11/1/16>
- Ripperda B, Bacchini F, Porth O, Most ER, Olivares H, Nathanael A, Rezzolla L, Teunissen J, Keppens R (2019) General-relativistic Resistive Magnetohydrodynamics with Robust Primitive-variable Recovery for Accretion Disk Simulations. *The Astrophysical Journal Supplement Series* 244(1):10. <https://doi.org/10.3847/1538-4365/ab3922>, URL <https://iopscience.iop.org/article/10.3847/1538-4365/ab3922>, publisher: IOP Publishing
- Robinson DC (1975) Uniqueness of the Kerr black hole. *Phys Rev Lett* 34:905–906. <https://doi.org/10.1103/PhysRevLett.34.905>
- Robles VH, Matos T (2012) Flat Central Density Profile and Constant DM Surface Density in Galaxies from Scalar Field Dark Matter. *Mon Not Roy Astron Soc* 422:282–289. <https://doi.org/10.1111/j.1365-2966.2012.20603.x>. [arXiv:1201.3032](https://arxiv.org/abs/1201.3032) [astro-ph.CO]
- Röder J, Cruz-Osorio A, Fromm CM, Mizuno Y, Younsi Z, Rezzolla L (2022) Comparison of Kerr and dilaton black hole shadows. *PoS EVN2021:024*. <https://doi.org/10.22323/1.399.0024>
- Röder J, Cruz-Osorio A, Fromm CM, Mizuno Y, Younsi Z, Rezzolla L (2022) Comparison of Kerr and dilaton black hole shadows. In: *European VLBI Network Mini-Symposium and Users' Meeting 2021*. p 24
- Röder J, Cruz-Osorio A, Fromm CM, Mizuno Y, Younsi Z, Rezzolla L (2023) Probing the spacetime and accretion model for the Galactic Center: Comparison of Kerr and dilaton black hole shadows. *Astron. Astrophys.*671:A143. <https://doi.org/10.1051/0004-6361/202244866>. [arXiv:2301.09549](https://arxiv.org/abs/2301.09549) [astro-ph.HE]
- Rodriguez C, Taylor GB, Zavala RT, Peck AB, Pollack LK, Romani RW (2006) A Compact Supermassive Binary Black Hole System. *Astrophys. J.*646(1):49–60. <https://doi.org/10.1086/504825>. [arXiv:astro-ph/0604042](https://arxiv.org/abs/astro-ph/0604042) [astro-ph]
- Roelofs F, Blackburn L, Lindahl G, Doleman SS, Johnson MD, Arras P, Chatterjee K, Emami R, Fromm C, Fuentes A, Knollmüller J, Kosogorov N, Müller H, Patel N, Raymond A, Tiede P, Traianou E, Vega J (2023) The ngEHT Analysis Challenges. *Galaxies* 11(1):12. <https://doi.org/10.3390/galaxies11010012>. [arXiv:2212.11355](https://arxiv.org/abs/2212.11355) [astro-ph.IM]
- Romero GE (2020) Large Latin American Millimeter Array. *arXiv e-prints* [arXiv:2010.00738](https://arxiv.org/abs/2010.00738). [arXiv:2010.00738](https://arxiv.org/abs/2010.00738) [astro-ph.IM]
- Rovelli C, Vidotto F (2014) Planck stars. *Int J Mod Phys D* 23(12):1442026. <https://doi.org/10.1142/S0218271814420267>. [arXiv:1401.6562](https://arxiv.org/abs/1401.6562) [gr-qc]
- Roy R, Yajnik UA (2020) Evolution of black hole shadow in the presence of ultralight bosons. *Phys Lett B* 803:135284. <https://doi.org/10.1016/j.physletb.2020.135284>. [arXiv:1906.03190](https://arxiv.org/abs/1906.03190) [gr-qc]
- Roy R, Vagnozzi S, Visinelli L (2022) Superradiance evolution of black hole shadows revisited. *Phys Rev D* 105(8):083002. <https://doi.org/10.1103/PhysRevD.105.083002>. [arXiv:2112.06932](https://arxiv.org/abs/2112.06932) [astro-ph.HE]
- Rubinur K, Das M, Kharb P (2019) Searching for dual AGN in galaxies with double-peaked emission line spectra using radio observations. *Mon Not R Astron Soc* 484(4):4933–4950. <https://doi.org/10.1093/mnras/stz334>. [arXiv:1902.00689](https://arxiv.org/abs/1902.00689) [astro-ph.GA]

- Ruderman MA, Sutherland PG (1975) Theory of pulsars - Polar caps, sparks, and coherent microwave radiation. *The Astrophysical Journal* 196:51–72. <https://doi.org/10.1086/153393>
- Saida H (2017) How to measure a black hole's mass, spin, and direction of spin axis in the Kerr lens effect 1: Test case with simple source emission near a black hole. *Progress of Theoretical and Experimental Physics* 2017(5):053E02. <https://doi.org/10.1093/ptep/ptx060>. arXiv:1606.04716 [astro-ph.HE]
- Sanchis-Gual N, Di Giovanni F, Zilhão M, Herdeiro C, Cerdá-Durán P, Font JA, Radu E (2019) Nonlinear Dynamics of Spinning Bosonic Stars: Formation and Stability. *Phys Rev Lett* 123(22):221101. <https://doi.org/10.1103/PhysRevLett.123.221101>. arXiv:1907.12565 [gr-qc]
- Sanders DB, Soifer BT, Elias JH, Madore BF, Matthews K, Neugebauer G, Scoville NZ (1988) Ultraluminous Infrared Galaxies and the Origin of Quasars. *Astrophys. J.*325:74. <https://doi.org/10.1086/165983>
- Sarkar A, Gupta AC, Chitnis VR, Wiita PJ (2021) Multiwaveband quasi-periodic oscillation in the blazar 3C 454.3. *Mon. Not. R. Astron. Soc.*501(1):50–61. <https://doi.org/10.1093/mnras/staa3211>. arXiv:2003.01911 [astro-ph.HE]
- Schive HY, Chiueh T, Broadhurst T (2014) Cosmic Structure as the Quantum Interference of a Coherent Dark Wave. *Nature Phys* 10:496–499. <https://doi.org/10.1038/nphys2996>. arXiv:1406.6586 [astro-ph.GA]
- Schnittman JD (2005) Interpreting the High-Frequency Quasi-periodic Oscillation Power Spectra of Accreting Black Holes. *Astrophys. J.*621(2):940–950. <https://doi.org/10.1086/427646>. arXiv:astro-ph/0407179 [astro-ph]
- Schnittman JD (2011) Electromagnetic counterparts to black hole mergers. *Classical and Quantum Gravity* 28(9):094021. <https://doi.org/10.1088/0264-9381/28/9/094021>, URL <https://doi.org/10.1088/0264-9381/28/9/094021>
- Schnittman JD, Bertschinger E (2004) The Harmonic Structure of High-Frequency Quasi-periodic Oscillations in Accreting Black Holes. *Astrophys. J.*606(2):1098–1111. <https://doi.org/10.1086/383180>. arXiv:astro-ph/0309458 [astro-ph]
- Schodel R, et al. (2002) A Star in a 15.2 year orbit around the supermassive black hole at the center of the Milky Way. *Nature* 419:694–696. <https://doi.org/10.1038/nature01121>. arXiv:astro-ph/0210426
- Sen A (1992) Rotating charged black hole solution in heterotic string theory. *Phys. Rev. Lett.*69(7):1006–1009. <https://doi.org/10.1103/PhysRevLett.69.1006>. arXiv:hep-th/9204046 [hep-th]
- Sen S (2018) Plasma effects on lasing of a uniform ultralight axion condensate. *Phys Rev D* 98(10):103012. <https://doi.org/10.1103/PhysRevD.98.103012>. arXiv:1805.06471 [hep-ph]
- Sengo I, Cunha PVP, Herdeiro CAR, Radu E (2023) Kerr black holes with synchronised Proca hair: lensing, shadows and EHT constraints. *J. Cosmol. Astropart. Phys.*2023(1):047. <https://doi.org/10.1088/1475-7516/2023/01/047>. arXiv:2209.06237 [gr-qc]
- Senovilla JMM (1998) Singularity Theorems and Their Consequences. *Gen Rel Grav* 30:701. <https://doi.org/10.1023/A:1018801101244>. arXiv:1801.04912 [gr-qc]
- Senovilla JMM, Garfinkle D (2015) The 1965 Penrose singularity theorem. *Class Quant Grav* 32(12):124008. <https://doi.org/10.1088/0264-9381/32/12/124008>. arXiv:1410.5226 [gr-qc]
- Shaikh R (2019) Black hole shadow in a general rotating spacetime obtained through Newman-Janis algorithm. *Phys Rev D* 100(2):024028. <https://doi.org/10.1103/>

- [PhysRevD.100.024028](#). [arXiv:1904.08322](#) [gr-qc]
- Shaikh R, Joshi PS (2019) Can we distinguish black holes from naked singularities by the images of their accretion disks? *JCAP* 10:064. <https://doi.org/10.1088/1475-7516/2019/10/064>. [arXiv:1909.10322](#) [gr-qc]
- Shaikh R, Banerjee P, Paul S, Sarkar T (2019a) Strong gravitational lensing by wormholes. *JCAP* 07:028. <https://doi.org/10.1088/1475-7516/2019/07/028>. [arXiv:1905.06932](#) [gr-qc]
- Shaikh R, Kocherlakota P, Narayan R, Joshi PS (2019b) Shadows of spherically symmetric black holes and naked singularities. *Mon Not Roy Astron Soc* 482(1):52–64. <https://doi.org/10.1093/mnras/sty2624>. [arXiv:1802.08060](#) [astro-ph.HE]
- Shakura NI, Sunyaev RA (1973) Black holes in binary systems. Observational appearance. *Astron Astrophys* 24:337–355
- Shankar F, Salucci P, Granato G, De Zotti G, Danese L (2004) Supermassive black hole demography: the match between the local and accreted mass functions. *Monthly Notices of the Royal Astronomical Society* 354(4):1020–1030
- Shankar F, Weinberg DH, Miralda-Escude J (2009) Self-Consistent Models of the AGN and Black Hole Populations: Duty Cycles, Accretion Rates, and the Mean Radiative Efficiency. *Astrophys J* 690:20–41. <https://doi.org/10.1088/0004-637X/690/1/20>. [arXiv:0710.4488](#) [astro-ph]
- Shao L, et al. (2015) Testing Gravity with Pulsars in the SKA Era. In: *Advancing Astrophysics with the Square Kilometre Array*. vol AASKA14. Proceedings of Science, p 042. [arXiv:1501.00058](#) [astro-ph.HE]
- Shashank S, Bambi C (2022) Constraining the Konoplya-Rezzolla-Zhidenko deformation parameters III: Limits from stellar-mass black holes using gravitational-wave observations. *Phys Rev D* 105(10):104004. <https://doi.org/10.1103/PhysRevD.105.104004>. [arXiv:2112.05388](#) [gr-qc]
- Shcherbakov RV, McKinney JC (2013) Submillimeter Quasi-periodic Oscillations in Magnetically Choked Accretion Flow Models of SgrA*. *Astrophys. J. Lett.* 774(2):L22. <https://doi.org/10.1088/2041-8205/774/2/L22>. [arXiv:1304.7768](#) [astro-ph.HE]
- Shen Y, Chen YC, Hwang HC, Liu X, Zakamska N, Oguri M, Li JIH, Lazio J, Breiding P (2021) A hidden population of high-redshift double quasars unveiled by astrometry. *Nature Astronomy* 5(6):569–574. <https://doi.org/10.1038/s41550-021-01323-1>, URL <https://doi.org/10.1038/s41550-021-01323-1>
- Sillanpaa A, Haarala S, Valtonen MJ, Sundelius B, Byrd GG (1988) OJ 287: Binary Pair of Supermassive Black Holes. *Astrophys. J.* 325:628. <https://doi.org/10.1086/166033>
- Silva HO, Sakstein J, Gualtieri L, Sotiriou TP, Berti E (2018) Spontaneous scalarization of black holes and compact stars from a Gauss-Bonnet coupling. *Phys Rev Lett* 120(13):131104. <https://doi.org/10.1103/PhysRevLett.120.131104>. [arXiv:1711.02080](#) [gr-qc]
- Simon J, Birrer S, Bechtol K, Chakrabarti S, Cyr-Racine FY, Dell’Antonio I, Drlica-Wagner A, Fassnacht C, Geha M, Gilman D, Hezaveh YD, Kim D, Li TS, Strigari L, Treu T (2019) Testing the Nature of Dark Matter with Extremely Large Telescopes. *Bulletin of the American Astronomical Society* 51(3):153. <https://doi.org/10.48550/arXiv.1903.04742>. [arXiv:1903.04742](#) [astro-ph.CO]
- Simpson A, Visser M (2019) Regular black holes with asymptotically Minkowski cores. *Universe* 6(1):8. <https://doi.org/10.3390/universe6010008>. [arXiv:1911.01020](#) [gr-qc]

- Singh BP, Ghosh SG (2018) Shadow of Schwarzschild–Tangherlini black holes. *Annals Phys* 395:127–137. <https://doi.org/10.1016/j.aop.2018.05.010>. arXiv:1707.07125 [gr-qc]
- Sorce J, Wald RM (2017) Gedanken experiments to destroy a black hole. II. Kerr–Newman black holes cannot be overcharged or overspun. *Phys. Rev. D* 96(10):104014. <https://doi.org/10.1103/PhysRevD.96.104014>. arXiv:1707.05862 [gr-qc]
- Sotiriou TP, Faraoni V (2012) Black holes in scalar-tensor gravity. *Phys Rev Lett* 108:081103. <https://doi.org/10.1103/PhysRevLett.108.081103>. arXiv:1109.6324 [gr-qc]
- Sotiriou TP, Vega I, Vernieri D (2014) Rotating black holes in three-dimensional Hořava gravity. *Phys. Rev. D* 90(4):044046. <https://doi.org/10.1103/PhysRevD.90.044046>. arXiv:1405.3715 [gr-qc]
- Spieksma TFM, Cannizzaro E, Ikeda T, Cardoso V, Chen Y (2023) Superradiance: Axionic couplings and plasma effects. *Phys. Rev. D* 108(6):063013. <https://doi.org/10.1103/PhysRevD.108.063013>. arXiv:2306.16447 [gr-qc]
- Staelens S, Mayerson DR, Bacchini F, Ripperda B, Kuchler L (2023) Black hole photon rings beyond general relativity. *Phys. Rev. D* 107(12):124026. <https://doi.org/10.1103/PhysRevD.107.124026>. arXiv:2303.02111 [gr-qc]
- Stelle KS (1978) Classical Gravity with Higher Derivatives. *Gen Rel Grav* 9:353–371. <https://doi.org/10.1007/BF00760427>
- Stephan AP, Naoz S, Ghez AM, Witzel G, Sitarski BN, Do T, Kocsis B (2016) Merging binaries in the Galactic Center: the eccentric Kozai–Lidov mechanism with stellar evolution. *Mon. Not. R. Astron. Soc.* 460(4):3494–3504. <https://doi.org/10.1093/mnras/stw1220>. arXiv:1603.02709 [astro-ph.SR]
- Strominger A, Vafa C (1996) Microscopic origin of the Bekenstein–Hawking entropy. *Phys Lett B* 379:99–104. [https://doi.org/10.1016/0370-2693\(96\)00345-0](https://doi.org/10.1016/0370-2693(96)00345-0). arXiv:hep-th/9601029
- Stuchlík Z, Schee J (2019) Shadow of the regular Bardeen black holes and comparison of the motion of photons and neutrinos. *Eur Phys J C* 79(1):44. <https://doi.org/10.1140/epjc/s10052-019-6543-8>
- Svrcek P, Witten E (2006) Axions In String Theory. *JHEP* 06:051. <https://doi.org/10.1088/1126-6708/2006/06/051>. arXiv:hep-th/0605206
- Tahura S, Pan Z, Yang H (2022) Science potential for stellar-mass black holes as neighbors of Sgr A*. *Phys. Rev. D* 105(12):123018. <https://doi.org/10.1103/PhysRevD.105.123018>. arXiv:2201.03154 [astro-ph.HE]
- Takahashi R (2004) Shapes and Positions of Black Hole Shadows in Accretion Disks and Spin Parameters of Black Holes. *Astrophys. J.* 611(2):996–1004. <https://doi.org/10.1086/422403>. arXiv:astro-ph/0405099 [astro-ph]
- Tchekhovskoy A, Narayan R, McKinney JC (2011) Efficient generation of jets from magnetically arrested accretion on a rapidly spinning black hole. *Mon. Not. R. Astron. Soc.* 418(1):L79–L83. <https://doi.org/10.1111/j.1745-3933.2011.01147.x>. arXiv:1108.0412 [astro-ph.HE]
- Teo E (2003) Spherical Photon Orbits Around a Kerr Black Hole. *General Relativity and Gravitation* 35(11):1909–1926. <https://doi.org/10.1023/A:1026286607562>
- Teodoro MC, Collodel LG, Kunz J (2021) Tidal effects in the motion of gas clouds around boson stars. *Physical Review D* 103(10):104064. URL <https://journals.aps.org/prd/abstract/10.1103/PhysRevD.103.104064>, publisher: American Physical Society

- Terrazas BA, Bell EF, Pillepich A, Nelson D, Somerville RS, Genel S, Weinberger R, Habouzit M, Li Y, Hernquist L, et al. (2020) The relationship between black hole mass and galaxy properties: examining the black hole feedback model in illustrating. *Monthly Notices of the Royal Astronomical Society* 493(2):1888–1906
- The LIGO Scientific Collaboration, the Virgo Collaboration, the KAGRA Collaboration, et al (2021) Tests of General Relativity with GWTC-3. arXiv e-prints arXiv:2112.06861. <https://doi.org/10.48550/arXiv.2112.06861>. arXiv:2112.06861 [gr-qc]
- Thirring H (1918) Über die Wirkung rotierender ferner Massen in der Einsteinschen Gravitationstheorie. *Physikalische Zeitschrift* 19:33
- Tiburzi C, Hobbs G, Kerr M, Coles WA, Dai S, Manchester RN, Possenti A, Shannon RM, You XP (2015) A study of spatial correlations in pulsar timing array data. *Monthly Notices of the Royal Astronomical Society* 455(4):4339–4350. <https://doi.org/10.1093/mnras/stv2143>, URL <https://doi.org/10.1093/mnras/stv2143>. <https://academic.oup.com/mnras/article-pdf/455/4/4339/4087311/stv2143.pdf>
- Tiede P (2022) Comrade: Composable modeling of radio emission. *Journal of Open Source Software* 7(76):4457. <https://doi.org/10.21105/joss.04457>, URL <https://doi.org/10.21105/joss.04457>
- Tiede P, Pu HY, Broderick AE, Gold R, Karami M, Preciado-López JA (2020) Space-time Tomography Using the Event Horizon Telescope. *Astrophys. J.*892(2):132. <https://doi.org/10.3847/1538-4357/ab744c>. arXiv:2002.05735 [astro-ph.HE]
- Tiede P, Johnson MD, Pesce DW, Palumbo DCM, Chang DO, Galison P (2022) Measuring Photon Rings with the ngEHT. *Galaxies* 10(6):111. <https://doi.org/10.3390/galaxies10060111>. arXiv:2210.13498 [astro-ph.HE]
- Titov O, Frey S, Melnikov A, Shu F, Xia B, González J, Tercero B, Gurvits L, de Witt A, McCallum J, Kharinov M, Zimovsky V, Krezinger M (2023) Astrometric Apparent Motion of High-redshift Radio Sources. *The Astronomical Journal* 165(2):69. <https://doi.org/10.3847/1538-3881/aca964>. arXiv:2302.12957 [astro-ph.GA]
- Tokovinin AA (1997) On the multiplicity of spectroscopic binary stars. *Astronomy Letters* 23(6):727–730
- Toshmatov B, Ahmedov B, Abdujabbarov A, Stuchlik Z (2014) Rotating Regular Black Hole Solution. *Phys Rev D* 89(10):104017. <https://doi.org/10.1103/PhysRevD.89.104017>. arXiv:1404.6443 [gr-qc]
- Tsujikawa S (2013) Quintessence: A Review. *Class Quant Grav* 30:214003. <https://doi.org/10.1088/0264-9381/30/21/214003>. arXiv:1304.1961 [gr-qc]
- Tsukamoto N (2018) Black hole shadow in an asymptotically-flat, stationary, and axisymmetric spacetime: The Kerr-Newman and rotating regular black holes. *Phys Rev D* 97(6):064021. <https://doi.org/10.1103/PhysRevD.97.064021>. arXiv:1708.07427 [gr-qc]
- Vagnozzi S, Visinelli L (2019) Hunting for extra dimensions in the shadow of M87*. *Phys Rev D* 100(2):024020. <https://doi.org/10.1103/PhysRevD.100.024020>. arXiv:1905.12421 [gr-qc]
- Vagnozzi S, Roy R, Tsai YD, Visinelli L, Afrin M, Allahyari A, Bambhaniya P, Dey D, Ghosh SG, Joshi PS, Jusufi K, Khodadi M, Walia RK, Övgün A, Bambi C (2023) Horizon-scale tests of gravity theories and fundamental physics from the Event Horizon Telescope image of Sagittarius A*. *Classical and Quantum Gravity* 40(16):165007. <https://doi.org/10.1088/1361-6382/acd97b>. arXiv:2205.07787 [gr-qc]
- Vecchio A (2004) Lisa observations of rapidly spinning massive black hole binary systems. *Phys Rev D* 70:042001. <https://doi.org/10.1103/PhysRevD.70.042001>, URL

- <https://link.aps.org/doi/10.1103/PhysRevD.70.042001>
- Vernieri D, Sotiriou TP (2012) Hořava-Lifshitz gravity: Detailed balance revisited. *Phys. Rev. D* 85(6):064003. <https://doi.org/10.1103/PhysRevD.85.064003>
- Vetsov T, Gylchev G, Yazadjiev S (2018) Shadows of Black Holes in Vector-Tensor Galileons Modified Gravity. arXiv e-prints arXiv:1801.04592. <https://doi.org/10.48550/arXiv.1801.04592>. arXiv:1801.04592 [gr-qc]
- Vigeland S, Yunes N, Stein L (2011) Bumpy Black Holes in Alternate Theories of Gravity. *Phys Rev D* 83:104027. <https://doi.org/10.1103/PhysRevD.83.104027>. arXiv:1102.3706 [gr-qc]
- Vigeland SJ, Hughes SA (2010) Spacetime and orbits of bumpy black holes. *Phys Rev D* 81:024030. <https://doi.org/10.1103/PhysRevD.81.024030>. arXiv:0911.1756 [gr-qc]
- Vincent FH, Gourgoulhon E, Herdeiro C, Radu E (2016a) Astrophysical imaging of Kerr black holes with scalar hair. *Phys Rev D* 94(8):084045. <https://doi.org/10.1103/PhysRevD.94.084045>. arXiv:1606.04246 [gr-qc]
- Vincent FH, Meliani Z, Grandclément P, Gourgoulhon E, Straub O (2016b) Imaging a boson star at the Galactic center. *Classical and Quantum Gravity* 33(10):105015. <https://doi.org/10.1088/0264-9381/33/10/105015>, URL <http://stacks.iop.org/0264-9381/33/i=10/a=105015?key=crossref.c60cc7dd0e0d9320c11658001038fd55>, publisher: IOP Publishing
- Vincent FH, Wielgus M, Abramowicz MA, Gourgoulhon E, Lasota JP, Paumard T, Perin G (2021) Geometric modeling of M87* as a Kerr black hole or a non-Kerr compact object. *Astron Astrophys* 646:A37. <https://doi.org/10.1051/0004-6361/202037787>. arXiv:2002.09226 [gr-qc]
- Visser M (2014) Physical observability of horizons. *Phys Rev D* 90(12):127502. <https://doi.org/10.1103/PhysRevD.90.127502>. arXiv:1407.7295 [gr-qc]
- Visser M, Wiltshire DL (2004) Stable gravastars: An Alternative to black holes? *Class Quant Grav* 21:1135–1152. <https://doi.org/10.1088/0264-9381/21/4/027>. arXiv:gr-qc/0310107
- Visser M, Barcelo C, Liberati S, Sonogo S (2008) Small, dark, and heavy: But is it a black hole? *PoS BHGRS:010*. <https://doi.org/10.22323/1.075.0010>. arXiv:0902.0346 [gr-qc]
- Völkel SH, Barausse E, Franchini N, Broderick AE (2021) EHT tests of the strong-field regime of general relativity. *Class Quant Grav* 38(21):21LT01. <https://doi.org/10.1088/1361-6382/ac27ed>. arXiv:2011.06812 [gr-qc]
- Volonteri M (2010) Formation of Supermassive Black Holes. *Astron Astrophys Rev* 18:279–315. <https://doi.org/10.1007/s00159-010-0029-x>. arXiv:1003.4404 [astro-ph.CO]
- Volonteri M, Habouzit M, Colpi M (2021) The origins of massive black holes. *Nature Rev Phys* 3(11):732–743. <https://doi.org/10.1038/s42254-021-00364-9>. arXiv:2110.10175 [astro-ph.GA]
- von Zeipel H (1910) Sur l'application des séries de M. Lindstedt à l'étude du mouvement des comètes périodiques. *Astronomische Nachrichten* 183(22):345. <https://doi.org/10.1002/asna.19091832202>
- Vos J, Mościbrodzka MA, Wielgus M (2022) Polarimetric signatures of hot spots in black hole accretion flows. *Astron. Astrophys.* 668:A185. <https://doi.org/10.1051/0004-6361/202244840>. arXiv:2209.09931 [astro-ph.HE]
- Waisberg I, Dexter J, Gillessen S, Pfuhl O, Eisenhauer F, Plewa PM, Bauböck M, Jimenez-Rosales A, Habibi M, Ott T, von Fellenberg S, Gao F, Widmann F, Genzel R (2018) What stellar orbit is needed to measure the spin of the Galactic centre

- black hole from astrometric data? *Mon. Not. R. Astron. Soc.* 476(3):3600–3610. <https://doi.org/10.1093/mnras/sty476>. arXiv:1802.08198 [astro-ph.GA]
- Wald RM (1999) *Gravitational Collapse and Cosmic Censorship*, Springer Netherlands, Dordrecht, pp 69–86. https://doi.org/10.1007/978-94-017-0934-7_5, URL https://doi.org/10.1007/978-94-017-0934-7_5
- Walker M, Penrose R (1970) On quadratic first integrals of the geodesic equations for type { 22} spacetimes. *Communications in Mathematical Physics* 18(4):265–274. <https://doi.org/10.1007/BF01649445>
- Walker RC, Hardee PE, Davies F, Ly C, Junor W, Mertens F, Lobanov A (2016) Observations of the Structure and Dynamics of the Inner M87 Jet. *Galaxies* 4(4):46. <https://doi.org/10.3390/galaxies4040046>. arXiv:1610.08600 [astro-ph.HE]
- Wang HM, Xu YM, Wei SW (2019) Shadows of Kerr-like black holes in a modified gravity theory. *JCAP* 03:046. <https://doi.org/10.1088/1475-7516/2019/03/046>. arXiv:1810.12767 [gr-qc]
- Wang X, Li PC, Zhang CY, Guo M (2020) Novel shadows from the asymmetric thin-shell wormhole. *Phys Lett B* 811:135930. <https://doi.org/10.1016/j.physletb.2020.135930>. arXiv:2007.03327 [gr-qc]
- Wang Z, Broderick AE (2023) Constraining the Existence of Axion Clouds in M87* with Closure Trace Analyses. arXiv e-prints arXiv:2311.01565 [astro-ph.HE]
- Wei SW, Liu YX (2021) Testing the nature of Gauss-Bonnet gravity by four-dimensional rotating black hole shadow. *Eur Phys J Plus* 136(4):436. <https://doi.org/10.1140/epjp/s13360-021-01398-9>. arXiv:2003.07769 [gr-qc]
- Weinberg NN, Milosavljević M, Ghez AM (2005) Stellar Dynamics at the Galactic Center with an Extremely Large Telescope. *The Astrophysical Journal* 622(2):878–891. <https://doi.org/10.1086/428079>. arXiv:astro-ph/0404407 [astro-ph]
- Weinberg S (1978) A New Light Boson? *Phys Rev Lett* 40:223–226. <https://doi.org/10.1103/PhysRevLett.40.223>
- Weinberger R, Springel V, Pakmor R, Nelson D, Genel S, Pillepich A, Vogelsberger M, Marinacci F, Naiman J, Torrey P, Hernquist L (2018) Supermassive black holes and their feedback effects in the IllustrisTNG simulation. *Mon. Not. R. Astron. Soc.* 479(3):4056–4072. <https://doi.org/10.1093/mnras/sty1733>. arXiv:1710.04659 [astro-ph.GA]
- Weltman A, et al. (2020) Fundamental physics with the Square Kilometre Array. *Publ Astron Soc Austral* 37:e002. <https://doi.org/10.1017/pasa.2019.42>. arXiv:1810.02680 [astro-ph.CO]
- Wharton RS, Chatterjee S, Cordes JM, Deneva JS, Lazio TJW (2012) Multiwavelength Constraints on Pulsar Populations in the Galactic Center. *The Astrophysical Journal* 753(2):108. <https://doi.org/10.1088/0004-637X/753/2/108>. arXiv:1111.4216 [astro-ph.HE]
- Wielgus M (2021) Photon rings of spherically symmetric black holes and robust tests of non-Kerr metrics. *Phys Rev D* 104(12):124058. <https://doi.org/10.1103/PhysRevD.104.124058>. arXiv:2109.10840 [gr-qc]
- Wielgus M, et al (2022) Millimeter Light Curves of Sagittarius A* Observed during the 2017 Event Horizon Telescope Campaign. *Astrophys. J. Lett.* 930(2):L19. <https://doi.org/10.3847/2041-8213/ac6428>
- Wielgus M, Akiyama K, et al (2020) Monitoring the Morphology of M87* in 2009–2017 with the Event Horizon Telescope. *Astrophys. J.* 901(1):67. <https://doi.org/10.3847/1538-4357/abac0d>. arXiv:2009.11842 [astro-ph.HE]

- Wielgus M, Horak J, Vincent F, Abramowicz M (2020) Reflection-asymmetric wormholes and their double shadows. *Phys Rev D* 102(8):084044. <https://doi.org/10.1103/PhysRevD.102.084044>. [arXiv:2008.10130](https://arxiv.org/abs/2008.10130) [gr-qc]
- Wielgus M, Moscibrodzka M, Vos J, Gelles Z, Martí-Vidal I, Farah J, Marchili N, Goddi C, Messias H (2022) Orbital motion near Sagittarius A* . Constraints from polarimetric ALMA observations. *Astron. Astrophys.*665:L6. <https://doi.org/10.1051/0004-6361/202244493>. [arXiv:2209.09926](https://arxiv.org/abs/2209.09926) [astro-ph.HE]
- Wilczek F (1978) Problem of Strong P and T Invariance in the Presence of Instantons. *Phys Rev Lett* 40:279–282. <https://doi.org/10.1103/PhysRevLett.40.279>
- Will CM (2008) Testing the general relativistic no-hair theorems using the Galactic center black hole SgrA*. *Astrophys J Lett* 674:L25–L28. <https://doi.org/10.1086/528847>. [arXiv:0711.1677](https://arxiv.org/abs/0711.1677) [astro-ph]
- Will CM (2014) The Confrontation between General Relativity and Experiment. *Living Rev Rel* 17:4. <https://doi.org/10.12942/lrr-2014-4>. [arXiv:1403.7377](https://arxiv.org/abs/1403.7377) [gr-qc]
- Witzel G, Eckart A, Bremer M, Zamaninasab M, Shahzamanian B, Valencia-S M, Schödel R, Karas V, Lenzen R, Marchili N, Sabha N, Garcia-Marin M, Buchholz RM, Kunneriath D, Straubmeier C (2012) Source-intrinsic Near-infrared Properties of Sgr A*: Total Intensity Measurements. *Astrophys. J. Suppl.*203(2):18. <https://doi.org/10.1088/0067-0049/203/2/18>. [arXiv:1208.5836](https://arxiv.org/abs/1208.5836) [astro-ph.HE]
- Witzel G, et al. (2012) Source-intrinsic near-infrared properties of Sgr A*: Total intensity measurements. *Astrophys J Suppl* 203:18. <https://doi.org/10.1088/0067-0049/203/2/18>. [arXiv:1208.5836](https://arxiv.org/abs/1208.5836) [astro-ph.HE]
- Wong GN (2021) Black Hole Glimmer Signatures of Mass, Spin, and Inclination. *Astrophys. J.*909(2):217. <https://doi.org/10.3847/1538-4357/abdd2d>. [arXiv:2009.06641](https://arxiv.org/abs/2009.06641) [astro-ph.HE]
- Wong GN (2021) Black Hole Glimmer Signatures of Mass, Spin, and Inclination. *Astrophys J* 909(2):217. <https://doi.org/10.3847/1538-4357/abdd2d>. [arXiv:2009.06641](https://arxiv.org/abs/2009.06641) [astro-ph.HE]
- Wong GN, Prather BS, Dhruv V, Ryan BR, Moscibrodzka M, Chan Ck, Joshi AV, Yarza R, Ricarte A, Shiokawa H, Dolence JC, Noble SC, McKinney JC, Gammie CF (2022) PATOKA: Simulating Electromagnetic Observables of Black Hole Accretion. *arXiv e-prints* [arXiv:2202.11721](https://arxiv.org/abs/2202.11721). [arXiv:2202.11721](https://arxiv.org/abs/2202.11721) [astro-ph.HE]
- Workman RL, et al. (2022) Review of Particle Physics. *PTEP* 2022:083C01. <https://doi.org/10.1093/ptep/ptac097>
- Xie Y, Zhang J, Silva HO, de Rham C, Witek H, Yunes N (2021) Square Peg in a Circular Hole: Choosing the Right Ansatz for Isolated Black Holes in Generic Gravitational Theories. *Phys Rev Lett* 126(24):241104. <https://doi.org/10.1103/PhysRevLett.126.241104>. [arXiv:2103.03925](https://arxiv.org/abs/2103.03925) [gr-qc]
- Yadav J, Das M, Barway S, Combes F (2021) A triple active galactic nucleus in the NGC 7733-7734 merging group. *Astron. Astrophys.*651:L9. <https://doi.org/10.1051/0004-6361/202141210>
- Yagi K, Yunes N, Tanaka T (2012) Slowly Rotating Black Holes in Dynamical Chern-Simons Gravity: Deformation Quadratic in the Spin. *Phys Rev D* 86:044037. <https://doi.org/10.1103/PhysRevD.86.044037>, [Erratum: *Phys.Rev.D* 89, 049902 (2014)]. [arXiv:1206.6130](https://arxiv.org/abs/1206.6130) [gr-qc]
- Yang H, Zimmerman A, Zenginoğlu A, Zhang F, Berti E, Chen Y (2013) Quasinormal modes of nearly extremal Kerr spacetimes: spectrum bifurcation and power-law ringdown. *Phys Rev D* 88(4):044047. <https://doi.org/10.1103/PhysRevD.88.044047>. [arXiv:1307.8086](https://arxiv.org/abs/1307.8086) [gr-qc]

- Yang SC, Luo H, Zhang YH, Zhang C (2022) Measurement of the Central Galactic Black Hole by Extremely Large Mass-Ratio Inspirals. *Symmetry* 14(12):2558. <https://doi.org/10.3390/sym14122558>. [arXiv:2207.01977](https://arxiv.org/abs/2207.01977) [gr-qc]
- Yoshino H, Kodama H (2012) Bosenova collapse of axion cloud around a rotating black hole. *Prog Theor Phys* 128:153–190. <https://doi.org/10.1143/PTP.128.153>. [arXiv:1203.5070](https://arxiv.org/abs/1203.5070) [gr-qc]
- Younsi Z (2024) Imaging black holes with the Event Horizon Telescope: an introduction. *Contemporary Physics*
- Younsi Z, Wu K (2015) Variations in emission from episodic plasmoid ejecta around black holes. *Mon. Not. R. Astron. Soc.* 454(3):3283–3298. <https://doi.org/10.1093/mnras/stv2203>. [arXiv:1510.01700](https://arxiv.org/abs/1510.01700) [astro-ph.HE]
- Younsi Z, Wu K, Fuerst SV (2012) General relativistic radiative transfer: formulation and emission from structured tori around black holes. *Astron. Astrophys.* 545:A13. <https://doi.org/10.1051/0004-6361/201219599>. [arXiv:1207.4234](https://arxiv.org/abs/1207.4234) [astro-ph.HE]
- Younsi Z, Zhidenko A, Rezzolla L, Konoplya R, Mizuno Y (2016) New method for shadow calculations: Application to parametrized axisymmetric black holes. *Phys. Rev. D* 94(8):084025. <https://doi.org/10.1103/PhysRevD.94.084025>. [arXiv:1607.05767](https://arxiv.org/abs/1607.05767) [gr-qc]
- Younsi Z, Psaltis D, Özel F (2023) Black Hole Images as Tests of General Relativity: Effects of Spacetime Geometry. *Astrophys. J.* 942(1):47. <https://doi.org/10.3847/1538-4357/aca58a>. [arXiv:2111.01752](https://arxiv.org/abs/2111.01752) [astro-ph.HE]
- Yu Q, Zhang F, Lu Y (2016) Prospects for Constraining the Spin of the Massive Black Hole at the Galactic Center via the Relativistic Motion of a Surrounding Star. *Astrophys. J.* 827(2):114. <https://doi.org/10.3847/0004-637X/827/2/114>. [arXiv:1606.07725](https://arxiv.org/abs/1606.07725) [astro-ph.HE]
- Yu Z, Jiang Q, Abdikamalov AB, Ayzenberg D, Bambi C, Liu H, Nampalliwar S, Tripathi A (2021) Constraining the Konoplya-Rezzolla-Zhidenko deformation parameters. II. Limits from stellar-mass black hole x-ray data. *Phys Rev D* 104(8):084035. <https://doi.org/10.1103/PhysRevD.104.084035>. [arXiv:2106.11658](https://arxiv.org/abs/2106.11658) [astro-ph.HE]
- Yuan GW, Xia ZQ, Tang C, Zhao Y, Cai YF, Chen Y, Shu J, Yuan Q (2021) Testing the ALP-photon coupling with polarization measurements of Sagittarius A*. *JCAP* 03:018. <https://doi.org/10.1088/1475-7516/2021/03/018>. [arXiv:2008.13662](https://arxiv.org/abs/2008.13662) [astro-ph.HE]
- Yuan GW, Shen ZQ, Tsai YLS, Yuan Q, Fan YZ (2022) Constraining ultralight bosonic dark matter with Keck observations of S2's orbit and kinematics. *Phys Rev D* 106(10):103024. <https://doi.org/10.1103/PhysRevD.106.103024>. [arXiv:2205.04970](https://arxiv.org/abs/2205.04970) [astro-ph.HE]
- Yuan Q, Zhang M, Liu X, Jiang PF, Kokhirova GI (2023) Correlation Analysis between OJ 287 Radio Jet Observables. *Astrophys. J.* 949(1):20. <https://doi.org/10.3847/1538-4357/acc5ec>
- Yunes N, Pretorius F (2009) Dynamical Chern-Simons Modified Gravity. I. Spinning Black Holes in the Slow-Rotation Approximation. *Phys Rev D* 79:084043. <https://doi.org/10.1103/PhysRevD.79.084043>. [arXiv:0902.4669](https://arxiv.org/abs/0902.4669) [gr-qc]
- Yunes N, Siemens X (2013) Gravitational-Wave Tests of General Relativity with Ground-Based Detectors and Pulsar Timing-Arrays. *Living Rev Rel* 16:9. <https://doi.org/10.12942/lrr-2013-9>. [arXiv:1304.3473](https://arxiv.org/abs/1304.3473) [gr-qc]
- Yunes N, Stein LC (2011) Non-Spinning Black Holes in Alternative Theories of Gravity. *Phys Rev D* 83:104002. <https://doi.org/10.1103/PhysRevD.83.104002>. [arXiv:1101.2921](https://arxiv.org/abs/1101.2921) [gr-qc]

- Zajaček M, Tursunov A, Eckart A, Britzen S (2018) On the charge of the Galactic centre black hole. *Mon Not Roy Astron Soc* 480(4):4408–4423. <https://doi.org/10.1093/mnras/sty2182>. [arXiv:1808.07327](https://arxiv.org/abs/1808.07327) [astro-ph.GA]
- Zamaninasab M, Eckart A, Meyer L, Schödel R, Dovciak M, Karas V, Kunneriath D, Witzel G, Gießübel R, König S, Straubmeier C, Zensus A (2008) An evolving hot spot orbiting around Sgr A*. In: *Journal of Physics Conference Series*. *Journal of Physics Conference Series*, vol 131. p 012008. <https://doi.org/10.1088/1742-6596/131/1/012008>. [arXiv:0810.0138](https://arxiv.org/abs/0810.0138) [astro-ph]
- Zanotti O, Rezzolla L, Del Zanna L, Palenzuela C (2010) Electromagnetic counterparts of recoiling black holes: general relativistic simulations of non-Keplerian discs. *Astronomy & Astrophysics* 523(1):A8. <https://doi.org/10.1051/0004-6361/201014969>, URL https://www.aanda.org/articles/aa/full_html/2010/15/aa14969-10/aa14969-10.html, publisher: EDP Sciences
- Zel'dovich YB (1971) Generation of Waves by a Rotating Body. *Soviet Journal of Experimental and Theoretical Physics Letters* 14:180
- Zeng XX, Zhang HQ, Zhang H (2020) Shadows and photon spheres with spherical accretions in the four-dimensional Gauss–Bonnet black hole. *Eur Phys J C* 80(9):872. <https://doi.org/10.1140/epjc/s10052-020-08449-y>. [arXiv:2004.12074](https://arxiv.org/abs/2004.12074) [gr-qc]
- Zhang F, Lu Y, Yu Q (2015) ON TESTING THE KERR METRIC OF THE MASSIVE BLACK HOLE IN THE GALACTIC CENTER VIA STELLAR ORBITAL MOTION: FULL GENERAL RELATIVISTIC TREATMENT. *The Astrophysical Journal* 809(2):127. <https://doi.org/10.1088/0004-637x/809/2/127>, URL <https://doi.org/10.1088/0004-637x/809/2/127>
- Zhao GY, Gómez JL, Fuentes A, Krichbaum TP, Traianou E, Lico R, Cho I, Ros E, Komossa S, Akiyama K, Asada K, Blackburn L, Britzen S, Bruni G, Crew GB, Dahale R, Dey L, Gold R, Gopakumar A, Issaoun S, Janssen M, Jorstad S, Kim JY, Koay JY, Kovalev YY, Koyama S, Lobanov AP, Loinard L, Lu RS, Markoff S, Marscher AP, Martí-Vidal I, Mizuno Y, Park J, Savolainen T, Toscano T (2022) Unraveling the Innermost Jet Structure of OJ 287 with the First GMVA + ALMA Observations. *Astrophys. J.* 932(1):72. <https://doi.org/10.3847/1538-4357/ac6b9c>. [arXiv:2205.00554](https://arxiv.org/abs/2205.00554) [astro-ph.HE]
- Zhu T, Wu Q, Jamil M, Jusufi K (2019) Shadows and deflection angle of charged and slowly rotating black holes in Einstein-Æther theory. *Phys Rev D* 100(4):044055. <https://doi.org/10.1103/PhysRevD.100.044055>. [arXiv:1906.05673](https://arxiv.org/abs/1906.05673) [gr-qc]
- Zilberman N, Casals M, Ori A, Ottewill AC (2022a) Quantum Fluxes at the Inner Horizon of a Spinning Black Hole. *Phys. Rev. Lett.* 129(26):261102. <https://doi.org/10.1103/PhysRevLett.129.261102>. [arXiv:2203.08502](https://arxiv.org/abs/2203.08502) [gr-qc]
- Zilberman N, Casals M, Ori A, Ottewill AC (2022b) Two-point function of a quantum scalar field in the interior region of a Kerr black hole. *Phys. Rev. D* 106(12):125011. <https://doi.org/10.1103/PhysRevD.106.125011>. [arXiv:2203.07780](https://arxiv.org/abs/2203.07780) [gr-qc]
- Zulianello A, Carballo-Rubio R, Liberati S, Ansoldi S (2021) Electromagnetic tests of horizonless rotating black hole mimickers. *Phys Rev D* 103(6):064071. <https://doi.org/10.1103/PhysRevD.103.064071>. [arXiv:2005.01837](https://arxiv.org/abs/2005.01837) [gr-qc]

Author affiliations*D. Ayzenberg*

Theoretical Astrophysics, Eberhard-Karls Universität Tübingen, D-72076, Tübingen, Germany.

ORCID: 0000-0003-0238-6181

Lindy Blackburn

Center for Astrophysics | Harvard & Smithsonian, 60 Garden Street, Cambridge, MA 02138, USA,

Black Hole Initiative at Harvard University, 20 Garden Street, Cambridge, MA 02138, USA.

ORCID: 0000-0002-9030-642X

R. Brito

CENTRA, Departamento de Física, Instituto Superior Técnico – IST, Universidade de Lisboa – UL, Avenida Rovisco Pais 1, 1049-001 Lisboa, Portugal.

ORCID: 0000-0002-7807-3053

S. Britzen

Max-Planck-Institut für Radioastronomie, Auf dem Hügel 69, D-53121 Bonn, Germany.

ORCID: 0000-0001-9240-6734

A. Broderick

Perimeter Institute for Theoretical Physics, 31 Caroline Street North, Waterloo, ON, N2L 2Y5, Canada,

Department of Physics and Astronomy, University of Waterloo, 200 University Avenue West, Waterloo, ON, N2L 3G1, Canada,

Waterloo Centre for Astrophysics, University of Waterloo, Waterloo, ON N2L 3G1 Canada.

ORCID: 0000-0002-3351-760X

R. Carballo-Rubio

CP3-Origins, University of Southern Denmark, Campusvej 55, DK-5230 Odense M, Denmark,

Florida Space Institute, University of Central Florida, 12354 Research Parkway, Partnership 1, 32826 Orlando, FL, USA.

ORCID: 0000-0001-6389-6105

V. Cardoso

Niels Bohr International Academy, Niels Bohr Institute, Blegdamsvej 17, 2100 Copenhagen, Denmark,

CENTRA, Departamento de Física, Instituto Superior Técnico – IST, Universidade de Lisboa – UL, Avenida Rovisco Pais 1, 1049-001 Lisboa, Portugal.

ORCID: 0000-0003-0553-0433

A. Chael

Princeton Gravity Initiative, Jadwin Hall, Princeton University, Princeton NJ 08544, USA.

ORCID: 0000-0003-2966-6220

K. Chatterjee

Department of Physics, University of Maryland, College Park, MD 20742, USA,
Institute for Research in Electronics and Applied Physics, University of Maryland,
College Park, MD 20742, USA,
Black Hole Initiative at Harvard University, 20 Garden Street, Cambridge, MA
02138, USA,
Harvard-Smithsonian Center for Astrophysics, 60 Garden Street, Cambridge, MA
02138, USA.
ORCID: 0000-0002-2825-3590

Y. Chen

Niels Bohr International Academy, Niels Bohr Institute, Blegdamsvej 17, 2100
Copenhagen, Denmark.
ORCID: 0000-0002-2507-8272

P. V. P. Cunha

Departamento de Matemática da Universidade de Aveiro and Centre for Research
and Development in Mathematics and Applications (CIDMA), Campus de Santiago,
3810-183 Aveiro, Portugal.
ORCID: 0000-0001-8375-6943

H. Davoudiasl

High Energy Theory Group, Physics Department, Brookhaven National Laboratory,
Upton, NY 11973, USA.
ORCID: 0000-0003-3484-911X

P. B. Denton

High Energy Theory Group, Physics Department, Brookhaven National Laboratory,
Upton, NY 11973, USA.
ORCID: 0000-0002-5209-872X

S. S. Doeleman

Center for Astrophysics | Harvard & Smithsonian, 60 Garden Street, Cambridge,
MA 02138, USA,
Black Hole Initiative at Harvard University, 20 Garden Street, Cambridge, MA
02138, USA.
ORCID: 0000-0002-9031-0904

A. Eichhorn

CP3-Origins, University of Southern Denmark, Campusvej 55, DK-5230 Odense M,
Denmark.
ORCID: 0000-0003-4458-1495

M. Eubanks

Asteroid Initiatives, LLC, USA.
ORCID: 0000-0001-9543-0414

Y. Fang

Perimeter Institute for Theoretical Physics, Waterloo, ON N2L2Y5, Canada,
Kavli Institute for Astronomy and Astrophysics, Peking University, Beijing 100871,
China.
ORCID: 0000-0003-0065-8622

A. Foschi

CENTRA, Departamento de Física, Instituto Superior Técnico – IST, Universidade de Lisboa – UL, Avenida Rovisco Pais 1, 1049-001 Lisboa, Portugal.
ORCID: 0000-0002-4636-637X

C. M. Fromm

Institut für Theoretische Physik und Astrophysik, Universität Würzburg, Emil-Fischer-Strasse 31, 97074 Würzburg, Germany,
Institut für Theoretische Physik, Goethe Universität Frankfurt, Max-von-Laue-Str.1, 60438 Frankfurt am Main, Germany,
Max-Planck-Institut für Radioastronomie, Auf dem Hügel 69, D-53121 Bonn, Germany.
ORCID: 0000-0002-1827-1656

P. Galison

Black Hole Initiative at Harvard University, 20 Garden Street, Cambridge, MA 02138, USA,
Department of History of Science, Harvard University, Cambridge, MA 02138, USA,
Department of Physics, Harvard University, Cambridge, MA 02138, USA.
ORCID: 0000-0002-6429-3872

S. G. Ghosh

Centre for Theoretical Physics, Jamia Millia Islamia, New Delhi 110025, India,
Astrophysics and Cosmology Research Unit, School of Mathematics, Statistics and Computer Science, University of KwaZulu-Natal, Private Bag 54001, Durban 4000, South Africa.
ORCID: 0000-0002-0835-3690

R. Gold

CP3-Origins, University of Southern Denmark, Campusvej 55, DK-5230 Odense M, Denmark.
ORCID: 0000-0003-2492-1966

L. I. Gurvits

Joint Institute for VLBI ERIC (JIVE), Oude Hoogeveensedijk 4, NL-7991 PD Dwingeloo, the Netherlands,
Faculty of Aerospace Engineering, Delft University of Technology, Kluyverweg 1, NL-2629 HS Delft, the Netherlands
ORCID: 0000-0002-0694-2459

S. Hadar

Department of Mathematics and Physics, University of Haifa at Oranim, Kiryat Tivon 3600600, Israel,
Haifa Research Center for Theoretical Physics and Astrophysics, University of Haifa, Haifa 3498838, Israel.
ORCID: 0000-0002-6960-0704

A. Held

Theoretisch-Physikalisches Institut, Friedrich-Schiller-Universität Jena, Max-Wien-Platz 1, 07743 Jena, Germany,
The Princeton Gravity Initiative, Jadwin Hall, Princeton University, Princeton, New Jersey 08544, USA.
ORCID: 0000-0003-2701-9361

J. Houston

Center for Astrophysics | Harvard & Smithsonian, 60 Garden Street, Cambridge, MA 02138, USA.

Y. Hu

Mullard Space Science Laboratory, University College London, Holmbury St. Mary, Dorking, Surrey, RH5 6NT, United Kingdom.
ORCID: 0000-0001-9252-0246

M. D. Johnson

Center for Astrophysics | Harvard & Smithsonian, 60 Garden Street, Cambridge, MA 02138, USA,
Black Hole Initiative at Harvard University, 20 Garden Street, Cambridge, MA 02138, USA.
ORCID: 0000-0002-4120-3029

P. Kocherlakota

Black Hole Initiative at Harvard University, 20 Garden St., Cambridge, MA 02138, USA,
Center for Astrophysics, Harvard & Smithsonian, 60 Garden St., Cambridge, MA 02138, USA.
ORCID: 0000-0001-7386-7439

P. Natarajan

Department of Astronomy, Yale University, 52 Hillhouse Avenue, New Haven, CT 06511, USA,
Department of Physics, Yale University, P.O. Box 208121, New Haven, CT 06520, USA,
Black Hole Initiative at Harvard University, 20 Garden Street, Cambridge, MA 02138, USA.
ORCID: 0000-0002-5554-8896

H. Olivares

Department of Astrophysics/IMAPP, Radboud University Nijmegen, P.O. Box 9010, NL-6500 GL Nijmegen, The Netherlands.
ORCID: 0000-0001-6833-7580

D. Palumbo

Center for Astrophysics | Harvard & Smithsonian, 60 Garden Street, Cambridge, MA 02138, USA,
Black Hole Initiative at Harvard University, 20 Garden Street, Cambridge, MA 02138, USA.
ORCID: 0000-0002-7179-3816

D. W. Pesce

Center for Astrophysics | Harvard & Smithsonian, 60 Garden Street, Cambridge, MA 02138, USA,
Black Hole Initiative at Harvard University, 20 Garden Street, Cambridge, MA 02138, USA.
ORCID: 0000-0002-5278-9221

S. Rajendran

Department of Physics and Astronomy, Johns Hopkins University, Baltimore, MD 21218, USA.
ORCID: 0000-0001-9915-3573

R. Roy

Anton Pannekoek Institute for Astronomy, University of Amsterdam, Science Park 904, 1098 XH, Amsterdam, The Netherlands.
ORCID: 0000-0003-3714-5310

Saurabh

P. D. Patel Institute of Applied Sciences, Charusat University, Anand, 388421 Gujarat, India.
ORCID: 0000-0001-7156-4848

L. Shao

Kavli Institute for Astronomy and Astrophysics, Peking University, Beijing 100871, China,
National Astronomical Observatories, Chinese Academy of Sciences, Beijing 100012, China.
ORCID: 0000-0002-1334-8853

S. Tahura

University of Guelph, Guelph, Ontario N1G 2W1, Canada,
Perimeter Institute for Theoretical Physics, Ontario, N2L 2Y5, Canada.
ORCID: 0000-0001-5678-5028

A. Tamar

124 Bank Enclave, First Floor, Laxmi Nagar, Delhi-110092, India.
ORCID: 0000-0001-8763-4169

P. Tiede

Center for Astrophysics | Harvard & Smithsonian, 60 Garden Street, Cambridge, MA 02138, USA,
Black Hole Initiative at Harvard University, 20 Garden Street, Cambridge, MA 02138, USA.
ORCID: 0000-0003-3826-5648

F. H. Vincent

LESIA, Observatoire de Paris, CNRS, Université Pierre et Marie Curie, Université Paris Diderot, 5 place Jules Janssen, 92190 Meudon, France.
ORCID: 0000-0002-3855-0708

L. Visinelli

Tsung-Dao Lee Institute (TDLI), 520 Shengrong Road, 201210 Shanghai, P. R. China,
School of Physics and Astronomy, Shanghai Jiao Tong University, 800 Dongchuan Road, 200240 Shanghai, P. R. China.
ORCID: 0000-0001-7958-8940

Z. Wang

Department of Physics and Astronomy, University of Waterloo, 200 University Avenue West, Waterloo, ON, N2L 3G1, Canada,
Waterloo Centre for Astrophysics, University of Waterloo, Waterloo, ON N2L 3G1,

Canada.

ORCID: 0009-0004-9417-2213

M. Wielgus

Department of Physics and Astronomy, University of 2 Max-Planck-Institut für Radioastronomie, Auf dem Hügel 69, 53121 Bonn, Germany,

Research Centre for Computational Physics and Data Processing, Institute of Physics, Silesian University in Opava, Bezručovám. 13, CZ-746 01 Opava, Czech Republic.

ORCID: 0000-0002-8635-4242

X. Xue

Institute of Theoretical Physics, Universität Hamburg, 22761, Hamburg, Germany,

Deutsches Elektronen-Synchrotron DESY, Notkestr. 85, 22607, Hamburg, Germany.

ORCID: 0000-0002-0740-1283

K. Yakut

Department of Astronomy and Space Sciences, Faculty of Science, University of Ege, 35100, İzmir, Turkey,

Ege Gravitational Astrophysics Research Group (eGRAVITY), University of Ege, 35100, İzmir, Turkey.

ORCID: 0000-0003-2380-9008

H. Yang

University of Guelph, Department of Physics, Guelph, ON N1G2W1, Canada,

Perimeter Institute for Theoretical Physics, Waterloo, ON N2L2Y5, Canada.

ORCID: 0000-0002-9965-3030

Z. Younsi

Mullard Space Science Laboratory, University College London, Holmbury St. Mary, Dorking, Surrey, RH5 6NT, United Kingdom.

ORCID: 0000-0001-9283-1191